PETROLOGY AND PETROGENESIS OF THE MOTZFELDT TA-MINERALISATION, GARDAR PROVINCE, SOUTH GREENLAND

Jamie Alan McCreath

A Thesis Submitted for the Degree of PhD
at the
University of St. Andrews

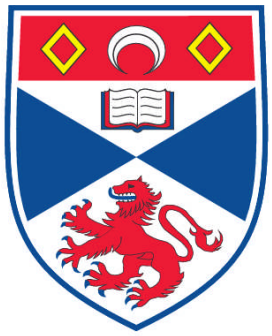

2009

Petrology and Petrogenesis of the Motzfeldt Ta-mineralisation, Gardar Province, South Greenland

Submitted for the degree of Doctor of Philosophy

School of Geography and Geosciences
University of St Andrews

Jamie Alan McCreath

February 3rd

2009

I, Jamie Alan McCreath, hereby certify that this thesis, which is approximately 50,500 words in length, has been written by me, that it is the record of work carried out by me and that it has not been submitted in any previous application for a higher degree.

Date signature of candidate

I was admitted as a research student in July, 2005 and as a candidate for the degree of Doctor of Philosophy in July, 2005; the higher study for which this is a record was carried out in the University of St Andrews between 2005 and 2009.

Date signature of candidate

I hereby certify that the candidate has fulfilled the conditions of the Resolution and Regulations appropriate for the degree of Doctor of Philosophy in the University of St Andrews and that the candidate is qualified to submit this thesis in application for that degree.

Date signature of supervisor

In submitting this thesis to the University of St Andrews we understand that we are giving permission for it to be made available for use in accordance with the regulations of the University Library for the time being in force, subject to any copyright vested in the work not being affected thereby. We also understand that the title and the abstract will be published, and that a copy of the work may be made and supplied to any bona fide library or research

worker, that my thesis will be electronically accessible for personal or research use unless exempt by award of an embargo as requested below, and that the library has the right to migrate my thesis into new electronic forms as required to ensure continued access to the thesis. We have obtained any third-party copyright permissions that may be required in order to allow such access and migration, or have requested the appropriate embargo below.

The following is an agreed request by candidate and supervisor regarding the electronic publication of this thesis:

Access to printed copy and electronic publication of thesis through the University of St Andrews.

Embargo on both, all, or part of printed copy and electronic copy for the same fixed period of two years on the following ground:

Publication would be commercially damaging to the researcher, or to the supervisor, or the University;

Date signature of candidate

Date signature of supervisor

Acknowledgements

I would like to thank the following people for their support, advice and general assistance during the production of this thesis. First and foremost I thank my supervisors Adrian Finch, Colin Donaldson and Ashlyn Armour-Brown for their encouragement, constructive discussions and general patience during the project.

Thanks must also go to those who braved the elements with me out in Greenland, including Teal Riley, Malcolm Wilkinson, Sarah Gordie, Julian Schilling, Gregor Markl, Ian Parsons and Sofka Amour-Brown. I would like to give special thanks to Johannes Schönenberger for his assistance in the field and during discussions both in the field and at various meetings over the past three years.

Within St Andrews there are a number of people who I would like to thank for their help. First I would like to thank Donald Herd for his assistance and patience during the long hours spent carrying out EPMA analyses. I would also like to thank Angus Calder for help with XRF analyses, Alix Cage and Chris Wurster for their help during stable isotope analyses and Stuart Alison for putting me up and keeping me fed and watered during the final stages of writing. Much appreciated. I would also like to thank Siri Simonsen for her help during LA-MC-ICPMS analyses and Tom Andersen for help with column chemistry whilst visiting the University of Oslo. I would also like to thank everyone from the Institut für Geowissenschaften, University of Tübingen for their help with fluid inclusion microthermometry and for making me feel welcome during my stay.

I am also grateful for the help and support of all my office mates; Georgina King, Tom Clemens, Cheryl Wood, Keziah Stott, and David Small. A special mention goes to Henrik Friis for being my partner in crime over the last three years.

I am also extremely grateful for the help and support I have received from my girlfriend Emily, particularly putting up with me during the final stages of the write-up. Thanks also go to all my friends for their moral support and for reminding me that there is life outside the office.

Finally I would like to thank my parents, Alan and Josephine, for their long-term investment in my education, not to mention their financial support along the way!

Abstract

The Motzfeldt centre is one of four major alkaline centres belonging to the Igaliko complex of South Greenland. The melts parental to the Motzfeldt centre are interpreted from Hf isotopes to be derived form a common mantle source which experienced subsequent isotopic contamination from older crustal components during the interval between segregation and emplacement. Magmatism within the centre commenced with the emplacement of the Motzfeldt Sø Formation at 1273 ± 8 Ma. This unit is unique within the Motzfeldt intrusion as it is characterised by a high degree of textural and mineralogical variability and hosts localised Nb, Ta, U, Th, Zr and REE mineralisation associated with pyrochlore and late-stage REE bearing carbonate phases. Biotite halogen contents show that in addition to enrichment of incompatible elements the MSF and Motzfeldt centre in general is particularly rich in F. The elevated F content is inferred to have extended the crystallisation interval of the melt and facilitated fractionation down to relatively low temperatures. The unusual enrichment of F and incompatible elements in the MSF is suggested to represent the first and most evolved melts extracted from the top of a stratified storage chamber at depth

The MSF is also characterised by pervasive subsolidus alteration, giving the rock and region a striking brick red colour. Pb-Pb pyrochlore studies indicate that alteration in the formation was effectively synchronous (1267 ± 6 Ma), with the magmatic age of emplacement. Fluid inclusion studies suggest that contemporaneous to the exsolution of juvenile, high salinity, F-rich fluids was the wholesale influx of hydrothermally convected low salinity groundwaters through the formation. The presence of pervasive late-stage hematite and calcite throughout the MSF suggests that the oxidation potential of the bulk fluid increased above the hematite-magnetite buffer during the waning stages of the hydrothermal phase. Mineralisation was promoted by this shift in fluid composition, reducing the complexing potential of fluid ligands and facilitating mineralisation within the high-levels units of the intrusion where alteration is most intense. Economic mineralisation associated with the centre is inferred to be largely sourced from the parental melts, however the role the hydrothermal phase played was particularly important in locally mobilising and concentrating incompatible elements within the high-level units of the formation.

Contents

Contents

Chapter 1

Introduction

1.1 Introduction

Since its discovery over 200 years ago tantalum (Ta) has become an important commodity in a number of diverse industries worldwide. The major consumer of world tantalum at present is the electronics industry where tantalum is used in the production of capacitors and high-power resistors. The physical and chemical properties of tantalum which make it such an important metal in this industry include high electrical conductivity and an excellent capacity to store and release electrical charge. In addition to the properties which make tantalum particularly useful in the electronics industry it also has an exceedingly high melting point (ca. 3,000°C), high corrosion-resistance and alloys well with other metals, making it perfectly suited for the production of super alloys for use in jet engines, chemical processing equipment, high-grade weaponry and nuclear reactors. The high resistance to corrosion which tantalum possesses is seeing it used more and more in surgical grade implants.

Over 130 tantalum and niobium bearing minerals are currently known to exist, however only a handful (tantalite, microlite, wodginite, euxenite, polycrase and fergusonite) are being used as raw materials in the tantalum industry. At present over half of the world's tantalum production comes from Australia and is dominated by the large pegmatite host tantalum deposits of Greenbushes and Wodgina in Western Australia (Partington *et al.,* 1995). Other principal suppliers of tantalum include Brazil, Canada, China, Ethiopia and Africa. Due to the increased world demand for tantalum, and the ethical and political problems surrounding resource exploitation in environmentally sensitive areas, exploration is now being carried out more diverse geological environments with a view to supplying the world demand for tantalum in the future. Areas currently under exploration include Greenland, Saudi Arabia, Egypt, USA, Canada and Finland. The present thesis is a study of a syenite host Ta-deposit in the Gardar alkaline igneous province of South Greenland. In 1999, the exploration company Angus and Ross plc obtained the exploration rights to the area east of the settlement of Narsarsuaq in the South of Greenland. The present study is an examination of the petrology and petrogenesis of the Ta-rich rocks of this region. This study explores the genesis of Ta-mineralisation in this area and evaluates the present concentrations of Ta and other economically interesting elements in the rocks of this region. Additionally the study places the

Ta-mineralisation in a broader context regarding the geology of the area, the centre, the Igaliko Complex, in which the rocks are hosted, and the Gardar province as a whole.

1.2 Alkaline magmatism

Although alkaline magmas only account for a small portion of igneous rocks in the Earth's crust (<1%) there is a large amount of literature devoted to their study (reviewed by Sørensen (1974) and Fitton and Upton (1987)). The large amount of literature devoted to the study of alkaline rocks is partly because they have remarkable mineralogical diversity, attracting the attention of mineralogists and petrologists alike, but also because of their economic interest as a result of their unusual enrichment of rare metals. The range of exotic mineral species found in alkaline rocks is due to the unusually high abundance of alkali elements (K and Na) and deficiency of silica, which makes alkaline environments ideal for the growth of mineral species that are unstable in silica-rich, alkali-poor magmas. In addition to academic interest, alkaline rocks also have great economic importance due to their extreme enrichment in large-ion lithophile elements (LILE) and high-field strength elements (HFSE), such as Zr, Nb, Ta, U and REEs, host within a variety of mineral species in and/or around alkaline igneous bodies. The effect of volatile components (H_2O, Cl, F and CO_2 principally) on the evolution of alkaline rocks has also been particularly well documented. Post-magmatic hydrothermal activity, associated with volatile fluids exsolved from the melt during crystallisation, has been demonstrated to import, export and remobilise elements within alkaline systems, localising and enhancing the grade of many economic mineral deposits associated with alkaline magmas (e.g. Kogarko, 1990; Kovalenko *et al.,* 1995; Salvi & Williams-Jones, 2006). In many cases the subsolidus activity of such volatile-enriched melts plays a more important role than the original magmatic phase.

One of the most celebrated and well studied alkaline provinces in the world is the mid-Proterozoic Gardar province of South Greenland (Upton & Emeleus, 1987). This area has been the site of much interest since the turn of the 19th Century because the excellent exposure and preservation of a diverse variety of rock types provide and excellent area for the study of ancient alkaline magma systems. In addition it is the host of several mineral deposits of worldwide importance, such as the cryolite deposit of Ivitût, the U and Be mineralisation of Ilimaussaq and the Ta-enriched deposits of the Motzfeldt region.

1.3 Geological setting of the Gardar Province

The Gardar province is located largely within the Ketilidian mobile belt of southern Greenland, comprising meta-sediments and meta-volcanics deformed and metamorphosed during the Ketilidian orogeny (1855-1794 Ma) (Gulson & Krogh, 1972; Garde *et al.,* 2002). The basement geology is reviewed in detail by Allaart (1976) and Garde *et al.* (2002), therefore only a brief overview is given here. The Ketilidian Mobile Belt extends from Kap Farvel in the south, up to the Ivigtût area in the northwest and to Ikermît in the northeast and comprises 4 distinct zones, each approximately 100 km wide extending NE-SW across the south of Greenland (Fig. 1.1). The northern border zone comprises supracrustal sediments and volcanics unconformably overlying Archaean age gneisses. The granite zone comprises a number of granite, diorite and orthogneiss units collectively termed the Julianehåb batholith, intruded over the interval 1854 ± 4 Ma to 1794 ± 1 Ma (Garde *et al.,* 2002) located within the root zone of the orogen. South of the granite zone is an area of complexly folded and metamorphosed granites, gneisses and migmatised Proterozoic sediments belonging to the folded migmatite zone. Extending south of the migmatite zone to the southern tip of Greenland is a flat-lying migmatite complex of high-grade meta-sediments, meta-volcanics and late Ketilidian age granite intrusives (Allaart, 1976: Garde *et al.,* 2002). The Julianehåb batholith now hosts most of the Gardar alkaline centres, with the exception of the Kûngnât, Ivigtût and Grønnedal-Ika centres, which are located within the northern border zone of the orogen (Fig 1.1). The siting of most Gardar magmatism within the Julianehåb batholith is interpreted to have been largely controlled by pre-existing structures generated during deformation of the orogen during Ketilidian times.

The Gardar alkaline province consists of essentially undeformed and unmetamorphosed alkaline intrusive centres and well exposed sequences of sub-aerial volcaniclastics, generated during episodic, rift-related magmatism during the mid-Proterozoic (Upton, 1974; Upton & Emeleus, 1987; Upton *et al.,* 2003). The province is exposed in the south of Greenland in a NE-SW trending graben structure developed during the tectono-magmatic evolution of the Proterozoic supercontinent, comprising North America, Greenland and Northern Europe. Transtensional tectonics generated during the break-up of this landmass promoted crustal anatexis and generation of mantle derived melts from which Gardar magmas were fractionated.

The province comprises approximately 10 major granite, syenite and nepheline syenite centres (Fig. 1.1) varying in size from several hundred meters in diameter (e.g. Ivigtût stock) up to ~50 km in diameter in the case of the Nunarssuit centre. All of the central complexes are generally recognised to be high-level passively emplaced bodies. Outcrops are commonly arcuate in plan and thought to be emplaced through a combination of block stoping, partial ring dyke formation and delamination of roofing material and earlier intrusive phases (e.g. Ilímaussaq, Motzfeldt and Igdlerfigssalik centres) (Emeleus and Harry, 1970; Parsons, 1979; Upton, 1962; Upton *et al*, 2003). The central complexes naturally fall into two catagories, those involving silica-oversaturated rocks such as granites and quartz syenites and those with silica-undersaturated chemistries, comprising typically variants of syenite and nepheline syenite. Several centres contain highly evolved peralkaline to agpaitic compositions of academic and economic interest, the most well know and well studied of these being the Ilímaussaq intrusion.

Igneous layering has been documented from many of the major intrusive centres of the province (Bohse *et al.,* 1971; Harry & Pulvertaft, 1963; Parsons, 1972; 1979; Sørensen, 1969; 1970) and reviewed by Ferguson and Pulvertaft (1963) and Upton (1961). Layering has been identified in anorthosites, gabbros, syenogabbros, augite syenites, nepheline syenites and granites throughout the Gardar, attributed to periodic changes in conditions (temperature, pressure, composition, etc) during crystal settling. Although crystal cumulates are often laterally continuous for hundreds of meters (e.g. kakortokites of the Ilímaussaq centre) many centres show pseudo-sedimentary igneous structures such as cumulate slump features, current cross lamination and irregularly deformed layers. The preservation of these features provides insights into the magmatic evolution of Gardar centres, showing evidence for temporal variations in magmatic convection in large magma chambers.

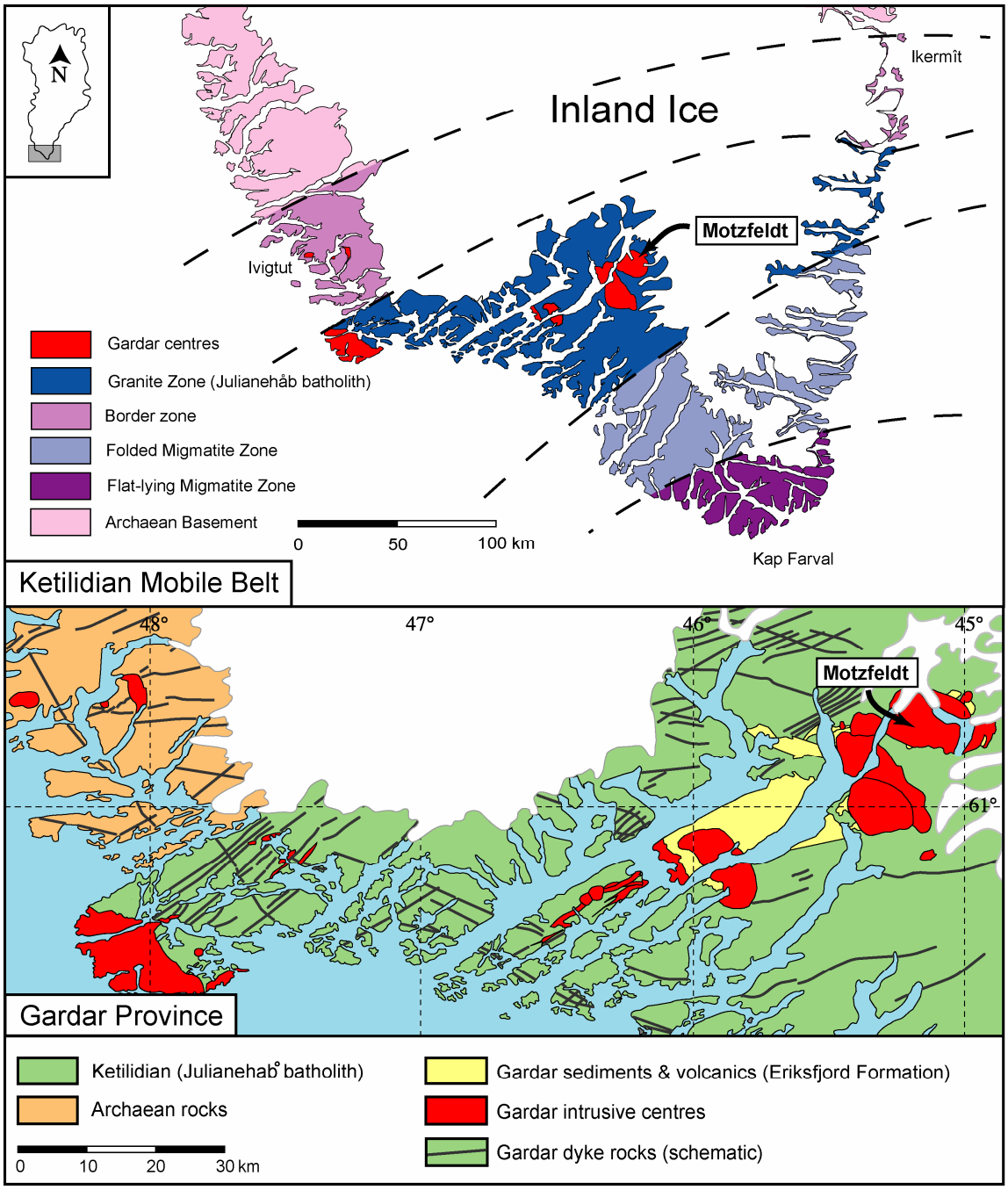

Figure 1.1. Geological sketch maps of South Greenland (after Garde *et al.,* 2002) and the Gardar Province (after Upton, 1974). The main zones of the Ketilidian orogen and major Gardar central complexes are shown. The location of the Motzfeldt centre is highlighted.

1.4 Geology of the Igaliko Complex

The present study focuses on the Motzfeldt centre, which is sited within the Igaliko complex in the north east of the province (Fig. 1.1). The Igaliko complex is the largest exposure of alkaline magmatism in the Gardar province, comprising ~250 km^2 of typically

silica-undersaturated syenite bodies located east of the major settlements of Narsarssuaq and Igaliko. The complex is recognised to consist of 4 major centres associated with 5 episodes of magmatism. These are, in order of emplacement, Motzfeldt, North Qôroq, South Qôroq, Early Igderfigssalik and Late Igderfigssalik (Coulson, 2003; Emeleus & Harry, 1970; Upton *et al.,* 2003). In addition to the 4 major centres there are a number of smaller satellite intrusions within the Igaliko complex, including the Østfjordsdal syenite (Salmon, in prep), Narsarssuaq stock (Salmon, in prep), North Motzfeldt centre (Finch *et al.,* 2001) and the silica-oversaturated Klokken intrusion (Parsons, 1972, 1979, 1981).

Central complex magmatism in the Igaliko complex initiated with the emplacement of the Motzfeldt centre at 1280 ± 30 Ma (Rb-Sr, Blaxland *et al.,* 1978) and terminated with the emplacement of the late Igdlerfigssalik centre and Klokken satellite stock at 1142 ± 15 Ma (Rb-Sr, Blaxland *et al.,* 1978) and 1166 ± 3 Ma (U-Pb badellyite date, Harper, 1988) respectively. However, the oldest igneous rocks associated with Igaliko magmatism occur as extrusive volcanic sequences belonging to the supracrustal Eriksfjord formation.

The type locality for the Eriksfjord formation is located on Narsaq peninsula between the Tunugdliarfik and Nordre Sermilik fjords and consists of ~3.5 km sub-aerial volcanics, interbedded fluvial and aeolian sandstones, ultrabasic carbonatites and lamprophyres (Andersen, 1997; Poulsen, 1964; Stewart, 1970; Tirsgaard and Øxenvad, 1989). Poulsen (1964) divided the formation into six members based on the exposures on the Narsaq peninsula; the Majût Mb, Massartût Mb, Naujarssuit Mb, Ulukasik Mb, Nunasarnq Mb and the Ilímaussaq Mb in order of stratigraphic sequence. In addition to exposures on the Narsaq peninsula, Eriksfjord rocks are found as outliers around, and xenoliths within, the major centres of Igaliko and in the Kungnat and Nunarsuit centres. The distribution of outliers and xenoliths of Eriksfjord rocks in many of the Igaliko centres and more southerly sited Gardar centres suggest that the sequence once covered much of the Igaliko complex, and indeed much of the Gardar province, suggesting that the base of the Eriksfjord predates the emplacement of the oldest Gardar centre.

1.5 Gardar chronology

Gardar magmatism has, until recently, been generally recognised as occurring during three principal periods; Early, Mid and Late Gardar, spanning the periods 1350-1300 Ma, 1280-1260 Ma and 1180-1140 Ma, respectively (Emeleus and Harry, 1970; Paslick *et al.,* 1993;

Upton & Blundell, 1978; Upton & Emeleus, 1987). However this work has since been refined with the development of more precise U-Pb age dating techniques (Table 1.1). New age determinations on the major Gardar centres suggest that a distinct Mid-Gardar period did not occur. Rather there is evidence only for two main episodes of igneous activity at ~1280 Ma and between 1180 and 1140 Ma (Upton *et al.,* 2003). Gardar magmatism thus spans at least 140 Ma, however the time at which Gardar magmatism initiated is still poorly constrained because of inaccurate dating of the Eriksfjord Formation. Therefore new age determinations for the Eriksfjord may see the interval of Gardar activity extend in excess of 200 Ma.

Table 1.1 *Published radiometric age dates for major Gardar centres*

Intrusion	Rock type	Age (Ma)	Initial $^{87}Sr/^{86}Sr$	Reference
Gronnedal-Ika	Nepheline Syenite	1299 ± 17	0.7032 ± 0.0004	Blaxland et al., 1978
Motzfeldt	Syenite	1280 ± 30	0.7024 ± 0.0004	Blaxland et al., 1978
North Qoroq	Nepheline Syenite	1268 ± 60	0.7052 ± 0.0030	Blaxland et al., 1978
North Motzfeldt	Nepheline Syenite	1226 ± 12	0.7054 ± 0.0019	Finch et al., 2001
Kungnat	Syenite	1275.2 ± 1.8*	-	Upton et al., 2003
Quassiarsuk	Carbonatite	1205 ± 12	0.7029 ± 0.0003	Andersen, 1997
South Qoroq	Nepheline Syenite	1106 ± 8	0.7029 ± 0.0004	Blaxland et al., 1978
Tugtutoq	Quartz Syenite	1165.7 ± 1.2*	-	Upton et al., 2003
Ilimaussaq	Agpaite/Syenite	1160 ± 5*	-	Waight et al., 2002
Orstfjordsdal	Syenite	1147.5 ± 3.2*	-	Salmon et al., (in prep)
Late Igdlerfigssalik	Nepheline Syenite	1142 ± 15	0.7029 ± 0.0007	Blaxland et al., 1978
Klokken	Gabbro	1166 ± 3*	-	Harper, 1988
Nunarssuit	Quarts Syenite	1130 ± 14	0.7043 ± 0.0002	Blaxland et al., 1978

Data shown are Rb-Sr dates which have been linearly regressed using the decay constants of Steiger and Jäger (1977). Dates marked with * are U-Pb ages. Errors for both Rb-Sr and U-Pb data are shown at the 2σ level.

A key uncertainty in Gardar chronology is dating the Eriksfjord Formation. This is a particular problem in the field area of the present study, where the Motzfeldt centre (1280 ± 30 Ma, Blaxland *et al.,* 1978) is found crosscutting the formation and rafts of Eriksfjord are hosted within the Motzfeldt syenites. Initial suggestions on the age of the Eriksfjord formation consider them to be one of the earliest expressions of rift-related magmatism in the Gardar, formed prior to the emplacement of the Motzfeldt centre. However, direct radiometric dates of ~1170 - 1200 Ma have been obtained from lavas within the Ulukasik Member on the Narsaq peninsula (Paslick *et al.,* 1993) and 1205 ± 12 Ma for the Mussartût member at Qassiarsuk (Andersen, 1997). These younger dates are inconsistent with the field evidence, which suggests the Eriksfjord to be older than the Motzfeldt and North Qôroq (1268 ± 60 Ma, Blaxland *et al.,* 1978) centres. Suggestions that the Eriksfjord represents a protracted period of magmatism attract little favour since there are few unconformities in the

sequence (Larsen, 1977). Textural features such as pahoehoe surfaces on lava flows are common, suggesting rapid and continuous lava production. Palaeomagnetic studies show that the entire Ulukasik sequence was erupted within a short magnetic reversal (Thomas & Piper 1992). Furthermore the close lithological similarities across the entire formation are inconsistent with a model where the Eriksfjord formation formed during several separate episodes of sedimentation and volcanism. Other interpretations suggest the younger dates obtained from the Ulukasik Member represent ages that have been wholly reset by younger magmatism (Piper *et al.,* 1999) and favour previously held opinions of an age of 1300 – 1350 Ma. It is clear that the age of the Eriksfjord formation remains contentious and will likely remain so until an accurate radiometric date is obtained.

1.6 Previous research

The Igaliko complex, including the Motzfeldt centre, the focus of the present study, was initially recognised during a number of reconnaissance flights carried out by the Geological survey of Denmark and Greenland (GEUS) (formerly the Greenland Geological Survey, GGU) during the late 1950s. This reconnaissance work was followed up by general geological surveying of the 4 major Igaliko centres during the field seasons of 1961, 1962 and 1963 by C.H. Emeleus and W.T.Harry. The results of this work included a geological map and description of the Igaliko complex (Emeleus & Harry, 1970). Of all the Igaliko centres, Motzfeldt received the least coverage during this work due to its large size, difficulty of access and extreme topography. As a result, the units NE of the Motzfeldt Sø lake were only visited briefly and were not surveyed in the detail received by the other Igaliko centres.

Initial mapping of the Motzfeldt centre by Emeleus and Harry (1970) distinguished 5 major syenite and nepheline syenite units, prefixed SM and numbered 1 to 5 in order of emplacement, and two satellite intrusions called North and East Motzfeldt. This nomenclature was used by Jones (1980) who described the petrography and geochemistry of the units established by Emeleus and Harry (1970) and added another agpaitic syenite unit (SM6) in the south of the centre, initially interpreted as highly metamorphosed basement rafts by Emeleus and Harry (1970).

In the late 1980s Bradshaw (1988) and Tukiainen *et al.* (1984) produced a revised field description for the centre and used a new nomenclature. They divided the Motzfeldt centre into three main formations, based on field and petrographic observations, called the

Geologfjeld, Motzfeldt Sø and Flinks Dal Formations (Fig. 1.2). Bradshaw (1985; 1988), Tukiainen (1985) and Tukiainen *et al.* (1984) identified much more detail in the rocks north east of Motzfeldt Sø in units previously belonging to the SM1 and SM3 units of Emeleus and Harry (1970), where reconnaissance work had been relatively superficial. These units are now considered part of the Motzfeldt Sø Formation (MSF) which comprises highly altered syenites and nepheline syenites. The Geologfjeld Formation (GF), in the north east of the centre, was previously grouped with the MSF in the SM1 and SM3 units of Emeleus and Harry (1970) and Jones (1980). Bradshaw (1985; 1988) considers this unit to be the earliest of the Motzfeldt intrusive members, representing an early satellite intrusion which predates the emplacement of the main partial ring-dykes of the 'Motzfeldt Ring Series' and considers this unit to be a "fresh" variant of the MSF, which was in some way impervious to the alteration process which affected the MSF. The remaining SM units of Emeleus and Harry (1970) and Jones (1980) (SM2, SM4, SM5 and SM6) are grouped in the Flinks Dal Formation (FDF), comprising three genetically related units of syenite and nepheline syenite. Previously the units east of Motzfeldt Sø were grouped as a separate satellite intrusion called the East Motzfeldt syenite (Emeleus & Harry, 1970). However Bradshaw (1985) identifies these units as an extension of the Motzfeldt Sø formation displaced laterally by the sinistral movement along the Flinks Dal fault.

1.7 Motzfeldt Sø Formation

The area NE of Motzfeldt Sø lake (Fig. 1.2), belonging to the MSF and GF, has been the site of much interest since detailed mapping commenced as part of the Syduran uranium exploration project under the Danish Ministry of Energy's research programmes of the 1981 and 1982 (Armour-Brown *et al.,* 1983, Tukiainen *et al.,* 1984). During this project more detailed mapping subdivided the MSF into three genetically related facies of syenite; the *MSF – marginal arfvedsonite syenite*, *MSF – altered syenite* and the *MSF – nepheline syenite*. Hosted within these three members are a number of late microsyenite sheets belonging to the *peralkaline microsyenite suite* of the MSF (Bradshaw, 1988; Tukiainen, 1988).

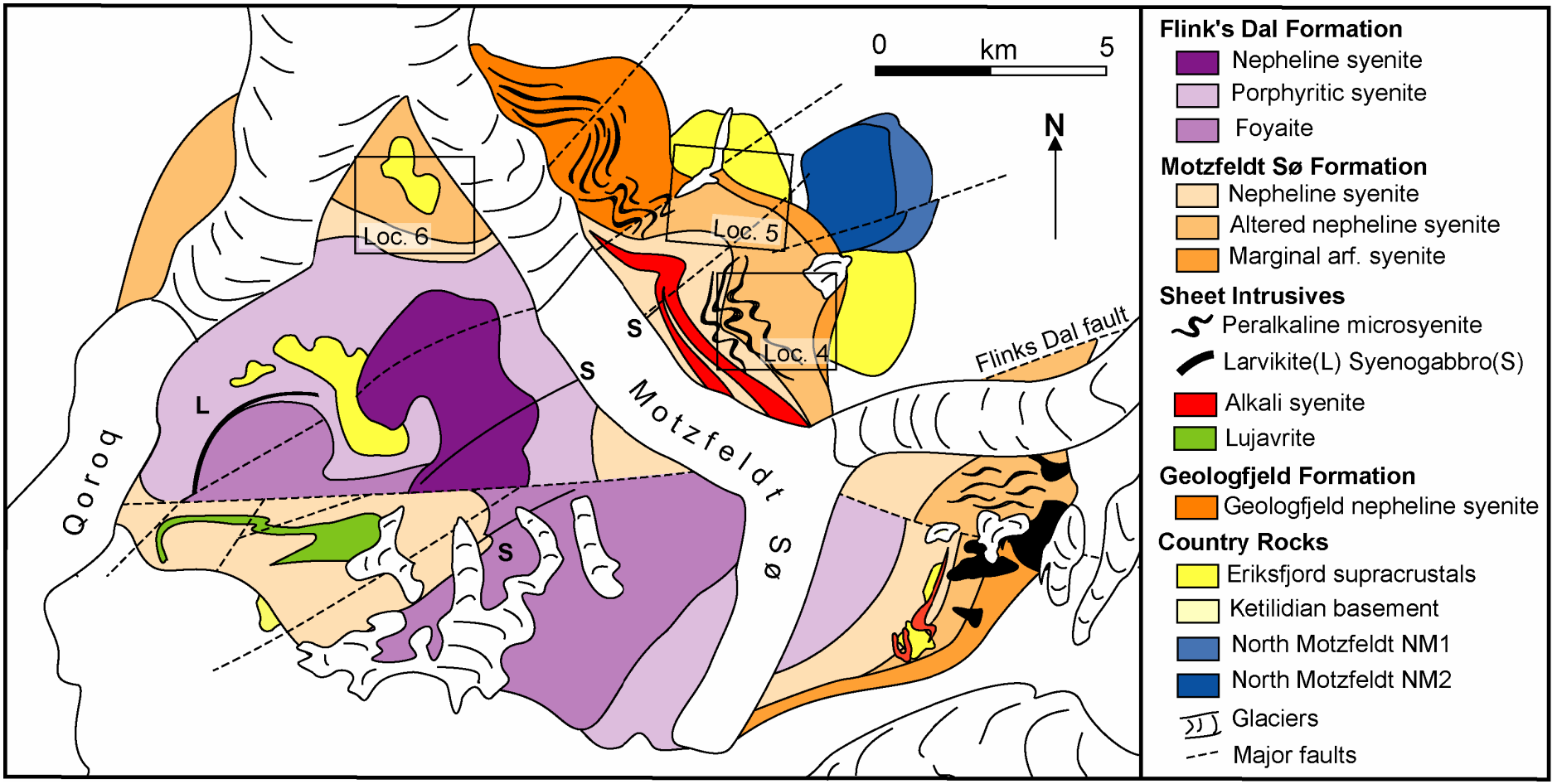

Figure. 1.2. Geological map of Motzfeldt alkaline centre showing major formations and unit subdivisions (after Bradshaw 1988; Jones 1980; Tukiainen *et al.,* 1984) Localities 4, 5 and 6 represent localities of economic interest within the Angus and Ross licence area.

Geochemical stream sediment sampling revealed particularly high levels of Nb and Ta associated with the MSF (Tukiainen, 1988). This discovery prompted further investigation into the economic potential of the area, instigating the establishment of the GEUS Pyrochlore project, jointly funded by GEUS and European Community's (formerly European Economic Community, EEC) Resources and Raw Materials Programme. The Pyrochlore Project revealed a number of localities containing economically interesting amounts of Nb, Ta, Th, U, Zr and LREE mineralisation hosted within the altered syenites of the MSF. The work of the Pyrochlore Project culminated in 1987 with a detailed airborne gamma-spectrometer survey over the 5 localities showing the greatest economic potential. It was calculated from the results of this work that the MSF-altered syenite had potential for over 500 x 10^6 tons of ore, containing over 1,400 ppm Nb, 120 ppm Ta, 60 ppm U and 90 ppm Th (Armour-Brown, 2001). On the basis of this potential Angus and Ross plc took out the exploration licence for the area towards the end of 1999. This was shortly followed up by a detailed surface sampling program of two of the main localities identified during the airborne survey. During the 2001 field season an extensive drilling program was undertaken by Angus and Ross plc in one of the localities in the MSF considered to have the highest economic potential. This revealed a preliminary resource potential of 15 million tonnes with an average grade in excess of 500 ppm Ta_2O_5 and 6,000 ppm Nb_2O_5, making the Motzfeldt centre one of the top ten potential Ta resources in the world (Armour-Brown, 2001).

1.8 The present study

This project focuses on the geology of units in the northeast of the Motzfeldt centre belonging to the MSF. The background geology has been studied in detail by Bradshaw Bradshaw (1985; 1988) and Tukiainen *et al.* (1984) and detailed maps of the area have been produced as a result of this work. The revised sketch map for the area after Bradshaw (1988), Jones (1980) and Tukiainen *et al.* (1984) (Fig. 1.2) shows the location of the present study in addition to localities of economic interest to Angus and Ross Plc.

When studying evolved alkaline igneous rocks, like those of the Motzfeldt centre, particular attention must be paid to the role volatile components (principally H_2O, Cl, F and CO_2) play during the generation, fractionation, emplacement and crystallisation of alkaline rocks. The enrichment of volatile components in alkaline melts is know to extend the crystallisation interval of the melt and lower the melt viscosity. However the most pronounced action of volatile components manifests itself during the final stages of the extended

crystallisation interval. At this stage volatile components are often exsolved into immiscible fluids which have been shown both experimentally and in nature to complex and mobilise rare metals through fluoride, chloride and carbonate complexing (Salvi & Williams-Jones, 2006; Wood, 1990). These volatile complexes play an important role in transporting and concentrating elements, often considered immobile, to elevated levels within alkaline rocks. In addition to volatile components exsolved from the melt externally derived fluids of meteoric origin (H_2O) also play an important part in the post crystallisation evolution of alkaline centres and shallow level intrusive complexes in general.

Within the Motzfeldt alkaline centre striking differences in textural character and inferred sub-solidus histories exist between individual syenite formations. The rocks of the MSF show features characteristic of pervasive fluid-rock interaction and sub-solidus alteration. However units belonging to the FDF and GF remain relatively unaltered, suggesting a distinctly different sub-solidus history to the one encoded in the rocks of the MSF. In addition to obvious textural differences between the MSF and the FDF and GF the MSF also contains localised Ta, Nb, U, Th, Zr and REE mineralisation which is largely absent from the unaltered rocks of the FDF. High concentrations of volatile components are inferred to have once existed in the majority of Gardar alkaline centres (e.g. Finch, 1995; Finch *et al.,* 1995; Parsons *et al.,* 1991). Bradshaw (1988) suggested that the volatile component of the MSF played an important part in the genesis of the mineralisation, yet the origin of the mineralisation and its relationships to the magmatic and sub-solidus histories of the centre are still unclear. The present study looks at the magmatic history and the subsolidus history of the Motzfeldt centre and evaluate the role each of these played in the genesis of the economic mineralisation in the MSF.

Chapter 2

Fieldwork and Sample Collection

2.1 Introduction

Fieldwork was carried out over two expeditions during the summers of 2005 and 2006. This time was spent examining units within the Angus and Ross plc exploration licence in the area to the NE of the Motzfeldt Sø lake within the Motzfeldt Sø and Geologfjeld formations (MSF and GF respectively). During the 2006 field season additional visits were made to the more central units of the Motzfeldt centre, SW of Motzfeldt Sø belonging to the Flinks Dal Formation (FDF) and to the smaller North Motzfeldt satellite intrusion (Finch *et al.,* 2001) to the north-east of the centre (Fig. 1.2) to examine rocks which may have experienced a similar magmatic history to the Motzfeldt centre prior to the pervasive alteration. Drill cores taken during the 2001 Angus and Ross plc drilling program were also examined and sampled to evaluate the extent of mineralisation at depth and to establish the textural character of the units in which mineralisation is largely host, in addition to examining the large range of textural heterogeneity the upper units of the centre show. Field work carried out during these expeditions sought to evaluate: 1) The extent of mineralisation within the MSF and the lateral and vertical variability of this. 2) The role the roof-zone of the MSF played in the magmatic and hydrothermal evolution of the centre and the effects of country rocks assimilation 3) The role the hydrothermal phase played in the genesis of the mineralisation. 4) The relationship between the MSF and FDF.

2.2 Sampling strategy

The Motzfeldt centre, particularly the Motzfeldt Sø Formation, is highly atypical in character to other Gardar rocks. This is due largely to the textural heterogeneity and highly altered nature of the rocks as a result of complex magmatic and sub-solidus histories. In many studies concerning the petrology and petrogenesis of evolved igneous rocks, relatively unaltered samples are sought for examination due to difficulties arising in the analysis and interpretation of samples which have experienced significant subsolidus modification. Particular problems arise from the mobilisation, redistribution and possible introduction or export of elements into/out of the system, during which the primary magmatic mineralogy is often obscured or lost through replacement reactions and formation of secondary mineral phases.

Alteration at Motzfeldt is expressed as pervasive oxidisation and alteration of alkali-feldspars giving the rocks of the MSF a characteristic brick red colour. The primary mafic mineralogy is also commonly replaced by secondary subsolidus phases. The most common replacement texture seen is the subsolidus replacement of primary amphiboles by secondary pyroxene and biotite micas. This is unlike other Gardar centres e.g. Klokken, Igdlerfigssalik and North Qôroq, which retain dark cryptoperthitic feldpars and retain near pristine primary mafic phases. Because much of the mineralisation is host within units that have experienced pervasive subsolidus alteration it makes sampling of unmodified rocks impossible. Therefore sampling must be carried out with a view to examining both the magmatic and hydrothermal histories. During this study the sampling strategy sought to sample from the altered units from the MSF, in which mineralisation is largely host. Field observations and sampling was also carried out in the less intensely altered Motzfeldt units of the FDF, in an attempt to construct a comprehensive model for the magmatic and hydrothermal evolution of the centre as a whole.

Samples were collected from each of the major syenite units and from areas showing particularly interesting textures and mineralogical features, as well as from dykes, rare pegmatites and aplitic units. Samples of vein and fracture filling fluorite, quartz and carbonate were also collected for fluid inclusion and stable isotope analyses. Sample sizes varied depending on the textural character of the unit. For coarser grain samples, or where mineral separation was to be carried out, samples up to 6 kg were collected. For finer grain microsyenitic or aplitic facies, fist sized samples were collected. Additionally, smaller chips and rock fragments were collected from areas of interest for thin section examination and fluid inclusion analysis. A location map of samples locations can be found in appendix A. Sample numbers referred to in the text can be cross referenced with locations on the map.

2.3 Geography and geomorphology of the region

The Motzfeldt centre lies to the northeast of Qôroq fjord in an area of undulating high ground dissected by steep sided glacial valleys. The freshwater lake of Motzfeldt Sø cuts the centre and it is bound to the northeast by the inland ice cap. Access to the area is difficult, with the units east of Motzfeldt Sø (MSF and GF) only accessible by helicopter. The topography of the area is severe and in many places highly unstable as a result of recent glaciation, with vertical cliffs rising from close to sea level up to 1400m high plateaus. The NE side of Motzfeldt Sø, for example, has a vertical face nearly 1 km high. In detail the edge of

the exposure is deceptively unstable, comprising unsupported chimneys and slabs. The sub-horizontal fabric to some rocks of the area, plus the crumbly nature of the feldspars, creates a terrain in which it is unsafe to study the very well-exposed rocks in the glaciated faces. Inland exposure is deceptively variable with much of the area covered in frost shattered regolith, glacial till, permanent snow and steep scree slopes. Within the river valleys, the till is typically 3 m deep, and in the bowl landscape which forms the centre of the North Motzfeldt centre, is upwards of 5 m deep. Solid outcrop is largely restricted to steep valley walls and scoured river valleys. As a result sampling of frost shattered regolith is adopted. However, it is considered that the regolith accurately represents the subsurface geology as rock fragments have been frost-shattered but not transported great distances since dykes can be followed across the terrain. Trenches cut into the regolith on top of Angus & Ross plc locality 4 showed the regolith to comprise ~1 m of disoriented syenite blocks in feldspar sand which was clearly disaggregated from the underlying bedrock (P. Taylor and A. Finch, pers. comm., 2001). However, caution must be taken to prevent sampling of glacially-transported erratics, particularly in the lower lying valley areas or on plateau tops.

2.4 Geological field relations

Each of the intrusive units has been sequentially emplaced into the Ketilidian basement up to a level controlled by the unconformity between the base of the Eriksfjord formation and the Ketilidian basement. At N61° 11' 34.5" N044 56' 36.0" and N61 13' 32.0" N044° 59' 30.9" in the MSF the Eriksfjord roof rocks are still preserved *in situ*. Extrapolating this level across the present field area suggests that the Eriksfjord once covered the entire area acting as a cap rock to the Motzfeldt intrusion. Recent glaciation has removed much of these rocks exposing the roof-zone of the centre and deeply dissecting into the upper units of the centre allowing excellent 3-dimensional examination of the complex (Fig. 2.1)

The area of interest during the present study is coincident with the MSF as defined by Bradshaw (1988). It extends from the area W of Motzfeldt Sø to the easternmost part of the Motzfeldt centre. The FDF has also been studied and is located SW of Motzfeldt Sø, bound to the west by Qôroq fjord and to the east by the eastern limb of Motzfeldt Sø. During this study the geological nomenclature of Bradshaw (1988) will be used but may be correlated with the SM scheme of Emeleus and Harry (1970) and Jones (1980) using the reference table 2.1

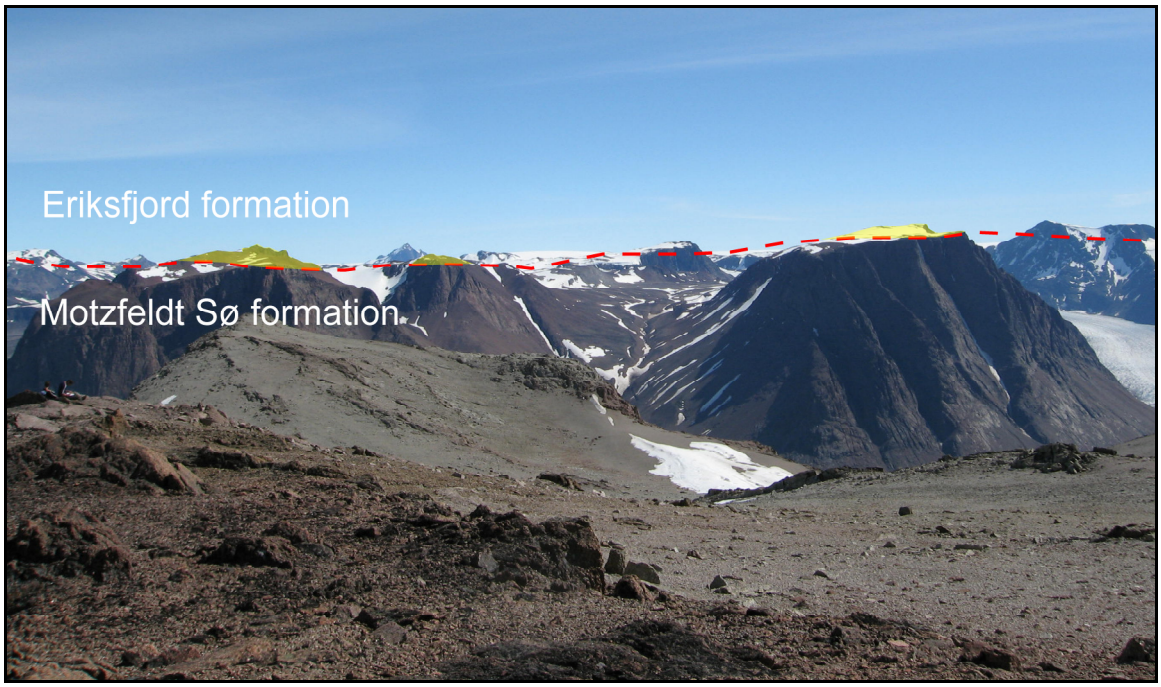

Figure 2.1. Flat topped roof zone of the Motzfeldt Sø formation dissected by deep glacial valleys. The red dashed line represents the extrapolated contact between the Eriksfjord sequence and Motzfeldt Sø Formation. Preserved sequences of in-situ Eriksfjord rocks are highlighted in yellow. Photograph taken from FDF looking NE towards MSF.

	Classification scheme of Bradshaw (1988)		Nomenclature of Emeleus and Harry (1970) and Jones (1980)
Hypabyssal Rocks	Sheet intrusions	Lujavrite	SM6
		Poikolitic arfvedsonite microsyenite	n.d.
		Peralkaline microsyenite suite	n.d.
	'Ring dyke' intrusions	Larvikite	SM5
		Laminated porphyritic syenite	n.d.
		Laminated alkali syenite	SM3
Plutonic Rocks	Flinks Dal Fm.	Nepheline syenite	SM5
		Foyaite	SM3/SM4
		Porphyritic nepheline syenite	SM2/SM4
	Motzfeldt Sø Fm.	Nepheline syenite	SM1
		Altered syenite	SM1
		Marginal syenite	SM1
	Geologfjeld Fm.	Geologfjeld Syenite	SM1

Table 2.1. New nomenclature of Bradshaw (1988) developed during the SYDURAN and Pyrochlore projects and correlation with the SM nomenclature or Emeleus & Harry (1970) and Jones (1980).

2.4.1 Motzfeldt Sø Formation

The units to the northeast of Motzfeldt Sø comprise syenite units belonging to the Motzfeldt Sø Formation (MSF) (Bradshaw & Tukiainen, 1983). These units have been described in detail by Bradshaw (1988) and are recognised to comprise three members; MFS-Marginal Arfvedsonite Syenite, MFS-Altered syenite and MFS-Nepheline syenite. Associated with the emplacement of the MSF is late-stage sheeting of evolved paralkaline microsyenite sheets. Detailed field relations are given by Bradshaw (1988). Subdivision of the region into these units is often subjective given the extreme textural and mineralogical heterogeneity within each unit and highly variable hydrothermal overprinting. As a result rocks of the present study will be described in detail and any assignment to the units of Bradshaw (1988) will only be made loosely.

The MSF shows an extremely high degree of heterogeneity. The syenites show striking textural variation from coarse-grained pegmatitic units to fine microsyenitic and aplitic units over distances of a few metres. The rock is typically a coarsely crystalline feldspathic syenite comprising euhedral brick-red oxidised alkali-feldspars, intercumulus amphiboles and subordinate green pyroxene (spherulitic occurrences are common at high levels). It includes facies which are porphyritic, containing large (ca. 15mm) alkali feldspars to phaneritic syenites with poikiolitic intergrowths of alkali-feldspar and arfvedsonite amphibole (Fig. 2.2a). Finer grained facies are also common, often having strongly porphyritic textures containing elongate tabular alkali-feldspars (ca. 10mm) in a microsyenite groundmass. This facies often exhibits a strong mineral alignment. Cutting much of the brick-red units of the MSF are sheets, isolated pods and lenses of brick-red aplitic syenites bordered by coarse pegmatites, this is best observed in cliff sections on the high plateaus of the MSF where the outcrop has a striped appearance where the concentration of these units is intense (e.g. N61° 11' 13.4" W044° 58' 16.2") (Fig. 2.2b).

Throughout the MSF localised occurrences of high concentrations of pyrochlore group minerals are found and have been the site of continued economic interest for Angus and Ross Plc. In addition to pyrochlore, zircon and other Nb, Ta and REE bearing minerals are found in this distinct facies syenite within the MSF. The characteristic pyrochlore host lithology is a leucocratic microsyenite, which occurs throughout the MSF as inclined sheets and isolated outcrops. This unit is attributed to the MSF – Peralkaline Microsyenite Suite (Bradshaw, 1988). At low elevations the abundance of this unit is low, though increases

traversing to high levels in the formation. On the high plateaus, in rocks inferred to be close to the roof of the formation, occurrences of this facies are relatively common, particularly in the Angus and Ross field locality 4 where the highest concentrations of economically interesting mineralisation are found.

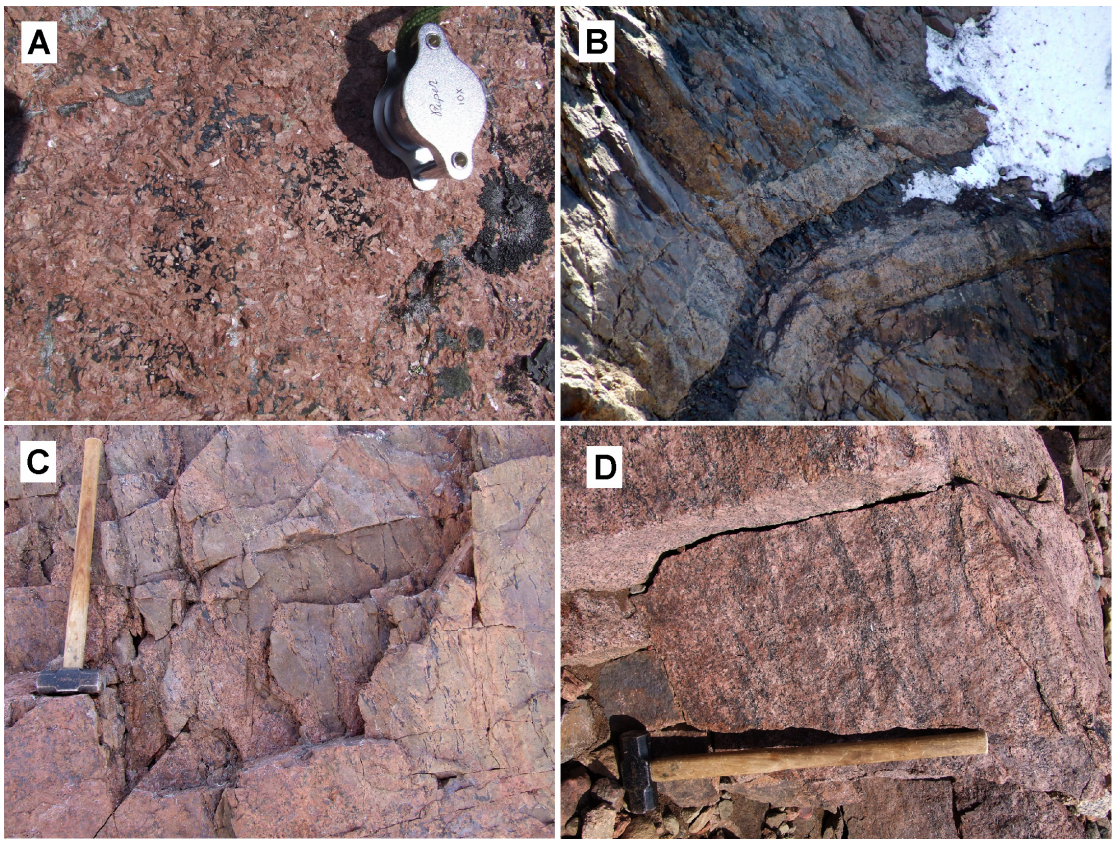

Figure 2.2. (a) Poikiolitic intergrowth of euhedral alkali-feldspars in black amphibole (hand lens for scale). (b) dark aplitic sheet bordered by coarse pegmatites. (c) Attenuated contact between texturally varying facies of altered MSF syenites (hammer handle is 80cm). (d) mafic cumulate mineral layering (hammer handle is 80cm).

The mineralogy of this distinct syenite facies is dominated by highly oxidised alkali-feldspar. Nepheline is also present but heavily altered. The mafic mode is generally very low and fine grained, occurring as sporadic clusters of amphibole, often replaced by secondary magnetite. Fluorite is abundant either as intercumulus rock forming minerals or as late veins. Pyrochlore group minerals have a dark brown to honey-yellow colouration in hand specimen and often have a halo of intense red oxidation in the feldspars surrounding them. Pyrochlore occurs disseminated throughout the rock, although several outcrops contain layers or horizons enriched in pyrochlore (Fig. 2.3), in which pyrochlore minerals make up 80-90 % of the mode. In general pyrochlores within the enriched horizons are larger (up to 3mm) than those

disseminated throughout the rock. Enriched horizons often parallel the mineral fabric of the rock suggesting that these may be pyrochlore rich cumulate horizons.

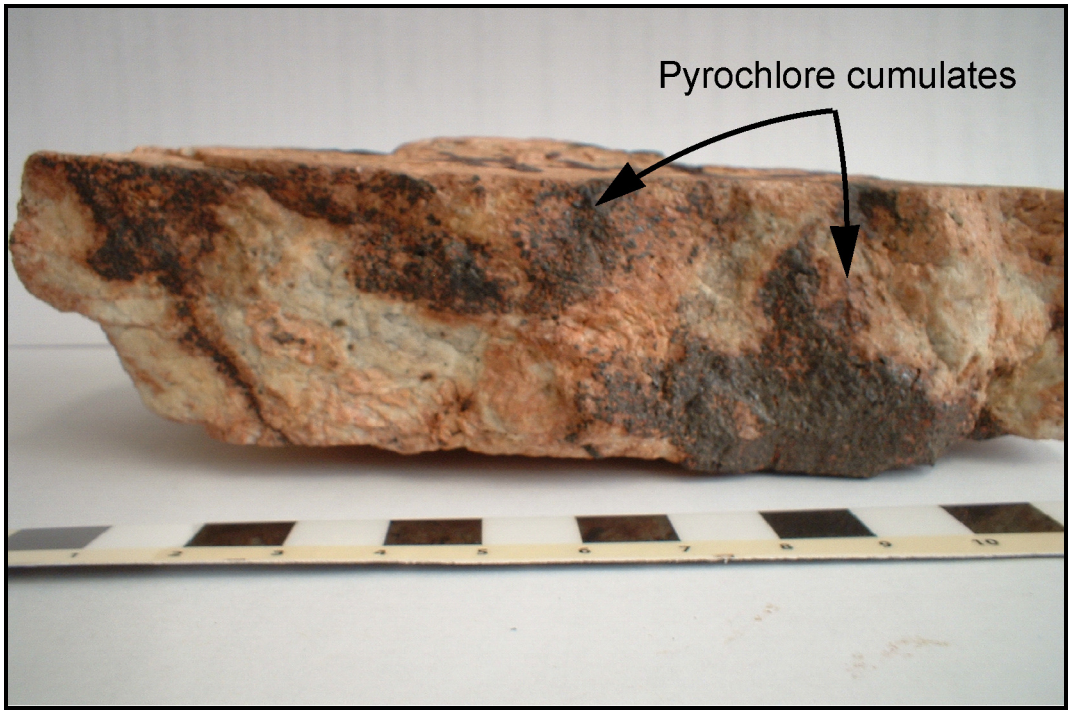

Figure 2.3. Hand specimen of pyrochlore rich sample GJM05-44. Pyrochlore is found disseminated through the samples though occurs in discrete enriched horizons where pyrochlore accounts for up to 90% of the rock's mineralogy.

Units located on the high plateaus show the most complex mineralogies and highest degree of textural variation. In addition to the many facies of syenite previously discussed there are occurrences of strongly pink coloured fine-crystalline syenite facies hosting large (ca. 10-15mm) pseudohexagonal green phenocrysts thought to represent alteration products of nepheline. Units close to the roof also show notable increases in the occurrence of intercumulus and vug-filling quartz. Intercumulus and vein filling purple fluorite is also common, making up 10 modal % of the rock in some areas. Contacts between texturally and mineralogically contrasting facies of syenite are rarely sharp and laterally traceable. In most areas several facies of syenite and nepheline syenite are found intimately intermingled over the scale of several meters (Fig. 2.2c). Areas where these textural relations are observed are often on the high plateaus or close to the highest surface exposure of the formation. From the field relations of these units it is suggested that the present land surface on the high plateaus is close to the roof of the formation. If this interpretation is correct, then the extraordinary textural heterogeneity may represent sheeting and rheomorphism near the roof, representing

the interplay of multiple melt batches interacting, mixing and mingling. This is supported by a lack of chilling on the contacts between units, suggesting that many of these melts were emplaced contemporaneously under very similar thermal and chemical conditions.

In addition to showing a high degree of textural variation rocks from high levels in the intrusion are also extremely friable through alteration of alkali-feldspars associated with the high degree of inferred subsolidus alteration. In addition to the pervasive oxidation of alkali-feldspars and secondary replacement of primary mafic phases discussed above, much of the outcrop east of Motzfeldt Sø contains macroscopic hematite, covering fracture surfaces and grain boundaries, giving intensely altered areas a distinctive blue-black sub-metallic lustre. In intensely altered samples the mafic mineralogy is often wholly replaced by hematite and other Fe-oxides and alkali-feldspars are coated by specular hematite.

The excellent 3-dimensional exposure provided by recent glaciation allows insights into the texture and alteration variability of units in the vertical dimension. A section from the high plateaus to the valley floor towards Motzfeldt Sø was carried out as part of the present study. On descending, the alteration becomes less intense and the rock loses the characteristic brick-red colouration. In low lying units close to Motzfeldt Sø shore at an elevation of <300 m, the rock becomes texturally more homogeneous and has a relatively fresh appearance and lacks the brick red alteration found at higher levels. At that locality, alteration is restricted to narrow zones of intense alteration and the rocks appearance is more similar to those units observed in the FDF. It is inferred that textural heterogeneity and alteration increase towards the top of the intrusion and is most intense on the high plateaus where the roof of the formation was.

Within the Angus and Ross licence area at Locality 5 (Fig. 1.2) an ~150 m vertical sequence of inter-bedded quartz conglomerates, quartz arenites and basaltic lavas, belonging to the Eriksfjord formation, are preserved in situ. Located at the base of the sequence, where the highly altered MSF syenite is in direct contact with quartz arenites, autobrecciation occurs for ~10 m into the quartzite (Fig. 2.4). Angular brecciated fragments of hematite coated quartzite, ranging in size from 5mm-30cm, are rimmed by cryptocrystalline quartz and supported by coarse crystalline euhedral fluorite. This contact represents the roof-zone contact of the MSF syenites with the base of the Eriksfjord formation. Localised fluorite mineralisation under the roof of the MSF suggests that fluorine levels in the roof of the formation were exceptionally high. The occurrence of intercumulus and fracture filling vein

fluorite throughout the MSF and the presence of extensive fluorite mineralisation in the preserved roof zone of the formation suggests that the fluorine content of the MSF melts was relatively high and exceptionally high in the roof-zone of the formation.

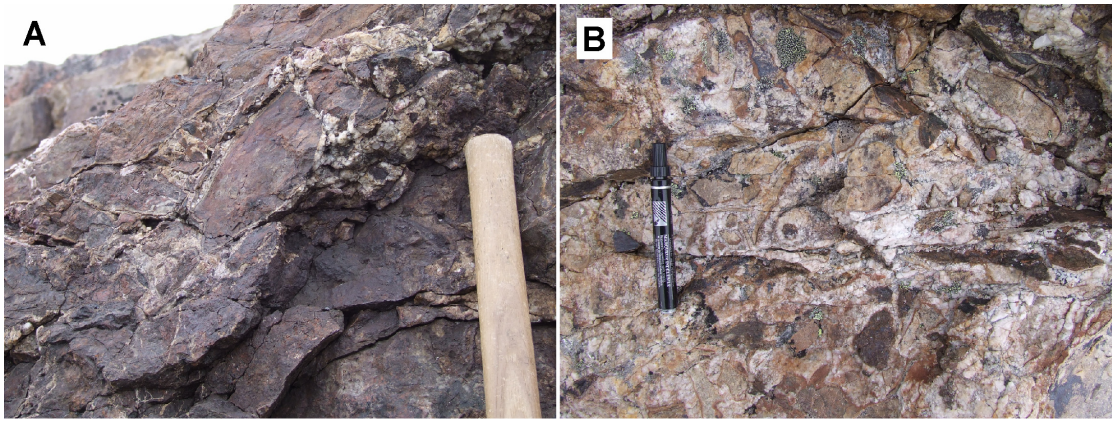

Fig. 2.4. (a and b) autobrecciated Eriksfjord arenites supported by crystalline fluorite. (a) shows fracture surfaces on the Eriksfjord are coated in specular hematite. (b) shows small angular quartzite fragments supported by coarse crystalline fluorite (pen for scale).

2.4.2 Flinks Dal Formation

Rocks south of Motzfeldt Sø are of noticeably different character to those of the MSF and are much more typical of Gardar rocks in general. Following the division of Bradshaw and Tukiainen (1983) these units belong to the Flinks Dal and Motzfeldt Sø Formations, though they bear little resemblance to the Motzfeldt Sø units east of the lake. The FDF has been divided into a number of intrusive members (Bradshaw, 1988 and Bradshaw and Tukiainen, 1983) sequentially emplaced inwards in a series of nested plutons. The three intrusive members of the FDF are the FDF – Nepheline syenite (SM5), FDF – Porphyritic nepheline syenite (SM2 and SM4) and FDF – Foyaite (SM4). Each of these intrusive phases are white nepheline syenites with differing textural and modal mineral abundances. These units have been previously described by Emeleus and Harry (1970), Jones (1980), Bradshaw (1988) and Schönenberger & Markl (2008) therefore the reader is referred to these sources for detailed descriptions. This section will overview field observations from each of the FDF units and will discuss features which can aid in the interpretation of the genesis of mineralisation in the MSF.

The largest and oldest of these units is the FDF - porphyritic nepheline syenite (SM2 & SM4). This unit is largely homogeneous over much of its outcrop area, comprising typically medium-grain porphyritic nepheline syenites. These typically contain phenocrysts of platy, tabular alkali-feldspars and squat euhedral nepheline in varying states of alteration (white, green or pink). The groundmass contains the same felsic mineralogy as the phenocryst assemblage. The mafic mineralogy is dominated by fresh blue-black interstitial amphibole and green pyroxene. One characteristic feature of this unit is the varying presence of porphyritic melanocratic enclaves. These vary in size from ca. 5 cm to 40 cm and have a phenocryst assemblage of elongate tabular alkali-feldspars up to 10 mm in length. The smaller inclusions are often well rounded (Fig. 2.5b), however larger examples often have more angular or sub-rounded shapes (Fig. 2.5a). The smaller inclusions may therefore represent the partially assimilated remnants of larger xenoliths or autoliths of earlier partially-crystallised syenite formed as part of the same magmatic episode. However, some samples show convolute margins and feldspar phenocrysts from the host syenite are frequently found penetrating the syenite-inclusion contact, suggesting that the porphyritic melanocratic units may have been partially molten during their incorporation. On the tops of plateaus there are localised areas which show weak red colouration from localised oxidation of alkali-feldspars, similar to that in the altered MSF units at low elevations.

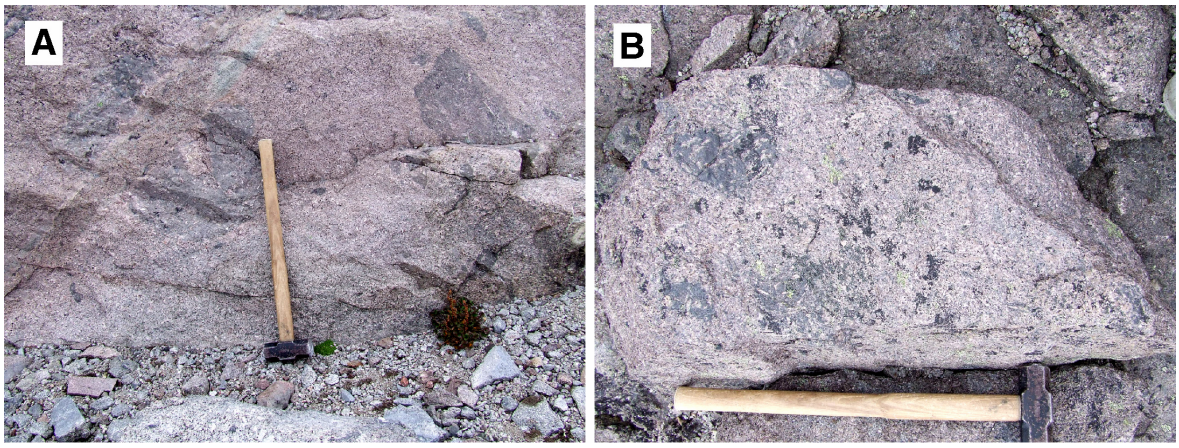

Figure 2.5. (a) Subangular melanocratic enclaves within FDF-porphyritic nepheline syenite (N61° 11' 40.5" W044° 06' 56.5"). (b) Samll rounded melanocratic enclaves in FDF-porphyritic nepheline syenite (N61° 11' 40.5" W044° 06' 56.5"). (hammer handle is 80 cm long).

The other major unit of the FDF is the FDF – nepheline syenite (SM5). Like the FDF – Porphyritic nepheline syenite, the FDF - Nepheline Syenite is homogeneous over its exposure. The unit is a grey/white coarse crystalline syenite outcropping in the centre of the

FDF, wholly surrounded by the FDF – porphyritic nepheline syenite and covering an area of about 10 km^2. Typically the unit contains squat rectangular alkali-feldspars up to 5 cm in length. Anhedral nepheline crystals up to 3 cm in size show varying states of alteration, similar to the FDF - porphyritic nepheline syenite. The mafic mineralogy is dominated by dark green pyroxenes and subordinate amphiboles. In some localities biotite is a secondary phase after pyroxene. On the high plateaus this rock takes on a yellowed and slightly oxidised colouration locally from alteration of feldspar and nepheline crystals, in a similar localised nature as observed in other FDF units. Within the FDF – Nepheline syenite are a number of porphyritic microsyenite units containing phenocrysts of elongate platy micas up to 5 mm in size.

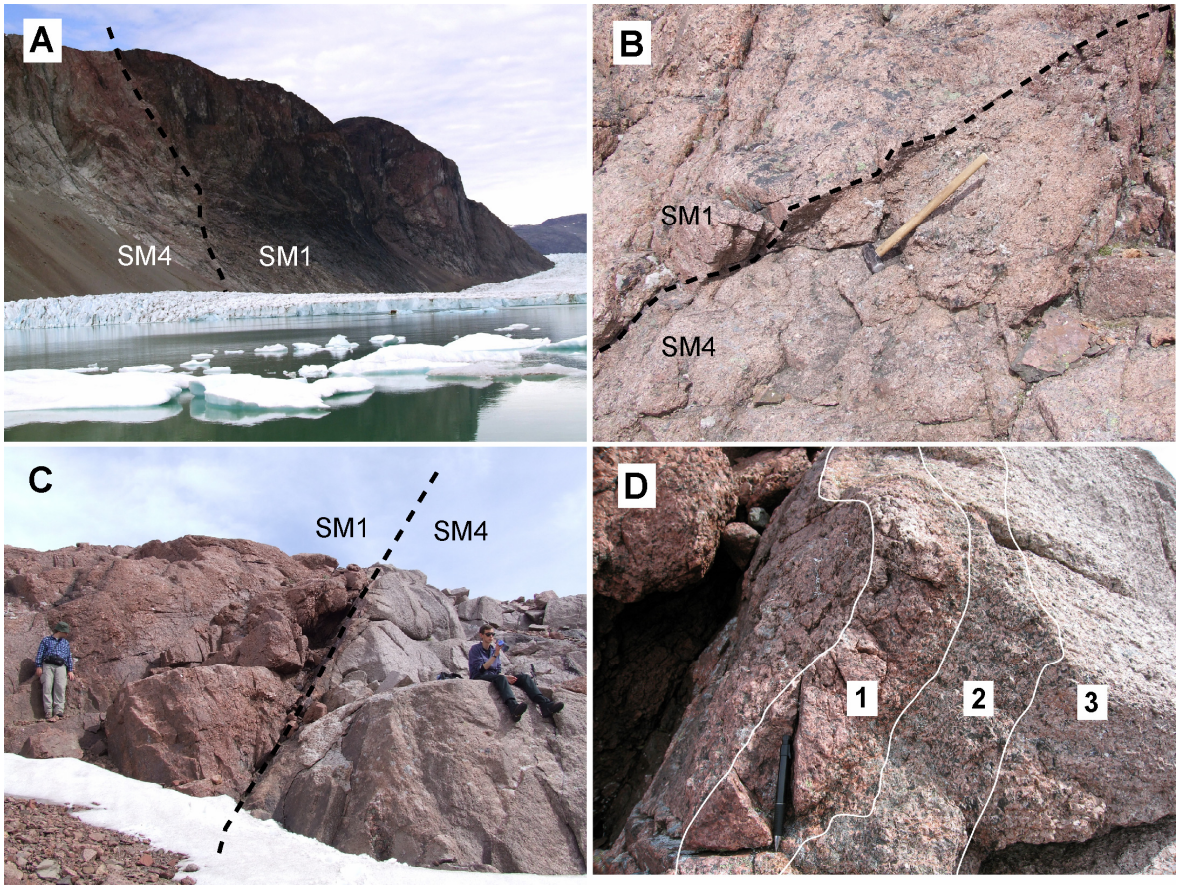

Figure 2.6. (a) Looking south from north of Motzfeldt Sø at contact between the FDF (left) and the MSF (right) showing dark brick red alteration. Viewer is standing at N61° 11' 44.9" W045° 01' 12.3" looking WNW. (b) Contact between FDF (bottom) and MSF (top). Both formations show pervasive brick red alteration. (hammer handle 80cm long) shows orientation of contact (N61° 12' 34.4" W045° 06' 19.5"). (c) Contact between light-coloured FDF (right) and redder MSF (left). Alteration is largely constrained to the MSF. (d) close-up of contact zone between altered MSF and unaltered FDF in C (pen for scale). 1.-chilled marginal facies of FDF. 2.-pyroxene rich marginal facies of FDF. 3.-Fresh FDF (N61° 12' 34.8" W045° 06' 23.8")

On the peninsula of land bordered by the Sermia Avanardleq and Qorqup Sermia glaciers there is an area of characteristic brick red altered syenite attributed to the MSF (SM1). The units in this region are very similar in character to the MSF northeast of Motzfeldt Sø. Although this area does not show as much textural heterogeneity as the units northeast of Motzfeldt Sø, it still has the characteristic brick-red colour and high degree of alteration as elsewhere in the MSF. The contact of the MSF in central Motzfeldt with the FDF – Porphyritic nepheline syenite can be traced laterally and vertically from the top of the current exposure on the high plateaus of central Motzfeldt (ca. 1300m) down to ca. 900m in the river valleys flowing north into Qôrqup Sermia. The contact can also be observed from north of Motzfeldt Sø, where it can clearly be seen in the cliffs above the lake (Fig. 2.6a). In the high elevation exposures the contact is sharp and follows an E-W trend dipping steeply towards the north (Fig. 2.6b&c).

The contact in this region shows a fine-medium grain chilled margin in the FDF, though chilling is not so significant as to suggest emplacement of the FDF into a cold host. The contact within approximately 30 cm is also characterised by enrichment of green pyroxenes (Fig. 2.6d). Despite the FDF being largely unaltered there is a marginal zone of alteration extending into the FDF for approximately 10 cm. Traversing to deeper levels in the centre the contact becomes less obvious as the contrasting alteration between the MSF and FDF is less pronounced (e.g. N61° ll' 44.9" W045° 01' 12.3") (Fig. 2.7a). At these lower elevations the boundary between the MSF and FDF is still a sharp intrusive contact with the same orientation, however there is little chilling and abundant xenoliths of largely unaltered and slightly coarser MSF syenites are hosted in the FDF (Fig. 2.7b), in addition to the porphyritic melanocratic enclaves discussed above. Close to and along the contact at lower elevations, rare pegmatitic patches up to several meters in thickness (Fig 2.7c) occur, containing very large euhedral feldspars up to 20cm in length, intercumulus nepheline, euhedral amphiboles and rare spherulitic growth of pyroxene needles (Fig. 2.7d). The occurrence of pegmatites is particularly rare in the FDF and during this study were only observed in few localities (e.g. N61° 12' 36.5" W045° 07' 57.5" and N61° 12' 34.9" W045° 07' 50.1"). The scarceness of pegmatites may be attributed to the relatively anhydrous nature of FDF melts.

Although the striking feature of the intrusive contact at higher elevations is the contrasting expression of sub-solidus alteration in the brick red MSF and the relatively fresh FDF, this is not true for all of the areas where the contact is well exposed. When viewed over

the region in the Inúngurassuaq area the intrusive contact appears to mirror the boundary between the altered MSF and relatively unaltered FDF. Although in many places the extent of alteration appears to follow the location of the contact, it is not controlled by it and in many locations the alteration is found penetrating well into the "unaltered" units of the FDF, likewise the "altered" units of the MSF appear relatively unaltered in areas at much lower elevations. Similar trends in alteration have been observed in the MSF north-west of Motzfeldt Sø.

Figure 2.7: (a) Intrusive contact between the MSF (top) and FDF (bottom). Both units appear relatively unaltered. (b) Xenoliths/enclaves of relatively unaltered MSF syenite host within unltered FDF. (c) pegmatite patches close to intrusive contact in FDF. (d) spherulitic pyroxene within FDF pegmatites. Hammer handle is 4 cm wide. All locations witin 20 m of N61° 12' 36.5" W045° 07' 54.6".

2.4.3 Eriksfjord Supracrustal Sequence

Throughout the MSF and FDF, well preserved sequences of Eriksfjord rocks are found on the high ground of the present study area. In some areas (e.g. N61° 12' 02.1" W044° 56' 15.1") extensive sub-horizontal rafts and xenoliths are found within the syenites of the

MSF and FDF. The character of Eriksfjord rocks varies depending on the formation it is found in. Eriksfjord rocks found in the immediate country rocks to the MSF at N61° 11' 34.5" W044° 56' 36.0" and N61° 13' 37.0" W044° 59' 30.9" are dominated by thick sedimentary sequences of typically pure quartz arenite, though occasionally horizons with a more dominant, and slightly coarse, feldspathic component occur. Remnant fluvial planar and cross-bedding features and ripple marks (Fig. 2.8a) are also preserved and are most easily observed in some of the more coarse grain, less well sorted facies. At N61° 11' 23.8" W044° 56' 36.9" the sedimentary units of the Eriksfjord are conglomeratic containing well-rounded pebbles (1-3cm) and small cobbles (5-20cm) of quartzite supported in a fine-medium grain quartz dominated matrix. Hematite coating is found close to the syenite contact where grain boundaries are mantled in hematite (Fig. 2.8b) giving the rock a dull blue-black sub-metallic lustre.

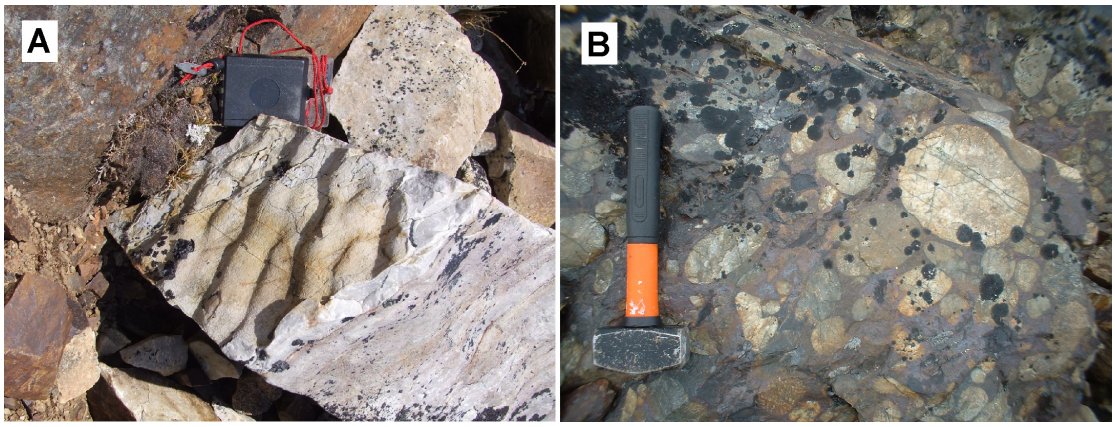

Figure. 2.8. (a) Ripple cross-laminations in loose Eriksfjord block (compass for scale) (N61° 13' 17.2" W044° 57' 22.4") (b) Well rounded conglomeratic unit within Eriksfjord sequence displaying intense hydrothermal hematite mineralisation (Hammer handle is 25cm) (N61° 11' 34.5" W044° 56' 34.0").

The basaltic component of the sequence has been observed in the roof zone of the centre preserved in Angus and Ross plc Locality 5 (N61° 13' 45.0" W044° 59' 39.5"). The best preserved sequence in locality 5 displays well preserved columnar jointing (Fig. 2.9a), pahoehoe flow textures (Fig. 2.9b) and vesicular flow surfaces (Fig. 2.9c). Cross sections through pillow basalts have also been observed (Fig. 2.9d) showing that many are truly volcanic. Rare occurrences of quartz pebbles are also found host within the basalt and are suggested to have been incorporated from the coarser quartzite units below. The presence of pahoehoe structures, pillow lavas and vesicular flow surfaces suggest many of the volcanics in

this area are sub-aerial and deposited in rapid succession. Aphyric and porphyritic trachytes have also been observed and represent the base of the sequence at this locality.

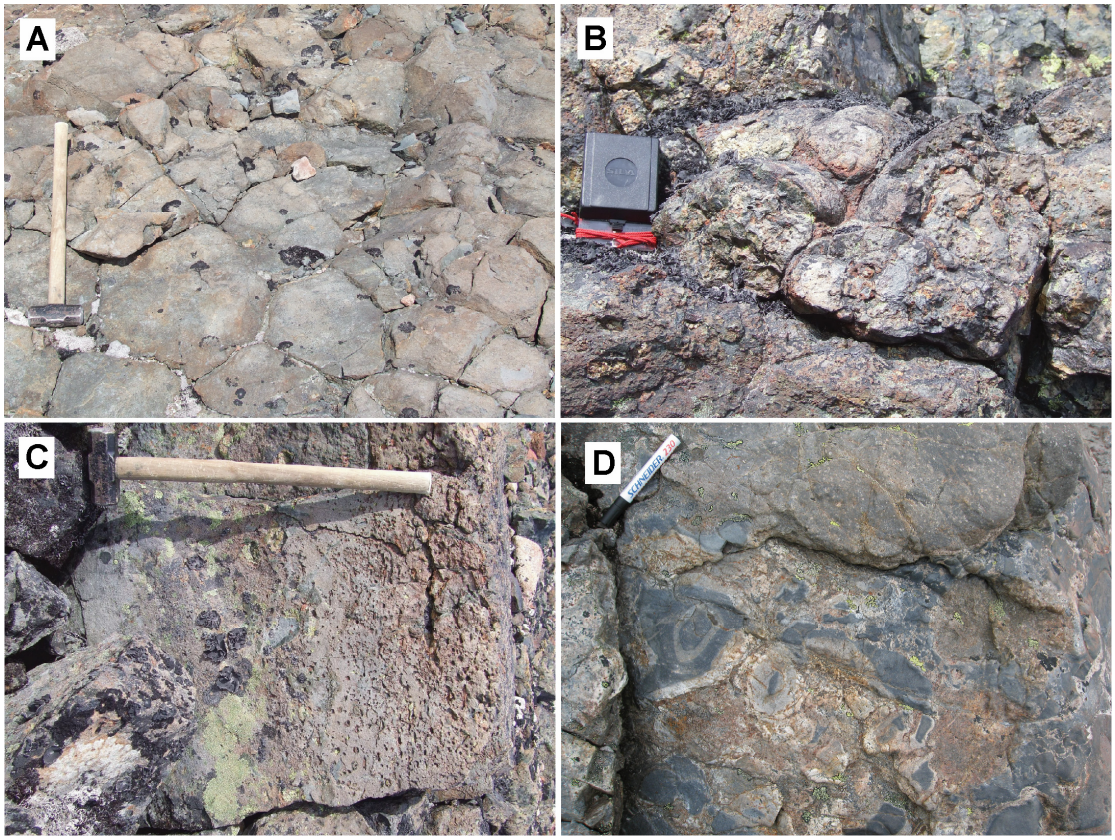

Figure 2.9. Textural features of the Eriksfjord volcanic successions preserved in the Motzfeldt roof zone. (a) Flow surface of a columnar jointed basalt (N61° 13' 30.0" W044° 58' 11.7") (hammer handle is 80 cm). (b) Ropey "pahoehoe" basaltic flow textures (N61° 13' 39.6" W044° 58' 54.6") (compass for scale) (c) Vesicular basalt. Vesicle density and size increase towards top of flow surface (right) (N61° 13' 39.6" W044° 58' 54.6"). (d) Basaltic pillow lavas (N61° 11' 34.8" W045° 06' 38.8") (pen for scale).

Outcrops of Eriksfjord in the FDF, southwest of Sermia Avanardleq, are strongly porphyritic trachytes containing platy feldspars up to ~1.5 cm in size. These are often found in direct contact with porphyritic syenite units belonging to the FDF, which are texturally very similar in appearance to the trachyte in a number of outcrops. These are overlain by units of altered basalt, preserving rare pillows. Minor amounts of quartz arenite are also found however the Eriksfjord rafts preserved in the FDF are dominated by volcanic components with subordinate sedimentary units. The dominance of sedimentary components in the Eriksfjord rocks local to the MSF and a distinct lack of sedimentary components in the FDF may suggest that rocks from the MSF were emplaced upto a different level within the Eriksfjord than the rocks of the FDF. The presence of a trachytic unit overlain by sequences

of arenite in the MSF is in good correlation with the Majût and Mussartût members of the Eriksfjord formation (Poulsen, 1964). Likewise the dominantly basaltic and trachytic components host as rafts within the FDF may be correlated with the Ilimaussaq member (Larsen & Tukiainen, 1985).

2.5 Conclusions

Rocks from the MSF and FDF show striking differences in texture and extent of alteration, relating to different the magmatic and hydrothermal histories. Present levels of exposure in the MSF offer a virtually 3-dimensional view of the formation providing an excellent opportunity for studying vertical variation within its rocks. At high levels in the formation, within ca. 100 m of the roof, the textural character of the rock is highly variable, comprising many facies of rock, ranging from microsyenite to coarse pegmatitic facies. Traversing to lower levels the rock becomes more homogeneous in character and texturally similar to rocks from the FDF. Extensive fluorite mineralisation, locally concentrated under the preserved roof-zone to the north of the centre, implies that fluorine levels in the MSF melts were exceptionally high and increasingly concentrated in the high-level units of the formation, where the greatest textural variability is found. High concentrations of fluorine in the MSF likely affected the physical and chemical properties of the melt, extending the crystallisation interval and increasing the melts potential to complex incompatable elements. This is most evident in the inferred roof-zone of the formation where late-stage pyrochlore bearing microsyenite sheets are most abundant.

The MSF is also characterised by pervasive and large scale hydrothermal alteration, which gives the formation its characteristic red oxide colouration. Alteration follows a similar trend to the magmatic heterogeneity. At high levels in the intrusion alteration is most intense. Traversing to low levels in the intrusion alteration decreases and the rock loses its characteristic oxidised colour. Correlation between the magamtic diversity and sub-solidus alteration at high-levels in the intrusion strongly suggests that the roof zone of the formation and the volatile component of the melt played an important role in the uniquel evolutionary history of the MSF.

The FDF is relatively uniform in texture and mineralogy, varying only slightly between intrusive units The alteration seen in the MSF is largely absent in the FDF and the rocks are remarkably similar in character to rocks found at low elevations in the MSF. The lack of

extensive fluorite mineralisation, subsolidus alteration and pegmatitic facies in the FDF implies that these magmas were less rich in volatile components than the adjacent MSF and were relatively anhydrous The genetic link between the MSF and FDF will be explored in subsequent chapters, however it may be suggested from the similarities between the FDF and the unaltered units of the MSF that these may represent the same unit. Throughout the Motzfeldt centre are a number of major fault lineaments, the most prominent being the Flinks Dal fault. East of Motzfeldt Sø Bradshaw (1988) identified sinistral displacement in the rocks of the MSF. The orientation of this fault follows the trend of the NW limb of Motzfeldt Sø. Although no vertical displacement was commented on it is possible that a vertical throw of ca. 800 m along a major fault in this region could displace the units of FDF upwards relative to the MSF, thereby juaxtaposing units which are hightly altered (MSF) with units from lower in the intrusive column which have experienced little sub-solidus alteration (FDF). Alternatively the FDF and MSF may infact be separate intrusive units and their present surface exposures are at different levels in the intrusive column. It may be that the present exposure of the FDF is lower in the intrusion than the present exposure of the MSF. Hence rocks at low levels in the MSF are at similar levels in the intrusive to the rocks on the plateaus in the FDF. These hypotheses will be explored further in subsequent chapters.

Chapter 3

Petrography

3.1 Introduction

This chapter describes the petrography of the major intrusive units of the Motzfeldt Sø Formation (MSF) and gives general petrographic observations from the major rocks types of the Flinks Dal Formation (FDF), as the focus of the present study was the MSF and the FDF was the subject of another studentship that operated in parallel (Schönenberger, 2008; Schönenberger & Markl, 2008). The chapter is based on the petrographic findings from samples collected during the present study but also draws on the work of Angus and Ross plc, sponsors of this research.

Previous petrographic investigations in the Motzfeldt centre include Emeleus and Harry (1970) and Jones (1980), focusing principally on the unaltered syenite units of the FDF. During these studies the altered units of the MSF were only briefly visited (Emeleus, pers comm., 1995), as a result the MSF is poorly characterised in those articles. Further detail to the NE was completed by Bradshaw (1988) as part of the GGU-SYDURAN project, who subsequently remapped the MSF and carried out a detailed structural and petrographic investigation. In addition to Bradshaw (1988) a number of GGU reports were published on the petrography of units within the MSF and GF (Tukiainen *et al.,* 1984; Tukiainen, 1985). General petrography of the mineralised units is given by Bradshaw (1988), however detailed descriptions of the mineralised units are not provided. This chapter therefore provides a general overview of the petrography of the MSF and FDF drawing on the work of others, particularly Jones (1980) and Bradshaw (1988) for the FDF and Bradshaw (1988) and Tukiainen *et al.* (1984) and Tukiainen (1985) for the MSF, but supplementing them with further petrological characterisation. Optical microscopy and cathodoluminescence petrography have been used during the present study. Instrumentation and operating conditions used during both techniques are described in appendix B. Table 3.1 summarises the general paragenetic relations of units studied from both formations. The descriptions presented here underpin the analytical studies that constitute the bulk of the thesis.

3.2 Motzfeldt Sø Formation

3.2.1 Optical Microscopy

The MSF hosts numerous facies of syenite and nepheline syenite varying in colour from red to pink to white. The unit was subdivided into three concentric members by Bradshaw (1988) termed the MSF – *Marginal arfvedsonite syenite*, MSF – *Altered syenite* and the MSF – *Nepheline syenite*. Throughout the present study classification of units into these three members has been avoided due to the unusually high degree of heterogeneity found with each.

Syenite samples located at low-levels in the MSF are more homogeneous and display a much lower degree of alteration that units at higher levels in the formation. Generally the rock is a coarsely crystalline syenite, though occurrences of microsyenite of similar mineralogy are also common. Typically this rock comprises alkali-feldspar primocrysts making up 60-70% of the mode. Feldspar are coarsely exsolved patch and braid perthite up to 1 cm long and ~1 mm wide (Fig. 3.1). Large crystals often show Carlsbad twins, perpendicular to which perthitic exsolution lamellae form, giving the feldspar a 'herringbone' texture. Although alteration is less intense in these units, feldspars often show turbidity, which in many samples is localised to one of the exsolved phases. Nepheline is present up to 15 modal %. In hand specimen this often has a pale pink coloration but in thin section nepheline often appears less turbid and altered than feldspars. The mafic mineralogy is dominated by characteristic pale olive green to brown pleochroic arfvedsonite amphiboles and bright green to yellow pleochroic aegirine pyroxene intercumulus to the felsic phases. Several occurrences of concentric zoning have also been observed under PPL, characterised by radiating pleochroism. Biotite is common, forming secondary to amphibole or growing as ragged red-brown crystals associated with magnetite. Fluorite is common in many syenite facies of the Motzfeldt centre and is present largely as an intercumulus phase or in microveins, often having a strong purple colouration. Accessory phases identified during the present study include elongate euhedral apatite, interstitial and vein filling calcite, zircon and euhedral pyrochlore crystals, which often show strong alteration haloes in the host feldspars. Other secondary accessory phases reported by Bradshaw (1988) include rinkite and låvenite, though these were not identified during the present study.

The degree of textural heterogeneity in the MSF increases vertically and the red-oxide staining (interpreted as alteration) which characterise the formation becomes more

widespread. Within ~200 m of the inferred roof of the formation there are a number of textural variants of syenite. These generally have similar mineralogy, although vary in mineral mode, textural character, type and degree of alteration. This section details the general petrology of these units and highlights some of the more unusual mineralogical and textural occurrences of the formation.

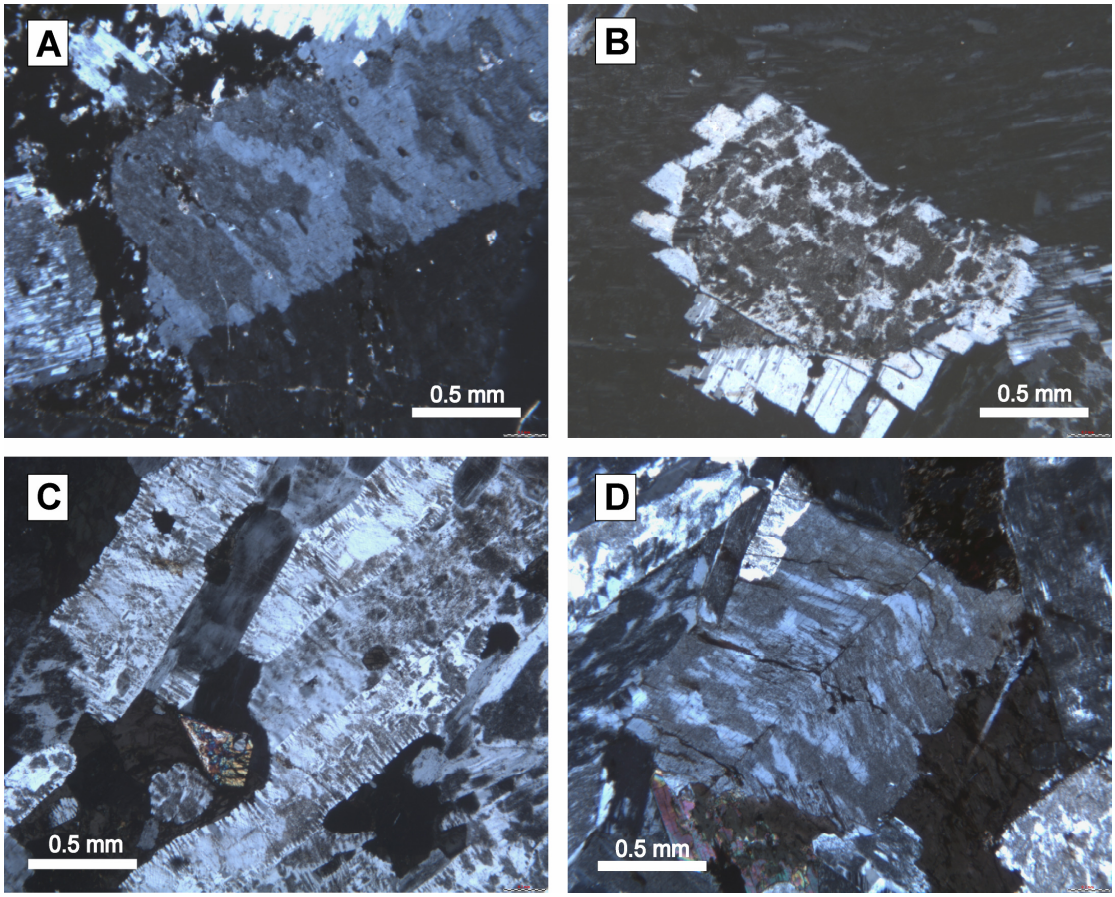

Figure 3.1. Textural relations of alkali feldspars from the Motzfeldt Sø formation. (a) Coarsely exsolved patch perthite and simple twinning in alkali-feldspar from low levels in the MSF (GJM06-13). (b) Altered exsolved alkali-feldspar with relatively fresh albite rims (GJM06-17). (c) Fine microperthite from altered alkali-feldspars (GJM06-32). (d) Coarsely exsolved and altered patch perthite with Carlsbad twinning from high-levels in the MSF (GJM06-36).

At high-levels in the intrusion, the most common facies of syenite is typically a coarse-grained and highly altered syenite composed predominantly of tabular brick shaped euhedral alkali-feldspars (mode: 70-80%) 5-15 mm in length with aspect ratios of ~2:1. Feldspar in this unit is coarsely perthitic displaying similar patch and braid textures to feldspar from lower in the intrusion. The high-level units of the MSF are characterised by the brick-red colour of feldspars. In thin section feldspars are turbid and have a dark brown or orange tinge in PPL,

reflecting the colour in hand specimen. Although very turbid (interpreted as highly altered), feldspar often shows rims which are relatively transparent in thin section (Fig. 3.1b). The brick red colour which characterises the feldspars of the MSF can be attributed to presence of microgranular iron oxides within the feldspar. In hand specimen many of the samples show specular hematite (Fe_2O_3) coating grain boundaries of feldspars giving samples a blue-black colour, this likely occurs as sub-microscopic inclusions within the altered areas of feldspar. Altered feldspar showing red/pink colour has been discussed by Putnis *et al.* (2007). The characteristic red-oxide colouration in all samples studied by these authors is generated through sub-microscopic growth of hematite rosettes and needles in the pore spaces of feldspar crystals, widely interpreted as forming during subsolidus re-equilibration in the presence of a fluid phase. The possible sources of Fe to form hematite are numerous, and include breakdown of primary Fe-bearing mafic phases, re-equilibration in the presence of Fe-rich externally sourced fluids and/or re-equilibration of a feldspar containing Fe in its structure (e.g. Fe^{3+} substituted for Al^{3+} in the tetrahedral site) with a solution, into which Fe is released and precipitated as hematite (Putnis *et al.,* 2007). Finch & Klein (1999) have shown that Gardar feldspars contain tetrahedral Fe^{3+} and discuss the possibility that they also contain nanoparticles of magnetite.

Nepheline is rare and only present in small amounts (<10%) in most samples but is typically heavily replaced by secondary zeolites and micas (an intergrowth referred to as 'gieseckite'). In many samples nepheline is entirely replaced and is only inferred from the relict crystal habit. The mafic mineralogy of high-level syenite facies of the MSF is dominated by dark green-brown pleochroic arfvedsonite amphibole. Despite the pleochroic scheme observed (which would make compositional zoning particularly obvious), few samples show optical zoning. Amphibole textures in the MSF are highly variable and dependent on the textural character of the particular facies of occurrence. In many samples arfvedsonite occurs intercumulus as anhedral to subhedral crystal clusters. A common feature in some samples (e.g. GJM06-34) is a feathered or embayed texture where amphibole is found in contact with relatively fresh albite rims of alkali-feldspars (Fig. 3.2). In the high levels, pyroxene is less common although striking radial rosettes of aegirine needles are found (e.g. GJM06-34). Sample GJM05-41 also has rare granular clusters of fine elongate aegirine crystals giving samples a spotty appearance with clusters up to 10 mm in diameter. In samples where clusters such as these occur, the texture of the sample as a whole is generally medium-grained (1-5 mm) and the felsic mineralogy is dominated by elongate tabular feldspars displaying a strong mineral alignment.

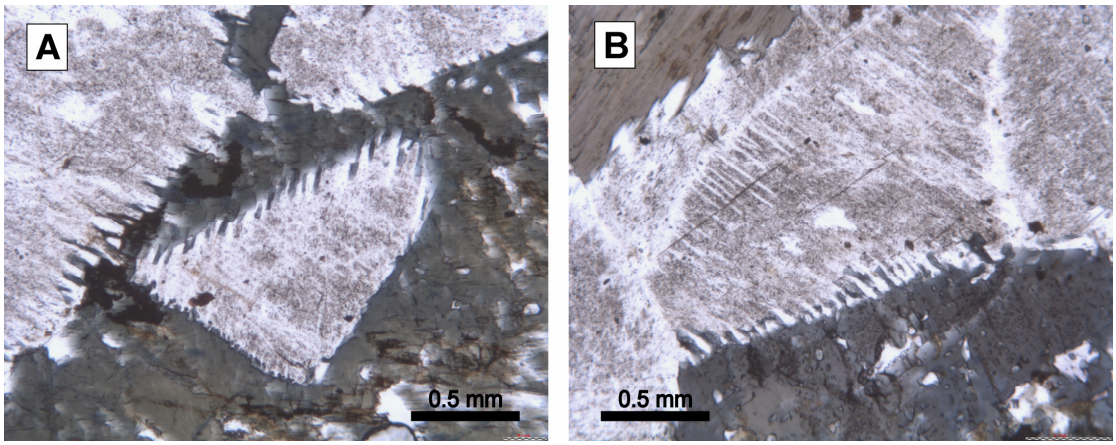

Figure 3.2. Feathered intergrowth between altered and exsolved alkali-feldspars and primary green-blue arfvedsonite amphibole (GJM06-34).

Biotite occurs throughout the altered facies of syenite in three distinct textural relationships. In many samples biotite is found as discrete primary crystals (Fig. 3.3a) or as a secondary phase intimately associated with intercumulus amphibole (Fig. 3.3c&d). Less common are large porphyritic plates of poikiolitic biotite up to 15 mm in diameter enclosing other common rock forming mineral phases, accessory zircon and rare pyrochlore crystals (Fig. 3.3b). In many samples small flakes of biotite are found growing as a rim surrounding clusters and individual crystals of magnetite (Fig. 3.3e&f). Textures like these have been described from other Gardar centres (e.g. Klokken intrusion, Parsons *et al.,* 1991 and Igdlerfigssalik, Finch *et al.,* 1995) and have been termed 'fringe biotites'. It is likely that the intercumulus and poikiolitic biotite grew directly from the silicate melt. Phase diagram shows that the phlogopite solidus temperature is too high, hence primary biotite phenocrysts must have been annite rich (Parsons *et al.,* 1991). It is not clear whether the fringe biotite grew through reaction of the residual silicate melt and accessory magnetite or through subsolidus reactions (Finch *et al.,* 1995). In samples where biotites grew as a product of subsolidus replacement reactions the term reaction corona may be applied to describe the textural relationship of the biotites. Several rare samples of large (ca. 40 mm) mica books with pseudohexagonal basal sections have also been observed in hand specimen from the MSF. Each of these textural occurrences of biotite is studied in subsequent chapters concerning their halogen chemistry (chapter 5).

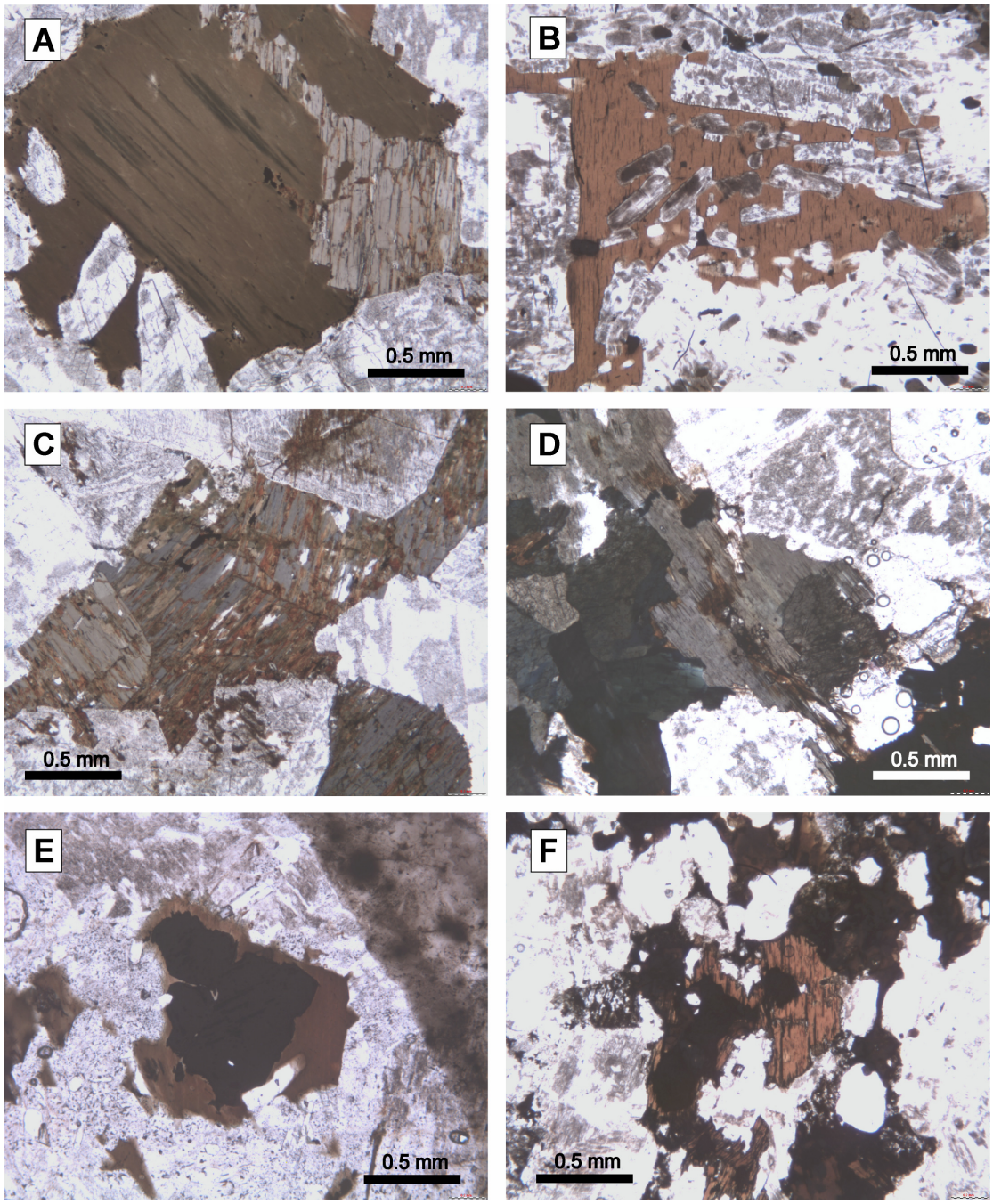

Figure 3.3. Textural occurrence of biotite micas in samples from the Motzfeldt Sø formation. (a) Large primary biotite crystal (GJM06-63). (b) Large poikiolitic biotite phenocryst hosting euhedral alkali-feldspar, apatite and magnetite (GJM06-31). (c & d) secondary biotite replacement of primary arfvedsonite (GJM06-63). (e & f) Fringe/reaction corona of secondary biotite (GJM05-23).

Fluorite is a common component of all samples of the MSF and makes up 10% of the rock, in many samples occurring intragranular, as fine veins and as cubic euhedral crystals in mineralised cavities. Associated with some fluorite samples are rims of zeolites on the boundary between fluorite and feldspar. In small miarolitic cavities, euhedral quartz has also been identified in association with fluorite. Both these phases host abundant fluid inclusions which have been the focus of microthermometric investigation (chapter 6). The presence of quartz in nepheline bearing syenites suggests that quartz host in miarolitic cavities is secondary in origin, associated with the late magamtic to subsolidus phase.

Pyrochlore minerals hosting economically important concentrations of Nb and Ta have been identified as an accessory phase in all facies of syenite from the MSF. However, throughout the MSF, distinct facies of fine-grained leucocratic syenite enriched in pyrochlore have been identified. These occur in greatest abundance close to the roof-zone of the formation. The pyrochlore host is composed almost entirely of euhedral, aligned tabular alkali-feldspar laths, giving the rock a strong fabric. Aside from pyrochlore the mafic mineralogy is restricted to rare clusters of highly altered mica, amphibole and magnetite.

Pyrochlore is typically disseminated throughout these samples (Fig. 3.4a&b), although cumulate horizons locally enriched in granular clusters of pyrochlore define particular pyrochlore-rich facies of syenite (Fig. 3.4c-f). Disseminated pyrochlore grains typically range in size from 0.5-2 mm across and are always euhedral. In cumulate-rich horizons, crystals are larger than the disseminated crystals (up to 4 mm) and often have strong octahedral crystal habit. Pyrochlore group minerals are often characterised by their strong honey-yellow colour in transmitted light. However crystals from the MSF show a dark reddish-brown to opaque colour in transmitted light suggesting alteration. Larger crystals from cumulate-rich horizons occasionally show subtle zoning which is enhanced by the dark zones of more intense alteration (e.g. Fig. 3.4e). Pyrochlore crystals in the MSF in general have a thin rim of hematite, similar to that observed mantling many of the primary phases in the formation, and may contain inclusions of alkali-feldspar, magnetite, fluorite and calcite. In cumulate-rich horizons intense fracturing of the host feldspars is common (e.g. Fig.3.4d) running between individual pyrochlore crystals and running parallel the mineral fabric of the rock.

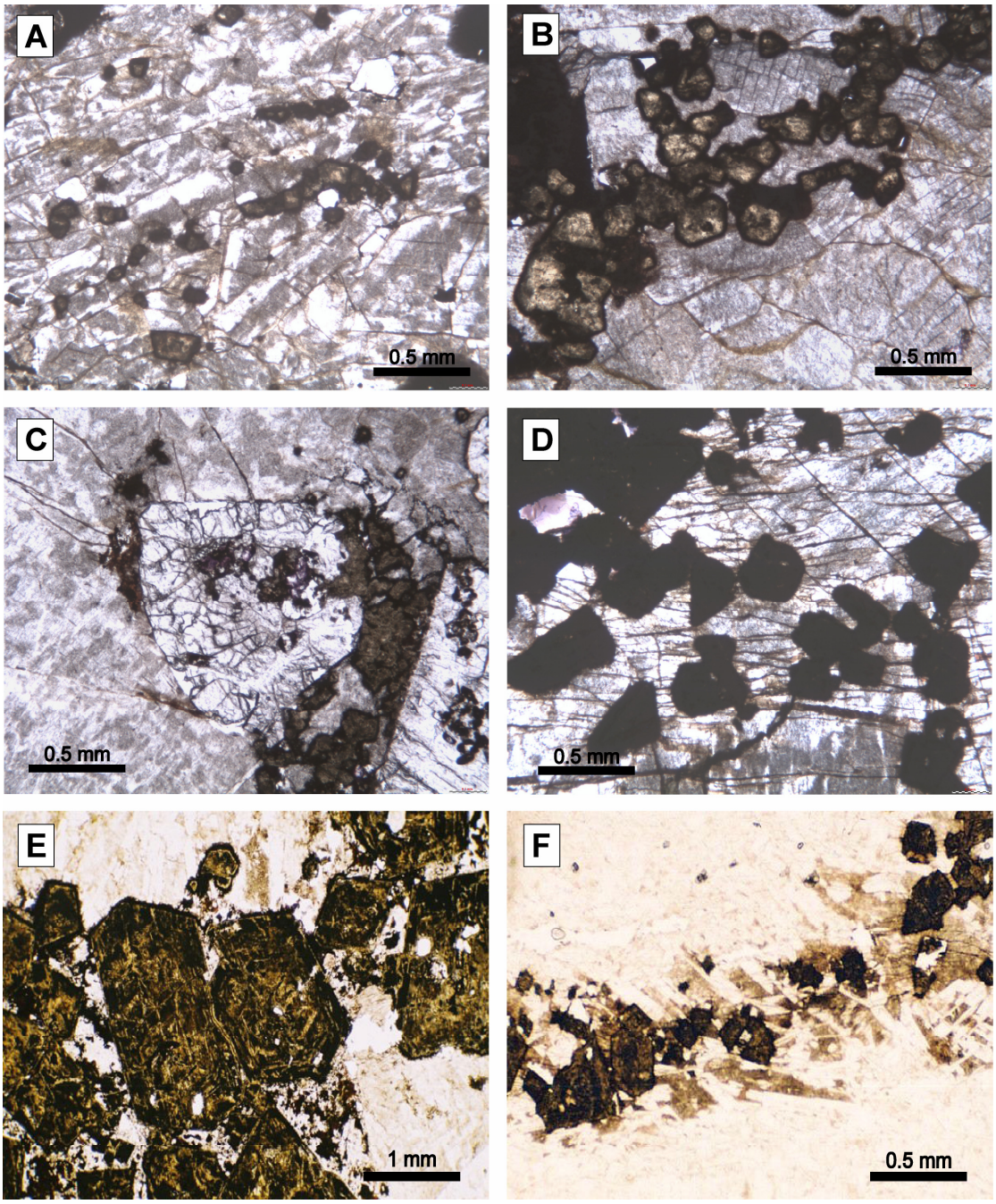

Figure 3.4. Occurrence and textural relationships of pyrochlore mineralisation in the Motzfeldt Sø Formation. (a&b) Disseminated pyrochlore crystals host in a leucocratic feldspar rich groundmass (GJM05-23, GJM06-18). (c) Granular mass of pyrochlore crystals intimately associated with large (1-2mm) high-relief zircon megacrysts (GJM06-65). (d-f) Dense concentration of pyrochlore crystals from locally enriched cumulate layers. Image D shows strong fracturing of host feldspars parallel to the cumulate layer. Image e shows weak zoning in larger crystals. Image f shows concentrated alteration in feldspars intimately associated with pyrochlore mineralisation (A&R 10520, GJM05-21).

3.2.2 Cathodoluminescence petrography

Cathodoluminescence (CL) petrography is an important technique in the study of metasomatic processes in alkaline environments. This technique has been used principally in the field of CL characterisation of alkali-feldspars which have experienced subsolidus alkali metasomatism (e.g. Finch & Klein, 1999; Lee *et al.,* 2007). In addition to the textural character of feldspars, CL is a useful tool for identifying submicroscopic mineral assemblages associated with late-magmatic and subsolidus processes and in identifying subtle compositional variations in accessory minerals.

The CL character of feldspars has been discussed by numerous authors since the original publications on the subject by Smith and Stenstrom (1965) and Long and Agrell (1965). These authors noted different luminescence of feldspars related to the degree of alteration. Mariano (1976) subsequently addressed the reasons for contrasting luminescence in feldspars inferred to have experienced different degrees of metasomatic alteration. This work demonstrated that, in general, metasomatised feldspars luminesced red and those which escaped or experienced less alteration display blue luminescence. This characteristic therefore provides a useful indication of the levels of metasomatic alteration alkaline rocks have experienced. The causes of different luminescent signatures in feldspars have been the subject of some debate since the pioneering work if Mariano (1976) and the subject is still the focus of much research. Discussion of each of the possible mechanisms of luminescence activation in alkali feldspars is a project in its own right, therefore detailed discussion of this will not be outlined here. For detailed reviews the reader is referred to the publications of Marshall (1988) and references therein. For more recent publications concerning the metasomatic alteration of feldspars in alkaline environments the reader is referred to the work of Finch and Klein (1999), Götze *et al.* (1999, 2000) and Lee *et al.* (2007). Generally the blue luminescence emission in alkali-feldspars is attributed to structural defects in the crystal lattice (Finch & Klein, 1999; Geake *et al.,* 1977) or to activation by Eu^{2+} (Mariano & Ring 1975; Götze *et al.,* 1999, 2000). Other interpretations include incorporation of trace amounts of Ti, Cu and Ga into the crystal lattice (Mariano, 1976; De St. Jorre & Smith, 1988), but these suggestions have not been supported by subsequent studies. Regardless of the mechanism for the generation of luminescence, blue luminescence is generally interpreted to represent relatively fresh alkali-feldspars which have experienced minimal fluid related alteration.

A change in the luminescence emission of alkali-feldspars from blue to red is generally considered to be a product of fluid-mediated recrystallisation during the subsolidus. The red luminescence of many metasomatised feldspar from alkaline complexes has been suggested to be due to the structural state of tetrahedral Fe^{3+} in the feldspar, introduced into the feldspar by the fluid (Mariano, 1976). Additionally Finch and Klein (1999) suggested that during re-crystallisation under subsolidus conditions crystal defects are removed through an increase in ordering, effectively inhibiting the blue luminescence of the feldspar.

In a similar trend to the degree of alteration and heterogeneity, the CL properties of feldspars in the MSF vary considerably from low levels in the intrusion into high level exposures on the high plateaux of the area. Alkali-feldspars from units located at lower altitude in the formation close to Motzfeldt Sø, show variable states of alteration reflected in the proportion of the feldspar giving off a red luminescence emission. The CL character of feldspars from low level samples is varied and largely dependent on the grain size of individual feldspars and the coarseness of the perthitic exsolution. Metasomatic reddening of feldspars is localised to grain boundaries and along exsolution lamellae (Fig. 3.5a&b). In many samples alteration related reddening is often restricted to one particular phase of perthitic exsolution. Such textures are typical of syenites throughout the Gardar province, including those of the Flinks Dal Formation (Finch, 1990). In crystals displaying higher degrees of alteration, the blue luminescence emission locally preserved in one exsolved phase is often lost or inhibited. These phases now show a dark blue or dull purple luminescence. Feldspars from low levels in the MSF therefore commonly display blue cores mantled by metasomatically altered red luminescing rims. This observation suggests that much of the fluid passing through these samples was restricted to passage along grain boundaries. Reddening of particular phases within the cores of some samples is likely caused by fluid flow through interconnected micropores within the feldspar structure (Worden *et al.,* 1990, Finch & Walker, 1991).

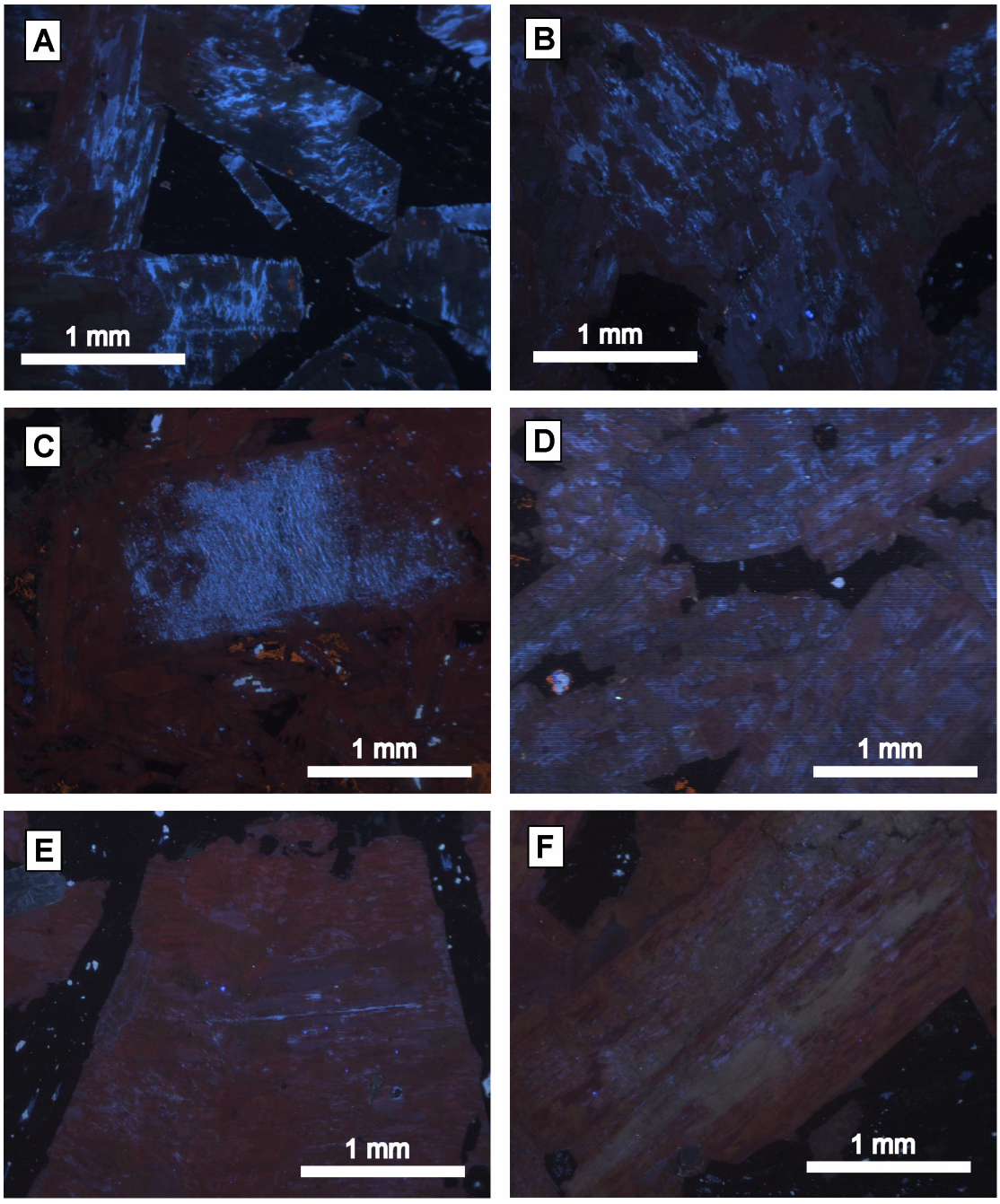

Figure 3.5. Cathodoluminescence character of alkali-feldspars from the Motzfeldt Sø Formation. (a&b) Blue luminescent magmatic perthite patches surrounded by red luminescent altered areas. Samples from low levels in the intrusion (GJM05-59). (c) Fine blue luminescent perthite bands preserved in an alkali-feldspar phenocryst surrounded by red luminescent alkali-feldspar groundmass (GJM05-41). (d) Variably altered feldspars showing weak blue luminescence in best preserved magmatic areas (GJM05-21). (e) Red luminescent metasomatically altered alkali-feldspar (GJM05-64). (f) Highly altered alkali-feldspar showing red and pale green luminescence, associated with clay mineral alteration (GJM05-64). Non-luminescent areas are mafic phases peppered with bright blue luminescent fluorite.

At higher levels in the formation, feldspar is orange/pink in colour in hand specimen and highly turbid in thin section. Under CL all samples show extensive reddening (Fig. 3.5e&f). In coarsely perthitic samples, the two exsolved phases are identifiable from contrasts in the luminescence intensity and the shade of the reddening. Many samples show a weakly luminescent green colour localised to particular patches of perthitic exsolution (Fig. 3.5f) which may represent the development of zeolite or clays (Götze *et al.,* 2002). Although many of the samples show intense reddening from fluid-rock interaction facies of finer grain syenite hosting large (5-10 mm) alkali-feldspar phenocrysts sometimes have cores or exsolved phases showing a weak blue luminescence, preserving the original magmatic CL signature of the crystal (Fig. 3.5c&d). The extensive reddening of the CL emission in feldspars from high-level units of the MSF is consistent with the interpretation that fluid-rock interaction and subsequent alteration was most intense in these units.

Throughout the MSF fluorite is found as a common rock forming mineral phase (10-15%). Under CL fluorite is characterised by a bright blue luminescence (much brighter than the blue emission of fresh alkali-feldspars) and is found as large discrete crystals throughout all samples of the present study (Fig. 3.6a-d). In addition to discrete crystals many thin sections are peppered with small bright blue specks of disseminated fluorite (Fig. 3.6e), often intimately associated with the mafic minerals. In many samples fluorite crystals are often associated with pyrochlore. Fluorite immediately juxtaposed with pyrochlore often shows a dull blue luminescent halo which is inferred to be generated through radiation induced structural damage (Fig. 3.6d), similar to radiation haloes often seen in optical microscopy of biotite hosting accessory zircon. In larger fluorite crystals irregular or weak zoning is observed (Fig. 3.6a&c), with duller blue cores and brighter luminescing rims. Within several crystals, fine interconnected networks of dark blue luminescent veins are observed (Fig. 3.6a-c) displaying similar luminescent properties to radiation haloes associated with pyrochlore crystals. In some crystals this texture takes on a mottled or patchy appearance as the dark blue luminescent areas increase in density.

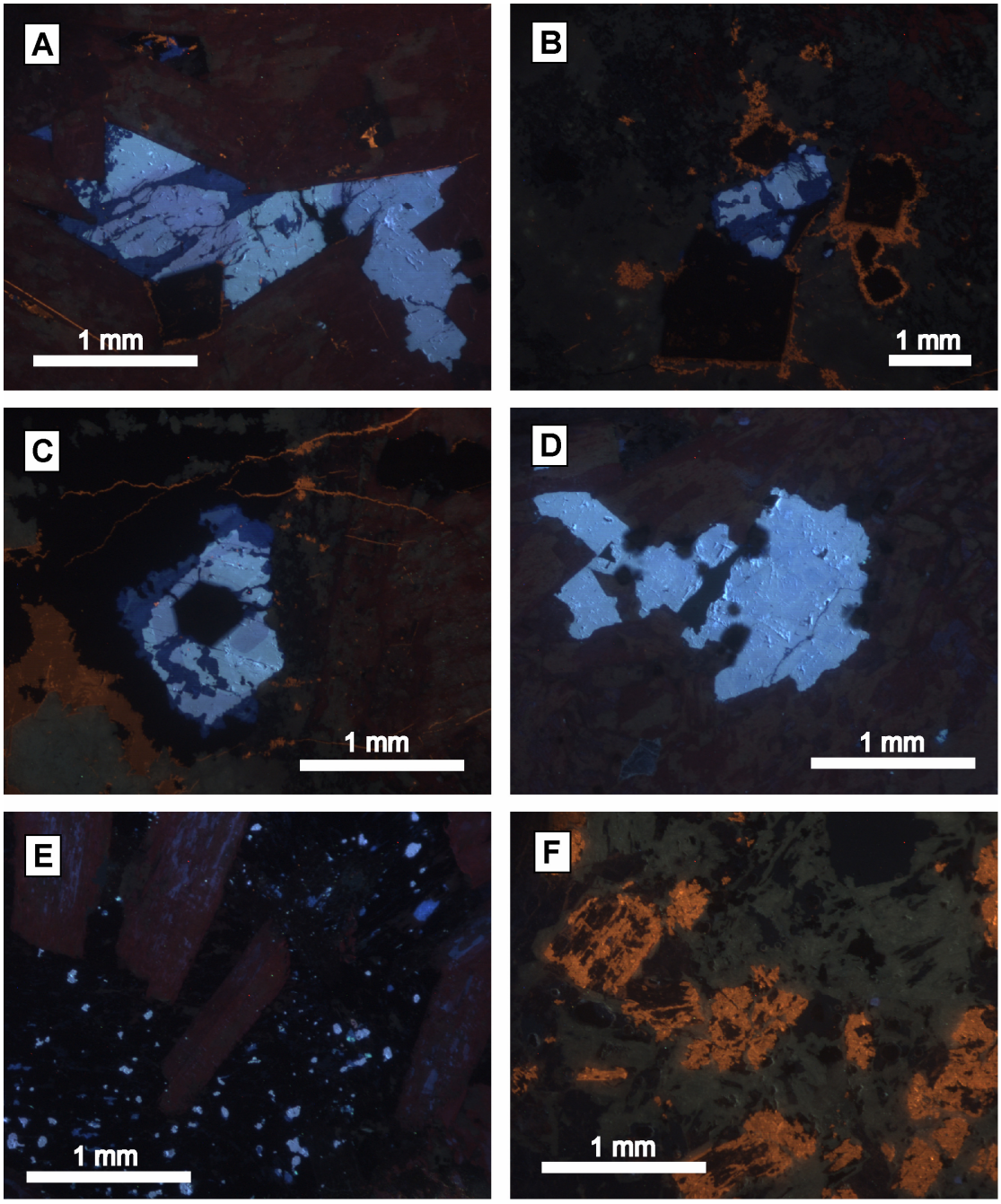

Figure 3.6. Cathodoluminescence of fluorite and calcite from the Motzfeldt Sø Formation. (a) Blue luminescent fluorite displaying weak zoning. Dark blue luminescent areas are associated with secondary alteration along microveins (9-037.7). (b) Bright blue luminescent fluorite showing dark blue secondary alteration. Euhedral non-luminescent pyrochlore surrounded by orange luminescent calcite (9-037.7). (c) Blue luminescent fluorite surrounding a euhedral pyrochlore crystal. Fluorite also shows dark blue luminescent alteration. Orange luminescent calcite veining and crystalline calcite are also present (9-037.7). (d) Bright blue luminescent fluorite showing dark blue radiation halos where in contact with non-luminescent pyrochlore (GJM05-23). (e) Blue luminescent specks of disseminated fluorite associated with mafic minerals (GJM05-35). (f) Orange luminescent calcite forming secondary to amphibole (2-024.5). Samples 9-037.7 and 2-024.5 from 2001 Angus and Ross plc drill cores.

The textural relationship of dark blue luminescent fluorite to light blue variants suggests against this being a primary growth feature, resembling more closely textures associated with alteration under subsolidus conditions. The microvein texture seen in Figure 3.6a suggests that the dark luminescence is generated through interaction between the fluorite and fluid migrating along microfractures in the crystal. Such microfracture networks have been identified optically and are often full of fluid inclusions. Possible causes of dark blue alteration may be 1) substitution of ions into the fluorite from the fluid, 2) radiation damage generated from ions carried in the fluid or 3) radiation damage from submicroscopic radioactive mineral phases precipitated in microfractures. Although the exact processes are unknown it is clear that these textures were generated post-crystallisation and are linked to the metasomatic fluid phase of the centre's history.

In addition to the brilliant blue fluorite peppering many samples from the MSF, orange and yellow luminescent calcite is also common. This is often intimately associated with alteration of non-luminescent mafic phases (Fig. 3.6f). Optically calcite is very difficult to identify in the highly altered syenites of the MSF, unless forming large veins. However when viewed under CL it becomes clear that it may make up as much as 5% of the mode in some samples. Fine veins of calcite are also common. Similar to fluorite, calcite is also often intimately associated with pyrochlore crystals where it often mantles individual grains (Fig. 3.6a&b).

Other luminescent mineral phases identified from the MSF are zircon and apatite. Apatite commonly shows weak yellow or pale blue luminescence, though are relatively uncommon in many of the sections from the MSF. The blue colour is interpreted by Hayward and Jones (1991) as resulting from Eu^{2+} in contrast to the yellowish-red luminescence of apatites containing Eu^{3+}. The mix of blue and red-yellow apatites hints at a magma with a varying redox potential. Zircon is characterised by a dark blue luminescence similar to fresh alkali-feldspars. Zircon from the MSF have been the focus of detailed isotopic study (chapter 7) and thin sections hosting zircons and zircon mineral separates have been the subject of detailed textural investigation. Zircon has been separated from samples GJM06-18 and GJM06-29 and will now be discussed. No zircons, with the exception of GJM06-18 (Fig. 3.7a), show oscillatory zoning. Instead samples show relatively homogeneous CL emissions with weak broad zoning and slight contrasts between the core and rim. All of the samples show evidence for late to post-magmatic modification, light blue luminescent patches of alteration penetrate into individual crystals from their margins and cross-cut any preserved

magmatic features (Fig. 3.7a-d). Magmatic parts of the crystal seem to have experienced post-magmatic alteration in the presence of a fluid-phase. The altered areas are characterised by bright blue emission colours compared to the dark blue CL emission in areas inferred to be remnant magmatic areas. The percentage of the total crystal that has experienced such alteration is highly variable, ranging from a narrow zone on the rim of the crystal to pervasive alteration where up to 40% of the crystal has been altered.

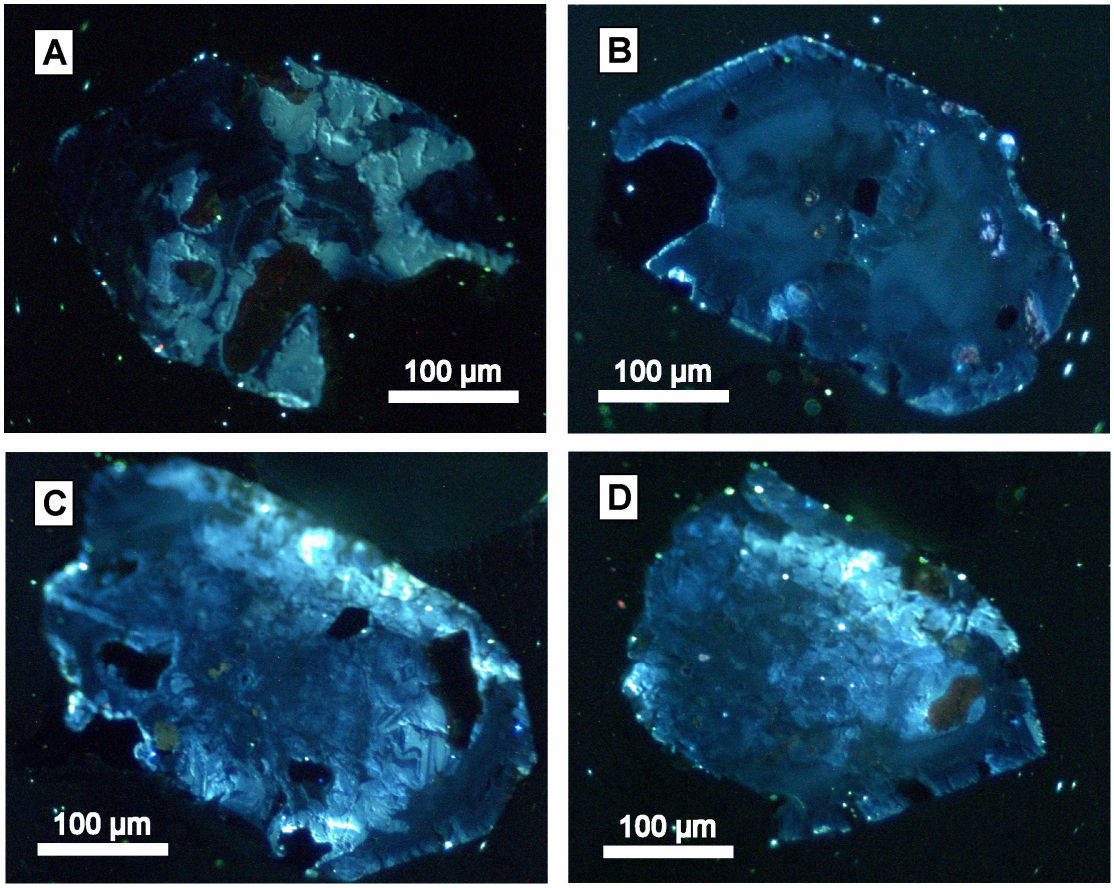

Figure 3.7. Cathodoluminescence character of zircon separates from the Motzfeldt Sø Formation. (a) Discontinuous areas of alteration, with bright blue CL emissions cutting across primary oscillatory zoned zircon showing a weaker dark blue luminescence (GJM06-18). (b-d) Blue luminescent zircon separates showing complex and convoluted secondary alteration textures. Primary zonation in largely masked or absent (GJM06-29).

3.3 Flinks Dal Formation

3.3.1 Optical microscopy

In contrast to the MSF, units from the FDF are relatively homogeneous. The petrology of the FDF has been discussed in detail by Bradshaw (1988), Jones (1980), Schönenberger and Markl (2008), therefore during this section a general overview outlining the main petrographic character of the formation will be given based on primary observations made as part of the present study and drawn from the work of previous authors.

The most common rock in the FDF is a medium to coarse grain porphyritic nepheline syenite, termed SM4 by Emeleus and Harry (1970). This nepheline syenite unit typically comprises large tabular or plate like alkali-feldspar, 10-20 mm in length. These are often coarsely perthitic displaying both patch and braid perthite textures (Fig. 3.8a-d). Carlsbad twinning is also common, where perthitic exsolution is present these crystals have a herringbone texture (Fig. 3.8a). Euhedral to subhedral nepheline (2-4 mm) often has a deep pink colouration in hand specimen and often turbid in thin section or altered to cancrinite, natrolite or sodalite (Finch, 1991; Jones, 1980). The mafic mineralogy is dominated by bright green intercumulus clinopyroxenes (aegirine-augite) which are often particularly Zr-rich (Jones & Peckett, 1980; Jones, 1984). Dark green to brown pleochroic amphibole is common in some samples though generally the mafic mineralogy is dominated by pyroxene. Fine fringe biotite is also commonly associated with magnetite. Accessory phases and secondary mineral assemblages include magnetite, zircon, apatite and pyrochlore crystals. Fluorite and calcite are also common in many rocks either as secondary alteration products of feldspar and amphibole.

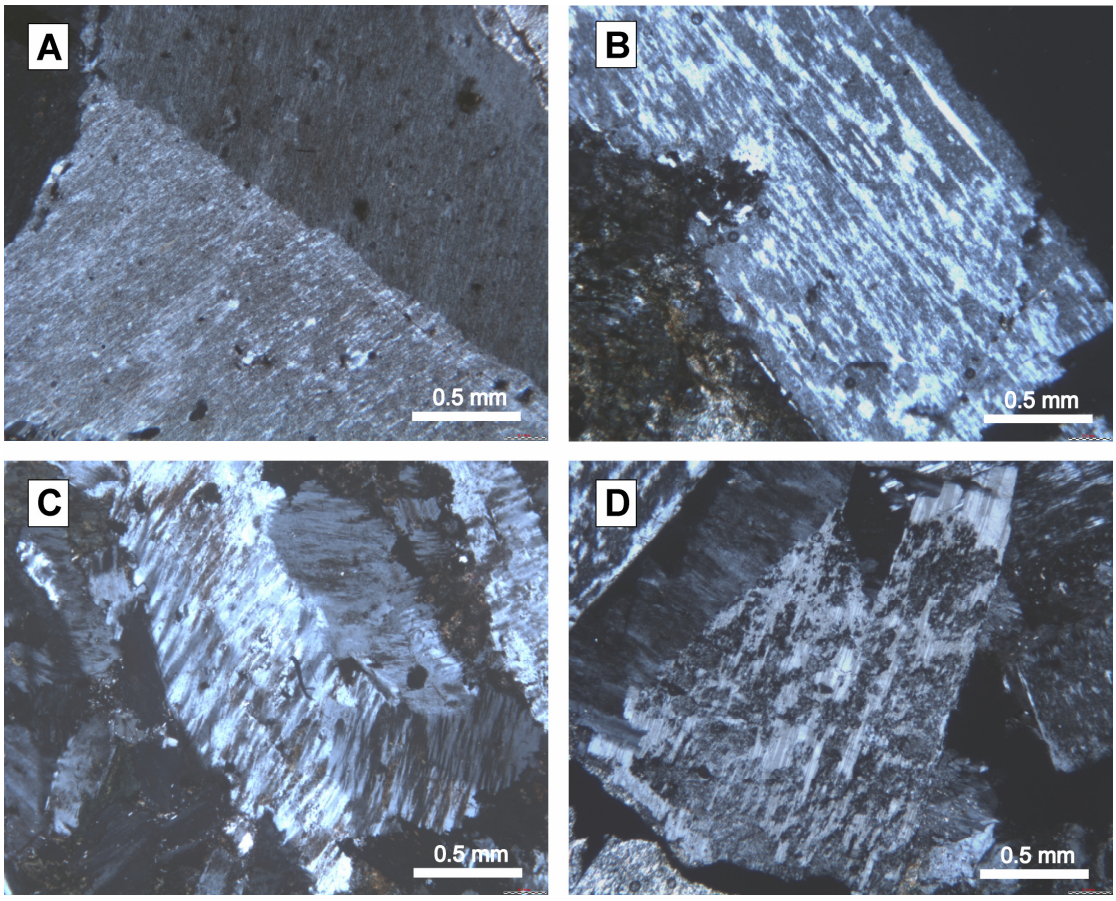

Figure 3.8. Textural relationships of alkali feldspars from the Flinks Dal Formation. (a) Fine microperthites and Carlsbad twin (GJM06-110). (b&c) Coarsely exsolved patch perthites (GJM06-85, GJM06-91). (d) Perthitic alkali-feldspar showing patches of micaceous alteration (GJM06-85).

Throughout the porphyritic nepheline syenite, occurrences of mafic-rich porphyritic enclaves are common. The mineralogy of these is predominantly fine aggregates of amphibole and pyroxene and euhedral microperthitic alkali-feldspar. Despite the relatively uniform mineral assemblages throughout the FDF, variation in the texture and modal composition of the rock is relatively common. Nepheline microsyenitic facies occur throughout the formation containing elongate, tabular laths of alkali-feldspar often coarsely exsolved and showing strong twinning. These are supported in a fine-grain groundmass of tabular alkali-feldspar, euhedral nepheline and intercumulus green pyroxene. Porphyritic biotite is also common in the microsyenite, occurring as 1-5 mm tabular sheets with a deep red-brown colour (Fig. 3.9a&b).

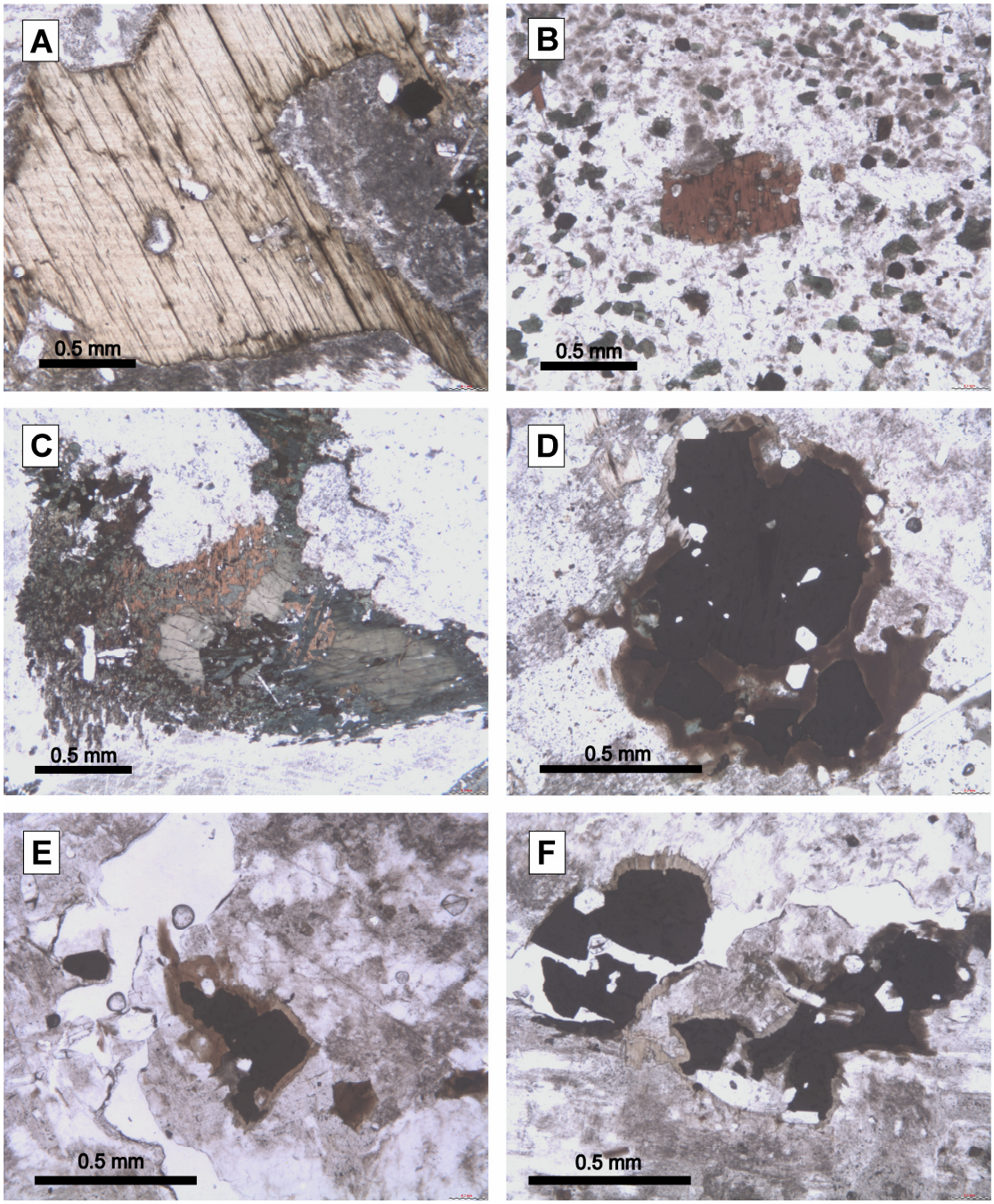

Figure.3.9. Textural relationships of biotite from the Flinks Dal Formation. (a) Large primary biotite crystal (GJM06-87). (b)Poikiolitic biotite phenocryst in microsyenite hosting inclusions of alkali feldspar and pyroxene (GJM06-99). (c) secondary biotite replacement of primary zoned pyroxene (GJM06-91). (d-f) Reaction corona of fringe biotite generated during the subsolidus reaction between magnetite and alkali-feldspar (GJM06-87).

The last and youngest major intrusive unit of the FDF is sited centrally within the Motzfeldt centre, north of the Flinks Dal fault (Bradshaw, 1988). This unit comprises a very coarse nepheline syenite. Typically 60-65 % of this rock comprises coarse rectangular and tabular alkali-feldspar which range in size from 10 to 40 mm and are often exsolved to coarse

perthite (Fig. 3.8c&d). Bradshaw (1988) also identified a second feldspar phase which mantles the larger primary phase as well as occurring as separate bladed crystals in the groundmass which may be identified by their finer perthitic texture. Euhedral to subhedral cloudy nepheline varying from 1-4 mm in length is also present. Alteration products after these minerals are common and include sodalite (Finch, 1991), analcite and secondary albite (Jones, 1980). The mafic minerals occur as clots of several minerals and small intercumulus phases. Pyroxene is most common and often shows concentric zoning under plane polarised light. Arfvedsonite amphibole is often intimately associated with pyroxene and regularly shows a strong pleochroic scheme of brown, green and blue. Biotite is also found in the mafic clusters of this nepheline syenite and quite often replaces primary amphibole and pyroxene (Fig. 3.9c). Fringe biotite reaction coronas have also been identified in a number of samples intimately associated with magnetite. Fluorite and calcite are also common in this rock. The accessory mineral assemblage of this rock is principally zircon and apatite.

Pyrochlore mineralisation in the MSF is relatively widespread and has been the focus of detailed investigation during the present study (chapter 4). In contrast, pyrochlore is largely absent in the FDF and to date has only been identified in one locality from the formation. Pyrochlore in the FDF occurs in a facies of syenite texturally similar to that hosting pyrochlore in the MSF. The rock is generally a hightly leucocratic microsyenite. The mineralogy of the leucosyenite is dominated by fine euhedral laths of alkali-feldspar, which may comprise 70-80% of the mineral mode. Unlike the pyrochlore host facies in the MSF, the feldspars of the FDF are largely pristine. Post-magmatic perthites are present though alteration related turbidity is much reduced. Alignment of feldspar also gives the rock a strong fabric, similar to the pyrochlore host facies in the MSF.

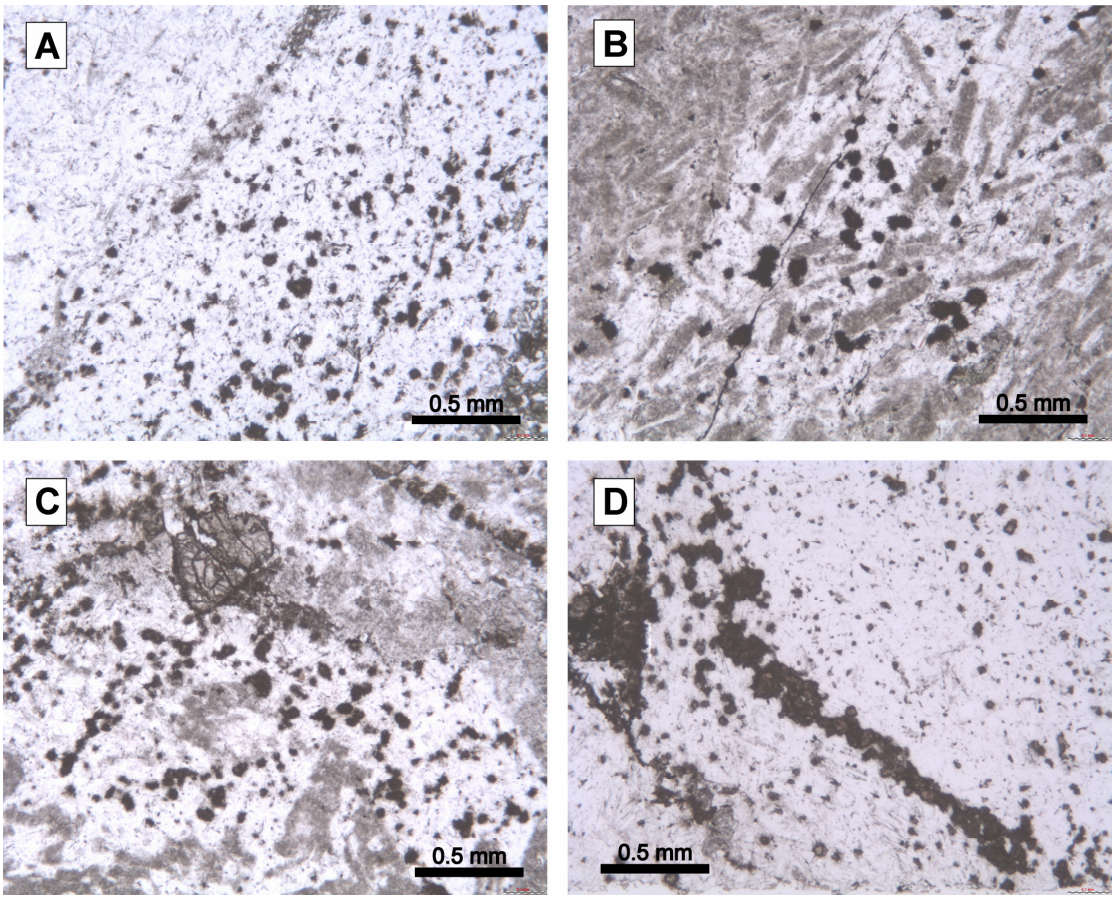

Figure 3.10. Photomicrographs of pyrochlore occurrence in samples from the Flinks Dal Formation (JS55, JS58 & JS66). All samples (a-d) show dark brown/yellow fine pyrochlore crystals disseminated throughout the rock. Image (d) shows cumulate horizons locally enriched in pyrochlore. Samples from collection of Johannes Schönenberger.

The mafic mineralogy of the rock is dominated by fine disseminated pyrochlore speckled throughout the rock (Fig. 3.10a-d). In addition to disseminated minerals cumulate horizons rich in pyrochlore also occur (Fig. 3.10d). These horizons are parallel or sub-parallel to the alignment of feldspar. Other mafic phases include small flakes of coppery biotite (10%) and small dark-green amphibole phenocrysts (<10%). Pyrochlore crystals are euhedral and often show cubic or octahedral crystal habit. These range from 1-4 mm in diameter and in transmitted light have a strong honey-yellow colour, often with a darker brown/yellow rim. Alteration (identified by turbidity and intracrystalline darkening) in pyrochlore from this sample is much lower than observed in samples from the MSF. Here samples retain the translucent honey-yellow colour characteristic of fresh pyrochlore and show no opaque alteration, as in pyrochlore from the MSF. The hematite mineralisation which mantles pyrochlores from the MSF is absent. From textural relationships pyrochlore in this facies of syenite is a primary phase, crystallised directly from the melt.

3.3.2 Cathodoluminescence petrography

The CL character of minerals in the FDF is almost identical to those studied from low levels in the MSF. Finch (1990) has also carried out cathodoluminescence studies on samples from the FDF and the reader is directed this work for supplementary information. Feldspar from the porphyritic nepheline syenite of the FDF display blue CL in their cores and dark red CL on the rims and exsolved perthitic phases of individual crystals (Fig. 3.11). Though approximately 40% of the blue magmatic phases of the crystal is preserved, in a number of samples reddening of individual grains occasionally exceeds 90% of the crystal. Similar luminescence was observed by Finch (1990) from the FDF. No luminescence was observed from the nepheline of the present study, however very pale blue luminescence was documented from nepheline from the FDF by Finch (1990) after long exposure.

Other luminescent minerals observed in the rocks of the FDF are fluorite, calcite, apatite and zircon. Fluorite occurs as discrete crystals with uniform bright blue CL or displaying weak broad zoning. Disseminated specks of fluorite are also common in turbid feldspars and, similar to the MSF, pepper the section when viewed under a low magnification. Calcite is common, displaying a bright orange to yellow luminescence and is often associated with the mafic minerals or as fine veins cutting the section and penetrating along mineral cleavage planes. Occasional zircon is also observed showing a light blue/grey luminescence and poor zoning. Apatite has also been observed showing a similar blue luminescence to zircon. Finch (1990) also observed yellow, mauve and orange luminescing apatites showing chaotic zoning. Sodalite was also observed by Finch (1990) as a secondary mineral phase after nepheline and displaying an orange-yellow to white luminescence.

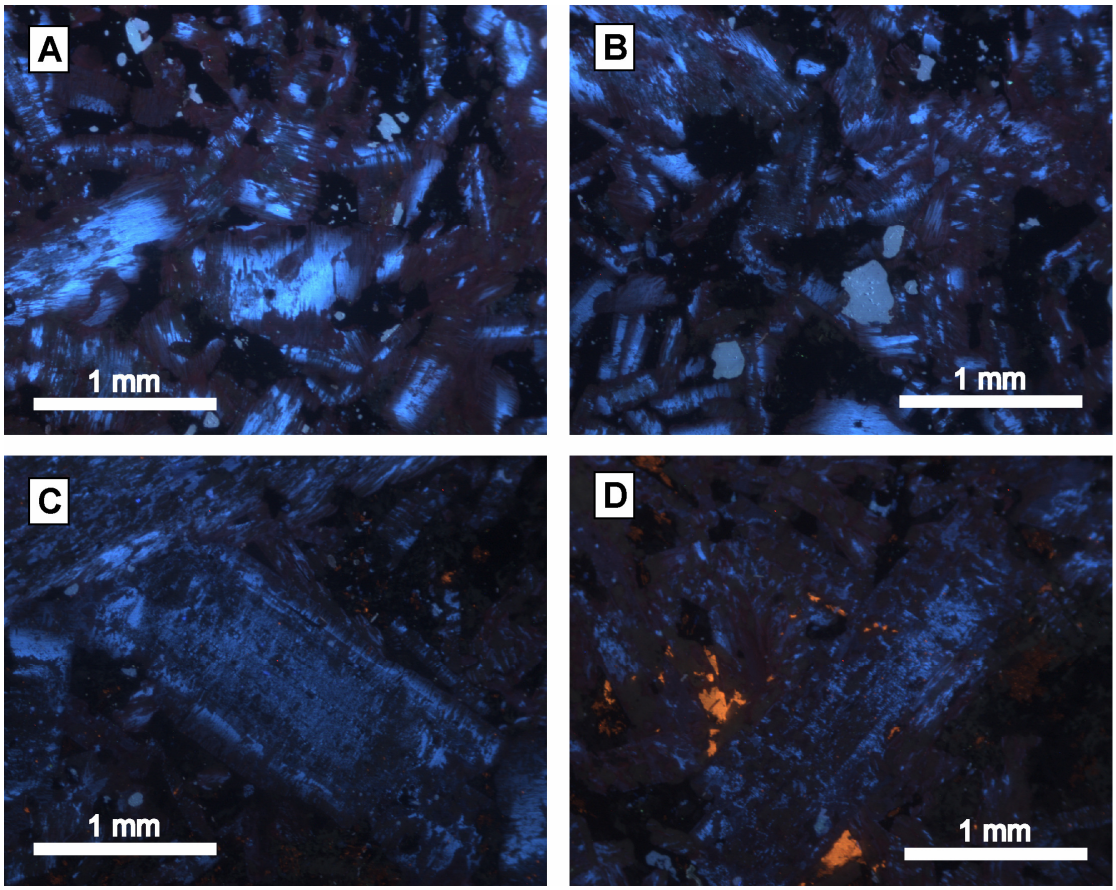

Figure 3.11. Cathodoluminescence character of alkali-feldspars from the Flinks Dal Formation. (a&b) Blue luminescent magmatic perthite patches surrounded by red luminescent altered areas (GJM06-85). (c) Fine blue luminescent perthite bands preserved in an alkali-feldspar phenocryst bright blue luminescent rims can also be seen (GJM06-91). (d) Variably altered feldspars showing weak blue luminescence in best preserved magmatic areas. bright orange luminescent minerals is intercumulus calcite (GJM06-91). Non-luminescent areas are non-luminescent mafic phases peppered with bright blue luminescent fluorite.

Table 3.1. Mineral Paragenesis from the Motzfeldt So and Flinks Dal Formations

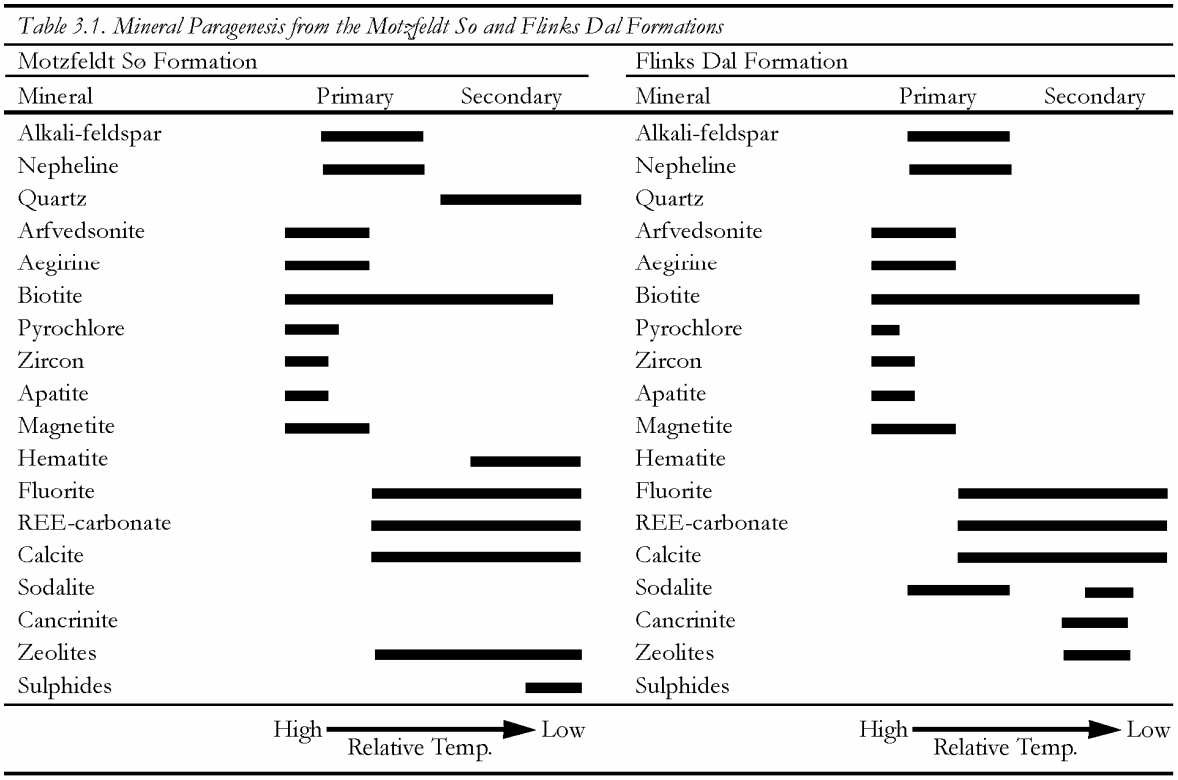

3.4 Discussion

In the previous chapter, it was suggested from the textural character and field relationships that rocks of the MSF encode a different evolutionary history to those of the FDF. From the character of the rocks in the field it is possible to conclude that the rocks from the MSF experienced a more complex magmatic history than those of the FDF and were also subject to a more intense and possibly longer hydrothermal phase. Petrographic observations from these formations confirm the suggestions of the previous chapter that the volatile components were higher and of greater activity in the MSF than the FDF and subsolidus activity in the MSF is higher than is inferred for the rocks of the FDF.

The felsic mineralogy of both formations is dominated by alkali-feldspar. In the MSF these show coarse patch perthites and many samples show finer lamellar microperthite at grain boundaries. In the FDF, patch perthites are also common, although are typically finer grained. Development and coarsening of feldspar exsolution textures is characteristic of large alkaline intrusions where the extended interval of cooling permits subsolidus diffusion of Na and K into like domains. The relatively higher degree of coarsening in the MSF suggests that subsolidus activity may have extended for a longer period than the subsolidus in the FDF. Overprinting much of the diffusion-related textures in feldspars from the MSF is intense and

pervasive alteration and secondary hematite mineralisation. This gives the feldspar a turbid red colour in plane polarised light and gives the rocks a characteristic brick-red colour in the field. In high-level units, hematite mantles the grain boundaries of feldspars and is found as fine specular hematite within the feldspar itself. In the FDF large scale hematite mineralisation, as found in the MSF, is largely absent. Feldspars from this formation only show coarsening of exsolved phases and a low degree of turbidity and alteration within individual crystals. The pervasive red alteration characteristic of the MSF is not present. Based on optical observations from feldspar, it is possible to conclude that both formations experienced interaction with a metasomatic fluid during the subsolidus, however the extent and form of alteration in the feldspars of the MSF encodes a more pervasive hydrothermal history than is found in the units of the FDF.

The CL character of feldspar from the MSF encodes the degree of subsolidus alteration particularly well. The degree of alteration, indicated by the percentage of the feldspar emitting a red luminescence, is greatest in the MSF where samples from high levels in the intrusion emit only red luminescence. Samples from lower in the intrusion preserve blue CL and red CL is restricted to exsolved phases and crystal boundaries. Feldspar luminescence in the FDF is indistinguishable from the luminescent character of feldspars from low levels in the MSF, retaining blue luminescent cores surrounded by red luminescing rims. The CL of feldspars from both formations is consistent with the observations from optical investigation that fluid activity was greatest in the MSF, particularly at high levels in the intrusion. In these samples fluid-rock interaction is greatest and permeates deep into individual crystals, whereas in the FDF and lower in the MSF fluid rock interaction is restricted to grain boundaries. Numerous studies concerning metasomatic alteration of alkali-feldspars suggest that intracrystalline microporosity controls the degree of alteration (Finch, 1990 and references therein). Finch and Walker (1991) demonstrated that in the Blå Måne Sø perthosite of South Greenland, there is a correlation between the degree of reddening in feldspars under CL and microporosity. This study and investigations by Worden *et al.* (1990) suggest that microporosity is generated during the exsolution of water from feldspars as they cool. The micropore network may be further enhanced by activity of late-stage hydrothermal fluids. Interconnected micropores in alkali-feldspars therefore provide a micro-scale channel network suitable for intragranular fluid flow, in addition to the dominant grain boundary fluid interaction. In the MSF, reddening of the CL emission in alkali-feldspars is most intense. Based on this observation it is suggested that fluid activity was greatest and that alteration occurred through fluid flow both along grain boundaries and through micropore networks in

the crystal. In the FDF and lower MSF, alteration is restricted largely to grain boundaries suggesting that interconnected microporosity is less well developed in these units, which may suggest a lower fluid activity in the units of this formation. Based on these observations it is suggested that fluid activity was greatest in rocks near the top of the MSF and generally less pervasive in the low level units of the MSF and in the present exposure of the FDF.

Pyrochlore mineralisation within the two main formations of the Motzfeldt centre is variable and largely restricted to the altered and texturally diverse units of the MSF. The occurrence of pyrochlore in this formation is restricted to one texturally distinct facies of syenite. Pyrochlore crystals from within this formation are always euhedral and are supported by highly altered alkali-feldspars. This textural relationship, in addition to pyrochlore-rich cumulate horizons within the rock, strongly suggest that pyrochlore grew as a primary mineral phase in the rocks of the MSF. Optical properties of pyrochlore from this facies of syenite deviate from the translucent honey-yellow expected in fresh pyrochlore crystals. Additionally all samples studied are mantled by a thin coat of hematite. Based on these observations it is likely that pyrochlore from the MSF have experienced a large degree of alteration associated with the subsolidus fluid activity inferred from the optical and CL properties of feldspars. Pyrochlore mineralisation in the FDF is largely absent, save the one locality described above. Texturally the character of the pyrochlore host rock from the FDF is indistinguishable from the pyrochlore host facies in the MSF, however pyrochlore from this formation retain the honey-yellow colour and hematite mineralisation is absent, suggesting that fluid-rock interaction and related alteration is reduced. From the optical properties of pyrochlore, it is not possible to determine the extent of alteration, therefore detailed investigation into fluid-pyrochlore interaction and alteration of pyrochlore minerals from the MSF and FDF will be presented in the following chapter.

Fluorite is a common rock-forming mineral in both formations of the Motzfeldt centre. Calcite is also common, forming in secondary veins and as alteration products of primary mineral phases. Throughout the MSF, fluorite accounts for 10-15 % of the rock and in previous chapters (chapter 2) extensive fluorite mineralisation has been discussed from within the in-situ roof-zone of the MSF. Although no extensive mineralisation is found in the FDF, fluorite is a common mineral in many samples studied. The presence of fluorine in undersaturated melts is not uncommon; however the extent of fluorite mineralisation in the Motzfeldt centre suggests that fluorine levels were exceptionally high in the melts and fluids associated with this formation. Investigation of fluorine activity within the Motzfeldt centre

will be addressed in subsequent chapters (chapter 5) examining the halogen content of biotite micas from both formations.

3.5 Conclusions

The textural character and degree of alteration in the Motzfeldt centre vary greatly between the MSF and FDF. Alteration is best observed under CL where feldspars display two phases of subsolidus alteration. During cooling, feldspars from both formations exsolved to coarse perthite. Under CL, alkali-feldspar shows alteration from primary blue to a secondary red luminescence. In the MSF, alteration is most intense and pervasive with feldspars displaying only red luminescence under CL, suggesting high levels of metasomatic, fluid-rock interaction associated with a prolonged and active subsolidus history. The green CL seen may be the formation of clays (Götze et al., 2002). Feldspars from the FDF retain blue luminescent cores and red altered areas are restricted to grain boundaries and exsolved phases. From these observations, the degree of fluid-rock interaction in the FDF, and also from low levels in the MSF, is inferred to be less than is observed higher in the MSF. This alteration trend is also reflected in the pyrochlore mineralisation from both formations. Pyrochlore from the MSF is largely opaque and mantled by specular hematite. In contrast, pyrochlore from the FDF is relatively fresh, retaining a translucent yellow colour and free of hematite.

Fluorite is common through out both formations suggesting that melts and exsolved fluids within both formations were exceptionally rich in fluorine. The role of fluorine in the evolution of the centre will be investigated and discussed in subsequent chapters. From field relationships (chapter 2) and the petrographic observations of the present chapter, it is clear that the MSF and FDF have experienced notably different magmatic and subsolidus histories. The magmatic evolution of the MSF is much more convoluted that the FDF additionally the textural character of minerals within this formation encode a sub-solidus history which was more pervasive than is observed in the FDF.

Chapter 4

Pyrochlore Mineral Chemistry

4.1 Introduction

Apart from occurring as a common accessory mineral in many facies of syenite in the Motzfeldt centre, pyrochlore group minerals also occur in zones of economic enrichment within the altered syenites of the Motzfeldt Sø Formation (MSF) and have also been identified in one locality from the Flinks Dal Formation (FDF). Although from the same centre, pyrochlores from the FDF and MSF show strikingly different textures and chemistries, attributed to markedly different sub-solidus histories. This chapter will look at the textural and microchemical character of pyrochlores from both these formations and will draw upon these observations to determine why such a striking variation exists between the MSF and FDF.

4.2 Structure and chemistry of pyrochlore group minerals

The pyrochlore group is a chemically diverse suite of minerals expressed by the general formula $A_{2-m}B_2O_{6-w}Y_{1-n}{\cdot}p\mathrm{H_2O}$, where *A* represents large cations in eight-fold (cubic) coordination, usually Na, Ca, Mn, Fe^{2+}, Sr, Cs, Ba, rare earth elements (REEs = Sc, Y and lanthanides), Pb, Bi, Th, U or site vacancies. The *B*-site is occupied by smaller cations in six-fold (octahedral) coordination and is occupied by smaller cations, typically Al, Nb, Ta, Ti, Fe^{3+}, Zr and Sn. *Y* is occupied by F, O, OH anions or site vacancies (Chakoumakos, 1984; Hogarth, 1977; Lumpkin & Ewing, 1995). Altered pyrochlores often show enrichment of large cations like Pb^{2+}, Ba^{2+} and K^{+}. The incorporation of these elements in the pyrochlore structure is problematic since their large ionic radii (1.18, 1.36 and 1.38 Å respectively, in octahedral co-ordination) makes accommodation in the *A* and *B* sites difficult. They may be accommodated through significant structural distortions and vacancy increases, but this would modify the overall stoichiometry. Lumpkin (1989) suggested they were located interstitially in the Wyckoff site 32e, which lies between the *A* and *Z*-sites, with the modified crystal structure resembling B_2O_6Z with *Z* occupied by the larger cation.

Up to ~10 wt% silica is also commonly found in altered pyrochlore group minerals (Johan & Johan, 1994), however its structural role has been long debated and as yet remains unclear. Several suggestions have been given. Hogarth (1977) suggested that high silicon contents are due to microcrystalline impurities of other silicate minerals, while Voloshin *et al.*

(1989) propose that high silicon content results from Si in an amorphous state. Bonazzi *et al.* (2006) suggest that 30-50% of silica detected by EPMA may be occupied in octahedral coordination in the *B*-site, whereas a larger fraction of 50-70% silicon is concentrated in radiation damaged crystal domains (though not specifically metamict). Octahedral silicon ($Si(OH)_6$) is known to be present in the structure of thaumasite (ideal structure $Ca_3Si(SO_4)(CO_3)(OH)_6 \cdot 12H_2O$) at room pressure (Edge & Taylor, 1969), however six-fold coordination of silicon is largely restricted to high pressure minerals such as stishovite (Finger & Hazen, 1991; Ross *et al.,* 1990). Vittorio *et al.* (2005) suggests that Si can be hosted within hexagonal channels running parallel to the c-axis of a defect pyrochlore structure as separate SiO_4 tetrahedra. Significant hydration is also associated with alteration in natural pyrochlores. In pyrochlores from nepheline syenites, Lumpkin and Ewing (1995) inferred H_2O contents, from analytical totals, to range from 2 to 14 wt% depending on the type and degree of alteration.

Classification of pyrochlore group minerals is based on the International Minerals Association (IMA) scheme of Hogarth (1977). Hogarth (1977) defined three sub-groups based on the atomic proportion of the major *B*-site cations, Nb, Ta and Ti: Microlite (Nb + Ta > 2Ti, Ta ≥ Nb), pyrochlore (Nb + Ta > 2Ti, Nb > Ta), betafite (2Ti ≥ Nb + Ta). Within each group individual species are defined with respect to the atomic proportion of *A*-site cations (Table 4.1).

Because of the large range in size and valence of elements which the pyrochlore structure can accommodate, a number of problems arise in assigning elements to structural sites. During this study the following site allocations are used. Al^{3+} and Zr^{4+} are assigned to the *B*-site in accordance with synthetic REE-Zr pyrochlores of Subramanian *et al.* (1983). All iron is assumed to be Fe^{2+} and assigned to the cubic *A*-site. Large cations such as Pb^{2+}, Ba^{2+} and K^+ are assigned to their traditional location in the *A*-site due to a lack of definitive data to suggest significant structural modification or siting within other sites. Silicon still remains problematic, and is particularly relevant to the present study since several altered samples from the MSF show notable enrichment of Si. During this section Si will be assigned to the *A*-site, however those samples showing particularly high Si contents (>3 wt%) will be viewed with suspicion as Si may be sourced from mixed analyses of silicate minerals, as amorphous silicon, or as complete SiO_4 species located in spaces in the defect pyrochlore structure (e.g. Vittorio *et al.* (2005)).

Table 4.1. *16 species of pyrochlore group minerals, after Hogarth (1977)*

SUBGROUPS defined by B-site cations: Nb, Ta & Ti			PYROCHORE Nb + Ta > 2Ti, Nb > Ta	MICROLITE Nb + Ta > 2Ti, Ta ≥ Nb	BETAFITE 2Ti ≥ Nb + Ta
SPECIES defined by A-site cations: K, Sn, Ba, REE, Pb, Bi & U	Na + Ca but no other A-site cations >20% total A-site		Pyrochlore	Microlite	Betafite
	One or more A-site cations, other than Na or Ca >20% total A-site Species named by most abundant A-site cation	K	Kalipyrochlore		
		Sn		Stannomicrolite	
		Ba	Bariopyrochlore		
		REE*	Yttriopyrochlore (∑Y > ∑Ce)# Ceriopyrochlore (∑Ce > ∑Y)		Yttrobetafite (∑Y > ∑Ce)
		Pb	Plumbopyrochlore	Plumbomicrolite	Plumbobetafite
		Bi		Bismutomicrolite	
		U	Uranpyrochlore	Uranmicrolite	Uranbetafite

*REE = Y + La→Lu; # ∑Y = Y + Gd→Lu; ∑Ce = La→Eu

Many studies into pyrochlore chemistry examine primary compositional variations generated during the magmatic growth of the crystal. However, like many minerals in the Motzfeldt centre, sub-solidus fluid-related activity has significantly altered the primary textures and composition of many pyrochlore crystals. During the present section pyrochlore crystals showing both primary magmatic textures and textural evidence for sub-solidus alteration will be described. Primary features include concentric and sector zoning developed during crystal growth. In the Motzfeldt centre such features are poorly preserved and are often obscured by complex secondary textures and chemistries attributed to alteration under sub-solidus conditions. The degree and form alteration takes in the pyrochlores of the Motzfeldt centre is largely dependant on the lithology and formation in which they are hosted. In the FDF alteration is only found in small areas of individual crystals and is much less pervasive than the alteration which will be described for the MSF. For this reason a framework must be used to describe different types and degrees of alteration. Such a framework has been developed through the work of Lumpkin and Ewing (1992, 1995 & 1996) for the progressive alteration of the three pyrochlore sub-groups (microlite, pyrochlore and betafite) under a range of hydrothermal conditions. Alteration in the Motzfeldt pyrochlores will therefore be described with reference to the framework of Lumpkin and Ewing (1992, 1995 & 1996) using the following criteria to describe phases of alteration based on textural and microchemical observations: 1) *Primary alteration*. In general, primary alteration is characterised by intracrystalline diffusion, associated with high-temperature interaction with juvenile magmatically derived fluids. 2) *Secondary alteration*. Secondary alteration is largely controlled by microfracturing of pyrochlore crystals and often associated elsewhere in the same sections

with the pervasive alteration of feldspars and micas to iron oxides and clays during interaction with lower temperature fluids. 3) *Transitional alteration*. This type of alteration is defined as alteration showing features characteristic of both primary and secondary, characterised by combination of intracrystalline diffusion and microfracture control (Lumpkin & Ewing, 1995). This type of alteration typically occurs in shallow crustal systems where a meteoric fluid component is present.

4.3 Flinks Dal Formation pyrochlores

4.3.1 Introduction and textural character

Pyrochlores from the FDF usually occur as fine (<80 μm) euhedral to subhedral crystals disseminated throughout the rock, occasionally in clusters or crystal aggregates, and present in amounts varying from 2-10 % mineral mode. BSE imaging of pyrochlores reveals well developed primary magmatic zonation (Fig. 4.1) identified by their excellent concentric growth zoning (e.g. Fig. 4.1a & b) developed on a 1-5 μm scale. The majority of samples however show sectors of compositional banding which is not continuous over the whole crystal (e.g. Fig. 4.1c).

Several pyrochlore samples from the FDF show textures that cannot be attributed to primary growth features. The BSE images in Figure 4.1e & f show pyrochlores with strong magmatic compositional zoning overprinted by irregular areas with a brighter BSE emission which are interpreted as areas of alteration overprinting the original magmatic textures of the crystal. Alteration penetrates the crystal in an irregular 'watermark' type texture from the crystal margin. The BSE contrast between mineral zones in the altered area is less intense than in primary, unaltered areas and has a generally brighter BSE emission, giving the altered area a washed out appearance. However, the alteration front is marked by a narrow zone with a dark BSE emission, aiding in the identification of such features. Figure 4.1f shows a weak fracture (arrow) penetrating into the crystal suggesting that alteration is to some degree fracture controlled. However in many examples preserved or annealed fractures cannot be seen, suggesting intracrystalline diffusion to be the dominant control of alteration.

4.3.2 Primary magmatic chemical zoning

Representative EPMA analyses of pyrochlores from the FDF are shown in Table 4.2. The complete data set can be found in appendix D. When plotted in the ternary Ti-Nb-Ta diagram (modified after Nickel, 1992), all of the pyrochlore samples from the FDF lie within the pyrochlore sub-group (Fig. 4.2) showing Nb enrichment. The other major cations in the *A*-site are principally Na and Ca. Typical ranges for these cations are 0.02 to 0.55 atoms per formula unit (apfu) for Na and 0.65 to 1.15 apfu for Ca. The other minor *A*-site cations; Mn, Fe, Sr, U, Th and Pb have maximum amounts of 0.11, 0.11, 0.08, 0.09, 0.01 and 0.03 apfu, respectively. The ∑REEs (La, Ce, Pr, Nd, Sm, Gd, Dy and Yb) are typically <0.06 apfu and dominated by La and Ce, which account for 65-85% of the total REE content. In many samples the heavier REEs are <0.01 apfu. None of the minor *A*-site cations exceed 20% of the *A*-site total, therefore pyrochlores from the FDF can be classified as pyrochlore sensu stricto (Hogarth, 1977).

Samples showing well developed concentric zonation were examined using EPMA on mineral traverses from core to rim (appendix C), with spot analyses on each of the dominant mineral zones. Each crystal (six separate pyrochlore crystals analysed from two pyrochlore rich samples) displays strong compositional variations over each of the contrasting BSE zones. Traverses from core to rim on all samples (Fig. 4.3) show a slight elevation of Ta in the core, decreasing towards the rim. Typical Ta values are 0.06-0.08 apfu in the core decreasing steadily to 0.02-0.03 apfu in the rim. Sample JS53-2 shows a slightly higher Ta content in one high-BSE zone, then continues on the same decreasing trend as before. Compositional variation between mineral zones is most obvious in the higher valency *A*-site elements; Mn^{4+}, U^{4+}, Ti^{4+} (Si^{4+} and Zr^{4+} show similar trends but are not shown in figure 4.3). Figure 4.3 shows that Ti, U and Mn are elevated in the bright, high-BSE zones and depleted in the dark, low-BSE zones. In contrast, the low-BSE zones display a slight elevation in the low-valency *A*-site elements, Na^{+} and Ca^{2+}, which are depleted in the high-BSE zones. Nb shows a flat profile regardless of mineral zonation. The relationship between compositional zoning and REE content is generally weak. In samples where F was analysed there is a strong relationship between high F content in bright-BSE zones.

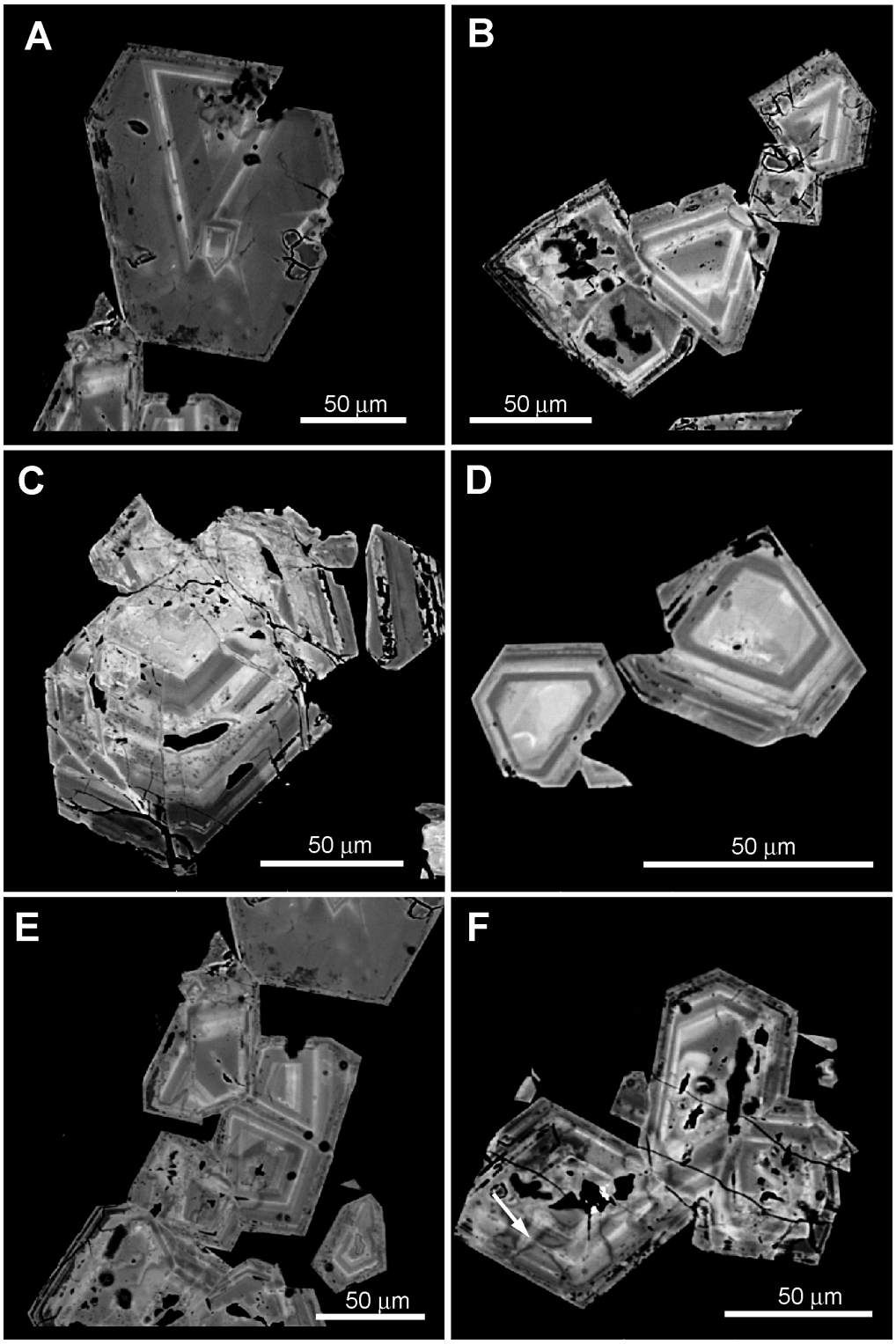

Figure 4.1. BSE images of select pyrochlores from the Flinks Dal Formation. (a), (b) and (d) Oscillatory zoned pyrochlore crystals; (c) Sector-zoned pyrochlore crystal; (e) and (f) oscillatory and sector-zoned pyrochlore crystals showing a dark BSE band interpreted as a diffusive alteration front and primary altered areas (light BSE washed-out areas).

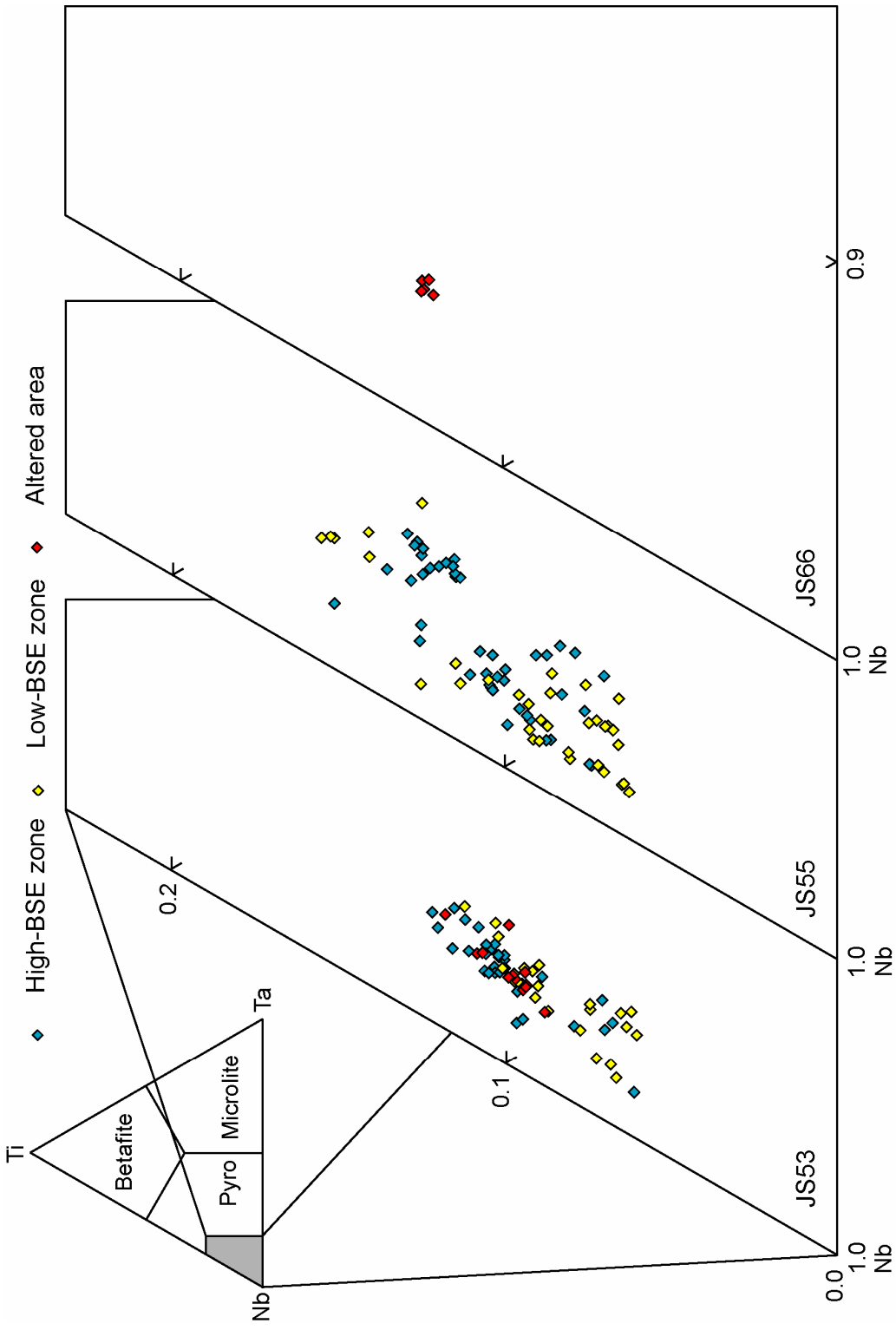

Figure 4.2. *B*-site element chemistry of pyrochlore group minerals from the Flinks Dal formation (samples JS53, JS55 and JS66), protected onto the Nb-Ta-Ti ternary diagram (Hogarth, 1977), modified according to the 50% rule of Nickel (1992).

***Table 4.2**. Representative EPMA analyses of pyrochlores from the Flinks Dal formation*

	Light BSE magmatic zones			Dark BSE magmatic zones			Altered zones		
Wt%	55-1-5	55-3-9	53-8-13	53-8-8	55-6-19	55-3-3	55-5-10	55-5-11	55-5-13
Na_2O	5.87	7.41	5.76	5.71	6.60	4.10	0.37	0.66	0.351
CaO	16.85	13.95	9.69	14.64	16.19	12.50	6.73	11.59	5.04
MnO	0.62	0.52	0.52	0.03	0.04	1.10	0.03	0.08	0.53
SrO	0.27	0.42	1.44	0.23	0.24	0.67	2.34	0.81	3.08
PbO	0.04	n.d	0.78	n.d	n.d	0.24	n.d	n.d	0.40
ThO_2	0.21	0.20	0.18	0.27	0.67	0.09	n.d	n.d	n.d
UO_2	2.66	2.53	4.31	1.22	1.59	3.03	2.17	1.80	1.76
La_2O_3	0.65	0.55	0.24	0.36	0.30	0.55	0.50	0.37	0.56
Ce_2O_3	1.72	1.32	1.28	1.24	0.94	1.59	0.89	0.63	1.12
Pr_2O_3	0.14	0.24	0.07	n.d	0.13	0.14	n.d	n.d	n.d
Nd_2O_3	0.45	0.24	0.48	0.42	0.43	0.73	0.43	0.50	0.38
Sm_2O_3	0.10	0.29	0.30	0.13	0.07	0.16	n.a.	n.a.	n.a.
Gd_2O_3	0.02	0.11	n.d	n.d	0.16	n.d	0.16	0.13	0
Dy_2O_3	0.06	n.d	0.30	n.d	0.12	n.d	0.17	0.92	0.39
Yb_2O_3	n.d	n.d	n.d	n.d	n.d	n.d	n.d	n.d	n.d
SiO_2	0.20	1.54	n.d	0.25	0.10	3.37	n.d	n.d	n.d
ZrO_2	0.58	0.91	1.37	2.26	0.82	0.16	2.18	1.66	2.38
Nb_2O_5	60.82	62.36	62.34	61.27	62.64	57.67	61.04	58.13	62.64
Ta_2O_5	1.34	1.52	2.63	3.28	1.57	1.02	2.71	2.40	2.72
TiO_2	4.07	3.63	4.39	3.82	3.89	5.00	4.02	3.72	3.98
FeO	0.21	0.35	1.04	0.27	0.03	2.06	0.57	0.68	0.72
F	3.00	3.93	3.59	6.16	3.60	3.02	n.a.	n.a.	n.a.
Total	**95.59**	**97.19**	**94.28**	**99.53**	**98.68**	**97.83**	**85.61**	**84.17**	**86.35**
Structural Formulae (∑B-site cations = 2)									
Na	0.364	0.444	0.340	0.382	0.398	0.259	0.022	0.042	0.020
Ca	1.155	0.923	0.632	0.916	1.080	0.873	0.445	0.813	0.325
Mn	0.034	0.027	0.027	0.001	0.002	0.061	0.019	0.005	0.027
Sr	0.010	0.015	0.051	0.004	0.009	0.025	0.084	0.031	0.108
Pb	0.001	-	0.013	-	-	0.004	-	-	0.006
Th	0.003	0.003	0.003	0.004	0.010	0.001	-	-	-
U	0.038	0.035	0.058	0.022	0.022	0.044	0.030	0.026	0.024
La	0.015	0.012	0.005	0.012	0.007	0.013	0.011	0.009	0.012
Ce	0.040	0.030	0.028	0.034	0.022	0.038	0.020	0.015	0.025
Pr	0.003	0.005	0.002	-	0.003	0.003	-	-	-
Nd	0.010	0.005	0.010	0.007	0.010	0.017	0.010	0.012	0.008
Sm	0.002	0.006	0.006	0.002	0.002	0.004	-	-	-
Gd	0.001	0.002	-	-	0.003	-	0.003	0.003	-
Dy	0.001	-	0.006	-	0.002	-	0.003	0.020	0.008
Yb	-	-	-	-	-	-	-	-	-
Si	0.012	0.095	-	0.004	0.006	0.220	-	-	-
Fe	0.011	0.018	0.053	0.027	0.002	0.112	0.029	0.037	0.036
∑A	**1.705**	**1.621**	**1.237**	**1.433**	**1.577**	**1.691**	**0.704**	**1.018**	**0.623**
Nb	1.759	1.742	1.715	1.720	1.763	1.700	1.702	1.720	1.705
Ta	0.023	0.026	0.043	0.042	0.027	0.018	0.046	0.043	0.045
Ti	0.196	0.169	0.201	0.175	0.182	0.245	0.187	0.183	0.180
Al	0.004	0.036	-	-	0.003	0.031	-	0.001	-
Zr	0.018	0.028	0.041	0.062	0.025	0.005	0.066	0.053	0.070
∑B	**2.000**	**2.000**	**2.000**	**2.000**	**2.000**	**2.000**	**2.000**	**2.000**	**2.000**
F	0.492	0.616	0.602	0.984	0.584	0.505	-	-	-

All sample numbers have prefix JS and were donated by J. Schöenenberger. Total Fe expressed as FeO. n.d = not detected. n.a. = not analysed. Fluorine is located in the *Y*-site and has not been included in structural recalculations.

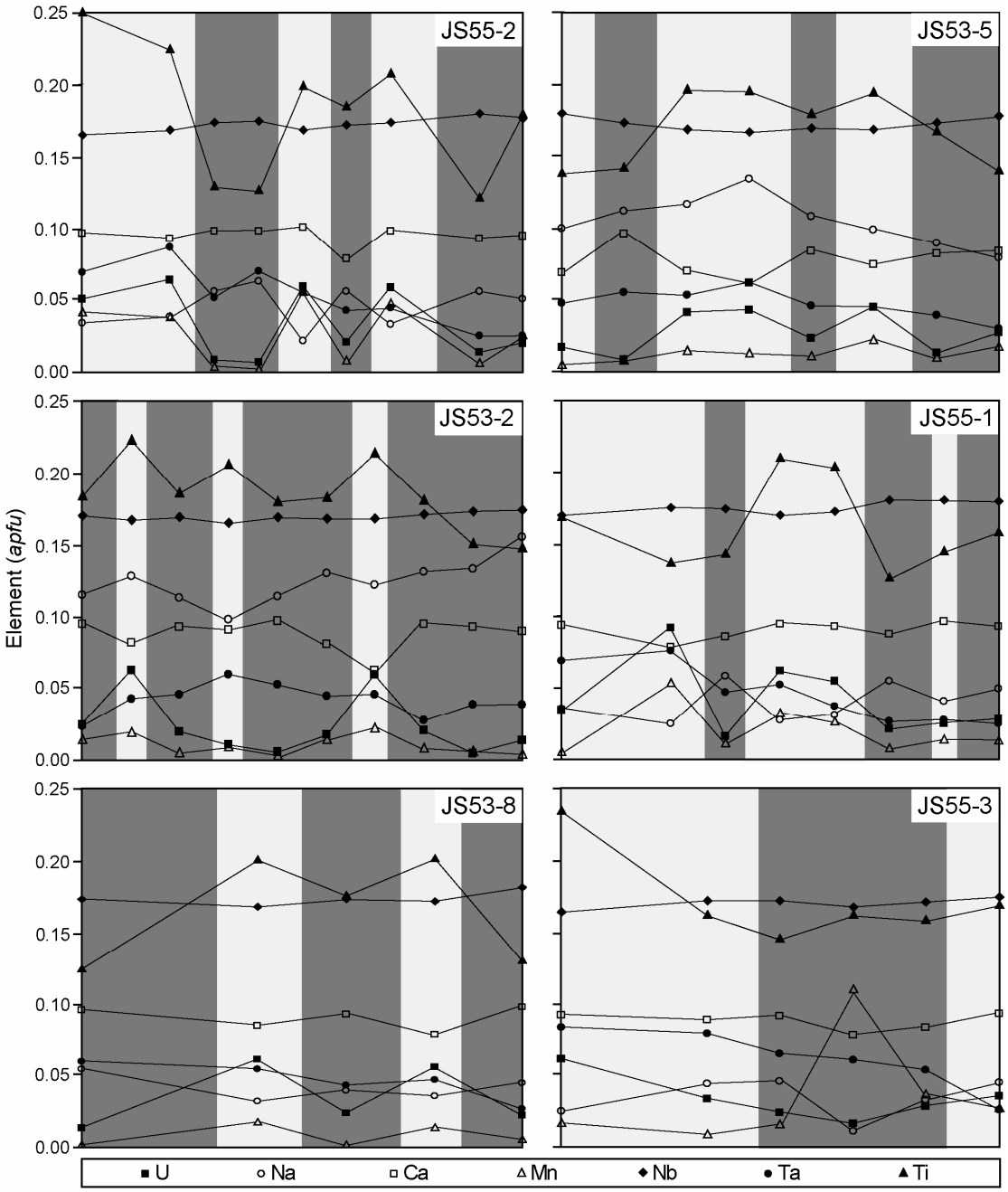

Figure 4.3. Distribution of Na, Ca, Mn, U, Nb, Ta and Ti across pyrochlore crystals from the Flinks Dal Formation. Na, Ca and Nb are shown as cation/10, apart from samples JS53-2 and JS53-5, which are shown as true values. Distribution profiles have been scaled and are not true traverse distances. Profile lines can be seen in appendix C.

4.3.3 Chemical effects of alteration

Several pyrochlore samples from the FDF show evidence for alteration penetrating the crystal in an irregular 'watermark' type texture from the crystal margin. Comparison of unaltered areas of the same crystal and unaltered crystals in the same sample show that

alteration is characterised by an increase in Sr and K and a decrease in the dominant *A*-site cations, Ca and Na (Fig. 4.4). Those zones interpreted as altered have increased values of Sr and K, typically increasing from ~0.02 to ~0.09 apfu and ~0.004 to ~0.02 apfu respectively during alteration. In three sample analyses K occurs up to 0.43 apfu. In the same traverses Ca decreases from 0.60-0.90 to <0.40 apfu and Na decreases from 0.09-0.14 to <0.05 apfu in the bright altered zones. Structural recalculation of altered and unaltered samples indicates development of *A*-site vacancies during alteration, with maximum values of 0.8 vacancies per formula unit. In samples where F was measured the F content appears to decrease slightly as a result of alteration. Alteration also appears to hydrate the pyrochlore structure significantly. H_2O contents inferred from low analytical totals suggest 2-7 wt% H_2O may be incorporated during alteration. Some samples show increases in U and Ti and minor decrease in Ta content in areas of alteration, though it is unclear whether this is the result of alteration or whether alteration is superimposed on original compositional heterogeneities associated with magmatic mineral zoning.

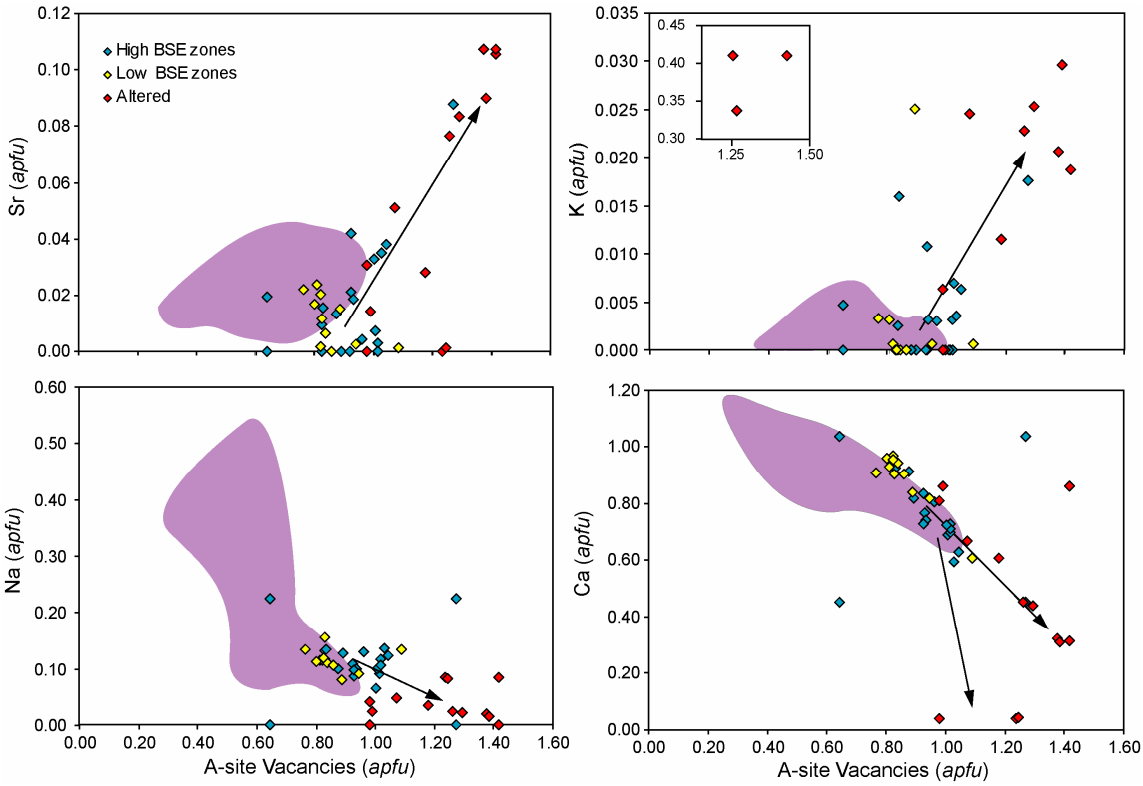

Figure 4.4. Variation diagrams (apfu) for large *A*-site cations (Sr, K, Na and Ca) vs. *A*-site vacancies for unaltered and altered pyrochlore areas. Arrows show alteration trends. Note that the decreases in Ca in high-BSE zones as a primary compositional feature and not a product of alteration. Purple shaded area shows field of entire data set of unaltered Flinks Dal Formation pyrochlore samples.

The behaviour of REEs during alteration is variable (Fig. 4.5). In the altered areas from samples JS53 the content of the heavier REEs shows variable increases and decreases, this is most apparent for Dy and Gd. In unaltered samples these elements both show a broad spread of values ranging from 0-0.02 apfu for Dy and 0-0.04 apfu for Gd. In altered samples the data range is generally slightly higher. La and Ce also vary during alteration with Ce becoming the more dominant LREE over La during alteration. Despite the slight variations noted above the normalised REE patterns do not appear to change significantly as a result of alteration.

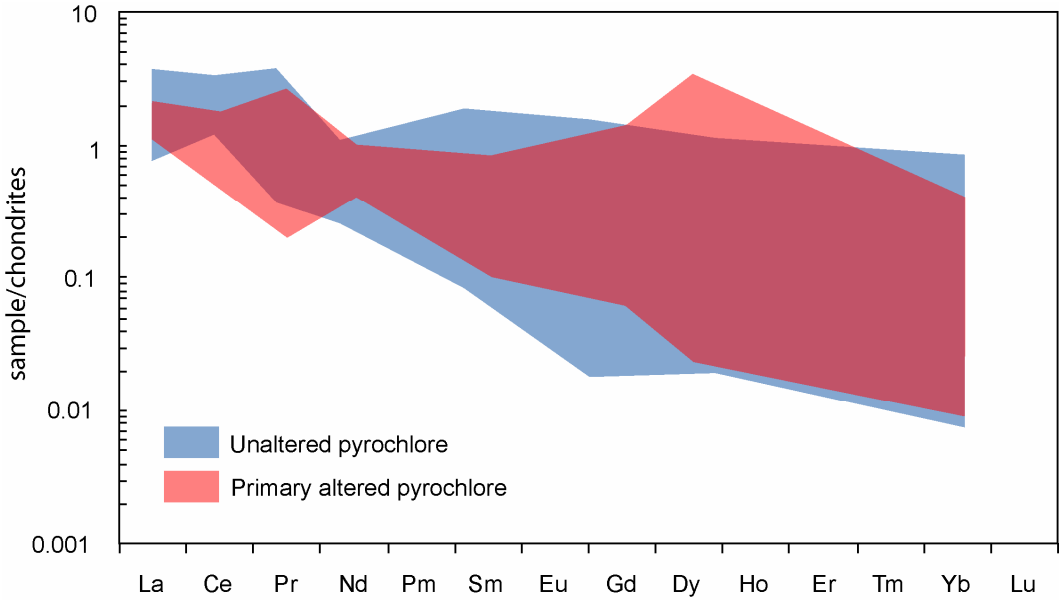

Figure 4.5. Chondrite-normalised REE distribution patterns for unaltered and altered pyrochlores from the FDF. Field for unaltered samples in blue. Field for altered samples in red.

Of all of the element exchanges that occur during alteration the larger cations (Sr and K) serve as the best chemical indicators of alteration. In unaltered samples Sr and K are generally at very low levels, however during alteration Sr can increase to 0.11 apfu, compared to typical unaltered values of 0-0.04. Similarly, K can occur up to 0.03 apfu compared to typical values of 0-0.005 apfu in unaltered samples. Following the framework of Lumpkin and Ewing (1995) for the progressive alteration of minerals within the pyrochlore sub-group, the textural and microchemical variations associated with alteration of pyrochlores from the FDF suggests a primary phase of alteration associated with high temperature juvenile fluids. The characteristic features of which are the loss of Na and F, *A*-site cation exchange for Sr, Ca, Fe and Mn, accompanied by variable changes in REE content and moderate increases in *A*-site vacancies (Lumpkin & Ewing, 1995).

4.4 Motzfeldt Sø Formation pyrochlores

4.4.1 Introduction and textural character

The units hosting pyrochlore east of the Motzfeldt Sø lake are in striking contrast to the pyrochlore-containing units in the FDF. The MSF is compositionally diverse and is atypical of other Motzfeldt units, and indeed units within the Gardar as a whole. FDF pyrochlores retain primary compositional zoning, whereas the MSF pyrochlore population show exclusively textures interpreted as evidence for high-levels of pervasive sub-solidus alteration associated with fluid-rock interaction. Pyrochlore crystals have been identified as accessory minerals in many of the syenite faces of the MSF, however the highest occurrence is largely constrained to lithologically distinct leucocratic microsyenite units containing fine disseminated euhedral pyrochlore crystals making up 5-15 % of the rock's mineralogy. Several examples contain bands or horizons enriched in cumulate clusters of pyrochlore, which are typically of larger size than disseminated crystals.

Pyrochlore group minerals are characterised by their octahedral habit and strong honey-yellow colour in transmitted light. In the FDF many of the unaltered pyrochlore crystals show these characteristic features. However, crystals from MSF show varying states of alteration. Although they have an octahedral crystal form they are characterised by a dark reddish-brown to opaque colour in transmitted light and are often rimmed by hematite and contain inclusions of alkali feldspar, magnetite, fluorite and LREE-rich carbonates, tentatively identified as bastnäsite or synchysite. BSE imaging of pyrochlores from the MSF reveals extremely complex internal textures (Fig. 4.6), with very few samples showing evidence of primary growth zoning. In samples which do retain evidence of primary zonation this is often weakly preserved as a result of secondary features partially masking or wholly overprinting the original magmatic features. Alteration textures within the MSF pyrochlores are more intense and pervasive than the irregular diffusion front observed in the FDF samples. MSF pyrochlores display alteration textures resembling a 'mosaic' or 'tortoise shell' pattern in BSE (Fig. 4.6). These textures are interpreted as intense alteration associated with fluid penetration along radiation-induced microfractures. The majority of pyrochlore crystals from the MSF have an intermediate to high-BSE emission which is cut by an interconnected network of lower BSE vein-like areas of alteration (Fig. 4.6f). It has been show in the FDF pyrochlores that primary alteration appears to increase the overall BSE emission of the crystal and give the samples a washed out appearance. In the MSF diffusion controlled alteration has likely

penetrated the whole crystal during a primary magmatic phase of alteration, increasing the overall BSE intensity of the crystal and washing out any primary features. These primary alteration features have been subsequently overprinted by a secondary phase of lower temperature alteration which appears dominantly fracture controlled.

Samples showing a network of fracture related alteration microfracture preservation are generally rare. Lumpkin and Ewing (1995) have shown that in heavily altered pyrochlores healing of microfractures can occur through hydration and volume expansion of the pyrochlore structure during a lower temperature secondary phase of alteration. Additionally, many pyrochlores showing strong alteration associated with annealed microfractures have strong radial fractures parallel to the crystal margins, which are attributable to volume expansion during hydration. This is particularly true for pyrochlores from the MSF which show H_2O estimates, inferred from low analytical totals, of 5-12 wt%.

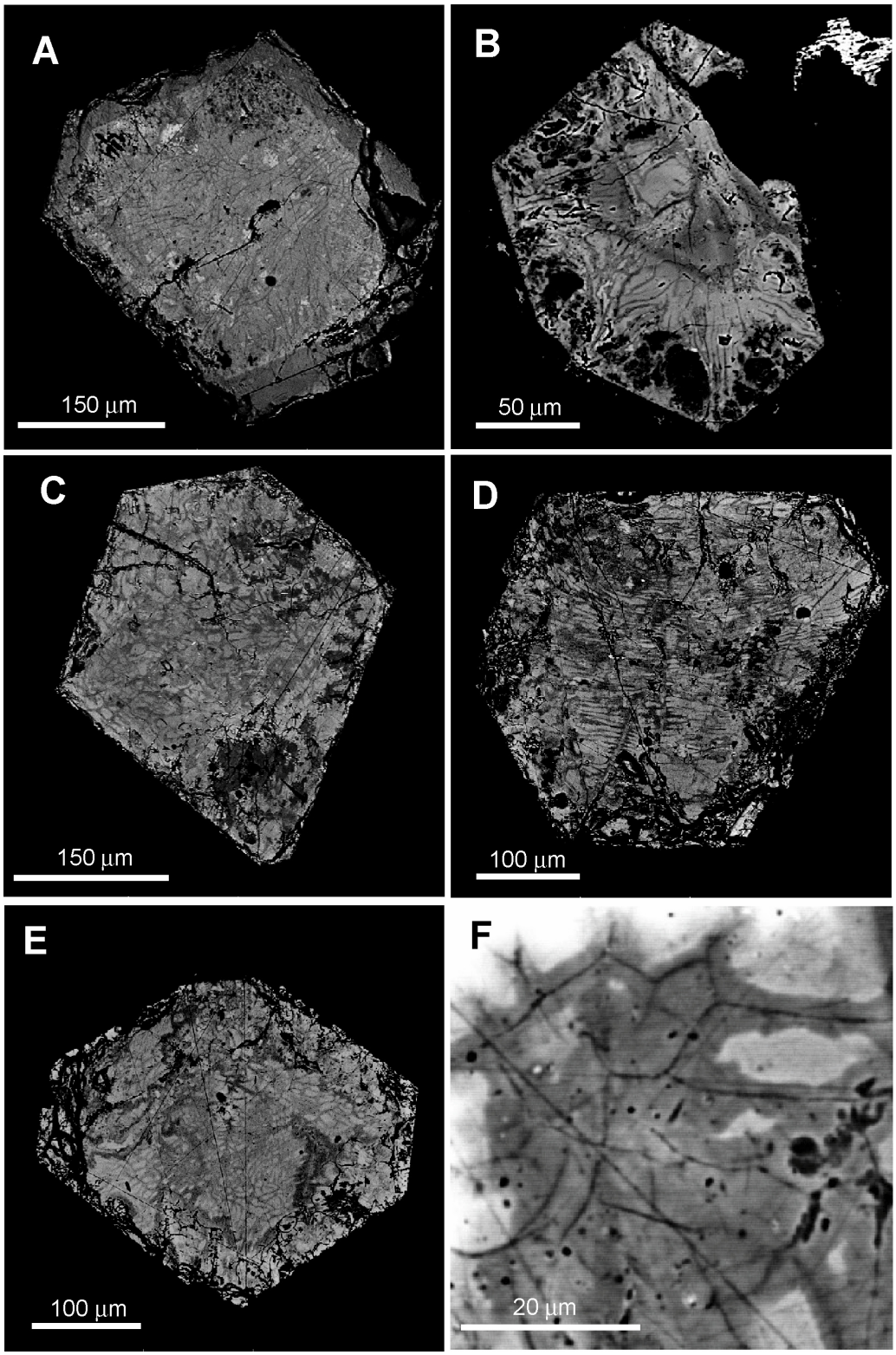

Figure 4.6. BSE images of select pyrochlores from the Motzfeldt Sø Formation. (a) and (b) Pyrochlores retaining weak primary zones overprinted by mosaic of alteration; (c), (d) and (e) Heavily altered pyrochlore crystals with intense network of microfractures penetrating the whole crystal (dark grey BSE) (f) close up of pyrochlore in (e) showing the network of microfractures and associated dark BSE alteration.

4.4.2 Chemical effects of alteration

Representative electron microprobe analyses and structural formulae of pyrochlores from the MSF are given in Table 4.3. The complete data set can be found in appendix D. The same elements analysed for samples belonging to the FDF have been analysed for the MSF. However for several samples Ba has been removed from the analyses and Sm has been analysed in its place. Similarly, in a number of samples F has not been analysed, however in those samples where F has been analysed the F content is extremely low (typically <1 wt %) and has been demonstrated to decrease with higher degrees of alteration.

When plotted in the Ti-Nb-Ta ternary diagram, modified after Nickel (1992), all of the pyrochlore samples form the MSF plot within the pyrochlore sub-group of Hogarth (1977) (Fig. 4.7). Despite the striking differences in texture and inferred alteration histories the composition of the major *B*-site cations in the MSF and FDF pyrochlores are very similar. Pyrochlores from the MSF show a slight depletion of Nb in preference for Ti. Pyrochlores from sample GJM06-64 show both secondary alteration and areas which retain primary magmatic features. It should be noted that although areas which appear unaltered in the MSF pyrochlores are referred to as 'primary' these likely represent areas which have previously undergone a primary phase of alteration (as is seen in the FDF pyrochlores) rather than representing true magmatic features. Regardless of the state of alteration (magmatic, primary or secondary alteration), there appears to be no change in the *B*-site composition of the Motzfeldt pyrochlores with reference to the grouping scheme of Hogarth (1977). This suggests that alteration associated with both high-temperature juvenile fluids and lower temperature evolved fluids does not significantly affect the major *B*-site cations (Nb, Ta and Ti). Therefore, any *B*-site compositional variation likely represents an inherent magmatic feature rather than a product of alteration. However, it has been demonstrated using electron microprobe element mapping that Nb is found in veins entering/exiting pyrochlores from sample GJM05-44. Whether Nb has been mobilised from the pyrochlore during the sub-solidus or is host within a sub-micron unidentified mineral phase is unclear.

Table 4.3. *Representative EPMA compositions of pyrochlores from the Motzfeldt Sø Formation*

	Magmatic pyrochlores					Altered pyrochlores				
Wt.%	64-20-3	64-20-4	64-5-3	64-5-5	64-21-6	64-5-18	64-20-9	64-8-12	65-13-3	64-5-17
Na_2O	7.20	6.00	4.69	4.71	3.23	1.98	1.36	0.66	0.77	n.d.
CaO	9.77	10.38	9.52	9.07	10.39	11.94	10.97	8.31	9.33	12.22
MnO	0.05	0.05	0.10	0.10	0.41	0.75	0.35	0.89	0.25	0.82
SrO	0.17	0.08	0.04	0.15	0.10	0.62	0.48	0.76	1.12	0.14
PbO	0.14	0.23	0.49	0.28	0.16	0.50	0.14	0.00	0.15	0.00
ThO_2	0.18	0.17	0.31	0.35	0.23	0.16	0.24	0.27	0.27	0.17
UO2	3.38	3.89	3.71	3.98	3.85	3.31	3.76	3.39	4.33	2.97
La_2O_3	1.15	0.96	1.54	1.38	1.05	1.60	0.85	0.72	0.80	1.98
Ce_2O_3	2.44	2.45	2.52	2.96	2.21	2.72	2.09	1.62	2.36	3.76
Pr_2O_3	0.25	n.d	0.40	n.d	0.19	0.19	0.05	0.12	0.24	0.57
Nd_2O_3	0.84	0.87	0.81	0.63	0.64	1.01	0.60	0.58	0.50	1.03
Sm_2O_3	0.06	0.21	0.18	0.14	0.16	0.06	n.d	n.d	n.d	0.18
Gd_2O_3	0.01	n.d	n.d	0.03	nd	0.13	n.d	0.11	0.02	0.01
Dy_2O_3	0.25	0.01	0.04	0.06	0.18	0.13	0.10	n.d	n.d	0.12
Yb_2O_3	n.d	n.d	0.12	n.d	n.d	0.07	n.d	n.d	0.04	n.d
SiO_2	1.69	1.52	1.33	1.06	2.41	1.99	1.46	4.48	6.57	2.04
ZrO_2	0.82	1.10	1.15	1.17	1.25	0.67	0.95	0.84	0.92	0.58
Nb_2O_5	57.21	55.70	56.07	54.83	58.41	52.95	57.44	55.36	48.90	55.87
Ta_2O_5	4.61	5.16	5.71	5.60	4.31	5.57	4.49	4.14	6.05	5.18
TiO_2	7.81	8.01	7.97	8.23	7.89	7.21	8.38	7.62	7.19	7.90
FeO	0.27	0.18	0.07	0.21	0.36	1.83	0.64	5.37	2.33	2.96
F	2.18	n.d	2.16	3.81	1.23	0.82	2.14	0.17	0.44	n.d
Total	**98.46**	**97.08**	**98.94**	**98.81**	**98.78**	**96.24**	**96.78**	**95.39**	**92.87**	**98.62**
Structural Formulae (∑B-site cations = 2)										
Na	0.418	0.351	0.272	0.276	0.183	0.123	0.077	0.040	0.050	-
Ca	0.627	0.671	0.610	0.586	0.652	0.819	0.692	0.551	0.675	0.795
Mn	0.003	0.003	0.005	0.005	0.020	0.041	0.018	0.047	0.014	0.042
Sr	0.006	0.003	0.001	0.005	0.003	0.023	0.017	0.027	0.044	0.005
Pb	0.002	0.004	0.008	0.005	0.003	0.009	0.002	-	0.003	-
Th	0.002	0.002	0.004	0.005	0.003	0.002	0.003	0.004	0.004	0.002
U	0.045	0.052	0.049	0.053	0.050	0.047	0.049	0.047	0.065	0.040
La	0.026	0.021	0.034	0.031	0.023	0.038	0.018	0.016	0.020	0.044
Ce	0.054	0.054	0.055	0.065	0.048	0.064	0.045	0.037	0.058	0.084
Pr	0.005	-	0.009	-	0.004	0.004	0.001	0.003	0.006	0.012
Nd	0.018	0.019	0.017	0.014	0.013	0.023	0.013	0.013	0.012	0.022
Sm	0.001	0.004	0.004	0.003	0.003	0.003	-	-	-	0.004
Gd	-	-	-	0.001	-	0.003	-	0.002	0.001	-
Dy	0.005	-	0.001	0.001	0.003	0.002	0.002	-	-	0.002
Yb	-	-	0.002	-	-	0.001	-	-	0.001	-
Si	0.101	0.092	0.080	0.064	0.141	0.127	0.086	0.277	0.444	0.124
Fe	0.014	0.009	0.003	0.011	0.018	0.098	0.032	0.278	0.132	0.150
∑A	**1.327**	**1.285**	**1.154**	**1.123**	**1.168**	**1.425**	**1.055**	**1.342**	**1.530**	**1.327**
Nb	1.524	1.519	1.515	1.495	1.548	1.536	1.530	1.550	1.493	1.536
Ta	0.089	0.085	0.093	0.097	0.069	0.097	0.072	0.070	0.111	0.086
Ti	0.354	0.364	0.358	0.373	0.348	0.347	0.371	0.355	0.365	0.360
Al	-	-	-	-	-	-	-	-	-	-
Zr	0.033	0.032	0.034	0.034	0.036	0.021	0.027	0.025	0.030	0.017
∑B	**2**	**2**	**2**	**2**	**2**	**2**	**2**	**2**	**2**	**2**
F	0.355	0	0.307	0.648	0.209	0.149	0.377	0.030	0.081	-

All sample numbers have prefix GJM06. Total Fe expressed as FeO. n.d = not detected. n.a = not analysed. Fluorine is located in the *Y*-site and has not been included in structural recalculations.

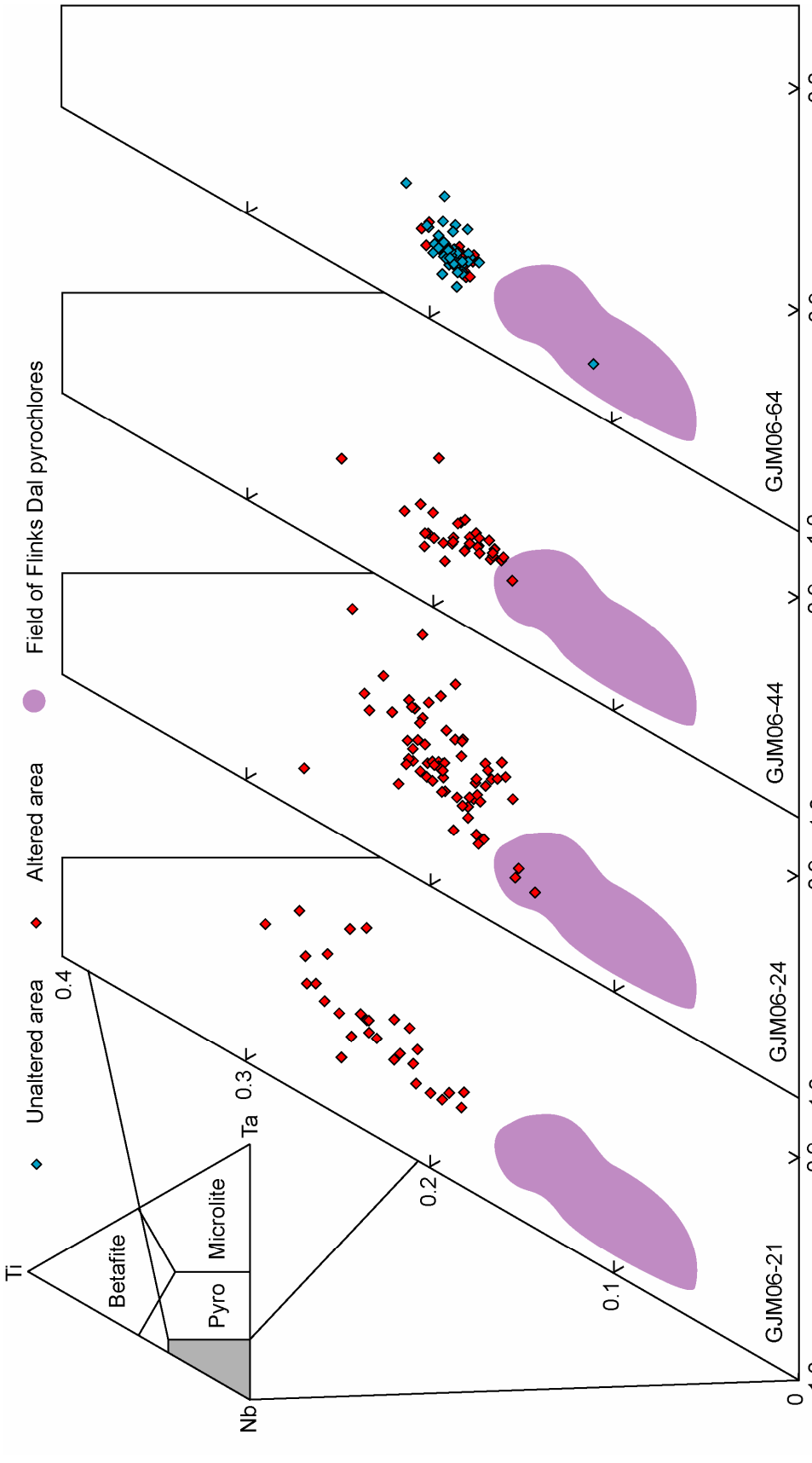

Fig.ure 4.7. *B*-site element chemistry of pyrochlore group minerals from the Motzfeldt Sø Formation (samples GJM06-21, GJM06-24, GJM06-44 and GJM06-64), projected onto the Nb-Ta-Ti ternary diagram (Hogarth, 1977), modified according to the 50% rule of Nickel (1992). Shaded area shows the field for unaltered pyrochlores from the Flinks Dal Formation.

None of the minor *A*-site cations exceed 20 % of the *A*-site total, with the exception of Pb which is found in two samples between 7-22 wt. %. Therefore the bulk of pyrochlores from the MSF can be classified pyrochlores senso stricto. Those containing high Pb may be classified as plumbopyrochlores according to the classification scheme of Hogarth (1977), however these samples will be discussed in detail below. Comparison of unaltered pyrochlores with pyrochlores showing alteration of primary and secondary origin shows no discernable variation in *B*-site cation behaviour, regardless of the state of alteration. However chemical exchange in the cubic *A*-site is much more variable with alteration. During primary alteration in the FDF pyrochlores show exchange in the *A*-site for K, Sr, Na and Ca and variable increases in Fe, Mn, REEs and *A*-site vacancies. Alteration within the MSF is characterised by similar trends though the more pervasive nature of the alteration has produced a higher degree of element mobility.

Examination of pyrochlores from sample GJM06-64 best demonstrate the chemical effects of this secondary phase of alteration as this sample hosts several pyrochlore crystals which retain areas of primary alteration and fresh magmatic areas, as well as areas overprinted by the pervasive microfracture controlled phase of alteration. Many of the other crystals examined have been intensely overprinted by a secondary phase of alteration and retain no chemical signature of earlier primary compositions. Therefore, these samples will be discussed with reference to the end composition of the alteration process, and any inferences on alteration trends will be made from sample GJM06-64.

Chemical effects of secondary alteration change the bulk crystal chemistry considerably form the primary compositions, this is particularly well recorded in several pyrochlores from sample GJM06-64. Unaltered areas of pyrochlore from this sample contain significantly higher amounts of Na, Ca and F compared to areas which have experienced a secondary phase of alteration. Typical ranges for Na in "unaltered" areas are 0.003 to 0.590 apfu. Similarly, Ca ranges from 0.179 to 0.973 apfu and in samples where F has been measured typical ranges are 0.010 to 1.420. In contrast, altered areas are characterised by variable addition or removal of Ca and near complete removal of Na and F. Typical compositions in altered areas are 0.000 to 0.297 for Na and 0.516 to 0.952 for Ca. F has been shown to generally decrease during primary alteration. During secondary alteration any remaining F is typically completely leached from the sample.

Sample GJM06-64 (Fig. 4.8) shows that monovalent (A^{+}) cations (principally Na) are preferentially removed until a point where all monovalent cations are leached from the structure and the composition moves towards the 'A-site vacancies' apex of the diagram, as divalent (A^{2+}) cations (largely Ca) are removed. This trend suggests that lower valence cations are preferentially removed at a faster rate than higher valance cations. For all other pyrochlore bearing samples from the MSF pyrochlore crystals show compositions plotting close or along the A^{2+} - A-site vacancies face, suggesting near or complete removal of monovalent Na, as is expected from the trend observed for the FDF and GJM06-64 MSF samples.

Secondary alteration results in variable decreases in the *A*-site cations Fe, Mn and Pb. Typical decreases in these elements through alteration are 0.660 to 0.025 apfu for Fe and 0.140 to 0.040 apfu for Mn. Increases in Pb are extremely variable and highly localised, with increases up to 0.450 apfu occurring in some areas. The localised nature of such high Pb content raises some uncertainty on its structural incorporation as the high content may represent mixed analyses of microcrystalline Pb-rich inclusions, which have not been identified. Inclusions of microcrystalline galena in pyrochlores from laterite deposits from the Harding pegmatite have been reported by Lumpkin *et al.* (1986). Additionally such high levels of Pb incorporation would require a large increase in site vacancies to accommodate the large Pb cation. However, structural recalculations for Pb-rich pyrochlores in the MSF only show an increase in A-site vacancies up to 0.2 vacancies per formula unit. It is therefore suggested that the high lead content represents mixed analyses of microcrystalline Pb bearing mineral phases hosted within the pyrochlore, rather than localised lead enrichment in the actual pyrochlore structure. This is further supported by the fact that the occurrence of Pb to these levels is only found within two crystals from the whole dataset. The structural incorporation of silicon into the pyrichlore structure is contentious. However in the altered pyrochlores from the MSF Si is seen to increase up to 0.8 apfu. Incorporation of the large Si^{4+} cation into the structure would likely introduce significant structural vacancies, however there is no clear correlation between increased Si content and increased A-site vancancies. It is therfore suggested that the increased Si content in altered samples represents either mixed analyses of secondary mineral phases or analyses of Si hosted within altered or metamict domains of the crystal structure.

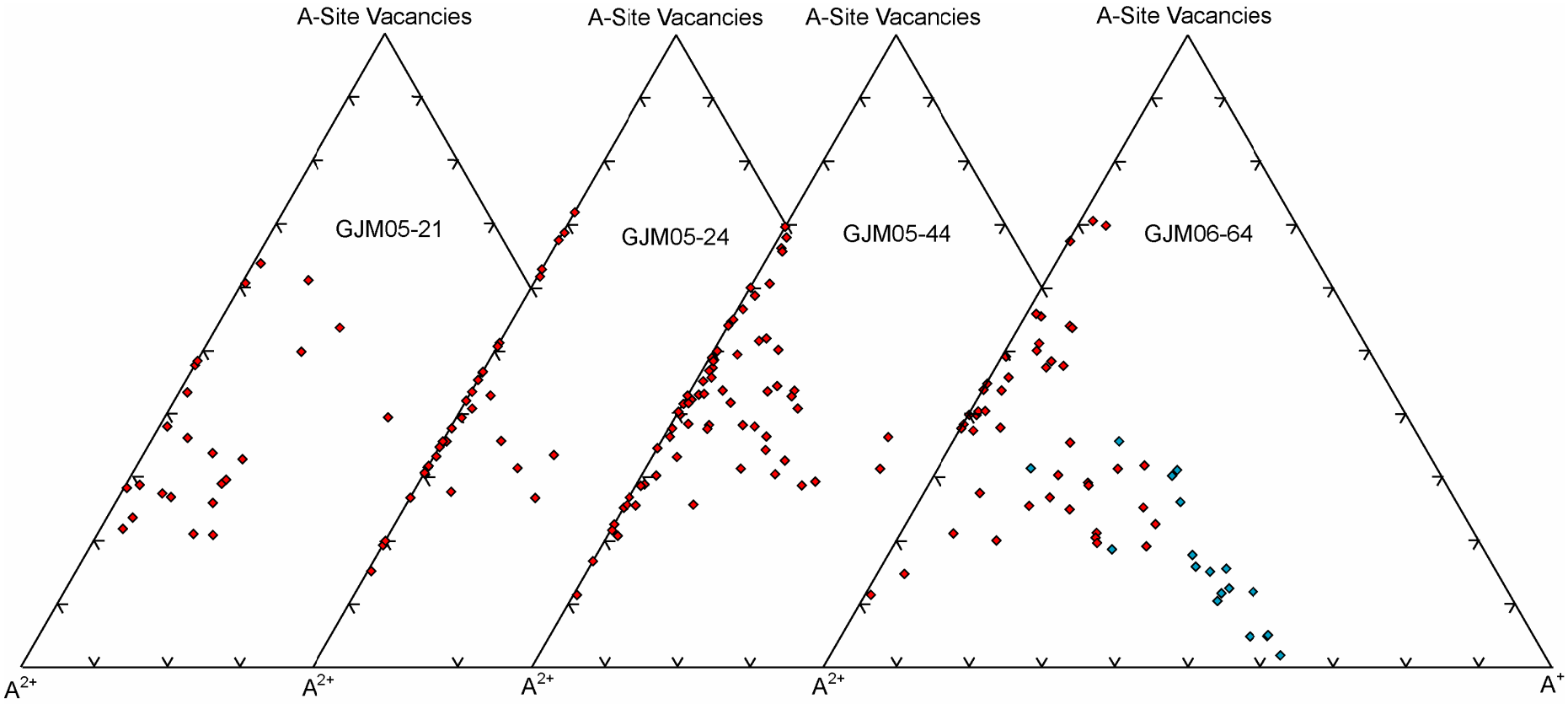

Figure 4.8. Ternary variation diagrams for divalent A-site cations (Ca, Fe, Mn and Sr), Monovalent A-site cations (Na) and A-site vacancies in samples from the MSF. Sample GJM06-64 shows analyses from "unaltered" areas (blue diamonds) in addition to analyses from altered areas in the same crystals (red diamonds). All other samples are from altered areas.

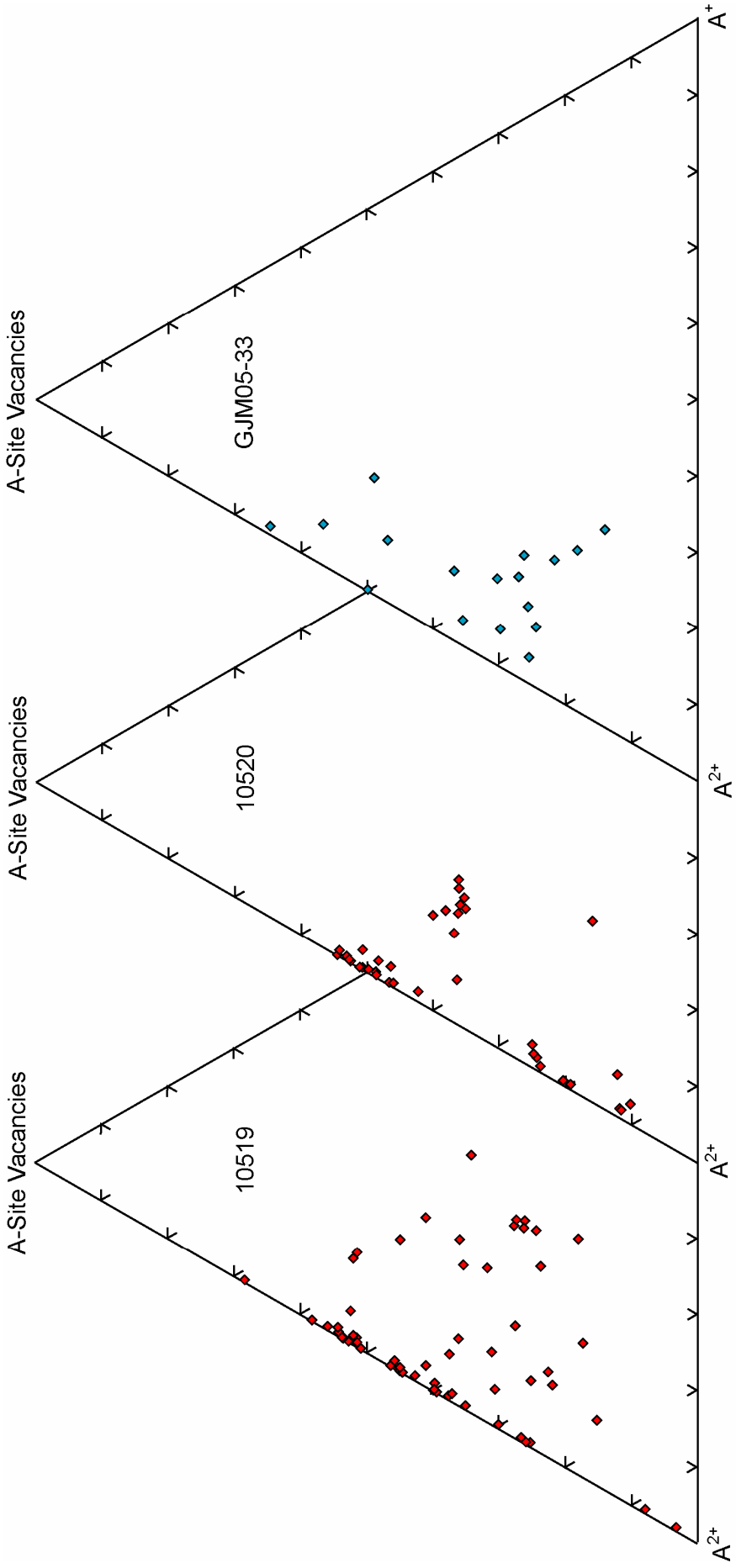

Figure 4.9. Ternary variation diagrams for divalent A-site cations (Ca, Fe, Mn and Sr), Monovalent A-site cations (Na) and A-site vacancies from secondary alreted pyrochlores from Angus and Ross samples (10519 and 10520) and unaltered accessory pyrochlores from sample GJM05-33.

As in the FDF, MSF pyrochlores are strongly enriched in the light lanthanides La to Sm. La and Ce are particularly enriched, accounting for 65-85% of total REE. Typical values for La and Ce are 0.3-2.6 wt% and 1.5-5.7 wt%, respectively. Lanthanides heavier then Sm were rarely found >0.1 wt% of the total, with the exception of Dy which typically occurs from 0.05-0.5 wt%, though found up to 1.7 wt% in some samples. Where Ba has been measured, altered samples have contents up to 3.5 wt%, though typically fall within the range 0.2-1.5 wt%.

U and Th contents remain relatively constant in all samples, regardless of the state of alteration. In the primary altered areas of crystals form sample GJM06-64 the U content ranges from 0.035 to 0.040 apfu and Th ranges from 0 to 0.007 apfu. The range for the secondary altered areas of the same sample is 0.040 to 0.075 apfu for U and 0.001 to 0.006 apfu for Th. The MSF pyrochlores, which have been pervasively altered and preserve no record of older compositions, show a broader range of values for U and Th, typically ranging from 0.028 to 0.105 and 0.001 to 0.015 respectively. Data from highly altered pyrochlores from samples GJM05-21, 24 and 44 (Fig. 4.8) and Angus and Ross samples 10519 and 10520 (Fig. 4.9) show similar compositions to the secondary altered zones observed in GJM06-64 suggesting similar trends of alteration from a similar start composition.

A result of the relatively high U content within the MSF pyrochlores (typically 3-5 wt. %) is a large number of samples showing features characteristic of radiation induced structural damage. The most characteristic of these is the presence of fractures, through which secondary alteration is intimately associated, and large radial and concentric fractures concentrated on the margins of the crystals. X-ray powder diffractograms (Fig. 4.10) for altered pyrochlores from samples GJM06-64 and GJM06-65 show low peak intensities and high background values. Diffraction peaks are also relatively broad and weakly defined. Each of these features suggests poor crystallinity and the presence of amorphous material, which are all characteristic of metamict or radiation damaged domains of the pyrochlore structure.

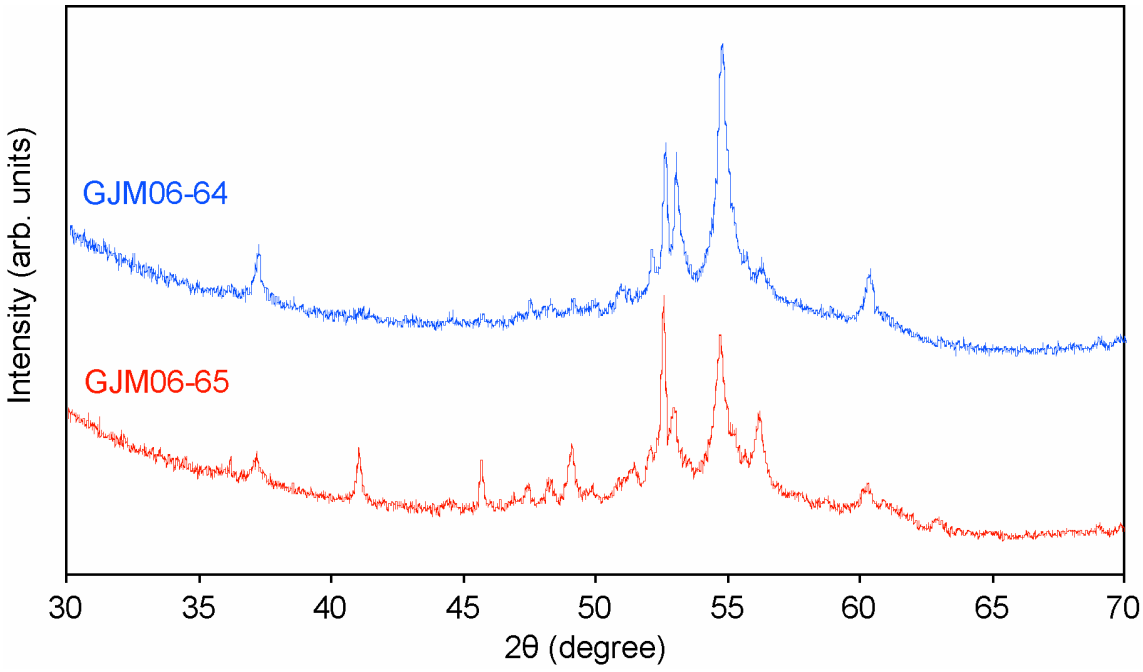

Figure 4.10. X-ray powder diffractograms from altered pyrochlore samples GJM06-64 and GJM06-65. See text for description.

4.5 Discussion

4.5.1 Genesis and conditions of alteration in the Flinks Dal Formation

The complex textures grading from simple oscillatory to more complex sector zoning in crystals from the FDF and microfracturing, radiation damage and intense compositional changes in the MSF indicate that pyrochlore group minerals from the Motzfeldt centre encode textural and chemical information relating to a complex magmatic history followed by multiple phases alteration during the sub-solidus. Spatial and temporal variations in the hydrothermal activity of the centre has allowed the progressive alteration of pyrochlore group minerals to be studied and has provided information on the contrasting sub-solidus histories found in the mineralised units of the MSF and the less altered syenites of the FDF.

Pyrochlores from the FDF show well preserved oscillatory and sector zoning. From core to rim FDF pyrochlores show a steady depletion of Ta and constant Nb content. Dark BSE zones show relative enrichment of Na, F and varied enrichment of Ca. U and Ti are notably depleted in the darker BSE zones and show a general depletion from core-to-rim. Several models have been developed to explain the generation of regular fluctuations in chemical composition and oscillatory zoning and are reviewed by Pearce (1994) and Shore and

Fowler (1996), with particular reference to the development of feldspar zonation. Hogarth *et al.* (2000) suggest the origin of oscillatory zoning and regular cyclic fluctuations in the composition of pyrochlore group minerals can be explained by a melt, supersaturated in Nb, Ta, U and other minor elements, evolving in-situ under relatively tranquil conditions. During cooling layers enriched in elements at their threshold saturation are successively precipitated at the liquid/crystal interface. Precipitation continues until the next threshold is reached and the process is repeated through disequilibrium feedback model. The planar nature of layer precipitation means that crystals maintain a euhedral faceted morphology throughout their growth history, providing a relatively stable crystallisation environment is maintained.

In a number of FDF pyrochlores sector zoning is also observed. Hodgson and Le Bas (1992) examined sector-zoned pyrochlores from carbonatites on the Cape Verde Islands. From their observation they suggest magma mixing to be the principal control, rather than the disequilibrium feedback model, suggesting convection and liquid mobility of the low viscosity melt would greatly inhibit the diffusion feedback mechanism. The presence of both sector and oscillatory zonation in the FDF pyrochlore minerals makes it difficult to model pyrochlore growth exclusively by one or the other of these models and is a problem raised by Hogarth *et al.* (2000). Therefore it may be suggested that such variations in zonation are a highly localised phenomena, attributed to small scale convection and mingling of comparable melts (similar P, T and *X*). Alternatively, there may be more than one generation of pyrochlore, of identical or similar age, formed as a result of several stages of crystallisation during the emplacement of the formation.

In addition to magmatic compositional variations, chemical changes associated with alteration are also observed in the FDF pyrochlore population. Crystals show irregular fronts of diffusive alteration cross-cutting primary growth zones. Alteration gives the crystal a washed-out BSE emission and is characterised chemically by a loss of Na, Ca and F, variable increases in Sr and K and generation of *A*-site vacancies. Intra-crystalline diffusion controlled alteration has been identified in a number of studies (e.g. Chakhmouradian and Mitchell, 1999, 2002; Chakoumakos and Lumpkin, 1990) and has been studied in detail by Lumpkin (1989) and Lumpkin and Ewing (1992, 1995 and 1996). Lumpkin and Ewing (1995) suggest primary alteration of pyrochlore sub-group minerals, hosted within evolved high-level alkaline complexes (alkaline pegmatites, nepheline syenites and carbonatites), to occur at relatively low temperatures. Experimental petrology and field observations suggest solidus temperatures as low as 400-600 °C for alkaline magmas, with a continuum into an alkaline hydrothermal phase

to temperatures as low as 200-350 °C. Chemical exchange between pyrochlore crystals and residual fluids suggest conditions of relatively high pH with high Na and Ca activity and elevated Sr activity. Despite the low degree of alteration observed in the pyrochlore crystals hydrothermal activity in the FDF was relatively restricted, when compared to the more heavily altered units of the MSF. Bradshaw (1988) demonstrated that the FDF, although enriched in F, Cl and C components (like many Gardar magmas), is relatively anhydrous. The elevated volatile content would have extended the crystallisation interval of the FDF, however deuteric alteration of primary mineral phases was restricted due to the low water content. Therefore the diffusive alteration observed in the FDF pyrochlores seems likely to be intimately associated with a residual fluid exsolved from the melt during the final stages of crystallisation, with little contribution from externally derived fluids.

4.5.1 Conditions of alteration in the Motzfeldt Sø Formation

Pyrochlores from the MSF show textural and chemical features distinctive of intense and pervasive sub-solidus alteration. Unlike the FDF, the MSF pyrochlore population preserves little or no evidence of original magamtic compositional variations. Primary magmatic zoning has been wholly overprinted by a primary phase of alteration, followed by subsequent development of a pervasive network of microfractures, associated with which is an intense secondary phase of alteration. Chemical exchange during secondary alteration is more extreme than the primary alteration encoded in the FDF pyrochlores and is characterised by near complete loss of Na and F, reduced Ca, varable increases in Fe, Mn and REEs and major increases in A-site vacancies. H_2O contents inferred from low analytical totals also show considerable increases.

The alteration encoded in pyrochlores from the MSF seems to have been generated through multiple phases of alteration, spanning a range of thermal and chemical conditions. From observations made from FDF pyrochlores, which are though to have crystallised from a relatively anhydrous melt, it seems likely that pyrochlore from the MSF have experienced an extended sub-solidus history developed under a more complex hydrothermal regime, unique to the MSF, where volatile rich magmatically-derived fluids evolved through interaction with hydrothermally circulated groundwaters (chapters 5 and 6). The MSF is recognised as being one of the first intrusive phases during the emplacement of the Motzfeldt centre (Emeleus and Harry, 1970), emplaced into the Majût and Massartût members of the lower Eriksfjord formation (Larsen & Tukiainen, 1985). These units comprise typically siliciclasitc sediments

and subordinate volcanic components. The FDF was later emplaced to a higher structural level into the Ilímaussaq member of the Eriksfjord, comprising trachytes and phonolites (Poulsen, 1970). Bradshaw (1988) suggested that the Majût and Massartût members, into which the MSF was emplaced, contained a higher proportion of formation water than the overlying Ilímaussaq member and were likely more permeable and susceptible to groundwater circulation. From this observation it is suggested that the interaction of juvenile fluids with thermally convecting groundwaters reduced the pH of the hydrothermal fluid, in the outer and upper units of the MSF, increasing the activity of Fe, Mn and REEs and promoting a secondary pervasive phase of alteration. Similar systems have been described by Andersen (1984, 1986 and 1987) for the Fen carbonatite massif in Norway and by Flohr (1994) for the Magnet Cove alkaline complex in Arkansas. The alteration observed in pyrochlores from the MSF is in agreement with the model of Bradshaw (1988) and shows many striking similarities to the models of Andersen (1984, 1986 and 1987) and Flohr (1994), suggesting fluid evolution leads from dominantly juvenile during the magmatic stage, during which primary diffusive alteration occurs, to groundwater-derived aqueous fluids during post-magmatic re-equilibration. In the FDF however only the primary phase of alteration generated through interaction with juvenile fluids is observed. Because the FDF is completely enclosed within the MSF this would have considerably reduced the circulation of groundwaters, inhibiting the secondary lower temperature phase of alteration generated through groundwater interaction.

4.6 Conclusions

Pyrochlore group minerals from the Motzfedlt centre show striking differences in texture and microchemical character depeding on which formation they are located. Samples from the FDF preserve primary magmatic compositional zoning and are overprinted in restricted areas by diffusive areas of primary alteration. In pyrochlore from the MSF primary features, as observed in the FDF, are wholly overprinted by pervasive alteration, characterising a different subsolidus history to the pyrochlores of the FDF. Pyrochlore crystals therefore serve as a useful indicator of the different geochemical conditions which the rocks of MSF and FDF experienced during the subsolidus evolution of the centre. Pyrochlore group minerals from the FDF display concentric growth zones characterising compositional fluctuation on the magma chamber during the evolution of the host melt. Although pyrochlore from the FDF are largely pristine a number of samples have undergone alteration under subsolidus conditions, characterised by mobility of Na & Ca and replacement with Sr & K. Textures associated with this phase of alteration form a clear diffusive front penetrating

into the crystal. The textural and microchemical characteristics of alteration in the FDF are consistent with a relatively high temperature phase of alteration associated with the final stages of crystallisation. Experimental work of Lumpkin and Ewing (1995) suggest that such textural and chemical features are generated in the presence of a high pH, juvenile magmatic fluid, over a temperature interval of ca. 500-300°C. In the MSF the textural character of alteration is intense and pervasive, penetrating pyrochlore throught a network of microfracures. During this phase of alteration pyrochlores are leached of cations and significantly hydrated. These features are consistent with lower temperature phase of alteration associated with low pH evolved fluids (Lumpkin & Ewing, 1995). The alteration encoded in the pyrochlores of the present study therefore reflects the different hydrothermal conditions the MSF and FDF experienced during the subsolidus.

Chapter 5

Biotites as Indicators of Fluorine Activity

5.1 Introduction

The mineral chemistry and halogen contents of micas have been the focus of much interest in the fields of petrology and geochemistry over the past few decades, as they can be used as potential indicators of the F and Cl contents of silicate melts and aqueous fluids associated with the emplacement of igneous bodies (Munoz, 1984, Munoz & Ludington, 1974). The basic biotite structure ($K_2(Fe,Mg)_6Si_6Al_2O_{22}(OH,F,Cl)_2$) comprises a unit containing two tetrahedral sheets and one octahedral sheet (Fig. 5.1). The tetrahedral sheet contains individual $(Si,Al)O_4$ tetrahedra linked together in a hexagonal mesh through sharing of the basal tetrahedral oxygens. The octahedral layer comprises a layer of *Y* cations (mainly Mg, Fe^{2+} and Al, though Mn, Cr, Ti and Li are also found) bound between two oppositely directed tetrahedral layers through sharing of the apical tetrahedral oxygen. Between each tetrahedral/octahedral unit is a layer of *X* cations (mainly K, Na and Ca) (Bailey, 1984). Within the biotite structure are OH groups in the centre of each 6-fold ring of $(Si,Al)O_4$ tetrahedra at the same level as the apical oxygens (Bailey, 1984; Deer *et al.,* 1992). The OH^- ion can be substituted by halides, particularly F^- and Cl^-. The halogen content of magmatic biotite therefore reflects the activities of these halogens at the time of biotite crystallisation. However, since halogen and OH groups are relatively weakly bonded in biotite they can readily substitute for F and Cl down to relatively low temperatures. Halogen contents of biotites are therefore not necessarily preserved from the magmatic OH, F and Cl composition of the melt but can be modified and therefore reflect the halogen content of late-stage fluids which interacted with biotites post-crystallisation.

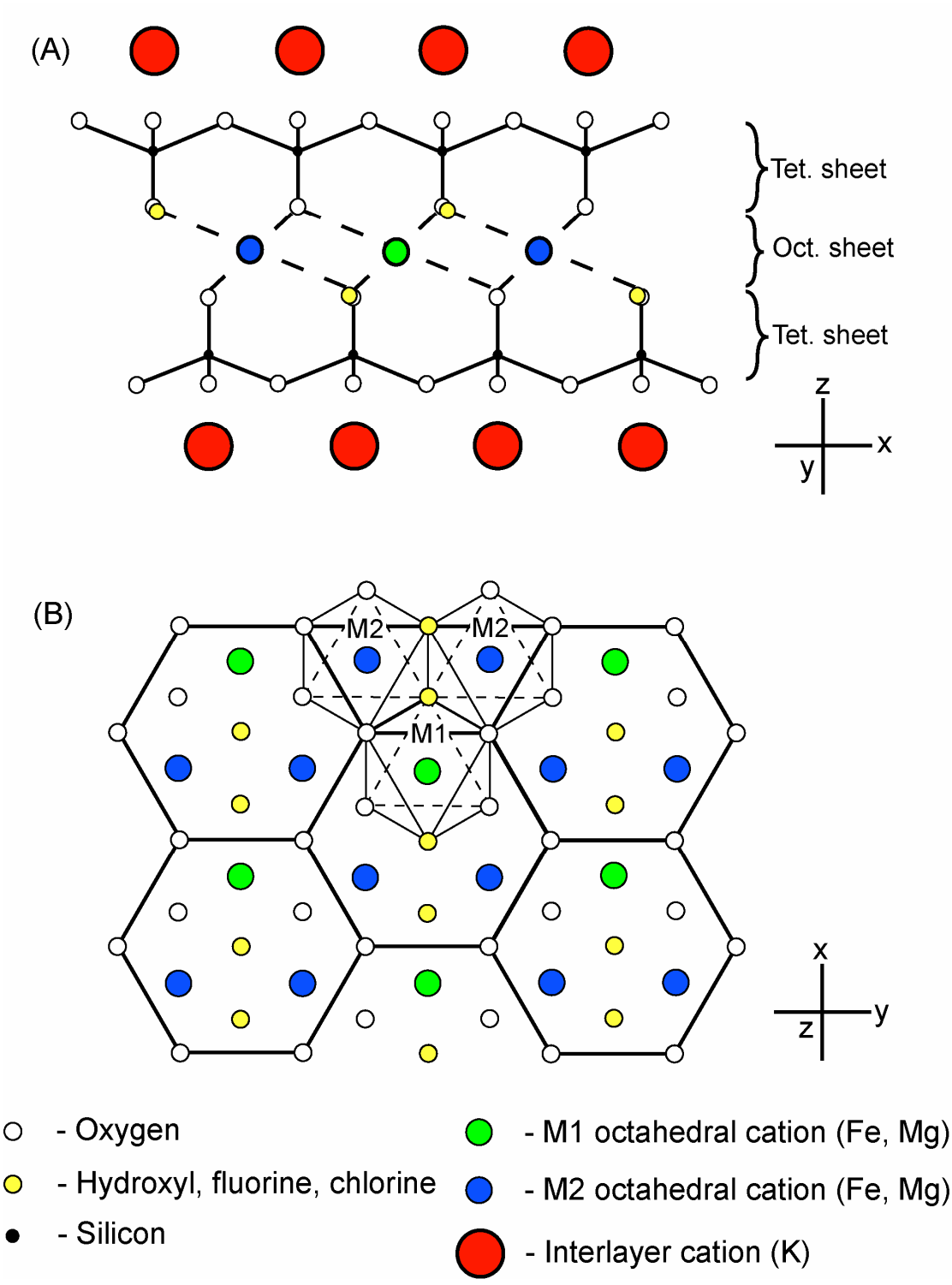

Figure 5.1. (a) Stylised crystal structure of biotite viewed down the y crystallographic axis, showing 1 octahedral sheet bound between 2 sheets of tetrahedra. (b) Stylised octahedral mica sheet showing the relative position of the M1 and M2 sites and hydroxyl sites.

5.2 Systematics of F-OH exchange in biotites

Fluorine is a common component of evolved mantle-derived alkaline melts and as such is a common constituent of micas associated with melts of this type. The substitution of fluorine and other halogens for OH groups in biotite micas is controlled by several factors which are dependant on the physiochemical character of the biotite and fluid. The controls of halogen exchange in biotite micas may be summarised as 1) the activity of the halide ion or halogen acid present during crystallisation and/or during sub-solidus fluid interaction; 2) the cations populating the octahedral sites (namely Fe^{2+}, Mg or Al); 3) the temperature of halogen-hydroxyl exchange, and 4) the effect of post-crystallisation leaching and interaction in the presence of (OH-rich) groundwaters (Munoz & Ludington, 1974; Munoz, 1984; Mason, 1992). Each of these factors will be discussed for the biotites from the MSF and FDF. However before samples of the present study are discussed, a review of the theoretical basis of halogen-hydroxyl exchange will be given to aid in the understanding of results presented during this chapter.

Halogen-hydroxyl exchange in biotite micas was first discussed in detail by Munoz and Ludington (1974) who showed that F:Cl:OH ratios in biotite micas may be reset post-crystallisation following re-equilibration with hydrothermal fluid(s) under sub-solidus conditions. The equilibrium exchange reaction between a biotite mica and fluorine-dominated silicate melt or fluid phase may therefore be defined as (ignoring Cl):

$$\mathrm{Mica(OH) + HF = Mica(F) + H_2O} \qquad (1)$$

An equilibrium constant, *K*, may be defined for this reaction by dividing the activities of the products by the activity of the reactants (where a_X represents the activity of $_X$) and may be written in logarithmic form as:

$$\log K = \log\left[\frac{a_{\mathrm{F}}}{a_{\mathrm{OH}}}\right]^{mica} + \log\left[\frac{a_{H_2O}}{a_{\mathrm{HF}}}\right]^{fluid} \qquad (2)$$

If we assume that each phase in this system behaves ideally at a pressure of 1 bar for a given temperature the fluid activity (*a*) can be replaced by fugacity (where f_X represents the fugacity of $_X$). Equation 2 can be further simplified by assuming that ideal mixing of F-OH occurs in the hydroxyl site of the mica, allowing substitution of mole fraction of anions for

activities in the mica (where X_X represents the mole fraction of $_X$). Therefore, following these assumptions equation 2 may be simplified to:

$$\log K = \log\left[\frac{X_F}{X_{OH}}\right]^{mica} + \log\left[\frac{f_{H_2O}}{f_{HF}}\right]^{fluid} \quad (3)$$

In addition to the speciation of the fluid, exchange in the hydroxyl site is also influenced by the temperature of the equilibrating fluid(s) and the composition of the mica, particularly the cationic occupancy of the octahedral sites to which OH or F are bound. Taking into account each of these variables Munoz and Ludington (1974) experimentally determined equilibrium constants for a range of synthetic biotite compositions (annite, phlogopite, siderophyllite) over a range of temperatures (Table 5.1). This work demonstrated that the fluoride-hydroxyl distribution coefficients (*K*) varied considerably between micas, notably between the two biotite solid-solution end-members annite $[K_2Fe_6(Si_6Al_2O_{22})(OH,F)_2]$ and phlogopite $[K_2Mg_6(Si_6Al_2O_{22})(OH,F)_2]$. They observed that biotites with high iron contents (high Mg/Fe ratios) were much less effective at removing F from the equilibrating fluid than those which have lower iron contents (low Mg/Fe ratios). This phenomenon has been observed in a number of studies concerning hydroxyl-bearing ferromagnesian silicate minerals (e.g. amphiboles, Oberti *et al.,* 1993). Because of the strong preference of F to exchange with minerals which are less rich in iron, the principal is referred to as "Fe-F avoidance" (Rosenberg & Foit, 1977).

Table 5.1. *Exchange equilibrium constants for halogen-hydroxyl exchange in biotites*

Composition	Log K
Phlogopite	2100/T + 1.523
Annite	2100/T + 0.416
Siderophyllite	2100/T + 0.200

Equilibrium constants defined by Munoz and Ludington (1974; 1977) for fluid pressures of 1 or 2 kbar over a temperature range of 673-1000 K.

Application of the equilibrium constants defined by Munoz and Ludington (1974) to natural micas is somewhat complicated through occupancy of the octahedral site by elements other then Fe^{2+}, Mg and Al. In many sample this includes, Fe^{3+}, Mn, Ti and Li. The second complication comes from uncertainties in determining the F:OH ratio of the hydroxyl sites and mixing in the octahedral site. Unfortunately there are no data available to evaluate deviation from ideal mixing in these sites. Therefore in order to apply the equations of Munoz

and Ludington (1974) to natural samples ideal mixing is assumed. For systems where ideal mixing (complete disorder) in a multi-site solid-solution occurs, Wood and Nichols (1978) demonstrated that an exchange reaction can be defined as $AX + BY = AY + BX$. Gunow *et al,* (1980) applied this expression to the biotite solid-solution for simultaneous mixing of Mg, Fe^{2+}, OH and F, assuming complete disorder in all sites concerned. This allows the expression of Wood and Nichols (1978) to be written as:

$$\text{phlogopite(OH)} + \text{annite(F)} = \text{phlogopite(F)} + \text{annite(OH)} \qquad (4)$$

Using the experimental data of Munoz and Ludington (1974) (Table 5.1) allows calculation of any intermediate (Mg, Fe)(OH, F) biotite using the methods defined by Gunow *et al.* (1980). For the phlogopite end member the reaction can be defined as follows, assuming ideal mixing:

$$\log K = \frac{2100}{T} + 1.523 = \log\left[\frac{a_{\text{Fph}}}{a_{\text{OHph}}}\right]^{bio} + \log\left[\frac{f_{H_2O}}{f_{\text{HF}}}\right]^{fluid} \qquad (5)$$

where a_{Fph} and a_{OHph} represent the activities of fluorine and hydroxyl anions in the phlogopite end member. Since 1.5 cationic sites exist for each hydroxyl site in biotite micas then according to the ideal mixing model the activity terms can be replaced by mole equivalents becoming: $a_{\text{Fph}} = X_{\text{Mg}}^{1.5} X_{\text{F}} \gamma_{\text{Fph}}$ and $a_{\text{OHph}} = X_{\text{Mg}}^{1.5} X_{\text{OH}} \gamma_{\text{OHph.}}$ Equation 5 can now be written as:

$$\log K = \frac{2100}{T} + 1.523 = \log\left[\frac{X_{\text{F}}}{X_{\text{OH}}}\right]^{bio} + \log\left[\frac{\gamma_{\text{Fph}}}{\gamma_{\text{OHph}}}\right]^{bio} + \log\left[\frac{f_{H_2O}}{f_{\text{HF}}}\right]^{fluid} \qquad (6)$$

Where γ_{Fph} and γ_{OHph} are the activity coefficients of F and OH for the particular Mg/Fe composition of the biotite, at a given temperature (Gunow *et al.,* 1980). The activity coefficients for both OH and F in phlogopite have also been defined experimentally by Wood and Nichols (1978) as:

$$\log \gamma_{\text{OHph}} = -X_{\text{Fe}} X_{\text{F}} \log K \qquad (7)$$

$$\log \gamma_{\mathrm{OHph}} = X_{\mathrm{Fe}} X_{\mathrm{OH}} \log K \tag{8}$$

If we assume the hydroxyl site is fully occupied and only contains F and OH, substituting $X_{OH} = 1 - X_F$ (Wood & Nichols, 1978) into equations 7 and 8 allows simplification to:

$$\log\left[\frac{\gamma_{\mathrm{Fph}}}{\gamma_{\mathrm{OHph}}}\right] = X_{Fe} \log K \tag{9}$$

Substituting this into equation 6 the equilibrium constant can be written as

$$\log K = \frac{2100}{\mathrm{T}} + 1.523 X_{\mathrm{Mg}} + 0.416 X_{\mathrm{Fe}} = \log\left[\frac{X_{\mathrm{F}}}{X_{\mathrm{OH}}}\right]^{bio} + \log\left[\frac{f_{\mathrm{H_2O}}}{f_{\mathrm{HF}}}\right]^{fluid} \tag{10}$$

Where X_{Mg} is molar fraction of octahedral Mg in the octahedral site. During this study X_{Mg} has been calculated as X_{Mg} = Mg/(Mg+Fe) which assumes the octahedral site contains only Mg and Fe and is fully occupied. Similarly, X_{Fe} is the molar fraction of Fe in the octahedral site and has been calculated as X_{Fe} = Fe/(Fe+Mg). Equation 10 may now be rearranged to calculate the fugacity ratio of the late-stage fluid (equation 11) in equilibrium with the biotite (Munoz, 1984). Similarly, equation 10 may also be rearranged to calculate the molecular ratio of F/OH in the biotite mica (equation 12) assuming the fluid fugacity is already known.

$$\log\left[\frac{f_{\mathrm{H_2O}}}{f_{\mathrm{HF}}}\right]^{fluid} = \frac{2100}{T} + 1.523 X_{\mathrm{Mg}} + 0.416 X_{\mathrm{Fe}} - \log\left[\frac{X_{\mathrm{F}}}{X_{\mathrm{OH}}}\right]^{bio} \tag{11}$$

$$\log\left[\frac{X_{\mathrm{F}}}{X_{\mathrm{OH}}}\right]^{bio} = \frac{2100}{T} + 1.523 X_{\mathrm{Mg}} + 0.416 X_{\mathrm{Fe}} - \log\left[\frac{f_{\mathrm{H_2O}}}{f_{\mathrm{HF}}}\right]^{fluid} \tag{12}$$

Munoz (1984) suggests further modifications to the basic equation to accommodate the siderophyllite (Al biotite end member) component of the biotite. However the siderophyllite component X_{sid} = (octahedral Al/0.167)(1-X_{Mg}) (Parsons *et al.,* 1991) of biotites from the Motzfeldt centre are zero, with the exception of two samples which will be discussed later. Therefore the siderophyllite component is ignored in the present study.

5.3 Chemistry of biotites from the Motzfeldt centre

Previous studies concerning the halogen contents of biotites from the Gardar province (Finch, 1990; Finch, 1995: Finch *et al.,* 1995) have shown that the Motzfeldt centre has one of the highest inferred halogen activities within the province, comparable to the fluorine-rich Late Igdlerfigssalik and altered South Qôroq units. Finch (1990) and Finch *et al.* (1995) found no systematic differences in the halogen content of biotites in individual units of the Motzfeldt centre. However, biotite analyses during these studies were restricted to the relatively homogeneous and largely unaltered units of the Flinks Dal Formation (Finch, 1990). Previous studies concerning the petrology of the Motzfeldt centre have hinted that the halogen content and fluid evolution of the Motzfeldt Sø Formation played an important role in the genesis of the mineralisation within this formation (Bradshaw, 1988; Jones, 1980), yet it still remains unclear why mineralisation and alteration is restricted to the MSF and is largely absent elsewhere in the Motzfeldt centre. During this study we examined biotite micas from the highly altered and locally mineralised syenite units of the Motzfeldt Sø Formation (MSF) and from the less altered nepheline syenites of the Flinks Dal Formation (FDF) to evaluate the halogen contents of these formations.

The petrography of biotites from the MSF and FDF have been discussed in detail in previous chapters (chapter 3) therefore only a short overview of their textural relations will be given here. Biotite is found throughout the Motzfeldt syenites in varying abundance from several small flakes per thin section to samples containing large poikolitic phenocrysts. Several samples of large "mica books" have also been sampled from within the MSF. Most commonly biotite occurs as an intercumulus phase forming irregularly shaped platelets growing intercumulus to pyroxene and amphibole (e.g. GJM06-63). Less common are samples (e.g. GJM06-31) contain large poikolitic sheets of biotite hosting a range of mineral inclusions. In many samples small flakes of 'fringe biotite' growing in reaction coronas mantling small magnetite accessory mineral phases is also found (e.g. GJM05-23 & GJM06-87). Textural occurrences of biotite throughout the Motzfeldt centre suggest multiple phases of growth, associated with the magmatic and sub-solidus phases of the centre's history. Fringe biotites mantling ilmenomagnetite grains have been identified by Parsons *et al.* (1991) and by Finch *et al.* (1995) from other Gardar centres. Their formation has been suggested to occur through the sub-solidus reaction:

$$\underset{\text{Sanidine}}{KAlSi_3O_8} + \underset{\text{Magnetite}}{Fe_3O_4} + \underset{\text{Water}}{H_2O} = \underset{\text{Annite}}{KFe_3AlSi_3O_{10}(OH)_2} + \underset{\text{oxygen}}{1/2O_2}$$

To generate Mg-bearing biotites Parsons *et al.* (1991) suggested involvement of other mineral phases, principally pyroxene, in the reaction. The various textural relationships of micas analysed during this study appear to have no influence on their fluorine or major element chemistry.

A total of 128 electron microprobe analyses of 84 biotites were made from texturally distinct variants of altered syenite from the MSF and 115 analyses of 62 biotites from each major syenite facies in the FDF. Representative electron microprobe analyses are given in table 5.2, including calculation of numbers of atoms per 22 oxygens and site allocations for all major elements. The complete data set and site allocations are provided in appendix E. In performing site allocations it is assumed that the tetrahedral site is always filled (8 atoms per 22 oxygens) by Si and then in turn by Al and Fe. Any excess Al or Fe is subsequently allocated to the octahedral site. The interlayer site is occupied by K, Ca or Na only. In addition to the elements considered here, biotite can also contain significant amounts of other ions, such as Li, Cl, Ba, Rb and Be (Bailey, 1984). During wavelength dispersive analysis (WDS) Cl, Rb and Ba were monitored using EDS spectra. Levels of these elements were generally very low and considered insignificant for the purposes of this investigation. Li and Be could not be determined using the EDS spectra. However previous ion microprobe analyses of biotite from the neighbouring Igdlerfigssalik centre and Klokken layered stock show typically low concentrations for both Li (1-25 ppm) and Be (<2 ppm) (Finch *et al.,* 1995; Parsons *et al.,* 1991). Although these elements are known to occur in appreciable amounts in the agpaitic rocks of the Gardar, they are not know to reach significant levels in the miaskitic rocks of the province, which the Motzfeldt centre is classed. Therefore these elements have not been analysed as they are typically in very low concentrations and considered negligible in the biotites of the present study.

The interlayer site of all biotites from the MSF and FDF is dominated by K, which in many samples is close to the theoretical 2 atoms per 22 oxygens. Na is generally low in many of the biotites analysed, typically ranging from 0.02-0.25 atoms per 22 O in the MSF and 0.02-0.20 atoms per 22 O in the FDF. However biotites from sample GJM06-07 from the MSF contain higher Na contents up to 0.34 apfu. In this sample Ca is also elevated, reaching 0.04-0.08 apfu. In all other biotites analysed Ca is typically absent, though in a few samples from

the FDF reaches 0.02 apfu. Elevation of Na and Ca in this one sample may represent sub-optical inclusions of plagioclase or pyroxene, or clay mineral alteration of the biotite.

Table 5.2. *Representative EPMA analyses of biotites from the Motzfeldt centre*

	MSF			FDF			FDF raft
Wt.%	23-2-2	29-7-2	66-1-1	87-4-6	87-16-1	91-9-2	84-3-1
Na_2O	0.47	0.89	0.47	0.60	0.40	0.70	0.32
MgO	3.64	3.27	3.43	10.18	7.44	4.92	1.99
Al_2O_3	9.38	10.03	9.75	12.78	15.35	9.79	18.06
SiO_2	37.01	36.48	36.83	36.69	34.59	36.51	31.96
K_2O	9.11	9.83	10.51	9.89	9.93	9.63	10.59
CaO	0.00	0.00	0.00	0.03	0.00	0.03	1.97
TiO_2	3.29	5.03	5.33	3.93	3.17	2.68	2.64
MnO	0.35	0.74	0.68	1.23	1.38	1.31	0.38
FeO	32.69	30.96	29.26	19.55	23.83	30.26	26.97
F	0.98	1.09	1.07	2.46	1.51	0.46	1.16
Total	95.94	98.34	96.26	97.35	97.59	95.83	96.04
O≡F	0.41	0.46	0.45	1.04	0.63	0.19	0.49
Total	**95.53**	**97.88**	**95.81**	**96.31**	**96.96**	**95.83**	**95.55**
Fe/(Fe+Mg)	0.83	0.83	0.82	0.52	0.64	0.77	0.88
Al/(Al+Si)	0.08	0.25	0.14	0.15	0.11	0.07	0.08
Cations per 22 oxygen							
K	1.89	2.00	2.15	1.95	1.98	1.99	2.19
Na	0.15	0.28	0.15	0.18	0.12	0.22	0.10
Ca	0.00	0.00	0.00	0.00	0.00	0.00	0.34
Interlayer site	**2.03**	**2.28**	**2.30**	**2.13**	**2.10**	**2.21**	**2.63**
Mg	0.88	0.78	0.82	2.34	1.73	1.19	0.48
Mn	0.05	0.10	0.09	0.16	0.18	0.18	0.05
Oct Fe	4.26	3.86	3.72	2.53	3.11	3.91	3.65
Oct Ti	0.40	0.60	0.64	0.46	0.37	0.33	0.32
Oct Al	0.00	0.00	0.00	0.04	0.28	0.00	0.70
Octahedral Site	**5.59**	**5.34**	**5.28**	**5.53**	**5.68**	**5.60**	**5.20**
Tet Al	1.83	1.92	1.88	2.33	2.60	1.90	2.82
Tet Fe	0.17	0.26	0.21	0.00	0.00	0.19	0.00
Si	6.00	5.81	5.91	5.67	5.40	5.91	5.18
Tetrahedral Site	**8.00**	**8.00**	**8.00**	**8.00**	**8.00**	**8.00**	**8.00**
F	0.50	0.55	0.54	1.20	0.74	0.23	0.60
Total Cations	**15.96**	**15.90**	**15.92**	**16.82**	**16.24**	**15.62**	**15.74**

All sample numbers have prefix GJM05. Tetrahedral site is filled by Si, Al and Fe in turn. Any excess Fe is allocated to the octahedral site. Oct = coctahedral, Tet = Tetrahedal

The octahedral site in biotite may be occupied by a range of elements including Cr, Mn, Co, Ni and Zn (Bailey, 1984), though in true micas the octahedral site is dominated by Mg, Fe^{2+}, Al and Ti. The octahedral Ti content of biotites from the MSF rarely exceeds 0.80

atoms per 22 O and typically falls within the range 0.60-0.70 apfu. A similar range is observed in the FDF although biotites from the FDF generally have a lower content, typically between 0.30 and 0.50 atoms per 22 O. With the exception of sample GJM06-07 (Al_{oct}=0.12), the octahedral Al content of MSF biotites never exceeds zero. Biotites from the FDF are slightly more aluminous than the MSF, spanning a range from 0.00 to 1.20 atoms per 22 O in the octahedral site. Mn rarely occupies more than 0.12 atoms per 22 O and never exceeds 1 wt% in any samples from the MSF. The Mn content of biotites from the FDF is slightly higher than the MSF spanning a range from 0.12 to 0.35 atoms per 22 O and reaching up to 3 wt% in several samples.

The greatest variation in biotites from the Motzfeldt centre comes from differences in the octahedral Fe and Mg content, relating to the annite-phlogopite solid solution. Variation within this solid-solution is the focus of this study and is expressed as the ratio of Fe/(Fe+Mg). Fe/(Fe+Mg) variation in biotites from the MSF is from 0.75 to effectively pure annite (Fe/(Fe+Mg) = 1.0). Similar to what is observed in the interlayer site and in the minor ion occupancy of the octahedral site, values of Fe/(Mg+Fe) from sample GJM06-07 are notably different from the main data. The composition of biotites from this sample range from 0.60 to 0.85. The Fe/(Fe+Mg) content of biotites from the FDF spans a much larger range (0.25-0.95). The octahedral site totals vary between 5.1 and 5.8 in the MSF and 5.5 and 6.0 in the FDF indicating the presence of vacancies in the octahedral sites of biotites from both formations. Vacancies may be present to balance Ti^{4+} in the octahedral site, by the exchange $2Mg^{2+} = Ti^{4+}$ + vac. Alternatively vacancies may be present to balance substitution of Fe^{3+} in the octahedral site. This may be particularly important in the MSF and will be discussed later.

5.4 Halogen content of biotites from the Motzfeldt centre

Fluorine contents in biotites from the MSF vary from 0.00 to 1.55 wt%, which relates to site occupancy between 0 and 0.78 atoms per 22 O (total is 2). The fluorine content of biotites from the FDF covers a much larger range of 0.00-3.35 wt%, relating to hydroxyl site occupancy of 0.00 to 1.67 atoms per 22 O. Since oxygen cannot be directly analysed using the electron microprobe the OH content of the hydroxyl site must be estimated by assuming complete occupancy of the hydroxyl site (2 hydroxyl ions for 22 oxygens). During the present study the OH content of the hydroxyl site was calculated by accepting OH = 2 - F (calculated to 22 oxygens). However several studies have shown that in addition to F, Cl and OH ions,

vacancies and substitution of O^{2-} into the hydroxyl site may also occur (Rancourt *et al.,* 1994: Rimsaite, 1970). During the present study Cl contents in all biotites have been shown by EDS analysis to be low, eliminating the problem of Cl-OH exchange. However introduction of vacancies and coupled substitution of $Fe^{2+} + OH^{-} = Fe^{3+} + O^{2-}$ may be significant enough in the samples of the present study to introduce errors in the occupancy of the hydroxyl site. Since no determination of the relative abundances of ferrous (Fe^{2+}) and ferric (Fe^{3+}) iron in the octahedral site are available and O^{2-} and vacancy populations cannot be determined directly, the estimated OH occupancy of the hydroxyl site provide maximum estimates.

The relationship between the F content and the Fe/(Fe+Mg) content of biotite micas has been the subject of some debate since Munoz and Ludington's original publication on the subject in 1974. Gunow *et al.* (1980) and Munoz and Ludington (1974) modelled F-OH exchange by assuming ideal mixing (complete disorder) in both octahedral and hydroxyl sites. Using the models of these authors plots of wt. % F versus Fe/(Fe+Mg) should yield curved traces for biotites which equilibrated with a single fluid at a given temperature. The plot of wt. % F versus Fe/(Fe+Mg) for biotites from the MSF and FDF are shown in figure 5.2. This plot shows that biotites from both formations generally have lower F contents as the annite component of the biotite increases, following the commonly observed "F-Fe avoidance" rule of Rosenberg and Foit (1977). Unlike the trends predicted by Munoz (1984) biotites from neither formation plot along distinct curves, increasing in F content logarithmically as the Fe content of the biotite decreases. Although the F content increases as Fe/(Fe+Mg) decreases, samples show considerable scatter at lower Fe/(Fe+Mg) ratios far beyond analytical uncertainty. This is particularly true for the FDF where F contents vary between 1.18 and 3.35 for Fe/(Fe+Mg) values between 0.5 and 0.6. Even within individual thin sections (GJM06-99 from the FDF) the F content varies from 0.0 to 0.6 wt. % at a constant Fe/(Fe+Mg) value of 0.82.

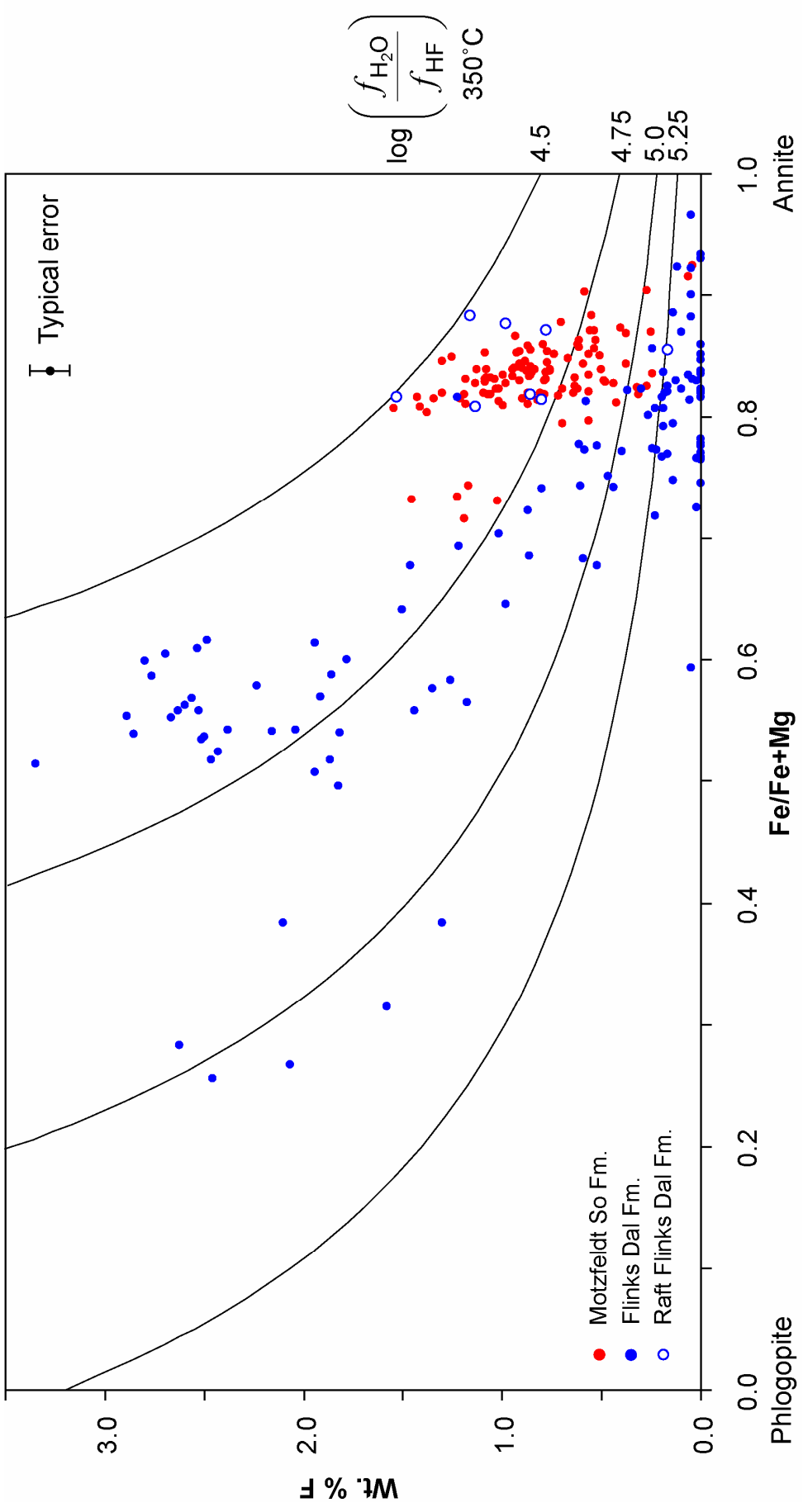

Figure 5.2. Plot of Fe/(Fe+Mg) versus weight percent F for samples from the Motzfeldt Sø Formation, Flinks Dal formation and sample from the underside of a basalt roof raft in the Flinks Dal Formation. Continuous curves illustrate the theoretical composition of micas in equilibrium with fluids of stated $\log(f_{H_2O}/f_{HF})$ for a temperature of 350°C.

Although the dataset from the MSF has a more restricted range, it similarly does not show the curved relationship between F and Fe/(Fe+Mg) predicted by Munoz (1984). Instead the FDF data have a slightly wedge-shaped distribution and samples from the MSF fit more closely to a straight line passing close to F = 0 when Fe/(Fe+Mg) = 1. In the MSF the slope of this line is much steeper than the slope defined by the FDF data. Similar trends were observed by Parsons *et al.* (1991) for the Klokken intrusion and Finch *et al.* (1995) and Finch (1995) from each of the major intrusive centres of the Gardar. Biotites from these studies plot in a right angled triangle, the hypotenuse of which presents the linear trend described by Parsons *et al.* (1991). The significance and possible causes of deviation from the model of Munoz (1984) will be discussed in the following sections. It is clear from figure 5.2 that there is a notable difference in the chemical composition of biotites from each formation. Although biotites from the MSF have lower absolute F contents the wt. % of F relative to the Fe/(Fe+Mg) ratio is much greater than observed in the FDF, suggesting that in the MSF the F-Fe avoidance rule may be violated more frequently compared to biotites from the FDF.

5.5 Composition of equilibrating fluids

Accepting that during biotite equilibration ideal mixing of F and OH occurs in the hydroxyl site and complete disorder of Fe and Mg in the octahedral site occurs the equilibrium exchange reaction (equation 11) of Munoz (1984) can be applied to the data sets of the MSF and FDF to estimate values for the fugacity ratio (log (f_{H2O}/f_{HF})) of fluid in equilibrium with both formations. Use of this equation requires an estimate for the temperature of last halogen-hydroxyl exchange. Previous authors have used a range of temperatures. Parsons *et al.* (1991) used a value of 1000 K (~730˚C) for the exchange temperature in the Klokken intrusion and Gunow *et al.* (1980) suggested that exchange in the Henderson molybdenite deposit occurs down to temperatures as low as 620 K (~350˚C). Estimating the final temperature of fluid-mica exchange is somewhat problematic since even slight differences in the temperature estimate used can produce significant differences in the final fugacity values (Finch, 1990; Munoz, 1984). This was particularly well demonstrated by Finch (1990) who showed graphically (Fig. 5.3) that for a biotite of composition Fe/(Fe+Mg) = 0.8 equilibrating with a fluid of $\log(f_{H2O}/f_{HF}) = 3.5$ at 900 K the F content should equilibrate to 1.47 wt. %. A deviation of just ±50 K from this temperature (credible values for precision on temperature from fluid inclusions, for example) introduces a variation of 1.00 < 1.47 < 2.38 wt. % F. This shows that the application of this technique to natural systems is of little use when absolute estimates of fugacity are sought. However, applied to several sample sets it provides a useful

indicator of *relative* fluid fugacities between samples which are inferred to have equilibrated over similar temperatures.

Fluid inclusion microthermometry carried out on fluorite and quartz host secondary inclusions suggest pressure-corrected trapping temperatures of 150-350°C (420-630 K) for late-stage fluids associated with both FDF and MSF. These temperatures provide a minimum temperature of the late-stage fluids which equilibrated with biotites. Therefore when estimating the $\log(f_{H2O}/f_{HF})$ value of this fluid we must assume that fluid-mica exchange continued down to these temperatures.

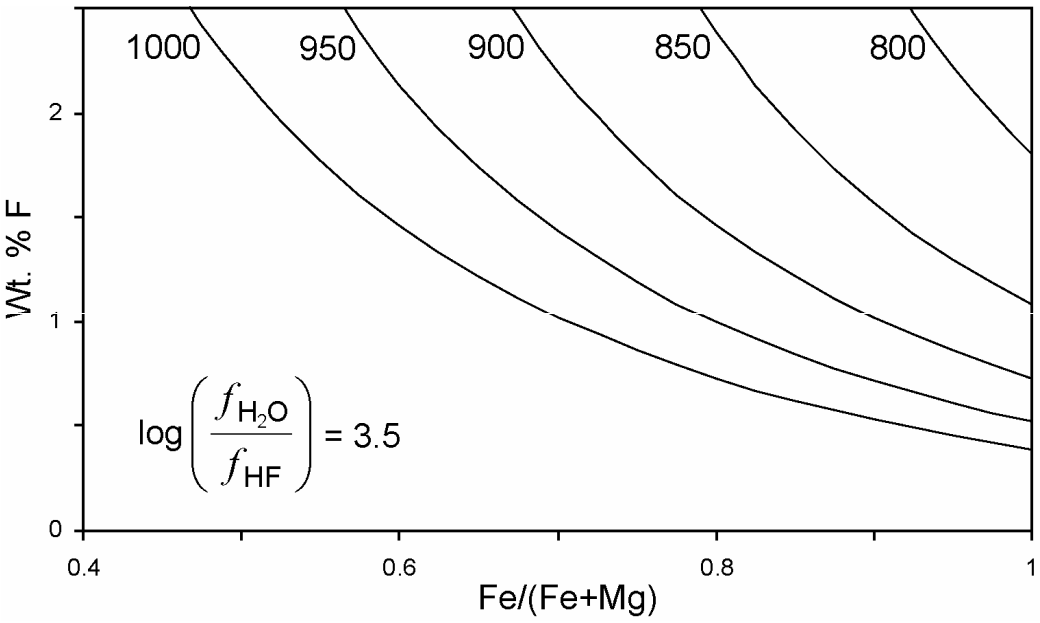

Figure 5.3. Plot of Fe/(Fe+Mg) versus weight percent F (after Finch, 1990). Curves are for various temperatures of equilibration (in Kelvin) at constant $\log(f_{H2O}/f_{HF})$. See text for description.

Using a temperature estimate of 350°C (630 K), for the final temperature of halogen-hydroxyl exchange in both formations, based on fluid inclusion data, estimates of $\log(f_{H2O}/f_{HF})$ for the MSF range between 4.2 and 5.8. Using the same temperature for FDF biotites, $\log(f_{H2O}/f_{HF})$ ranges between 3.6 and 6.3. Taken at face value these data suggest that each formation equilibrated with fluids of different compositions, which themselves show considerable spatial variation in F activity. A family of curves calculated using the equations of Munoz (1984) for $\log(f_{H2O}/f_{HF})$ values of 4.5, 4.75, 5 and 5.25 at 350°C are shown in figure 5.2. Comparing the biotite data of the present study to the fugacity curves shows that data from neither formation plot along the modelled curves. At lower Fe/(Fe+Mg), samples from

the FDF appear to plot closer to the curve for a fugacity ratio of 4.75 at 350°C, though at higher Fe/(Fe+Mg) ratios this trend breaks down. Samples from the MSF cut across the curves for fugacity ratios of 4.5, 4.75 and 5.

Another expression of biotite halogen data is to plot $\log(X_F/X_{OH})$ against Fe/(Fe+Mg). By rearranging equation 12 above plotting data in this way should yield a straight line with a slope gradient of -1.107, providing the suite of biotites equilibrated with a single fluid of fixed fugacity (Parsons *et al.,* 1991). Plotting data from the MSF and FDF in this way yield weak slopes with considerable scatter (Fig. 5.4). Straight lines fitted to these by least squares yield slope gradients of -4.70 ± 0.30 and -3.99 ± 0.63 (1σ) respectively for the MSF and FDF. Comparing these data to the theoretical slope calculated using the rearranged equation of Munoz (1984) the slope of both Motzfeldt data sets is considerably steeper than those predicted experimentally by Munoz (1984). The same was found by Parsons *et al.* (1991) for the Klokken intrusion. Theoretical slopes for fluids of fixed fugacity at 350°C are also shown on figure 5.4. Data sets from both formations clearly cross cut these.

From these observations it can be suggested that biotites from the MSF and FDF equilibrated with fluid phases which showed considerable spatial variation in fugacity within each formation. This may be true given that fluid inclusion investigations suggest a hybrid fluid in both formations, containing components from both magmatic and meteoric sources. However samples GJM06-99 from the FDF and GJM06-66 from the MSF have estimated fugacity ratios from 4.7-6.2 and 4.4-5.2 respectively within individual thin sections. It is highly unlikely that on the scale of a thin section the fluid fugacity ratio could vary by such an amount. Alternatively, the observed trend may be explained through equilibration with a single fluid of fixed fugacity but over a range of temperatures. Temperature gradients within the large intrusive units of the Motzfeldt centres are likely given the size of the intrusion. However to generate the fugacity range of 4.4 to 5.2 observed in section GJM06-66 the thermal range would need to be ~120°C. Such variation is credible on the scale of the whole intrusion but within an individual thin section is most unlikely.

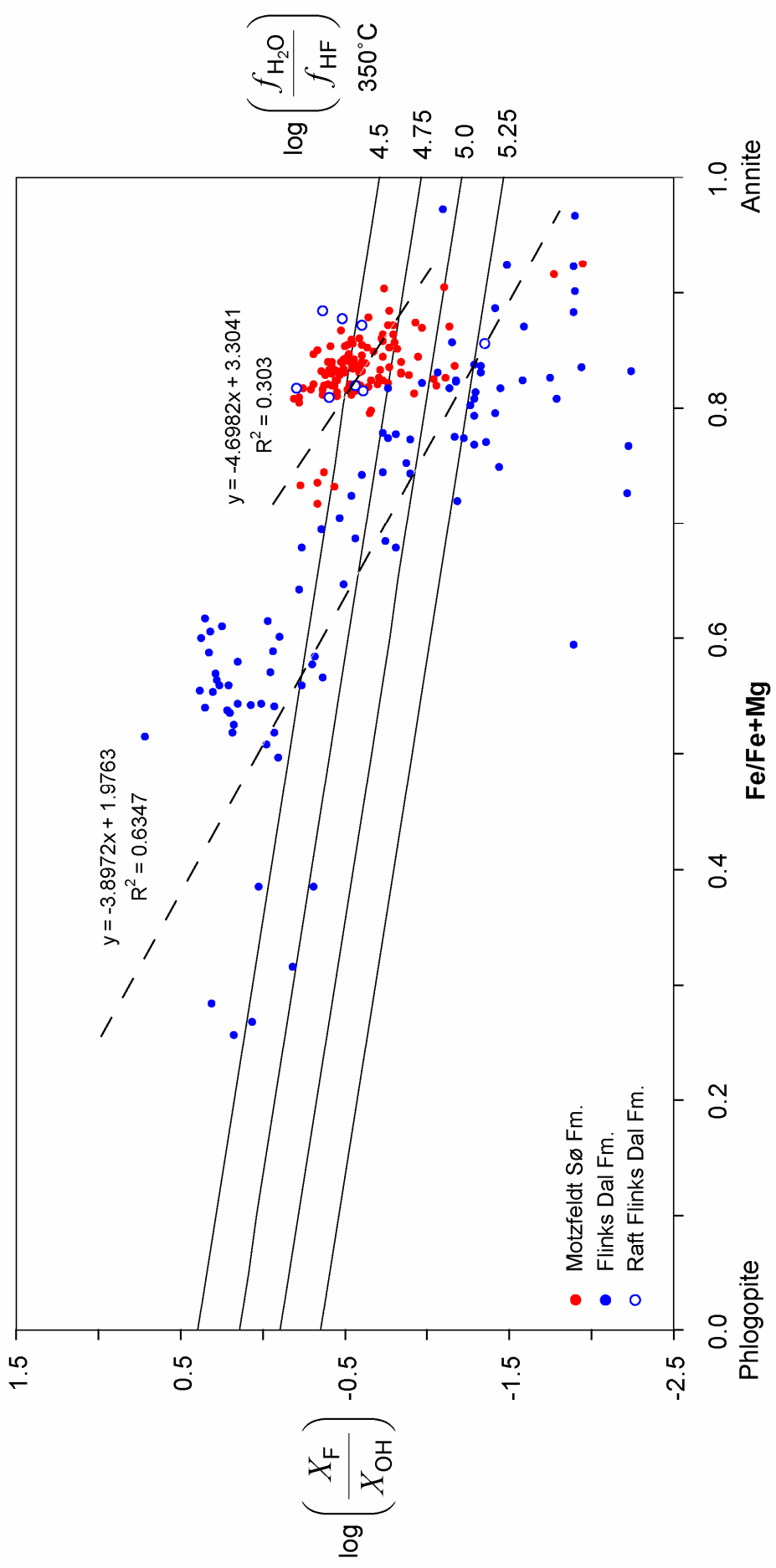

Figure 5.4. Plot of Fe/(Fe+Mg) versus log (X_F/X_{OH}) for samples from the Motzfeldt Sø Formation, Flinks Dal Formation and sample from the underside of a basalt roof raft in the Flinks Dal formation. Solid lines represent the theoretical slope of micas in equilibrium with fluids of stated log(f_{H2O}/f_{HF}) (Munoz, 1984) for a temperature of 350°C. Dashed lines represent the slope of data for individual formations fitted by least squares.

From these observations it is suggested that, although spatial variations in the fugacity ratio and temperature of the equilibrating fluid occurred in each formation in the Motzfeldt centre, and were likely the principal controls on the halogen content of Motzfeldt biotites, they are not the only control over halogen-hydroxyl exchange in the Motzfeldt centre. Based on these data, it is clear that the reciprocal exchange reaction for the biotite solid solution is not suited to biotites of the present study and the equations of Munoz (1984) inaccurately model halogen-hydroxyl exchange in the Motzfeldt centre. The limitations of the Munoz model in natural systems have been highlighted by previous authors (e.g. Gunow *et al.,* 1980: Parsons *et al.,* 1991; Finch *et al.,* 1995; Lanier *et al.,* 1978; Imeokparia, 1982) and have been critically reviewed by Zhu and Sverjensky (1992) and Finch *et al.* (1995) who discussed the many possible factors which can influence fluorine incorporation onto the biotite structure. The following section will highlight some of the major discrepancies in the Munoz model and will discuss the major factors which influenced fluorine uptake in the biotites of the Motzfeldt centre.

5.6 Factors affecting fluorine uptake in Motzfeldt biotites

5.6.1 Site occupation and ordering in the octahedral site

The experimental models of Munoz and Ludington (1974) and Munoz (1984) assume ideal mixing in the octahedral site, implying that the distribution of cations in the octahedral site is disordered. However, in natural samples complete disorder is this site is unlikely. Within the octahedral layer two crystallographically distinct octahedral sites occur, termed *M1* and *M2*, which are present in a ratio of 1:2, *M1:M2* (Fig. 5.1b) (Bailey, 1984). Cations in these sites are coordinated with 6 anions, 4 of which are O in the tetrahedral layer and the remaining two are either OH or F in the hydroxyl site. Sharing of ions between the octahedral and tetrahedral layers means that each OH or F is bonded to three octahedral metal cations (2 *M2* cations and 1 *M1* cation). In biotites where the octahedral site is fully occupied by Fe^{2+} and Mg, such as the biotites of the present study, there are 4 possible ways in which the octahedral sites (*M1* and *M2*) can be occupied when bonded to a F-OH site; Mg_3, Mg_2Fe, $MgFe_2$ and Fe_3 (Mason, 1992). However if the Fe-F avoidance rule is maintained, the only possible configuration which will permit F substitution into the hydroxyl site is for Mg to occupy all the *M* sites (Mg_3). If Mg is randomly distributed in biotite, there will inevitably be some F/OH sites bound to 3Mg. However, the probability of this configuration is greatly improved if the structure orders the octahedral ions into Mg- and Fe-rich domains. Ordering on this scale is

referred to a short-range order (SRO) and results in formation of domains within the octahedral layer which are Mg-F- and Fe-OH-rich (Stanz & Stone, 1979, 1983; Manceau *et al.,* 1990). If Fe-F avoidance is the overriding control on F-partitioning, ordered micas will accommodate more F than disordered ones at the same F fugacity (Mason, 1992). Under conditions of complete Fe-OH order and Mg-F order, the maximum amount of F to substitute into biotite is equal to the mole fraction of Mg $\left(X_F^{\max} = X_{Mg}\right)$. This function is shown on figure 5.5 by the bold dashed line. This line will subsequently be referred to as the 'Mason Maximum Fluorine Line'.

From the present study, it is assumed that the effect of cations other than Mg and Fe^{2+} on F-OH exchange is minimal given their relatively low concentrations in biotite. However two oxidation states of iron are possible and although Fe^{2+} is assumed as the standard state in many studies, Fe^{3+} can also make up a significant amount of the total Fe. Some Fe^{3+} may substitute on the tetrahedral site for Al^{3+}. The site allocation scheme adopted above assumes that all Al substitutes on the tetrahedral site until that is filled and excess occurs in the octahedral site. Rancourt *et al,* (1994) showed that ferric iron may be partitioned between the octahedral and tetrahedral sites in the proportion 2:1, favouring the octahedral site. Fe^{3+} partitioned into the tetrahedral sites is not directly bound to the hydroxyl site and has no interaction with this site. It may be that Fe^{3+} and Al^{3+} partition between tetrahedral and octahedral sites, causing overestimates Fe/(Fe+Mg) (since all Fe is assumed to be octahedral) and violating the assumption that X_{sid}=0. Since many studies concerning biotite chemistry are carried out using electron microprobe analyses, Fe is always reported as FeO from which the relative amounts of Fe^{2+} and Fe^{3+} are undetermined. Mössbauer spectroscopic studies of biotites from magnetite-bearing metamorphic assemblages have been shown to have up to 22% of total Fe as Fe^{3+} and biotites from hematite bearing assemblages as high as 46% total Fe as Fe^{3+} (Guidotti & Dyar, 1991). Similarly fluorannites from the Katugin Ta-Nb deposit, Russia contain 22% of total Fe as Fe^{3+} (Brigatti *et al.,* 2007). Although no quantitative assessment of the effects Fe^{3+} has on F-OH partitioning is possible it is know that high Fe_2O_3 contents in biotites influence F-OH exchange (Zhu & Sverjensky, 1992).

5.6.2 Non-ideal mixing in the F-Cl-OH site

Another limitation of the Munoz model is the assumption of ideal mixing of F, Cl and OH in the hydroxyl site. The ionic radii of F^- and OH^- are similar, 1.30 Å and 1.35 Å

respectively. Therefore based solely on ionic radii the ideal mixing models of Munoz (1984) may accurately represent F-OH exchange in the phlogopite-annite solid solution. However the radius of Cl^- (1.81 Å) is much larger than that of F^- and OH^- (Shannon, 1976). Hence in biotites containing Cl^- ideal substitution into the hydroxyl site is less probable, given the size difference between Cl^- and OH^-. Volfinger *et al.* (1985) suggested that incorporation of the large Cl^- ion onto the hydroxyl site will generate substantial distortion of the biotite structure, hence in natural systems Cl incorporation rarely reaches high levels. Zhu and Sverjensky (1992) suggested that in systems where Cl^- is low (i.e. <0.76 wt% = 0.05 mol%), the Cl component of the systems will likely obey Henry's law and the F-OH component will be close to ideal. Therefore Zhu and Sverjensky (1992) suggest that biotites with Cl contents lower than 0.05 mol% may be accurately modelled by the equations of Munoz (1984).

In systems where the hydroxyl site is occupied solely by F^- and OH^- ions, as is the case in the Motzfeldt centre (so long as there are no vacancies or O^{2-}), ideal mixing is assumed because of the similar ionic radii of F and OH (Gunow *et al.,* 1980; Munoz & Ludington, 1974; Munoz 1984). However Robert *et al.* (1993) demonstrated that in samples where vacancies are introduced into the octahedral site, mixing of F and OH may not be ideal since OH^- ions are preferentially located next to site vacancies. Therefore even through ideal mixing is inferred in the F-OH system, the introduction of vacancies in the octahedral site can cause the hydroxyl site to favour OH^- over F^- ions.

5.6.3 Speciation of the fluid-phase

During the studies of Munoz and Ludington (1974) and Munoz and Swenson (1981), experimental exchange reactions were internally buffered for halogen-hydroxyl exchange between HF and HCl species. However in natural systems it is unlikely that these are the only reacting species. Although in many shallow mineralising systems HF and HCl are often regarded as the most important halogen species, under sub-solidus conditions F and Cl can form associations with a range of metals in supercritical solutions. In many mineralised porphyry copper deposits, halogen complexing of metals is often the main mineralising process in such systems. However it still remains unclear whether these complexes are available for exchange at low temperatures. Experimental studies carried out by Volfinger *et al.* (1985) and Volfinger and Pascal (1989) on Cl exchange between biotite and muscovite micas and aqueous KCl solutions demonstrated that KCl species are not readily available for exchange with micas. In addition to KCl species, Al and Na associations may also be

important during exchange, particularly in the sub-solidus metasomatic phase of alkaline magmas. In shallow level intrusions, under sub-solidus conditions HCl and HF can become dissociated to ionized F^- and Cl^- (Frantz & Marshall, 1984), which is further enhanced by the high pH of fluids associated with alkaline melts. Exchange evolving these species may also be important during biotite equilibration.

5.7 Fluid equilibrium in the Motzfeldt centre

From the previous sections it is clear that in addition to the F-activity of late-stage fluids associated with the Motzfeldt centre there are a number of other crystallographic uncertainties which are unaccounted by the models of Munoz (1984) which can strongly influence halogen-hydroxyl exchange in biotites. Because of the deviation of the natural samples of the present study from the relationships predicted from experiment, quantitative comparison of the halogen activities in the MSF and FDF is avoided as it does not yield realistic values. Therefore discussion of data is based on a qualitative comparison of fluid activity based in the structural controls and fluid characteristics outlined above and discussed in previous chapters. Data from the MSF and FDF, although inadequately modelled by the Munoz equations, still define distinct fields on the wt. % F vs Fe/(Fe+Mg) diagram (Fig. 5.2). In both centres the F content decreases with increasing Fe/(Fe+Mg), demonstrating that in general F-Fe avoidance is maintained. This trend resembles the predictions of Mason (1992) based on F-Fe avoidance as the dominant structural control over the fluorine content of natural micas.

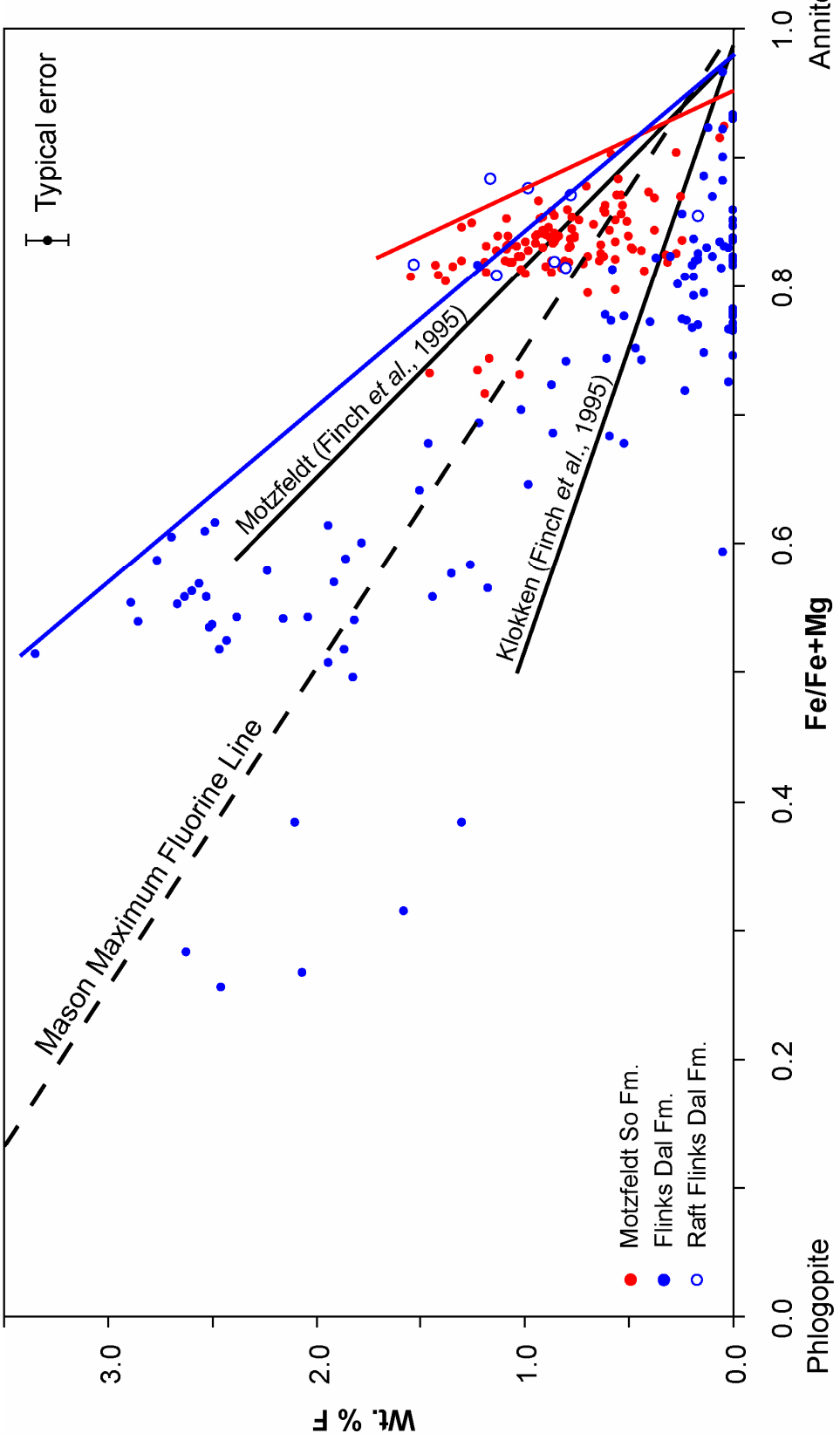

Figure 5.5. Plot of Fe/(Fe+Mg) versus weight percent F for samples from the Motzfeldt Sø Formation, Flinks Dal Formation and sample from the underside of a basalt roof raft in the Flinks Dal formation. Suggested Maximum Fluorine Lines are shown for each formation, representing the limiting maximum F levels observed as a function of Fe/(Fe+Mg). Also shown are the Maximum Fluorine Lines for the Motzfeldt centre and Klokken intrusion from Finch *et al.* (1995). The bold dashed line represents $XF = XMg$ (Mason Maximum Fluorine Line).

Samples from the FDF plot in a weak wedge shaped distribution. Similar trends are observed in the MSF, though the distribution fits slightly closer to a linear relationship than for the FDF. What is clear from both formations is that F increases with decreasing Fe/(Fe+Mg). From this observation a Maximum Fluorine Line may be fitted to each formation showing the maximum amount of F for a given Fe/(Fe+Mg) value. The slope of this line therefore reflects the relative F content of the late-stage fluids associated with each formation. Hence for a suite of samples the steeper the slope of the Maximum Fluorine Line, the higher the inferred F content of the late-stage fluid and the higher the degree of SRO in the biotites. Finch *et al.* (1995) and Finch (1995) applied this method to each of the major intrusive centres in the Gardar. Of the centres studied, Motzfeldt demonstrated the highest F contents inferred from the Maximum Fluorine Lines. It should be noted here that Maximum Fluorine Lines are merely a guide to the eye and although the exact position of the lines is open to debate, the qualitative differences are clear.

Comparison of the data of the present study with the data of Finch *et al.* (1995) (Fig. 5.5) demonstrates the strong similarity between the Maximum Fluorine Line from the FDF of this study and the Motzfeldt centre of Finch *et al.,* (1995). The samples of Finch *et al.,* (1995) were restricted to the FDF (Finch, 1990). Comparison of the Maximum Fluorine Lines for the MSF and FDF clearly shows that the slope is notably steeper for the MSF (Fig.5.5). Taken at face value this can be used to infer that fluids associated with the MSF are the most F-rich in the Motzfeldt centre. Figure 5.5 also shows that the Maximum Fluorine Lines of both formations are steeper than the Maximum Fluorine Line of Mason (1992), with the majority of samples from the MSF and around half of the samples from the FDF plotting above the Maximum Fluorine Line of Mason in the field of "Fe-F avoidance violated" (Mason, 1992). Theoretically biotites plotting along this line will show complete Fe-OH and Mg-F order. Samples plotting to the left of this line may posses full SRO but there is insufficient F to fill all available sites. For the centres studied by Finch *et al.* (1995) a high degree of order was inferred from the relatively steep slope of Maximum Fluorine Lines fitted to each centre. Based on this observation it is suggested that the biotites of the present study are also highly ordered. Given the large size of the Motzfeldt centre and the prolonged cooling history, high degrees of Fe-OH, Mg-F order in biotite are expected. The fact that Motzfeldt data plot beyond the Mason Maximum Fluorine Line indicates that some Fe-F bonding must occur. The inference is that late-stage fluids associated with both formations were extremely F-rich to the degree that Fe-F bonding took place even though it is unfavourable. Although the F content of biotites from the FDF reaches higher absolute amounts, samples from the MSF are inferred to have

experienced equilibrium in the presence of the most F-rich fluids since biotites from this formation have considerably higher F contents at higher Fe/(Fe+Mg) ratios.

The notably higher F content of the MSF is thought to reflect the stratigraphic location of this formation in the overall scale of the intrusion. The present exposure of the MSF is immediately underneath the roof of the formation capped by a thick sequence of arenite and basalt supracrustal rocks, whereas the roof-zone of the FDF is interpreted as some 500 m above current exposure. It is suggested that the roof of the MSF acted as in impermeable barrier to the vertical migration of F-rich late-stage fluids exsolved from the formation as it cooled, effectively allowing the rocks of the MSF to 'stew' in their own fluid as it ponded in high-levels of the intrusion. This is encoded in the biotites of the formation where F contents exceed the theoretical maximum permitted through Fe-F avoidance and F is forced into the biotite structure as it cools. Although samples from the FDF also violate the Fe-F avoidance it is not to such a high degree as those from the MSF. It is likely that fluids associated with the FDF were also F-rich, though not to the extent and volume associated with the MSF. These fluids may have migrated to the high-levels of the formation which are no longer present. Therefore in the roof zone of the FDF fluorine levels may have been comparable to those now observed in the MSF. Although the roof to the FDF is absent, large xenolithic rafts that have sunk into the chamber are exposed on the high plateaux of the area. Biotite from units on the underside of these rafts have significantly higher F for comparable Fe/(Fe+Mg) values (Fig. 5.4) than the bulk of the FDF, and indeed closely resemble values from the MSF. F contents up to 4.5 wt% were noted by Finch *et al.* (1995) from a xenolith raft within the FDF. This observation is in agreement with the findings of the present study. The interpretation of these anomalously high F values is that F-rich fluids migrating vertically in the FDF ponded under the large impermeable rafts. Localised concentration of these F-rich fluids in the syenite units under such rafts resulted in exceptionally F-rich biotites, similar to those in the MSF. In effect, the F-rich equilibrium found locally under the rafts of the FDF represents an microcosm of the MSF.

Previous studies concerning the stable isotopic nature of fluids associated with the Motzfeldt centre and Gardar centres report $\delta^{18}O$ values from feldspar separates of typically 4-7‰ for Motzfeldt, Klokken, Tugtutôq, Puklen and Kûngnât (Finch *et al.,* 1995; Sheppard, 1986) indicative of fluid interaction involving juvenile magmatic melts only. However more recent stable isotope work on North Qôroq (Coulson *et al.*, 2003), Ivigtût (Köhler *et al.,* 2008) and Motzfeldt (chapter 8) suggest fluids associated with these centres contain a notable

contribution from a groundwater component. From the fluid inclusion and stable isotope investigations of the present study (chapters 6 and 8) it has been suggested that the influence of meteoric fluids is greatest in the MSF. Why biotites from the Motzfeldt centre retain a halogen content indicative of equilibration with a high-F fluid, despite stable isotopic evidence suggesting that fluids of meteoric origin, generally of low F content, were significant in the late-stage fluids circulating in the centre, is unclear. It is possible that the isotopic record of meteoric fluid interaction post-dates the closure temperature of halogen-hydroxyl exchange in the biotites of the Motzfeldt centre. Fluid inclusion microthermometry shows low salinity secondary inclusion assemblages with trapping temperatures as low as 150°C. During the present study it has been assumed that fluid-mica exchange continued down to a closure temperature of ~350°C. Therefore any influence of fluids below this temperature will not be reflected in the halogen content of the biotites. It may be suggested that isotopic exchange with meteoric fluids occurred at temperatures lower than the closure temperature for the Motzfeldt biotites since fluids were clearly still circulating throughout the centre down to temperatures as low as 150°C. Pyrochlore group minerals from the MSF display textures indicative of deuteric alteration down to ~150°C (chapter 4), suggesting that the influence of meteoric fluids may post-date the high-F, dominantly juvenile fluid.

5.8 Conclusions

The halogen content of biotites from the Motzfeldt centre is dominated by fluorine, ranging from 0-3.35 wt. % in the FDF and 0-1.55 wt. % in the MSF. Data from both formations exhibit weak linear relationships with Fe/(Fe+Mg), passing close to 0 wt. % F at pure annite compositions. Although both formations show this trend, neither conforms in detail to the antipathetic relationship between F and Fe (Fe-F avoidance). The Fe-F avoidance rule breaks down in the biotites of the present study to permit incorporation of more F under the extremely F-rich subsolidus conditions inferred for both formations. Comparison of biotites from both formations shows clear differences in fluorine contents. Maximum Fluorine Lines fitted to both formations show the MSF to be the most F-rich formation of the centre. Since biotites may be used as direct indicators of the halogen content of late-stage fluids, it is inferred from this data that late-stage fluids associated with the MSF were some of the most F-rich fluids in the centre. Based on the current exposure level of the MSF, it is suggested that the activity of late-stage fluids in this region was locally elevated through ponding of F-rich fluids from depth under the roof. A similar model is suggested for the rafts within the FDF which represent microcosms of the behaviour at the MSF. Although the roof

zone is no longer exposed in this formation large supracrustal rafts provide localised insights into the fluid evolution which may have occurred at high levels in the FDF.

Although relative fluid fugacity values have been estimated for both formations following Munoz (1984), biotite from neither formation is accurately modelled by a fluid of a single composition at a single temperature. It is concluded that the equilibrium exchange reaction given by Munoz (1984) is inapplicable to biotites of the present study. Several crystallographic controls which are not accommodated into the models of Munoz have been suggested, and these may have a strong influence on F-uptake in the biotite. It is concluded that late-stage fluids in equilibrium with biotites from the Motzfeldt centre were extremely F-rich and predominantly juvenile origin. Variations in the F-content of biotites between formations are thought to reflect a combination of stratigraphic location within each formation and the overall fluorine content of the fluid. The influence of meteoric fluids is not encoded in the boities of the Motzfeldt centre, which may suggest that the influence of these fluids was at temperatures lower than the closure temperatures of the Motzfeldt biotites.

Chapter 6

Fluid Inclusion Investigations

6.1 Introduction

Previous studies concerning the genesis and evolution of peralkaline fluids within the Gardar have principally focused on the Ilímaussaq intrusion (Konnerup-Madsen, 2001; Konnerup-Madsen & Rose-Hansen, 1982; 1984). Konnerup-Madsen *et al.,* (1985) further compared fluid inclusions from the Ilímaussaq intrusion with other alkaline complexes in the Gardar Province, showing that Gardar fluid inclusions varied in compositions from saline aqueous fluids to CO_2–CH_4 and CO_2–CH_4–H_2O mixtures. The application of fluid inclusion studies has proved particularly useful in understanding fluid evolution associated with ore genesis within a range of geological environments, particularly our understanding of ore transport, deposition and host rock alteration associated with sub-solidus fluid activity. The Motzfeldt centre shows evidence for some of the most elevated volatile contents in the Gardar province (Finch *et al.,* 1995) and its rocks, specifically those belonging to the MSF, encode an alteration history unlike any other intrusive centre within the province. Understanding the role juvenile magmatic fluids and hydrothermally circulated groundwaters played during the unique sub-solidus history of the Motzfeldt centre will provide insights into the genesis and timing of mineralisation in the centre and will help to understand the processes which contributed to the unique hydrothermal regime of the MSF. This chapter will study fluid inclusion from the two dominant intrusive phases of the Motzfeldt centre, the MSF and FDF, to show differences in fluid chemistry which have had a strong influence on the genesis and evolution of mineralisation hosted within the rocks of the centre.

6.2 Fluid inclusion petrography

Fluid inclusions were analysed from magmatic fluorites from the Motzfeldt Sø (MSF) (GJM06-30, GJM06-68, GJM06-69, GJM06-70, GJM06-79 and GJM06-81) and Flinks Dal (FDF) formations (GJM06-96, GJM06-100 and GJM06-120) and from secondary fluorite (GJM06-48) and quartz veins (GJM06-68) from the Motzfeldt Sø Formation. Fluorite has been the mineral most commonly analysed during the present study as it is abundant throughout the altered MSF and less altered FDF, occurring in late stage fracture filling veins or growing intercumulus (i.e. magmatic) in many samples. Fluorite hosts abundant secondary and (pseudo)secondary fluid inclusions in addition to rare primary inclusions. Occurrences of

mariolitic quartz are relatively common in the altered units of the MSF (notably in the roof zone if the formation and associated with highly altered facies of syenite) however preparation of these samples proved difficult due to the relatively fine grain nature of the quartz sampled, therefore only one sample (GJM06-68) from the roof zone of the MSF has been analysed.

Fluid inclusions were examined optically prior to and during microthermometric analysis and classified as primary, secondary or pseudosecondary according to the classification scheme of Roedder (1984) and Shepherd *et al.* (1985). Primary inclusions, by definition, are trapped during crystal growth and commonly occur parallel to mineral growth zones in non-deformed euhedral crystals. These inclusions are often isolated from adjacent inclusions by distances greater than five times the diameter of the inclusion and may contain a solid phase which occurs as a mineral inclusion in the fluid inclusion host crystal. Secondary inclusions can be trapped at any time *after* the growth of the crystal, often occurring in planar groups or trails cutting across mineral zones and occasionally across grain boundaries (Van den Kerkhof & Hein, 2001). Secondary inclusions are often irregularly-shaped having elongate, thin or flat morphologies outlining healed secondary fractures. The phase proportions of secondary inclusions are often relatively uniform within individual inclusion trails. Fluid inclusions which formed in microfractures *during* crystal growth are referred to as pseudosecondary inclusions and are identified by inclusion trails which are truncated by younger mineral growth zones. During this study the principal inclusions analysed were of secondary or pseudosecondary origin. Of these inclusions two inclusion types were distinguished from MSF and FDF samples: 1) saline-aqueous two-phase inclusions containing a liquid and vapour phase (L + V) and 2) saline-aqueous three-phase inclusions containing liquid, vapour and solid phases (L + V + S).

6.2.1 Saline-aqueous two-phase inclusions

Saline-aqueous two-phase inclusions (L + V) are the most common type of inclusion in the fluorite samples studied. These inclusions occur in both the MSF and FDF and predominantly occur along inclusion trails interpreted as secondary and pseudosecondary. Secondary inclusions typically have irregular shape and vary in diameter between 10-40 μm and are found along inclusion rich planes (Fig. 6.1a, b & c). The degree of fill (*F*), defined as the volumetric proportion of the inclusion occupied by the liquid phase relative to the total volume of the inclusion ($F = V_{(liquid)}/V_{(liquid)} + V_{(vapour)}$), is typically 0.95 in most secondary inclusions. However a few rare inclusions have no vapour phase at room temperature and are

classed as monophase secondary aqueous inclusions. No further work was carried out on these inclusions. Pseudosecondary inclusions show a variety of shapes. Many have irregular to rounded shapes, though a number display a negative crystal shape having a rectangular or cubic form (Fig. 6.1f) and are commonly 10-40 μm in diameter. The degree of fill in pseudosecondary inclusions is typically 0.90-0.95, though a few have 0.80-0.90. A small number of large isolated inclusions (Fig. 6.1d) occur between (pseudo)secondary inclusion trails and are interpreted to be primary in origin. These are 20-50 μm in diameter and their shape is usually well rounded or slightly sub-angular. The degree of fill is typically 0.90-0.95.

6.2.2 Saline-aqueous three-phase inclusions

In addition to the two-phase saline-aqueous inclusions, several inclusions containing a solid phase were identified. The inclusions are often found in the same trails as the secondary and pseudosecondary two-phase inclusions described above (Fig. 6.1g) and are considered either secondary or pseudosecondary in origin. In general 3-phase inclusions have a similar size to the two-phase inclusions. They typically have a sub-angular shape, though occasionally show rounded shapes also, regardless of whether they are secondary or pseudosecondary. The phase proportions (L + V + S) in these inclusions are relatively constant, with typical volumetric proportion estimates of L = 0.85, V = 0.1 and S = 0.05. Several fluorite-host inclusions have been identified containing a large (S = 0.2) solid phase (Fig. 6.1h). Whether this is a mineral inclusion trapped during the formation of the inclusion or is a true daughter mineral crystallised from the fluid after trapping remains unclear. The implications of both origins will be discussed later. The identity of the solid phase within three-phase aqueous inclusions has not been directly determined during the present study, however Raman spectroscopic analyses carried out by Schönenberger and Markl (2008) on fluorite host three-phase inclusions from the MSF identified calcite as the principal daughter mineral.

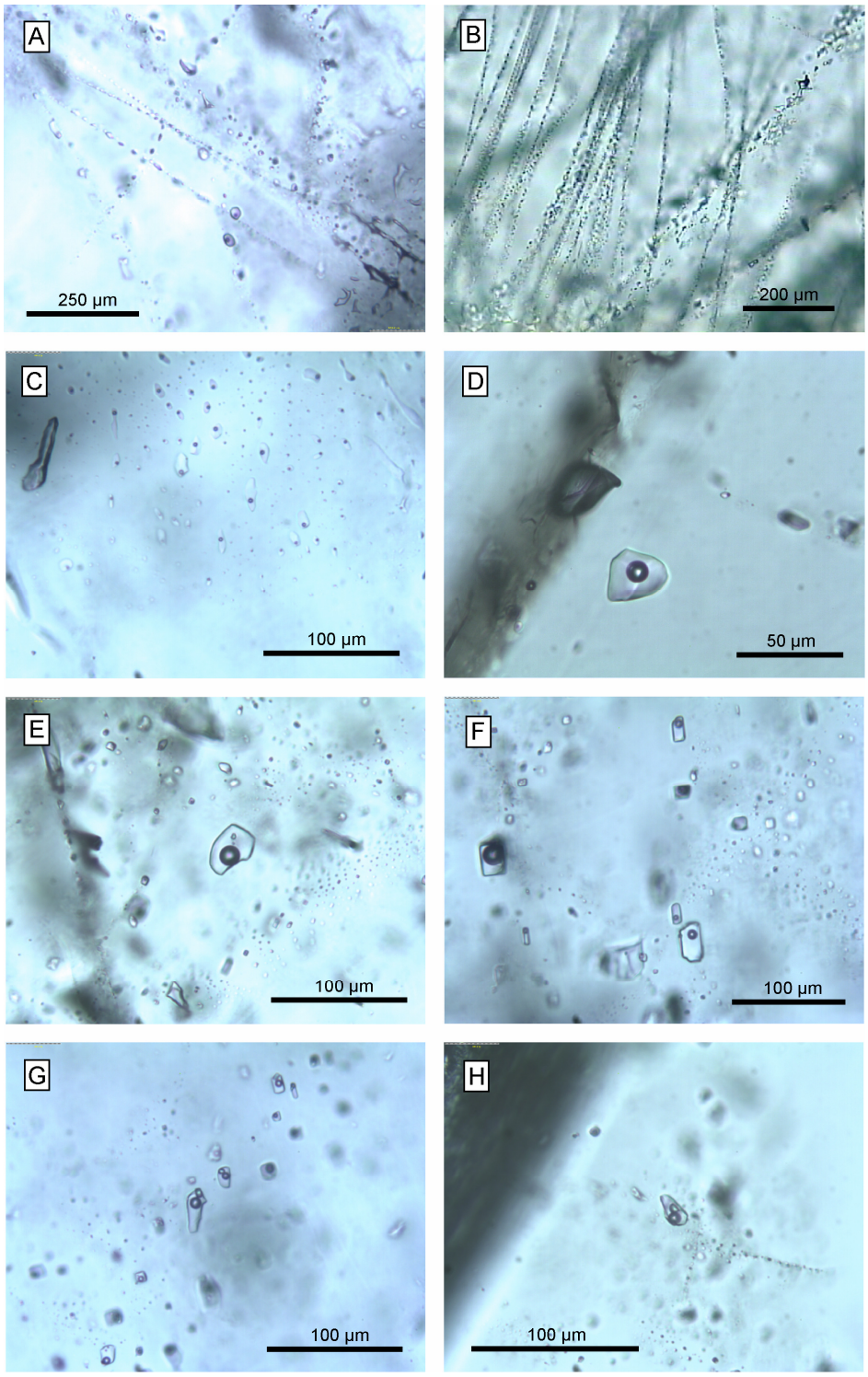

Figure 6.1. Typical fluid inclusions in fluorite from the Motzfeldt centre. (a) Secondary and pseudo-secondary inclusions from MSF. (b) Secondary fluid inclusion trails from the FDF. (c) Secondary 2-phase fluid inclusions from the MSF (photograph parallel to plane of inclusions). (d) Primary 2-phase aqueous inclusion from the MSF. (e) Primary 3-phase aqueous inclusion (centre of photograph) from the MSF. (f) Pseudo-rectangular pseudosecondary 2-phase aqueous inclusions from the MSF. (g) Trail of pseudosecondary 3-phase aqueous inclusions from the MSF. (h) pseudosecondary 3-phase inclusion with large solid phase.

6.3 Fluid inclusion microthermometry

Microthermometry was carried out on inclusions from both formations at the Institut für Geowissenschaften, University of Tübingen in Germany. Sample preparation and analytical techniques are outlined in appendix B. All aqueous inclusions (two-phase and three-phase) display a bi-modal distribution of final ice melting temperatures ($T_m H_2O$). Typically the bulk of the inclusions analysed show final ice melting temperatures between 0 and -5°C, however a number of inclusions show melting temperatures between -9 and -16°C (Fig. 6.2). These inclusions are most common in the MSF, though there are several pseudosecondary inclusions in fluorite samples from the FDF which show final ice melting temperatures of -10°C and -17°C. Eutectic melting temperatures (T_{me}) from two- and three-phase inclusions are between -50 and -25°C (Table 6.1) in inclusions from both formations. During initial rapid cooling to freezing the inclusions often show a pale brown colour (Fig. 6.3b), which might suggest the presence of dissolved salt cations other than Na (e.g. Ca^{2+}, Mg^{2+} and Fe^{2+}) which were not directly determined during this study (Davis *et al.,* 1989; Shepherd *et al.,* 1985)

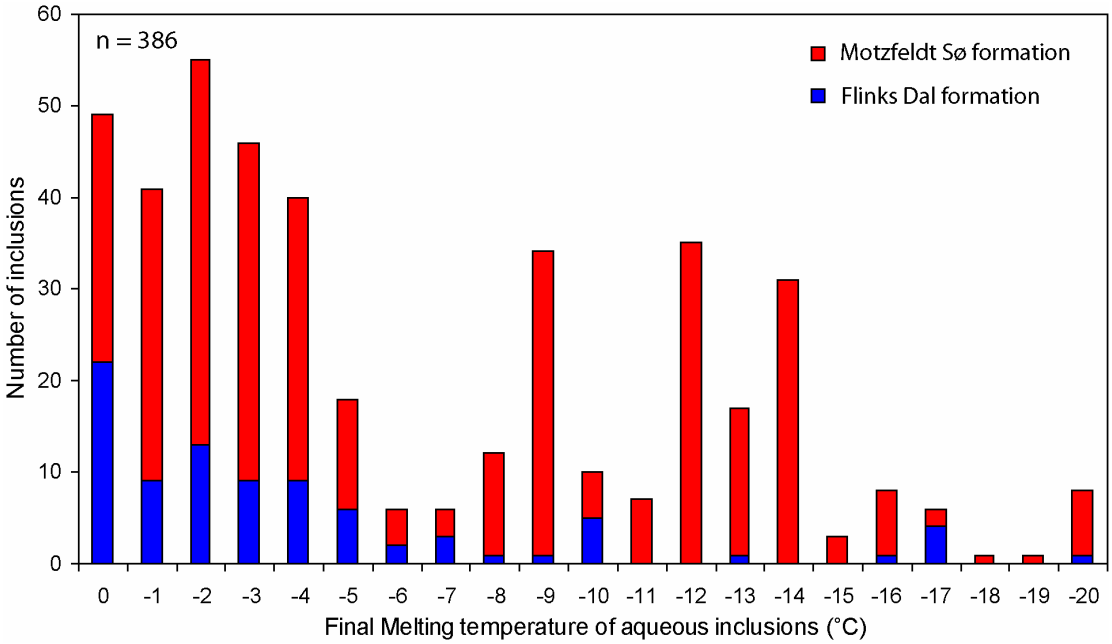

Figure 6.2. Histogram of final ice melting temperatures (T_m) for aqueous fluid inclusions from the MSF and FDF.

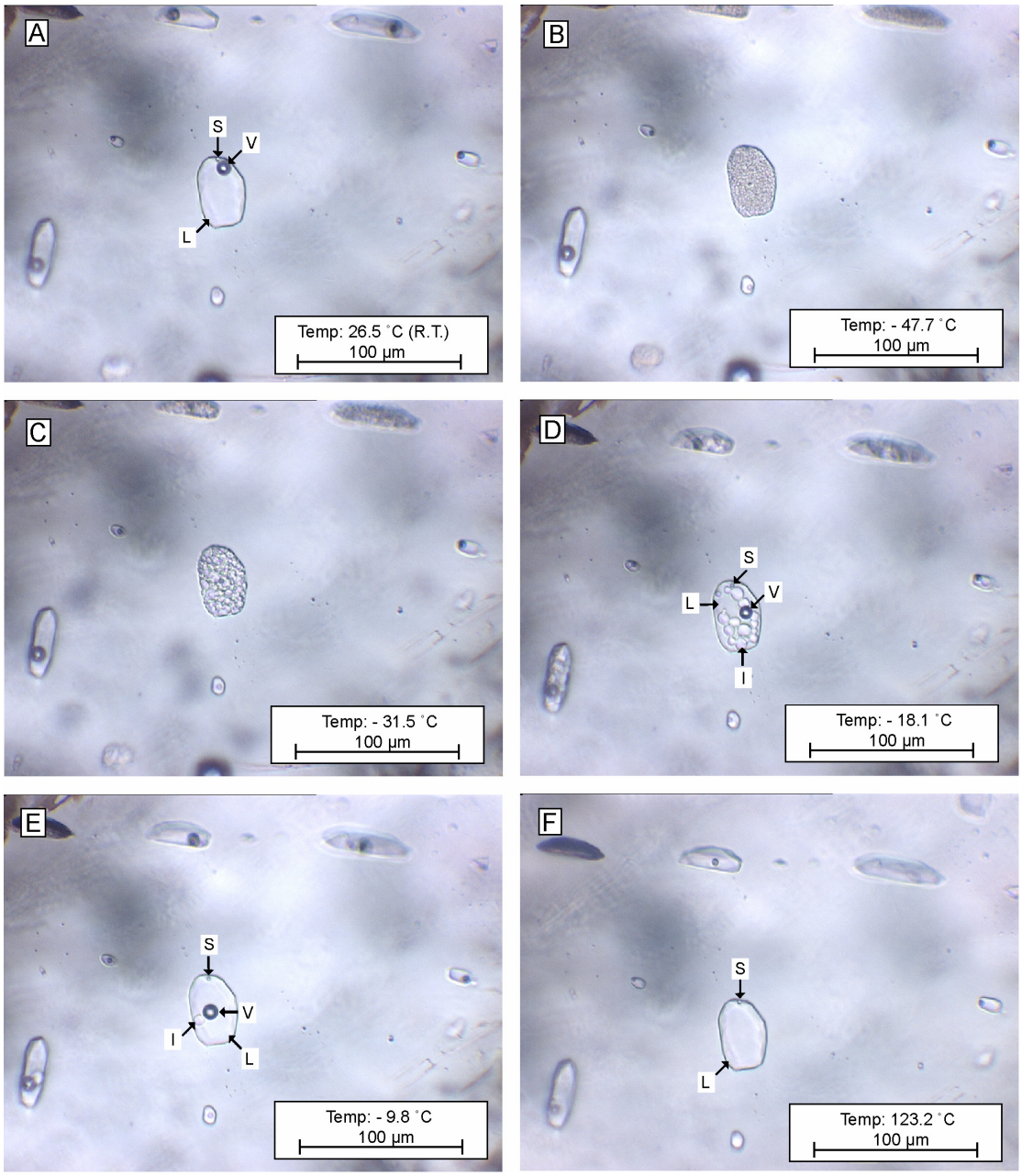

Figure 6.3. Sequence of photographs showing the major phase changes observed for a primary three-phase aqueous inclusion in fluorite from the MSF with an NaCl equivalent of 13.2 wt. %. Abbreviations in the following images are L - aqueous liquid, V - vapour, S - solid daughter mineral, I - ice crystals. (a) On freezing from room temperature (26.5°C) the inclusion supercools to -112°C before solidification is triggered. The vapour phase is crushed at this point. (b) On heating the inclusion becomes a pale brown colour and has a grainy appearance at -47.7°C, just above the temperature of first melting (T_{fm}). (c) -31.5°C; inclusion appears very granular and contains a mass of ice crystals and a saline liquid phase. The refractive index (RI) of the liquid phase is similar to the host fluorite making the inclusion margin difficult to observe. (d) -18.1°C; further melting of ice and vapour phase becomes visible again. RI of liquid decreased. (e) -9.8°C; Small ice crystal attached to the vapour bubble at a temperature close to final ice melting (T_m). (f) 123.2°C temperature of homogenisation into liquid phase.

The bi-modal distribution observed for final ice melting temperatures is mirrored in the inclusion salinities, expressed as the equivalent amount of dissolved NaCl in a standard H_2O-NaCl system (calculated using the revised equation of Bodnar, 1993). It should be noted here that although salinity is expressed as wt. % of dissolved NaCl, other salt cations such as Ca, Mg, K, Fe, and Br may also be present, though only in small amounts. Previous ion chromatography work on inclusions from the Motzfeldt centre has shown that Na is the dominant cation (Schönenberger & Markl, 2008). The next most abundant cations are Ca and K, though compared to Na which regularly reaches 10 wt. %, Ca and K rarely exceed 2.5 wt. % and 0.4 wt. % respectively. From this observation it is safe to model salinities using a simple H_2O-NaCl system. Samples from the MSF contain two groups of inclusions with different salinities (Fig. 6.4). The dominant group has salinities which are typically < 9 wt. % NaCl equiv. The other shows salinities between 12-20 wt. % NaCl equiv. Within the higher salinity group there are two prominent peaks at 14 wt. % NaCl equiv. and 17 wt. % NaCl equiv. The FDF is characterised by salinities of typically < 9 wt. % NaCl equiv., though a few anomalous inclusions show higher salinities at 15 wt. % NaCl equiv and around 20 wt. % NaCl equiv.

Table 6.1. *Microthermometric data for fluid inclusions from the Motzfeldt centre*

Sample	Fm	Mineral	*n*	Type	$T_{(me)}$ (°C)	$T_{(m)}$ H_2O (°C)	$T_{(h)}$ H_2O (°C)	Salinity (wt% NaCl eq.)
GJM06-30	MSF	Flt(P)	18	L-V	-26 to -45	-1.2 to -7.2	102 – 274	2.1 - 10.7
GJM06-48	MSF	Flt (S)	50	L-V	-25 to -40	-0.6 to -19.6	81 - 380	0.7 - 22.1
GJM06-48	MSF	Flt(S)	4	L-V-S	-35 to -40	-15.9 to -16.3	355 - 367	19.4 - 19.7
GJM06-68	MSF	Flt (S)	94	L-V	-26 to -51	-0.6 to -23.0	92 - 237	0.7 - 24.3
GJM06-68	MSF	Flt (S)	7	L-V-S	-26 to -35	-1.6 to -14.3	142 - 215	2.7 - 18.0
GJM06-68	MSF	Qtz (S)	17	L-V	-20 to -35	-3.2 to -14.1	106 - 234	5.4 - 17.8
GJM06-69	MSF	Flt (P)	87	L-V	-18 to -54	-0.8 to -23	116 - 236	1.0 - 18.2
GJM06-69	MSF	Flt (P)	9	L-V-S	-24 to -40	-1.8 to -3.0	106 - 225	3.1 - 4.9
GJM06-70	MSF	Flt (P)	59	L-V	-20 to -35	-0.4 to -23.7	84 - 248	0.3 - 24.8
GJM06-79	MSF	Flt (P)	32	L-V	-25 to -45	-0.1 to -14.4	85 - 242	0.2 - 17.9
GJM06-81	MSF	Flt (P)	52	L-V	-10 to -20	-0.1 to -8.2	82 - 329	0.2 - 11.9
GJM06-96	FDF	Flt (P)	46	L-V	-15 to -50	-0.6 to -31.2	70 - 273	0.7 - 29.4
GJM06-100	FDF	Flt (P)	43	L-V	-10 to -30	-0.1 to -5.2	80 - 251	0.2 - 8.1
GJM06-100	FDF	Flt (P)	6	L-V-S	-20	-2.0 to -3.0	102 - 283	3.1 - 4.9
GJM06-120	FDF	Flt(P)	14	L-V	-18 to -35	-0.8 to -4.2	96 - 246	1.0 - 6.7

n – number of inclusions analysed in sample; $T_{(me)}$ – eutectic (first) melting; $T_{(m)}$ H_2O – final melting of ice; $T_{(h)}$ H_2O – total homogenisation temperature to liquid (N.B. solid phase did not dissolve in any multiphase inclusions). Inclusions analysed in: Flt (P) – primary magmatic fluorite; Flt (S) – hydrothermal vein fluorite; Qtz (S) – hydrothermal vein quartz. Fluid type: L-V – liquid-vapour two-phase aqueous inclusion; L-V-S – liquid-vapour-solid three-phase aqueous inclusion; salinities calculated using the equation of Bodnar (1993). Full data set can be found in appendix F.

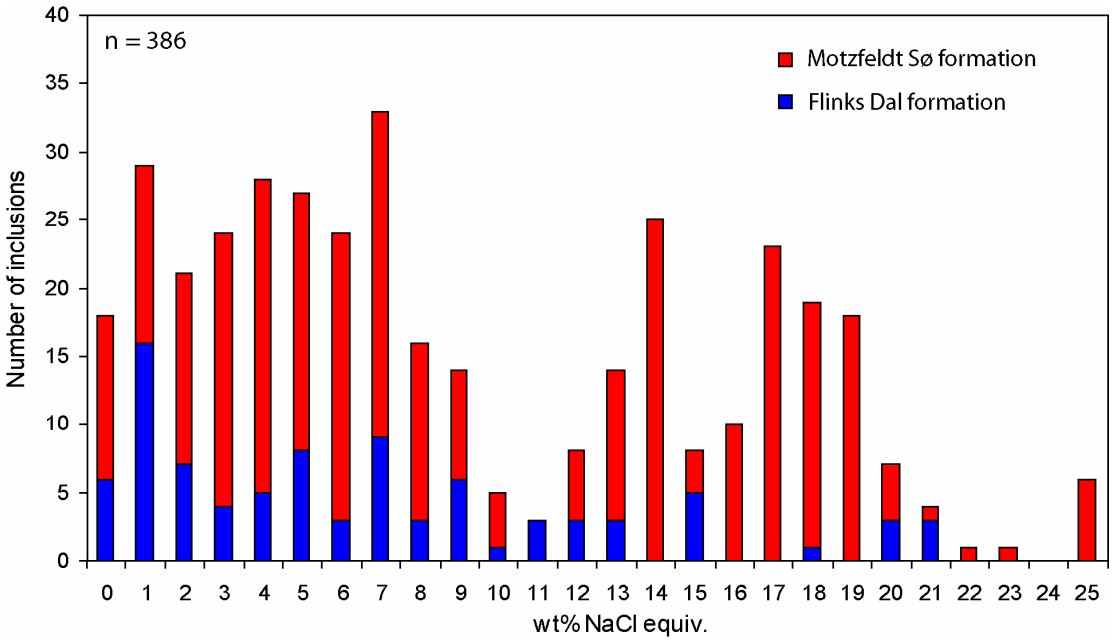

Figure 6.4. Histogram of wt% NaCl equivalent of all aqueous fluid inclusions from the MSF and FDF.

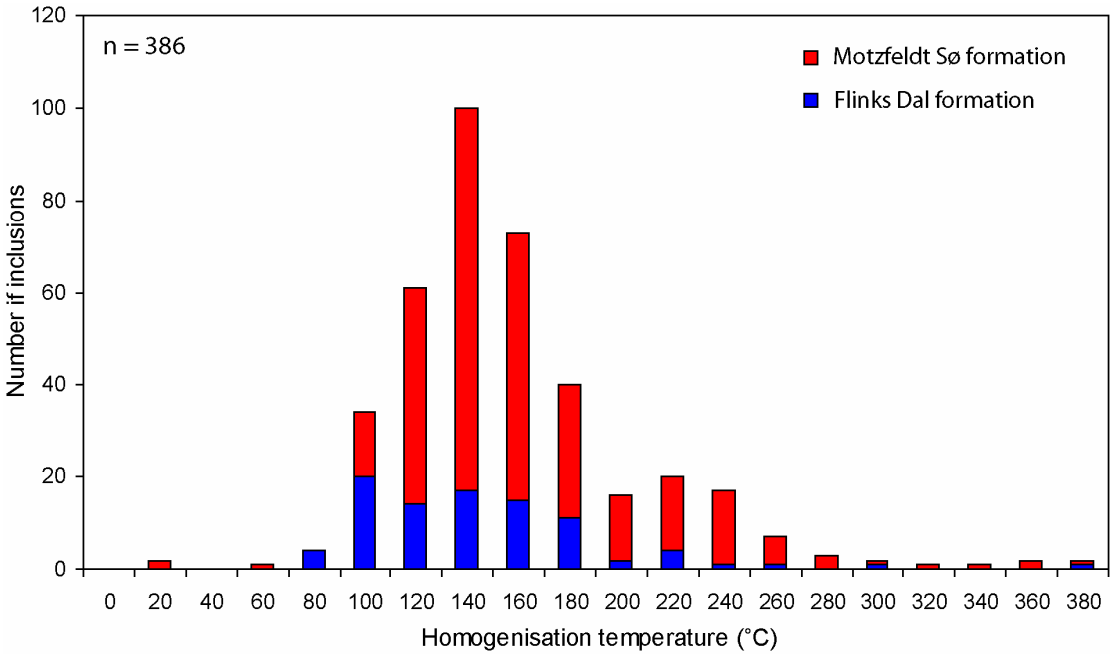

Figure 6.5. Histogram of homogenisation temperatures (T_h) of all aqueous fluid inclusions from the MSF and FDF.

All fluid inclusions analysed, regardless of whether they are two- or three-phase, homogenise to a single liquid phase over the temperature interval 100 - 260°C. This is observed in both formations (Fig. 6.5). However, within this range the homogenisation

temperatures (T_h) display a slight bi-modal distribution. Up to 80% of the inclusions from the MSF, and 90% of inclusions from the FDF, homogenise within the range 100 - 180˚C. The remaining inclusions homogenise in the range 220 - 260˚C. The majority of low-salinity inclusions (< 9 wt. % NaCl equiv.) show homogenisation temperatures over the range 100 – 240˚C, but higher salinity inclusions (12 - 20 wt. % NaCl equiv.) from the MSF have lower homogenisation temperatures (100 - 160˚C, Fig. 6.6). Inclusions with higher salinities and lower homogenisation temperatures were analysed from fluorite-rich rocks immediately underneath the roof-zone of the MSF (Samples GJM06-68, GJM06-69 and GJM06-70). Therefore these samples may encode the fluid character of locally evolved, lower temperature fluids beneath the roof of the formation, rather than being representative of the MSF as a whole. During heating of three-phase aqueous inclusions to approximately 450˚C (or until decrepitation of the inclusion) the daughter mineral phase (suggested to be calcite) did not dissolve into the liquid phase, nor were any signs of partial dissolution observed. Similarly there appears to be no systematic difference in T_h, T_m or salinity between 2- and 3-phase aqueous inclusions.

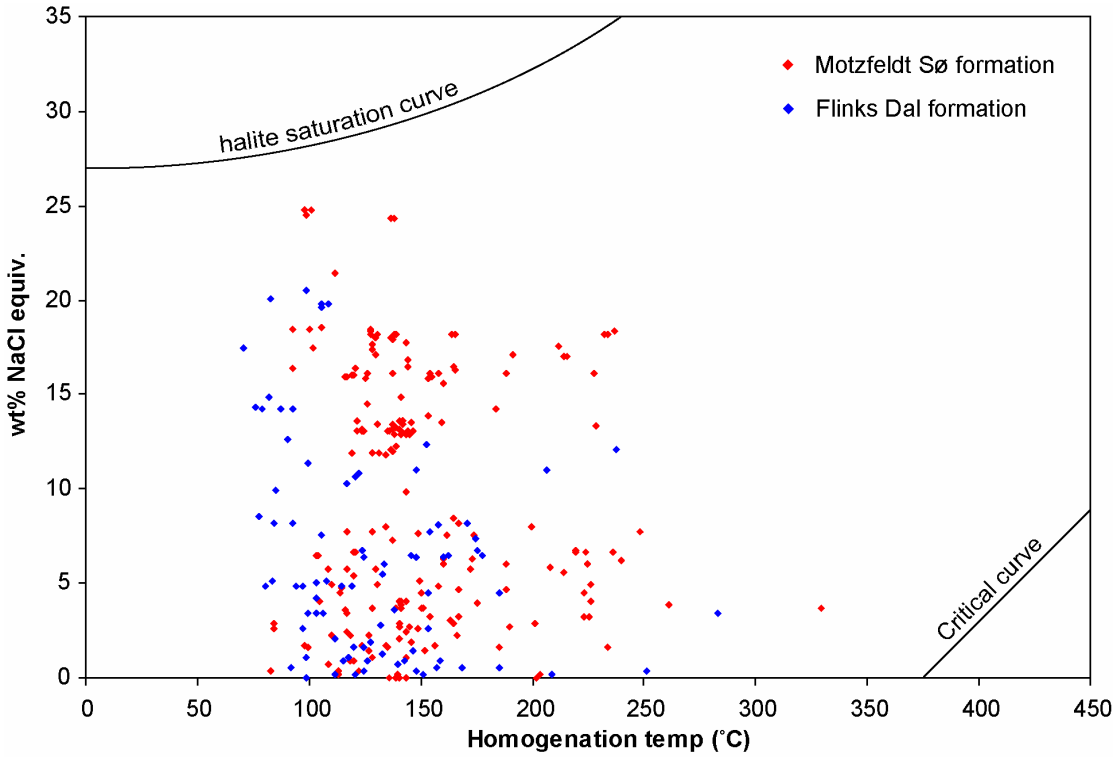

Figure 6.6. Salinity (wt. % NaCl equiv.) versus homogenisation temperature for aqueous inclusions from the MSF and FDF. Halite saturation curve represents salinity after which halite daughter minerals precipitate on cooling. The critical curve represents the composition and temperature range where aqueous inclusions homogenise by gradual fading of the meniscus between the liquid and vapour phases (Shepherd *et al.,* 1985).

6.4 Discussion of fluid inclusions

6.4.1 Fluid origin and evolution in the Motzfeldt Sø Formation

Fluid inclusions from the MSF commonly show salinities of <9 wt. % NaCl equiv. and homogenise over a relatively broad temperature range (100 - 260˚C). However a number of inclusions show notably higher salinities (12 - 20 wt. % NaCl equiv.) and homogenise over a more restricted temperature range (100 - 160˚C). Fluorite samples which host these inclusions are located immediately underneath the preserved roof-zone of the centre, where it is suggested that fluorine-rich fluids have ponded under the preserved roof of the formation.

The origin of high-salinity (NaCl-saturated) fluid inclusions has received much attention over the past decade (e.g. Webster, 2004; Zhang *et al.,* 1997; Zhang *et al.,* 2007) due to their importance in understanding the evolution of ore-forming fluids. The geological and economic significance of hypersaline fluids is great due to their ability to complex and transport elements, usually considered immobile, within magmatic-hydrothermal systems (e.g. Kogargo, 1980; Salvi & Williams-Jones, 2006). This is particularly apparent in evolved alkaline melts where considerable amounts of high field strength elements (HFSE) are often locally concentrated. The transport capacity of such high-salinity fluids is often linked to the halogen, particularly fluoride, activity of the aqueous solution, which can determine the fluids capacity to transport REE and HFSE as fluoride complexes (Wood, 1990). This is particularly important in understanding the evolution of the MSF, which had unusually high fluorine activity, inferred from halogen exchange in micas (chapter 5), and contains many elements locally enriched to economically significant amounts.

High-salinity fluids are common in many intrusion-related mineral deposits and as a result have been the focus of a large number of studies, particularly on porphyry copper and ephemeral intrusion related hydrothermal systems (e.g. Fall *et al.,* 2007; Zhang *et al.,* 1997 and Zhang *et al.,* 2007). Formation of high-salinity fluids can occur though a number of mechanisms (Fig. 6.7), however the two principal mechanisms are; 1) boiling of a lower-salinity fluid, concentrating dissolved salts in the residual liquid phase as the volatile component (H_2O) is boiled off, or 2) direct exsolution of a high-salinity fluid from a melt during the final stages of crystallisation (Bodnar, 1994; Wilkinson, 2001).

Before discussing the origin of the higher salinity inclusions in the MSF it should be noted that the trapped fluid in the MSF was not sufficiently saturated in NaCl to permit precipitation of halite daughter minerals on cooling. Therefore these inclusions are not high-salinity inclusions in the strict sense (i.e. greater than approximately 27 wt% NaCl at room temperature) as they are not sufficiently saturated with NaCl to crystallise a halite daughter mineral. However for the purposes of the discussion they will be referred to as high-salinity inclusions to differentiate from the main assemblage of low-salinity inclusions.

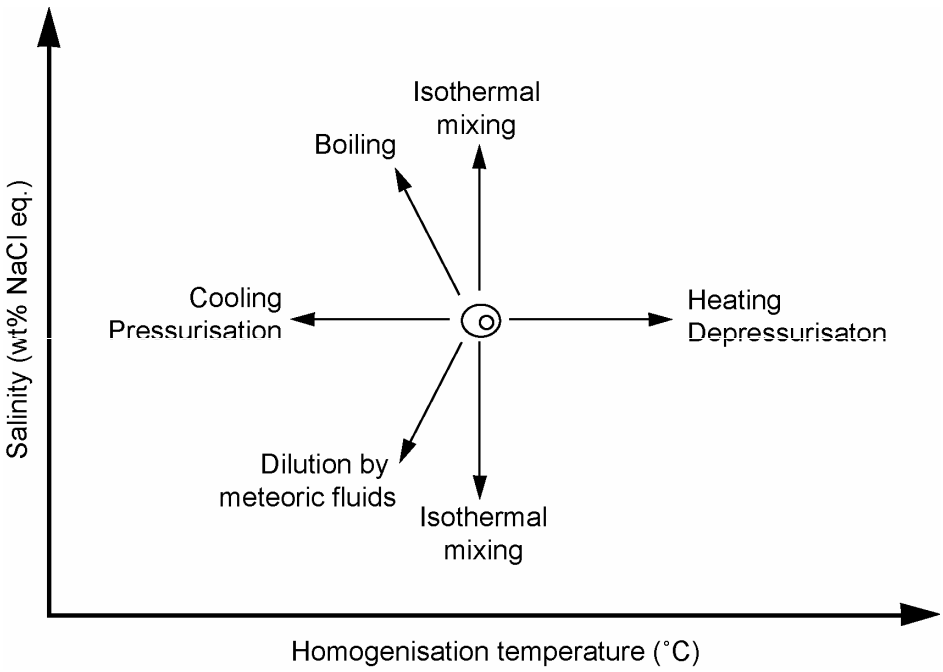

Figure 6.7. Schematic diagram showing typical trends of fluid evolution during common hydrothermal processes (after Wilkinson, 2001).

The high-salinity inclusions in the MSF are intimately associated with localised fluorite mineralisation concentrated in the roof-zone of the formation. It may be argued that the localisation of high-salinity inclusions only in the roof-zone of the formation suggests boiling of the exsolved residual magmatic fluid at low lithostatic/hydrostatic confining pressures, removing the volatile (H_2O, amongst other volatiles) component of the fluid and effectively concentrating the dissolved salts in the residual liquid. A similar model was suggested by Bradshaw (1988) to be the principal driving force for continued migration of incompatible element rich juvenile fluids to the roof-zone of the MSF from lower in the intrusion. To satisfy this model vapour-rich fluid inclusions (V + L), which homogenize to the vapour state (V + L → V), should be present and should show identical homogenisation temperatures to

inclusions in the same assemblage which homogenise to the liquid state (L + V → L) (Bodnar, 1994; Roedder & Bodnar, 1980; Shepherd *et al.,* 1985; Wilkinson, 2001). None of the inclusions analysed during this investigation show homogenisation into the vapour state. Similarly, phase proportions in all high-salinity 2-phase aqueous inclusions are relatively uniform at room temperature, suggesting that during fluid trapping there was no liquid - vapour separation, as would be expected during boiling. Therefore, although fluid boiling may have occurred at high levels in the intrusion, it is not a feasible mechanism in the samples of this study for locally concentrating more saline fluids within the roof-zone of the MSF.

The homogenisation temperatures of the high-salinity inclusions, though relatively restricted, lie within the same temperature interval as the main low-salinity inclusions. Similar homogenisation temperatures at contrasting salinities, as seen in the MSF, may be explained by isothermal mixing/mingling of fluids with contrasting salinities (Shepherd *et al.,* 1985, Wilkinson, 2001). Several observations have been made during this study (see chapters 4 and 8) to suggest influx and thermal convection of meteoric waters throughout the MSF (and to a lesser extent in the FDF). The dominant low-salinity (<9 wt. % NaCl equiv.) inclusion assemblage from the MSF may therefore represent a hybrid fluid generated through mixing of juvenile, moderate- to high-salinity magmatic waters with lower salinity, externally derived meteoric groundwaters. The effect of meteoric water influx would be to dilute early, moderate-to high-salinity magmatic waters resulting in the low- to moderate-salinity fluids, which now characterise the main inclusion assemblage.

The high-salinity inclusions preserved locally in the roof-zone of the MSF may therefore represent a fluid with a greater component of a juvenile moderate- to high-salinity fluid exsolved from the melt as it crystallised, prior to dilution by meteoric waters. Why this fluid is preserved exclusively within the roof zone is problematic, as it would be expected that fluid activity and interaction with externally derived meteoric fluids would be greatest at high-levels in the intrusion. Preservation of the high-salinity fluid may be explained by the fluid mixing work of Henley and McNabb (1978). They demonstrated that fluids with markedly different densities (and hence salinities) are extremely slow to mix. As a result many fluid inclusion assemblages tend to preserve salinity extremes of the two "end member" fluids, rather than showing a mixing trend between the contrasting fluids. In the case of the MSF the trapped fluids may therefore represent a high-salinity dominantly magmatic fluid and a lower salinity hybrid fluid which is dominated by a meteoric component. Since many of the inclusions analysed during this study are of secondary origin, trapped in fractures and planes

of fluid movement, they therefore postdate the crystallisation of the fluorite, which is recognised as one of the final mineral phases to crystallise during the liquid-fluid transition. This suggests that the juvenile component of fluids trapped in the MSF may be significantly less than the contribution from hydrothermally convected groundwaters.

Fluids exsolved early in the evolution of silicate melts tend to have lower salinities than those exsolved late in crystallisation history (Zhang *et al.,* 2007). It may be suggested that the fluids exsolved from much of the MSF were of lower salinity than those exsolved from the mineralised melts close to the roof. Alternatively, inclusions in the roof-zone represent a trapped fluid which exsolved from more evolved units at depth and migrated towards the top of the chamber where they ponded under the largely impermeable roof. The lower homogenisation temperatures of these inclusions can also be explained if these fluids exsolved late in the crystallisation of the MSF and ponded in the roof-zone. During migration through the formation these fluids would have undergone adiabatic expansion and some degree of interaction with lower salinity meteoric fluids resulting in a cooling of the fluid. Similar high-salinity inclusions were also identified by Schönenberger and Markl (2008) from vein fluorite sampled within the mineralised units of the MSF. In addition to having an elevated NaCl component (up to 25 wt. % NaCl equiv) Schönenberger and Markl also noted an increase in the Cl/Br ratio of inclusions from this sample, which they attributed to either a mixing of high- and low-salinity fluids and/or a different fluid generation. These observations are consistent with the observations of the present study.

It should be noted that the confining pressure at which these inclusions were trapped was notably higher than the present day surface exposure. Stratigraphic reconstructions on the Eriksfjord formation suggest that the base of the Mussartût member, into which the MSF was emplaced, was approximately 2 km below the top member of the formation. Similarly Jones (1980) suggested pressure conditions between 1 and 2 kbar for the emplacement conditions of the Motzfeldt centre. Konnerup-Madsen and Rose-Hansen (1984) obtained similar emplacement pressures for the Ilímaussaq intrusion, some 40 km southwest of the Motzfeldt centre. Based on the work of Konnerup-Madsen and Rose-Hansen (1984) a pressure correction of 50 - 100°C has to be applied the measured homogenisation temperatures to determine the pressure corrected original trapping temperatures (T_T) of inclusions from the Motzfeldt centre. Homogenisation temperatures for the MSF and FDF typically range from 100 - 260°C for the main low-salinity population, suggesting trapping temperatures of between 150 and 360°C for secondary and pseudosecondary inclusions from both formations. The

higher salinity population homogenise over a slightly more restricted range of 100 - 160°C, suggesting trapping temperatures of 150 - 260°C, which provides an approximate minimum temperature of the fluid which interacted with the rocks of the Motzfeldt centre during the sub-solidus.

Though the origin of the high-salinity inclusions can only be speculated upon, it is likely that these inclusions represent a trapped fluid which has experienced minimal dilution by meteoric waters and may characterise a fluid salinity close to the parental composition of the most evolved units of the MSF. These inclusions may not be representative of the bulk fluid which interacted with the MSF, however they provide useful insights into the fluid evolution of the centre and demonstrate the potential the parental melt (and fluids it exsolved) had to concentrate dissolved elements to economic levels.

6.4.2 Fluid origin and evolution in the Flinks Dal Formation

Despite the striking textural differences between the MSF and FDF, the fluids associated with the FDF show striking similarities to those which interacted with the MSF, showing similarly low salinities to the main inclusion population of the MSF and spanning a similar range of homogenisation temperatures. The trapping of fluids comparable to the MSF may be explained using same fluid mixing model suggested for the main MSF inclusion assemblage. However the melts of the FDF have been shown to be relatively anhydrous yet retain high concentrations of dissolved volatiles (F, Cl and C compounds) (Bradshaw, 1988) and unlike the MSF incompatible elements are relatively evenly distributed throughout the formation and highly mineralised zones are absent. Therefore during crystallisation the relative amount of juvenile fluids exsolved from the melts would be much reduced in comparison to the MSF. Similarly the influence of meteoric influx is also reduced; the brick-red staining and hematite mineralisation characterising the MSF is largely absent in the FDF and restricted to a relatively narrow zone along the magmatic contact with the MSF and the undersides of foundered basalt and trachyte rafts. The reduced influence of meteoric fluids in the FDF is also reflected in the stable isotope characteristics of late-stage carbonates (chapter 8) and in the alteration encoded in pyrochlore group minerals from the formation (chapter 4). From these observations it is suggested that the MSF, which now envelops the FDF, acted as a barrier reducing the large-scale circulation of externally derived waters in the FDF. The fluid inclusion assemblage in the FDF therefore represents a similar fluid mixing model as found in the MSF, though the exsolved juvenile fluid was of lower volume and possibly of lower

salinity. The subsequent interaction with meteoric waters was also reduced and restricted to high levels in the intrusion which are no longer present. If the high levels of the FDF were still preserved fluid inclusion assemblages associated with these units may have displayed similarly high-salinity characteristics as are observed in the MSF, however this is purely speculative. Another hypothesis which has been speculated (A. Finch, personal communication, 2008) is that the FDF my in fact be the same unit as the MSF offset vertically by displacement along a major fault lineament which now lies concealed under Motzfeldt Sø. Sinistral movement along the major Flinks Dal Fault has been commented on by several authors (Bradshaw, 1988; Jones, 1980; Upton *et al.,* 2003), though the vertical displacement still remains somewhat unknown. Using the base of the Eriksfjord Formation as a guide a vertical down-throw of up to 500 m can be suggested for units north of the Flinks Dal fault (MSF), Therefore it is not unlikely that displacement along a similarly large fault concealed beneath Motzfeldt Sø may also occur.

Accepting the interpretation that the MSF represent a high-level unit of the FDF the similarities in the fluid inclusion salinities and temperatures may be explained by the same fluid mixing model suggested above for the MSF. The FDF experienced some interaction with meteoric waters but the major component of the fluid was of low- to moderate-salinity and juvenile origin. Local preservation of a high salinity fluid under the roof is likely due to the large volume of fluid migrating towards the roof, certain samples, which had little time to mix with less saline meteoric fluids, retain a fluid chemistry close to the original juvenile fluid exsolved from the melt. This interpretation is speculative and cannot be supported without evidence to confirm the presence of a major fault within Motzfeldt Sø. However given the amount of vertical displacement suggested on the Flinks Dal Fault it is not unlikely that vertical displacement associated with a major fault concealed under the freshwater lake of Motzfedlt Sø may be significant enough to juxtapose the less altered units of the FDF alongside the highly altered high-level units of the MSF.

6.4.3 Origin of three-phase inclusions

The most common secondary and pseudosecondary inclusions in both formations are 2-phase saline aqueous inclusions (L + V), however throughout both formations three-phase saline-aqueous inclusions (L + V + S) are also found. From the inclusions, it cannot be clearly determined if the solid phases represent crystalline calcite trapped during inclusion formation, or if they are daughter minerals crystallised from the fluid after trapping. Phase proportions (L

+ V + S) in many three-phase inclusions are relatively uniform (with the exception of rare inclusions containing a larger than average solid phase) which suggest that these are true daughter minerals crystallised from the trapped fluid. Additionally, secondary trails of three-phase inclusions are also common (e.g. Fig. 6.1g) in fluorites from the MSF, favouring post entrapment crystallisation over accidental inclusion for the genesis of the solid phases. Although it is argued that solid phases represent true daughter minerals, it cannot be ruled out that in some inclusions the solid phase was accidentally trapped. This process can account for rare inclusions hosting large calcite crystals. The presence of both two- and three-phase aqueous inclusions in the MSF and FDF suggests that during the evolution of these formations the fluid was dominantly characterised by H_2O and NaCl with variable dissolved Ca. Although both inclusion types have been identified the sample material did not allow for the relative chronology of each inclusion type to be determined by cross-cutting relations.

6.5 Conclusions

The results of this study show that fluids associated with the highly altered and mineralised MSF are remarkably similar in character to fluids associated with the largely unaltered and unmineralised FDF. Fluid inclusion assemblages from both formations cover a similar range of homogenisation temperatures (100 - 240˚C) and salinities (<9 wt. % NaCl equiv.). However, fluid inclusions from close to the roof zone and from high-levels in the MSF show notably higher salinities (12 - 20 wt. % NaCl equiv) and homogenise over a smaller and lower temperature range (100 - 160˚C). This fluid is considered to represent a virtually pristine juvenile magamatic fluid exsolved late in the crystallisation history of the MSF. The lower salinity inclusions, which characterise fluids from the bulk of the MSF are considered to represent a hybrid fluid comprising components of both juvenile magmatic and externally derived meteoric origin. The model suggested for the fluid evolution of the MSF, based on the observations of this study, is that juvenile fluids exsolved from the melt as it crystallised interacted with hydrothermally convected meteoric waters, diluting the magmatic component of the fluid and effectively lowering the bulk salinity of the main fluid phase. Preservation of a juvenile high-salinity fluid in the high-level units of the formation is somewhat enigmatic, however it is suggested that this fluid exsolved late in the sub-solidus history of the formation from more evolved units and was of notably higher salinity than fluids exsolved early in the sub-solidus (e.g. Zhang *et al.,* 2007). Ponding of large volumes of these fluids under the roof of the MSF permitted preservation of a fluid composition which has experienced minimal dilution by meteoric fluids.

Fluid evolution in the FDF is inferred to have developed under a similar hydrothermal regime as the MSF, though the proportion of the fluid which is of juvenile origin is suggested to be lower and of generally lower salinity. Similarly the component of meteoric waters is also inferred to be less in the FDF as the MSF appears to have acted as a barrier to the large scale circulation of meteoric fluids within this formation. From these observations it is suggested that the fluids associated with the MSF and FDF have evolved through the same processes where variable amounts of mixing between two fluids of contrasting salinity have occurred. The high salinity inclusions hosted in fluorite mineralisation in the roof-zone preserve a fluid which is though to be close to the juvenile fluid exsolved from the melt. The presence of extensive fluorite mineralisation and highly saline brines demonstrates the physiochemical potential the melts and fluids of the MSF had to complex, transport and concentrate elements to economic amounts.

Chapter 7

Radiogenic Isotope Analysis

7.1 Introduction

Isotopic analysis is often applied to igneous provinces for the purposes of a) arriving at age estimates of particular events, b) examining the source regions of magmas and c) understanding the chemical and provenance of hydrothermal fluids. Previous isotopic studies on Gardar rocks have principally been concerned with dating the major intrusions of the province. Early Rb-Sr whole-rock radiometric analysis (Blaxland *et al.,* 1978) provided age estimations for each of the major central complexes and divided igneous activity in the Gardar divided into three principal events. More recent U-Pb work (summarised by Upton *et al.,* 2003) has further constrained Gardar magmatism in favour of two main phases of igneous activity. Despite the recent attention Gardar centres have received there have been relatively few isotopic studies carried out on the centres of the Igaliko complex, as a result the early extent of Gardar magmatism still remains somewhat contentious.

Other than the publications concerning the timing of Gardar magmatism there has been little research into the isotopic evolution of individual complexes. Taylor and Upton (1993) presented Pb-isotope data for the Kûngnât complex and Tugtutôq Younger Giant Dyke complex and suggested that isotopic variation between these complexes could be attributed to variable contributions from two isotopically distinct crustal components, derived from Proterozoic (Tugtutôq) and Archaean (Kûngnât) crust. Similarly, Andersen (1997) demonstrated using Sm-Nd and Pb-Pb isotope systems that the carbonatites and alkali-silicates of the Qassiarsuk volcanic sequence, though dominantly mantle derived, show evidence for a significant contribution from a locally-derived crustal component. Goodenough (1997) and Goodenough *et al.* (2000) demonstrated using Rb-Sr, Sm-Nd and Pb-Pb isotopes that both the Kûngnât and Ivigtût complexes show evidence for crustal contamination prior to isotopic disturbance through fluid activity. Each study demonstrated that although alkaline magmas within the Gardar are predominantly mantle derived, contributions from crustal components, either at depth and/or during emplacement, played a significant role in the overall chemistry of the centres.

The present study aims to provide a new age estimate for the events within the Motzfeldt centre. This is explored using methods by which the magmatic and hydrothermal

ages can be deconvoluted and demonstrate how some of the problems associated with dating centres with complex hydrothermal histories can be overcome. In addition the provenance of rocks within the Igaliko complex is also poorly understood, particularly their evolution from mantle source to emplacement. This chapter attempts to identify the provenance of the Motzfeldt centre and to characterise the major components which controlled the geochemical and isotopic composition of these magmas.

7.2 U-Pb systematics of Motzfeldt Sø Formation zircons

A total of 40 in situ laser ablation multi collector inductively coupled plasma mass spectrometry (LA-MC-ICPMS) spot analyses were made on 21 zircon separates (samples GJM06-18 & GJM06-29) from the altered syenites of the Motzfeldt Sø Formation (Table 7.1). Analyses were made on areas of zircon with dark blue CL luminescence (interpreted as preserving magmatic zones, chapter 3) and from regions with light blue luminescence (showing textural evidence for alteration under sub-solidus conditions). U-Pb spot analyses from both regions are plotted on the U-Pb Concordia diagram (Fig. 7.1). The U-Pb Concordia (Fig. 7.1a) shows a large range of isotopic compositions with a strong grouping of points around 1300 Ma on the Concordia curve and a significant number of points plotting outwith this cluster, defining a line of discordia between 350 and 900 Ma. The cluster of concordant points yield a Concordia age (Ludwig, 2003) of 1273 ± 8 Ma (Fig. 7.1b). The Rb-Sr isochron age estimate for the Motzfeldt centre by Blaxland *et al.,* (1978) was 1282 ± 30 Ma (recalculated using decay constants of Steiger and Jäger (1977)), although those data show significant scatter with an MSWD of 18.06. Finch *et al.* (2001) noted that the residuals from the Motzfeldt isochron of Blaxland *et al.* (1978) are greatest for samples collected north of Motzfeldt Sø, belonging to the MSF, suggesting either that these samples have significantly different initial $^{87}Sr/^{86}Sr$ ratios relative to the units south of Motzfeldt Sø (FDF), or that rocks of different ages have been considered together. Removal of samples belonging to the MSF provides a higher precision Rb-Sr isochron age of 1287 ± 4 Ma for the emplacement of the FDF. The greater spread of age dates using the Rb-Sr system are to be expected since most Rb and Sr in the rocks is hosted in feldspars and micas and these minerals are heavily altered in most Motzfeldt samples, particularly so in MSF samples. Hence the precision on the Rb-Sr age estimate is a larger value and the accuracy may be suspect due to open system isotope behaviour.

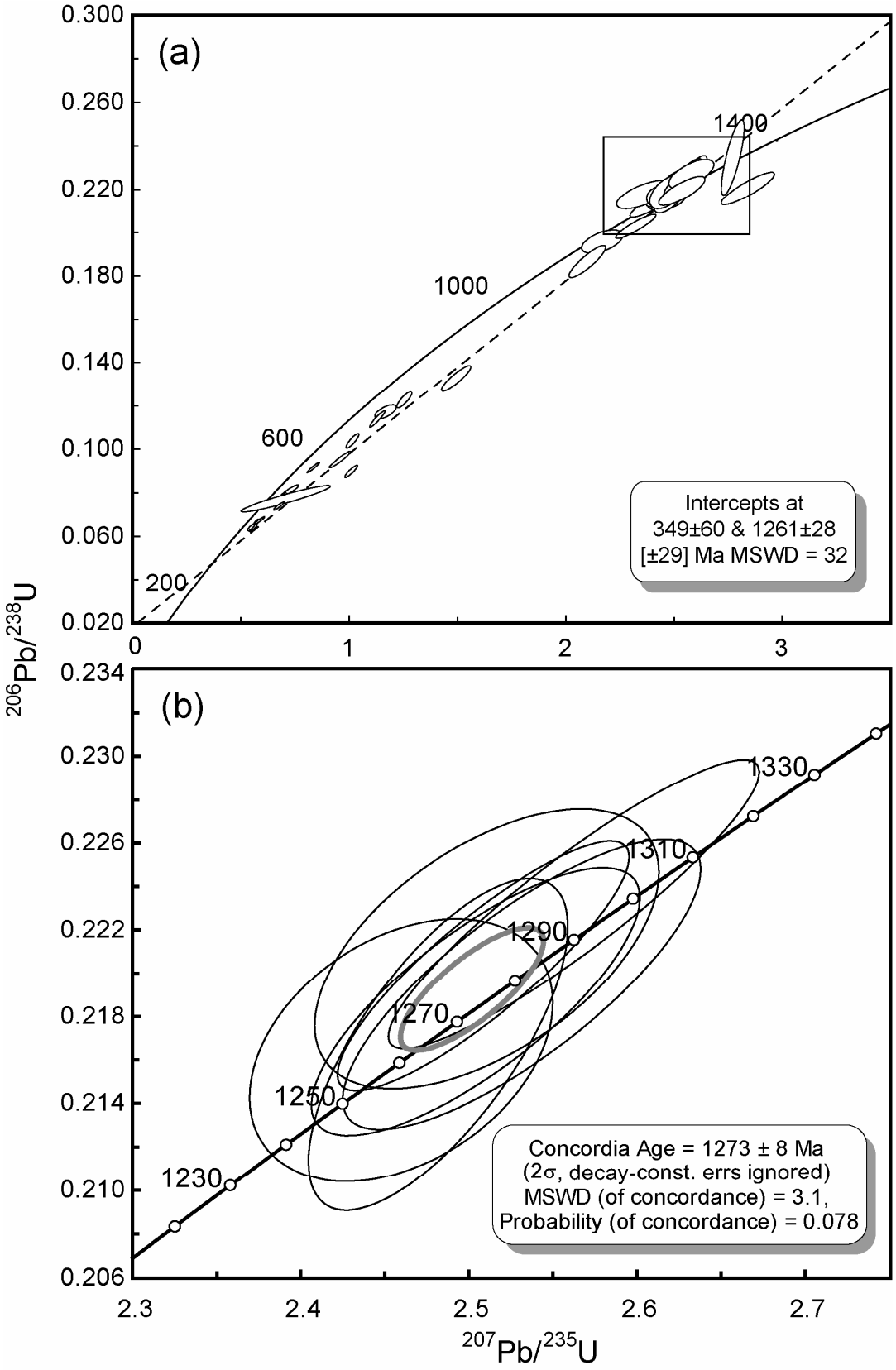

Figure 7.1. (a) U-Pb Concordia diagram of 40 spot analyses on 21 zircon samples dated by U-Pb LA-MC-ICPMS. Box shows area of concordant analyses. (b) Concordant zircon analyses from preserved magmatic zones defining strong Concordia age of 1273 ±8 Ma (MSWD = 3.1). Zircon analyses are shown as ± 2σ error ellipses.

The Concordia diagram (Fig. 7.1a) also shows a number of normally discordant points plotting along a discordia line. These points generally correlate with analyses from altered areas of zircon characterised by homogeneous textures with bright blue CL and dark BSE emissions. Figure 7.2 shows an idealised illustration of zircon sample GJM06-18-1 in CL (see Fig. 3.7a for CL image), with dark blue oscillatory zoned magmatic zircon and light blue homogenous patches of alteration. This illustrates the strong correlation between areas of alteration and isotopic discordance.

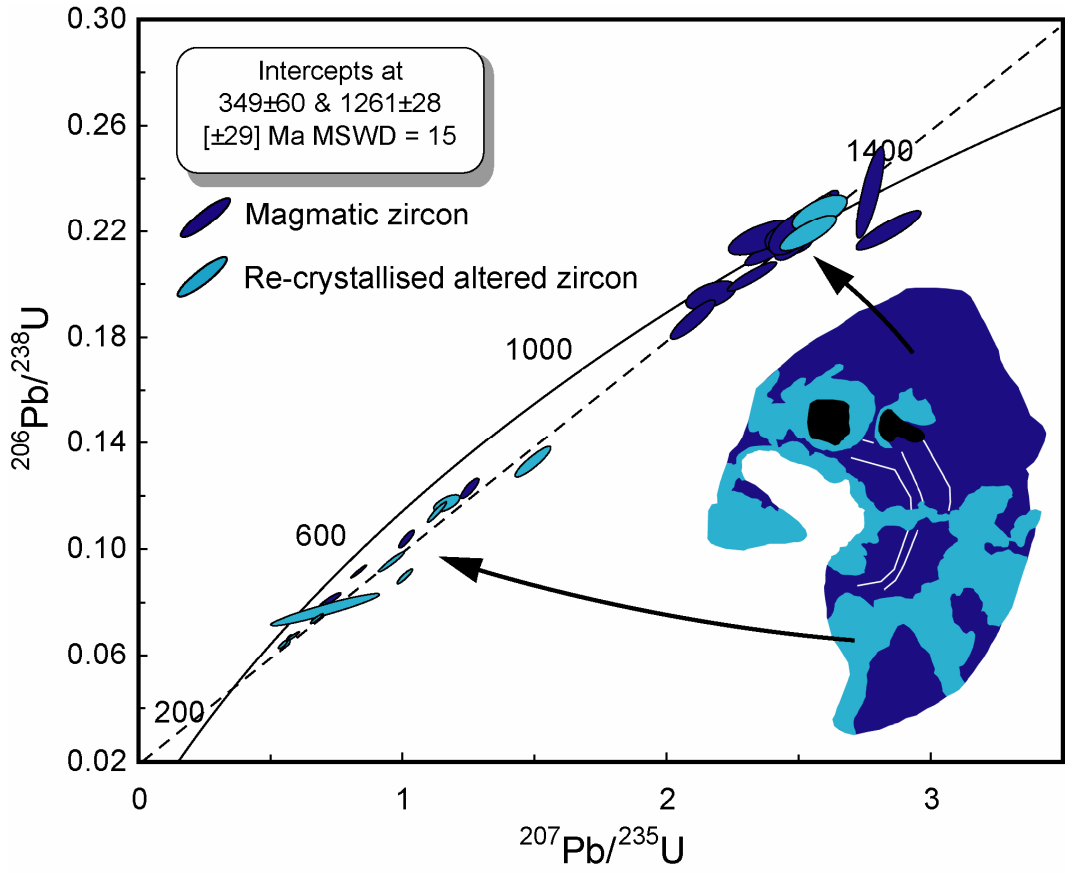

Figure 7.2. U-Pb Concordia diagram of all zircon points analysed by LA-MC-ICPMS. Idealised illustration of zircon sample GJM06-18-1 showing correlation between discordant points displaying a bright blue CL emission (dark BSE), interpreted to have experienced alteration and re-crystallisation during the sub-solidus. Analyses from areas representing preserved magmatic zones generally provide Concordant ages. Zircon analyses are shown as ± 2σ error ellipses.

Table 7.1 *U-Pb data for zircons from the Motzfeldt Sø Formation*

Magmatic areas	$^{207}Pb/^{206}Pb$	2σ	$^{207}Pb/^{235}U$	2σ	$^{206}Pb/^{238}U$	2σ
GJM06-18-2a	0.08824	0.00208	2.76907	0.02133	0.23489	0.0071
GJM06-18-2b	0.09346	0.00111	2.83803	0.05071	0.22067	0.00312
GJM06-18-2c	0.0821	0.00052	2.52509	0.03224	0.22343	0.00324
GJM06-29-03a	0.08199	0.00049	2.55308	0.03135	0.22624	0.00327
GJM06-29-03b	0.0818	0.00063	2.4656	0.0344	0.219	0.0032
GJM06-29-04a	0.06034	0.00034	0.55336	0.00654	0.06648	0.00083
GJM06-29-05a	0.07115	0.00041	1.1214	0.01513	0.11432	0.00156
GJM06-29-06a	0.06325	0.00029	0.68194	0.00766	0.07813	0.00094
GJM06-29-06b	0.07007	0.00042	1.00668	0.01207	0.10428	0.00135
GJM06-29-06c	0.08202	0.00042	2.57572	0.03071	0.22798	0.00322
GJM06-29-07a	0.07343	0.00042	1.24743	0.01418	0.12305	0.00156
GJM06-29-07c	0.08309	0.00041	2.48174	0.03152	0.21673	0.00312
GJM06-29-07d	0.08206	0.00042	2.50565	0.03055	0.22153	0.00316
GJM06-29-07e	0.08166	0.00043	2.49129	0.02962	0.22136	0.0031
GJM06-29-08a	0.0821	0.00076	2.5107	0.04183	0.22112	0.00263
GJM06-29-09a	0.08104	0.00103	2.09513	0.03534	0.18694	0.00303
GJM06-29-09b	0.08256	0.0007	2.31879	0.03745	0.20311	0.00226
GJM06-29-10	0.082	0.0007	2.45967	0.03748	0.21709	0.00242
GJM06-29-11a	0.07811	0.00101	2.35705	0.0522	0.21786	0.00278
GJM06-29-11b	0.08239	0.00063	2.50864	0.03544	0.22034	0.00235
GJM06-29-12	0.0831	0.00077	2.56248	0.04508	0.22318	0.00272
GJM06-29-13c	0.06493	0.00046	0.82477	0.01274	0.09215	0.00101
GJM06-29-13d	0.0637	0.00083	0.71659	0.01672	0.08158	0.001
GJM06-29-14a	0.08312	0.00067	2.50407	0.03991	0.21869	0.00252
GJM06-29-14b	0.08192	0.00065	2.46276	0.03903	0.2182	0.00251
GJM06-29-14c	0.0825	0.00061	2.45974	0.03684	0.21646	0.00247
GJM06-29-15a	0.08151	0.00083	2.40164	0.04486	0.21372	0.0026
GJM06-29-16b	0.0801	0.00088	2.16215	0.03904	0.19597	0.00221
Altered areas						
GJM06-29-04b	0.08034	0.00044	0.99812	0.01208	0.09018	0.00113
GJM06-29-05b	0.07115	0.00041	1.1214	0.01513	0.11432	0.00156
GJM06-29-07b	0.07189	0.00061	0.94793	0.02027	0.09569	0.00159
GJM06-29-07b	0.07189	0.00061	0.94793	0.02027	0.09569	0.00159
GJM06-29-08b	0.08338	0.00077	2.53148	0.04352	0.21948	0.00273
GJM06-29-09c	0.06156	0.00049	0.57725	0.00924	0.06783	0.00069
GJM06-29-13a	0.08215	0.00072	2.57574	0.04334	0.22742	0.00275
GJM06-29-13b	0.07143	0.00065	1.15834	0.01972	0.11756	0.00131
GJM06-29-14d	0.06033	0.0004	0.53698	0.00752	0.06462	0.00064
GJM06-29-15b	0.08097	0.00084	1.48618	0.02748	0.13331	0.00236
GJM06-29-15c	0.06116	0.00046	0.54379	0.00812	0.06456	0.00065
GJM06-29-16a	0.06483	0.00052	0.66432	0.01025	0.07444	0.00074
GJM06-29-16c	0.06517	0.00391	0.69721	0.08454	0.07768	0.00245

The upper intercept age of 1261 ± 28 Ma is within error of the concordant age from preserved magmatic zircon analyses. The lower intercept age on Concordia diagrams is often considered to record a secondary event during which most or all of the radiogenic Pb accumulated since the time of isotopic closure may be lost from the zircon (e.g. Geisler *et al.,* 2007; Harley & Kelly, 2007 and Wetherill, 1956, 1963). Isotopic discordance usually occurs

during the superposition of a younger, real, geological event on a suite of zircons and is often associated with the growth of new zircon crystals. Therefore the lower intercept value can be used to record the age of an episodic Pb-loss event, assuming the zircon lost all previously accumulated radiogenic Pb. However in the south of Greenland there is no recorded geological event which could correlate with the lower intercept age of 349 ± 60 Ma from the MSF zircons. Given the textural relationship between hydrothermal alteration and the discordant points in the zircons of the present study, the lower intercept age should provide an age for the hydrothermal event. Taking these discordant data on face value, it would suggest that the hydrothermal alteration is substantially (i.e. ~900 Ma) younger than the magmatism. There is a possible correlation with Caledonian events, which occur in East Greenland ~1000 km to the NE, but there is no evidence of Caledonian events in South Greenland. The lower intercept age is therefore interpreted as a spurious age relating to open system behaviour. One suggestion for this trend may be that alteration and damage to structural domains in the zircon, associated with the alkaline hydrothermal phase, has resulted in partial and steady diffusive loss of radiogenic Pb (i.e. Tilton, 1960) in confined domains of the zircon, resulting in a series of variably discordant analyses spread out along a single discordia. However there are no points along the Concordia, which would be expected if constant diffusion through time where the control. The lack of points along the Concordia makes suggesting diffusive loss of Pb from altered domains somewhat problematic. Although the exact control over the isotopic discordance is uncertain it is clear that elevated hydrothermal activity associated with the final stages of crystallisation has played an important role in the isotopic systematics of the MSF zircon population.

7.3 Lu-Hf systematics of Motzfeldt Sø Formation zircons

In addition to U-Pb isotope analyses, the same zircon separates were analysed for Lu-Hf isotopes using LA-MC-ICPMS (Table 7.2). Figure 7.3 shows the time corrected $^{176}Hf/^{177}Hf$ ratios plotted against age determined from U-Pb analyses. The U-Pb data (Fig. 7.1) from zircon separates shows that several samples contain areas displaying strong isotopic discordance from re-crystallization and open-system behaviour of U-Pb isotopes under sub-solidus conditions. This raises a problem as there is a possibility that post-magmatic modification may have a similar effect on Hf isotopic compositions, permitting open-system behaviour of the Hf isotopes. This issue has been addressed in several studies (e.g. Hoskin & Black, 2000; Patchett *et al.,* 1981; Patchett, 1983; Smith *et al.,* 1987) examining variably discordant zircon populations from a variety of geological environments to investigate

systematic disturbance to the Lu-Hf system with isotopic discordance in the U-Pb system. Patchett (1983) showed that zircons yield identical $^{176}Hf/^{177}Hf$ ratios in both near-concordant and highly discordant areas of the same zircons. This work was later confirmed by Hoskin and Black (2000) who demonstrated that zircons may lose U, Th and radiogenic Pb during post-magmatic modification, associated with metamorphism or hydrothermal activity, yet retain primary abundances of Lu and Hf from crystallisation. Both these studies suggest that whilst samples experience notable disturbance of the U-Pb system, showing strong isotopic discordance, the Lu-Hf system retains the primary isotopic signature acquired during initial crystallisation. This is particularly important for the present study as many of the zircons display strong U-Pb isotopic discordance. Hf isotope analyses made on discordant areas of zircon have been corrected before plotting on the $^{176}Hf/^{177}Hf$ diagram in Figure 7.3 and are plotted using concordant U-Pb ages obtained from fresh magmatic areas of the same crystal. These point analyses are shown with light blue circles on Figure 7.3.

Crustal residence ages of zircon can be constrained in two ways using the Hf isotope system; by the depleted mantle model age or depleted mantle zircon age. The depleted mantle model age (t_{DM}) of a mineral or rock in the Earth's crust records the time since the hafnium content of the mineral or rock being analysed was last at equilibrium with a depleted (high Lu/Hf) mantle reservoir (Fig. 7.4). Therefore the depleted mantle model age is an estimate of the age of the protolith from which a particular rock or mineral was sourced (Griffin *et al.,* 2000). However because of the low Lu/Hf ratio found in zircon (<0.002) model ages calculated solely from the measured $^{176}Hf/^{177}Hf$ values will only yield a minimum age for the protolith of the zircon; this is termed the depleted mantle zircon age (t_{DMZ}). However, if the crystallisation age of the zircon is available from U-Pb analysis, a more realistic model age can be calculated for the protolith. This is the depleted mantle whole-rock age (t_{DMW}) (Fig. 7.4 and 7.5). The t_{DMW} age is achieved by modelling a growth curve for a model reservoir with an appropriate Lu/Hf ratio through the initial $^{176}Hf/^{177}Hf$ ratio of the zircon (Andersen *et al.,* 2002). For samples where no whole-rock data are available, the t_{DMW} value can be estimated from the measured $^{176}Hf/^{177}Hf$ and $^{176}Lu/^{177}Hf$ ratios. During the present study the only available data were in situ U-Pb ages and Lu/Hf ratios from zircon separate analysis, therefore a growth curve was forced for the system using the available data with a $^{176}Lu/^{177}Hf$ value of 0.010. This value is recognised as the $^{176}Lu/^{177}Hf$ ratio of a felsic protolith.

Table 7.2. *Lu-Hf data for zircons from the Motzfeldt Sø Formation*

Magmatic areas	$^{176}Hf/^{177}Hf$	2σ	$^{176}Lu/^{177}Hf$	2σ	$^{176}Yb/^{177}Hf$	2σ
GJM06-18-1a	0.282085	0.000015	0.001321	0.000002	0.067065	0.000850
GJM06-18-1b	0.281856	0.000038	0.000212	0.000002	0.012096	0.000082
GJM06-18-1c	0.282014	0.000029	0.001734	0.000045	0.082415	0.002000
GJM06-29-4a	0.282106	0.000011	0.002044	0.000014	0.129009	0.001500
GJM06-29-4b	0.282118	0.000013	0.002486	0.000089	0.156211	0.007100
GJM06-29-5a	0.282122	0.000013	0.001537	0.000055	0.102472	0.004900
GJM06-29-5b	0.282051	0.000015	0.000903	0.000020	0.059087	0.001000
GJM06-29-7a	0.282080	0.000016	0.000558	0.000006	0.033722	0.000260
GJM06-29-7b	0.282195	0.000018	0.002477	0.000012	0.156269	0.001800
GJM06-29-7c	0.282108	0.000014	0.002521	0.000013	0.154161	0.000830
GJM06-29-8a	0.282114	0.000022	0.002947	0.000007	0.186717	0.001400
GJM06-29-9b	0.282062	0.000019	0.001218	0.000041	0.080377	0.002600
GJM06-29-10a	0.282044	0.000022	0.000926	0.000005	0.058614	0.000910
GJM06-29-10b	0.281996	0.000026	0.000529	0.000026	0.034495	0.001600
GJM06-29-11c	0.282266	0.000019	0.002257	0.000006	0.144449	0.001500
GJM06-29-12a	0.282051	0.000015	0.001765	0.000036	0.098801	0.002300
GJM06-29-12b	0.282109	0.000021	0.001502	0.000059	0.088994	0.004000
GJM06-29-13a	0.282219	0.000016	0.002907	0.000012	0.158817	0.000770
GJM06-29-13b	0.282180	0.000012	0.002492	0.000005	0.136304	0.001400
GJM06-29-14a	0.282233	0.000012	0.002704	0.000020	0.145718	0.001800
GJM06-29-14b	0.282054	0.000017	0.001165	0.000006	0.060063	0.000660
GJM06-29-15a	0.282150	0.000017	0.002759	0.000032	0.138645	0.002000
GJM06-29-15b	0.282176	0.000016	0.002954	0.000032	0.154832	0.002300
GJM06-29-16a	0.282062	0.000012	0.001230	0.000018	0.060977	0.001600
GJM06-29-16b	0.282182	0.000014	0.002550	0.000017	0.127228	0.001300
GJM06-29-17a	0.282161	0.000016	0.004363	0.000022	0.209153	0.002200
GJM06-29-17b	0.282081	0.000014	0.003117	0.000044	0.161674	0.003400
GJM06-29-18a	0.282104	0.000012	0.002564	0.000026	0.121904	0.001600
GJM06-29-20a	0.281980	0.000013	0.001996	0.000071	0.102131	0.004200
GJM06-29-20b	0.282110	0.000011	0.001648	0.000058	0.080533	0.002200
Altered areas						
GJM06-29-3a	0.281993	0.000019	0.001096	0.000043	0.071600	0.004000
GJM06-29-3b	0.282060	0.000014	0.001852	0.000049	0.112460	0.002900
GJM06-29-6b	0.282344	0.000029	0.003386	0.000130	0.247007	0.009300
GJM06-29-8b	0.282116	0.000014	0.001711	0.000007	0.108418	0.000440
GJM06-29-10c	0.282104	0.000018	0.001174	0.000031	0.081223	0.002900
GJM06-29-9a	0.281973	0.000020	0.000717	0.000060	0.049237	0.004600
GJM06-29-11a	0.282149	0.000023	0.002031	0.000004	0.126982	0.001500
GJM06-29-11b	0.282117	0.000018	0.001176	0.000009	0.072052	0.001400
GJM06-29-19a	0.282151	0.000014	0.002196	0.000009	0.102587	0.001000
GJM06-18-1b	0.281929	0.000013	0.000898	0.000120	0.043960	0.005800

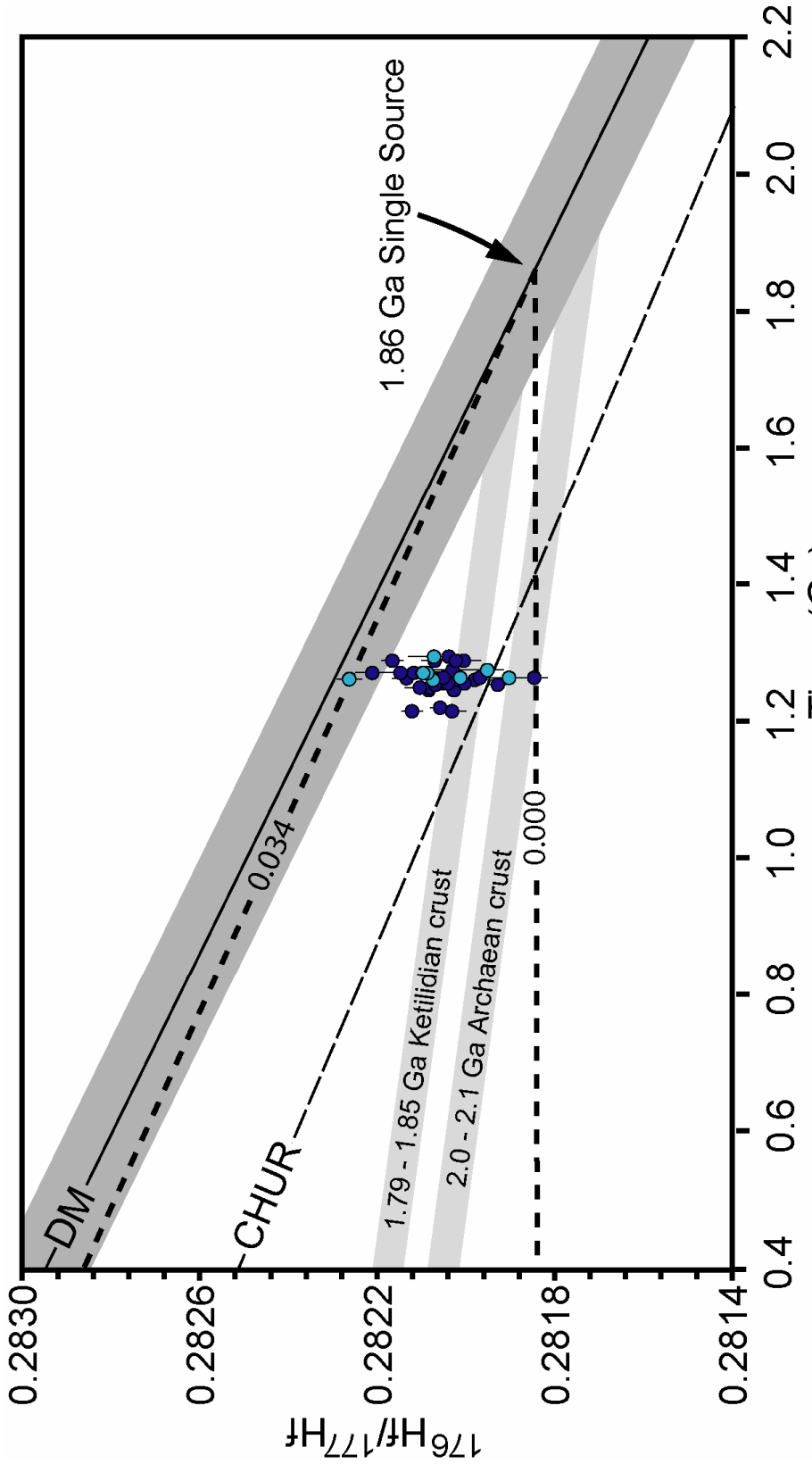

Figure 7.3. Hf isotope evolution diagram for 38 LA-MC-ICPMS spot analyses on 21 zircon separates. Data points are colour coded with the same colours in Fig. 7.2. Age plotted as $^{207}Pb/^{206}Pb$ zircon ages. Growth curves are shown for chondrite uniform reservoir (CHUR) (Blichet-Toft and Albarède, 1997) and depleted mantle (DM) (Griffin *et al.*, 2000). The shaded field surrounding the DM curve represents a range of 3 ε_{Hf} units. Theoretical fields for the 1.79-1.85 Ga Ketilidian crust (Garde *et al.*, 2002) and 2.0-2.1 Ga Archean basement (Knudsen *et al.*, 2001) are show as possible protolith sources. Each sample is shown with 2σ error bars for $^{176}Hf/^{177}Hf$.

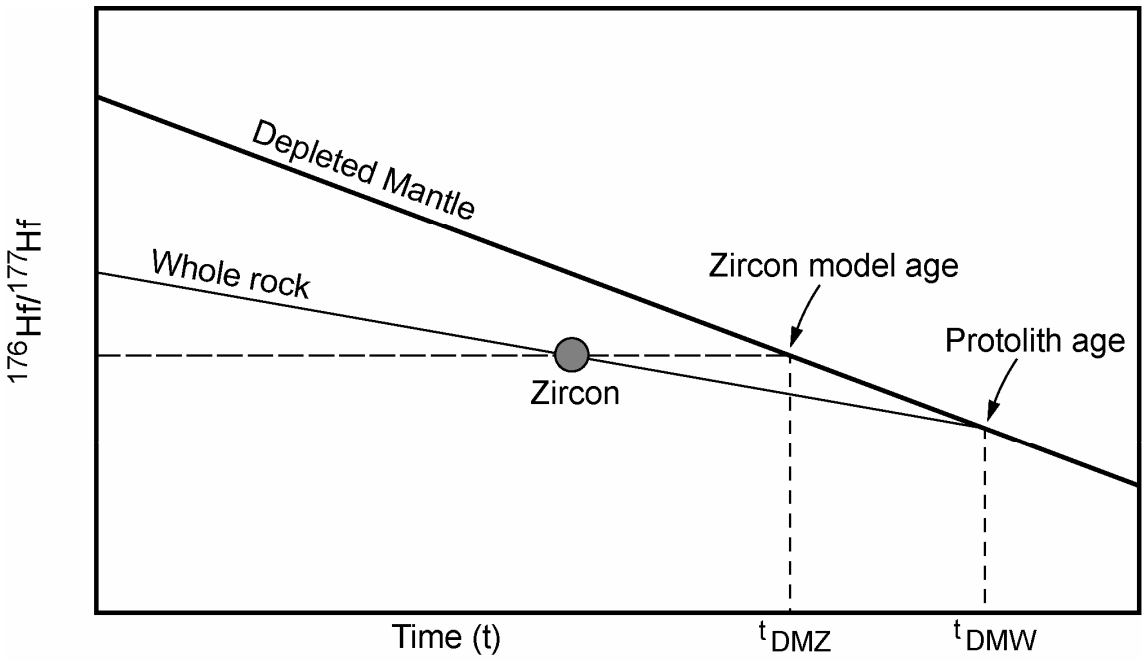

Figure 7.4. Example of the principle of Hf isotope model age calculation after Andersen *et al.,* (2002), showing the difference between the zircon model age (t_{DMZ}) and the depleted mantle whole-rock age (t_{DMW}), which is a more realistic model age for the protolith of the zircon host rock. The t_{DMW} is calculated by modelling a model growth curve with and $^{176}Lu/^{177}Hf$ ratio, corresponding to the host rock, through the initial ratio ($^{176}Hf/^{177}Hf$) of the zircon.

The zircon population from the MSF show a broad range of $^{176}Hf/^{177}Hf$ ratios between 0.28185 and 0.28226 ± 0.00003 (2 standard deviations), corresponding to epsilon (ε_{Hf}) values of -3.96 - 8.96. Using concordant U-Pb ages obtained from the same zircon separates the $^{176}Hf/^{177}Hf$ values yield crustal residence ages between 1.33 - 2.02 Ga using the depleted mantle whole-rock method (t_{DMW}). Using the depleted mantle zircon method (t_{DMZ}) a range between 1.31 - 1.85 Ga is calculated for the model age range of the protolith. Since the crystallisation ages of the MSF zircon population are available the calculated t_{DMW} residence ages are preferred over the t_{DMZ} residence ages as these are thought to provide a more accurate estimate of the protolith age.

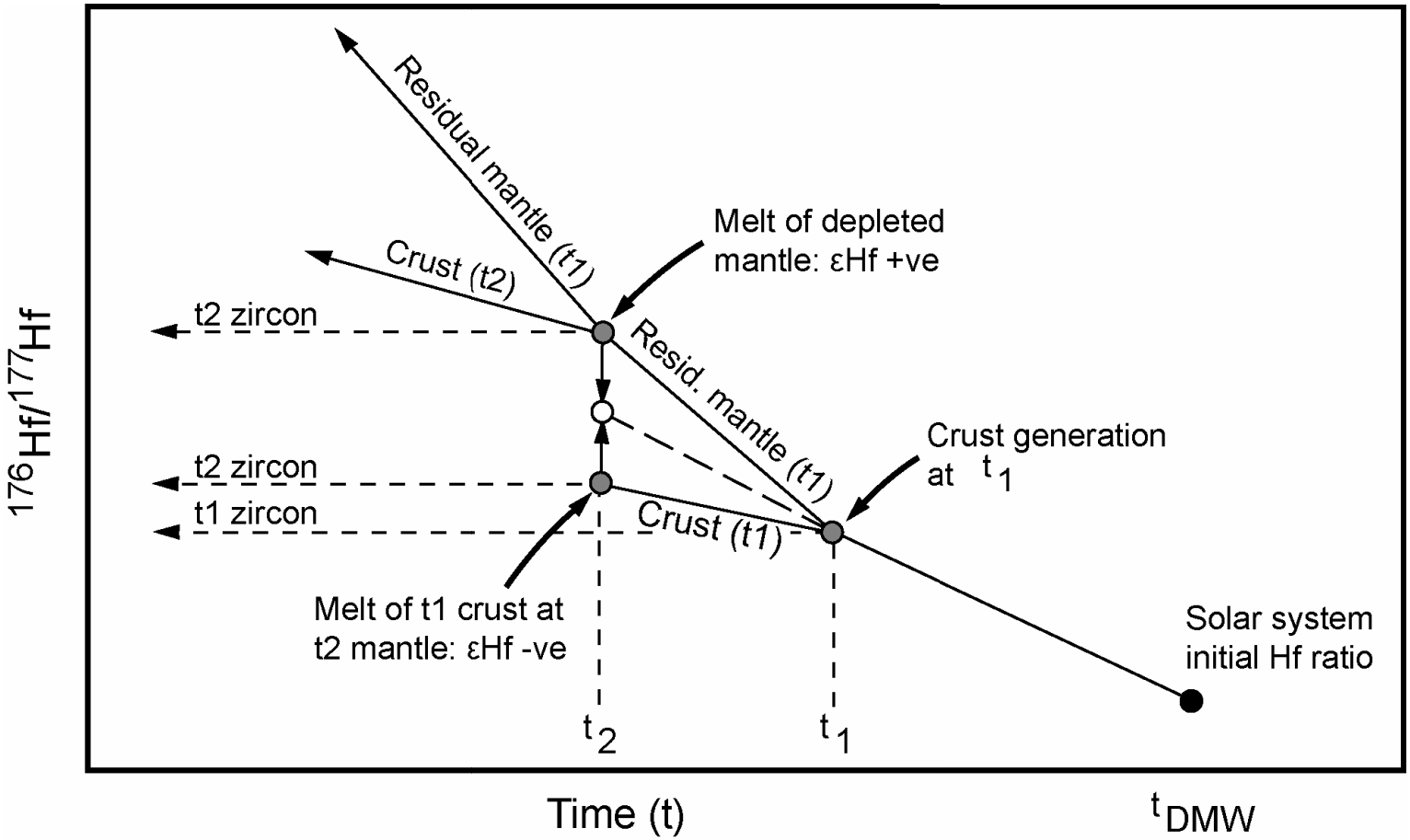

Figure 7.5. Schematic Hf evolution diagram, modified after Patchet *et al.* (1981) and Kinny and Maas (2003), for an episode of partial melting of the Earth's mantle. Partial melting at time t_1 results in divergent Hf isotope evolution paths for the newly generated crust (low Lu/Hf) and the residual, depleted mantle (high Lu/Hf). Zircons formed in the crust at time t_1 will preserve the initial $^{176}Hf/^{177}Hf$ ratio. At time t_2 a variety of sources may contribute to newly formed crust. If derived solely from the depleted mantle the εHf of zircons formed at time t_2 will be positive. However if there is mixing with a crustal component enriched in Hf the εHf value will be weakly positive, zero or negative, depending on the relative proportions of each component. Any inherited zircons at t_2 will have cores with lower εHf than the newly crystallized rims.

The range of $^{176}Hf/^{177}Hf$ values and corresponding model ages from the MSF zircons span a range between the depleted-mantle (DM) and chondritic uniform reservoir (CHUR) growth curves (Fig. 7.3) with several samples displaying $^{176}Hf/^{177}Hf$ values lower than the CHUR line. The spread of $^{176}Hf/^{177}Hf$ values observed in the zircons of the present study suggests either: 1) Segregation of a single melt from a heterogeneous source region of uniform age yet variable Lu/Hf ratio and hence variable $^{176}Hf/^{177}Hf$, or 2) mixing of melts from two or more source rocks with different crustal residence ages, and hence different Hf isotopic compositions. To evaluate how realistic a single source model is for the Hf isotopic evolution of the Motzfeldt centre, the range of $^{176}Lu/^{177}Hf$ needed to obtain the $^{176}Hf/^{177}Hf$ values from the zircons must be estimated. The minimum age of a single source region is provided by the intersection of a horizontal line ($^{176}Lu/^{177}Hf = 0$) through the zircon with the lowest $^{176}Hf/^{177}Hf$ value with the depleted mantle (DM) curve (Andersen *et al.,* 2007). Applying this to the data set of the present study, a minimum crustal residence age of 1.86 Ga is obtained, which is comparable with ages obtained for the Ketilidian basement (1854 ± 4Ma – 1794 ± 1Ma, Garde *et al.,* 2002). To account for the range of $^{176}Hf/^{177}Hf$ obtained from the Motzfeldt zircons the $^{176}Lu/^{177}Hf$ signature of the single 1.86 Ga heterogeneous source must vary from zero to 0.034 (Fig. 7.3). Given that the minimum crustal residence age is consistent with age estimates for the Ketilidian, the single source model is consistent with derivation exclusively from the Ketilidian crust. However the maximum $^{176}Lu/^{177}Hf$ value (0.034) is considerably higher than average crustal values. The 1.86 Ga crustal residence age determined for the source region only provides a minimum age by assuming the source region is Lu free (i.e. $^{176}Lu/^{177}Hf = 0$). This is highly unrealistic. If the source region is older than 1.86 Ga the $^{176}Lu/^{177}Hf$ must be greater than zero. Therefore for an older source region, the $^{176}Lu/^{177}Hf$ value of the zircon with the lowest $^{176}Hf/^{177}Hf$ value must be greater than zero. Similarly the maximum $^{176}Lu/^{177}Hf$ value must also increase to greater then 0.034. This model is unlikely given that the geochemical and petrological character of all Gardar intrusions strongly suggest derivation from a mantle component, rather than a crustal component. Based on this evidence and the Hf isotopic data, a single source model inadequately models the isotopic character of zircons from the Motzfeldt centre.

A model envisaging multiple source regions complies with wider perceptions on the source of Gardar magmas and may more closely model the Hf evolution of the Motzfeldt centre. Although parent melts to all Gardar intrusions are generally considered to be mantle derived, an exclusively mantle character is unlikely given the fact that the ascending magmas

have penetrated a thick section of continental crust and crustal contamination is inferred. Deviation from an exclusively mantle derived isotopic signature may be achieved through contamination of depleted mantle residua (high Lu/Hf) with an earlier segregated crustal component (low Lu/Hf). A crustal component is favoured as Hf is preferentially partitioned into liquids more readily than Lu, therefore differentiated continental crust acquires a Lu/Hf ratio lower than the residual melt from which it was derived.

The relatively wide range of $^{176}Hf/^{177}Hf$ values and corresponding range of t_{DMW} ages found in the MSF zircons suggest that source rocks with notably different $^{176}Hf/^{177}Hf$ values contributed to the final melt. To generate the $^{176}Hf/^{177}Hf$ range of the present data set would require source rocks with $^{176}Hf/^{177}Hf$ <0.28185 and > 0.28226 respectively. At 1.27 Ga the only possible component with a $^{176}Hf/^{177}Hf$ >0.28226 is from the global depleted mantle source with a $^{176}Hf/^{177}Hf_{1.27\ Ga}$ = 0.2823-0.2824. This suggests that the principal source of the radiogenic Hf component was dominantly depleted mantle in origin. For the data set to span the range observed, contribution from one or more additional components with a lower Lu/Hf ratio are also required.

Figure 7.3 shows the suggested $^{176}Hf/^{177}Hf$ range for Ketilidian crust of 1.79-1.85 Ga age (Garde *et al.,* 2002) and the corresponding $^{176}Hf/^{177}Hf$ range for the time interval suggested by Knudsen *et al.* (2001) for the generation of a primitive Archaean continental crust between 2.0-2.1 Ga. Ketilidian age rocks outcrop throughout the south of Greenland and host the Motzfeldt centre and a majority of the major Gardar central complexes. Although earlier Archaean age rocks are found within the Border zone of the orogen in the Ivigtût region of the province, the extent of such rocks at depth remains unknown. The $^{176}Hf/^{177}Hf$ values of zircons from the present study ranges between the depleted mantle (DM) curve and the fields suggested for Ketilidian and Archaean age continental crust. The data therefore define a mixing array between the depleted mantle and Ketilidian and Archaean crust, suggesting that in addition to a dominantly mantle derived source with a high Lu/Hf signature there has been subsequent contamination during ascent and emplacement by a crustal component with a much less radiogenic Hf signature. The mixing array between the depleted mantle and crustal rocks strongly suggests that Ketilidian and Archaean rocks were the principal contaminant sources in the rocks of the Motzfeldt centre, however contributions from older primitive crustal components at depth cannot be ruled out. Similar suggestions have been given by Andersen (1997) for the evolution of the nearby Qassiarsuk volcanic complex, by Taylor and Upton (1993) for the evolution of the Tugtutôq Younger Giant Dyke and Kûngnât Fjeld and

by Goodenough (1997) who noted that the Pb isotopic composition of Gardar magams may be used to demonstrate the nature of the crustal contaminants. Similarly Upton and Thomas (1980) also hypothesised that the variation in degree of silica saturation in the Tugtutôq Younger Giant Dyke complex may be due to variable degrees of crustal assimilation. The Hf isotopic data from zircon from the MSF therefore suggest that in addition to the dominantly mantle derived source, there was a significant contribution from earlier differentiated pre-Gardar crustal rocks.

7.4 Pb-Pb Isochron dating of Motzfeldt Sø Formation pyrochlores

A total of 34 pyrochlore separates were analysed for Pb isotopes from two pyrochlore bearing samples (GJM06-18 & GJM06-64) within the altered MSF. Additionally, 15 whole rock Pb isotope analyses were carried out on syenite units in the MSF and FDF (Table 7.3). The whole rock data show a relatively restricted isotopic range and fall along a relatively straight line on the $^{206}Pb/^{204}Pb$ vs $^{207}Pb/^{204}Pb$ plot (Fig. 7.6). The Pb-isotopes for the MSF typically range from 18.3 - 31.6 for $^{206}Pb/^{204}Pb$, 15.3 - 16.5 for $^{207}Pb/^{204}Pb$ and 38.4 - 44.9 for $^{208}Pb/^{204}Pb$. Sample GJM05-24 shows higher ratios (84.0, 20.8 and 45.5 respectively for $^{206}Pb/^{204}Pb$, $^{207}Pb/^{204}Pb$ and $^{208}Pb/^{204}Pb$) due to the sample containing up to 10 modal % pyrochlore. The FDF has a smaller and generally lower range of 16.3 - 20.0 for $^{206}Pb/^{204}Pb$, 15.2 - 15.5 for $^{207}Pb/^{204}Pb$ and 35.8 - 39.4 for $^{208}Pb/^{204}Pb$. Two samples of Eriksfjord basalt and sandstone have also been analysed and are shown in Fig. 7.7 for reference.

In contrast to the restricted range observed for the whole rock samples, the LA-MC-ICPMS data for altered pyrochlores from the MSF show a much larger range of isotopic compositions. Uranogenic lead ($^{207}Pb/^{204}Pb$) shows a range of 15.5 - 112.1 with a $^{206}Pb/^{204}Pb$ range of 17.1 - 1183.5. Data for both pyrochlore and whole-rock uranogenic lead are plotted in Figure 7.6. When the pyrochlore and whole rock data are regressed together an imperfectly fitted line (MSWD = 161) is obtained with an isochron age of 1266 ± 4 Ma (Model 2 solution, Ludwig, 2003). Without the whole-rock data, the linear regression is greatly improved (MSWD = 4.5), with a model 2 age of 1267 ± 6 Ma (Ludwig, 2003). This age is indistinguishable from the magmatic U-Pb zircon age of 1273± 8 Ma.

Table 7.3 *Pb-Pb data from pyrochlores from the Motzfeldt Sø Formation*

	$^{208}Pb/^{204}Pb$	1σ	$^{207}Pb/^{204}Pb$	1σ	$^{206}Pb/^{204}Pb$	1σ
Pyrochlores						
GJM06-18-1a	46.459	0.280	27.072	0.480	160.725	5.900
GJM06-18-1b	45.365	0.091	23.707	0.170	119.532	2.100
GJM06-18-1c	46.908	0.140	28.896	0.180	182.830	2.200
GJM06-18-2a	53.003	0.720	51.097	2.200	448.276	27.000
GJM06-18-2b	52.180	0.560	45.182	1.600	377.442	19.000
GJM06-18-3a	46.713	0.093	28.691	0.160	181.891	2.000
GJM06-18-4	44.763	0.054	27.213	0.440	162.911	5.400
GJM06-18-5	50.332	0.270	31.798	0.630	217.428	7.600
GJM06-18-6	48.568	0.290	28.560	0.710	179.922	8.600
GJM06-18-7a	45.975	0.110	29.425	0.530	189.713	6.400
GJM06-18-7b	46.749	0.100	25.209	0.250	138.190	3.200
GJM06-18-9a	47.480	0.110	34.115	0.200	245.978	2.300
GJM06-18-9b	47.812	0.440	35.329	1.200	260.253	14.000
GJM06-18-9c	47.567	0.650	34.566	1.700	250.304	21.000
GJM06-18-10	103.058	0.310	65.864	0.550	632.243	5.200
GJM06-18-13	47.768	0.083	31.049	0.390	208.423	4.700
GJM06-18-15	45.118	0.110	22.504	0.230	105.439	2.800
GJM06-18-17	47.105	0.250	28.049	0.660	172.179	8.100
GJM06-18-19	47.674	0.330	35.055	0.730	256.913	8.700
GJM06-18-24	54.089	0.370	35.099	0.590	259.237	7.300
GJM06-64-6a	54.478	0.180	66.177	0.810	632.746	9.700
GJM06-64-6b	67.303	0.210	111.149	0.420	1174.410	5.100
GJM06-64-7	68.421	0.220	112.058	0.620	1183.540	7.900
GJM06-64-8	62.880	0.260	100.485	0.750	1044.050	9.000
GJM06-64-10	37.650	0.018	21.588	0.061	92.925	0.750
GJM06-64-13	39.050	0.072	26.554	0.250	153.291	3.000
GJM06-64-14	61.137	0.300	91.159	0.910	931.214	11.000
GJM06-64-17	52.062	0.830	60.616	2.600	565.273	32.000
GJM06-64-19a	59.968	0.540	87.803	1.600	895.138	19.000
GJM06-64-19b	48.553	0.400	52.316	1.500	465.593	18.000
GJM06-64-22	61.302	0.810	69.974	1.600	675.604	19.000
GJM06-64-23	63.017	0.120	101.656	0.440	1060.520	5.500
GJM06-64-25	65.296	0.120	96.640	0.290	998.934	3.600
GJM06-64-26	44.640	0.100	40.517	0.300	336.128	3.100
Whole rock						
GJM06-51	25.984	0.010	16.050	0.004	44.913	0.013
GJM05-59	18.753	0.007	15.450	0.004	38.425	0.011
GJM06-62	19.344	0.007	15.472	0.004	38.902	0.011
GJM05-21	23.741	0.009	15.877	0.004	40.097	0.012
GJM06-12	18.253	0.007	15.336	0.004	38.930	0.011
GJM06-34	15.804	0.006	14.936	0.004	35.992	0.010
GJM06-72	20.865	0.008	15.593	0.004	40.033	0.012
GJM05-24	84.032	0.033	20.765	0.006	45.455	0.013
GJM06-33	18.329	0.007	15.499	0.004	37.835	0.011
GJM06-110	18.221	0.007	15.401	0.004	37.618	0.011
GJM06-116	31.607	0.012	16.530	0.005	41.053	0.012
GJM06-119	19.094	0.007	15.474	0.004	38.741	0.011
GJM06-125	20.019	0.008	15.516	0.004	39.420	0.011
GJM06-98	18.740	0.007	15.397	0.004	38.535	0.011
GJM06-90	16.267	0.006	15.251	0.004	35.843	0.010

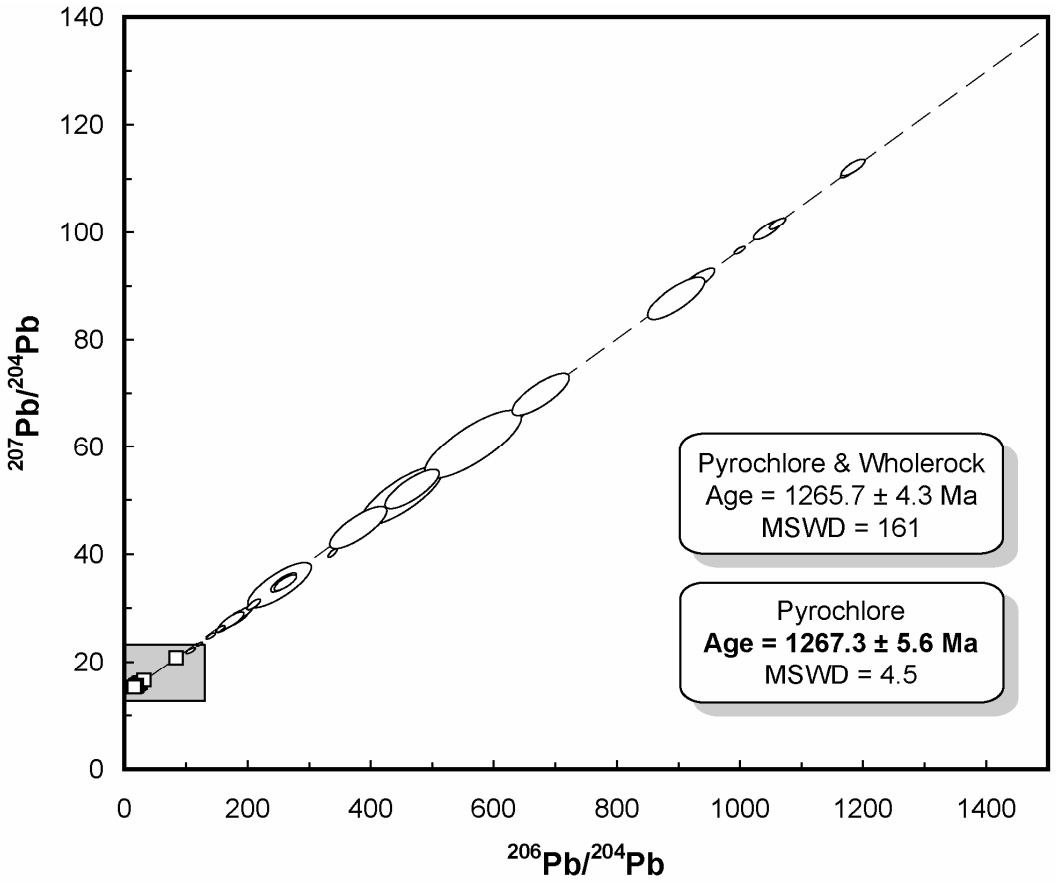

Figure 7.6. Pb-Pb isochron diagram for pyrochlore separates and whole rock analyses from the MSF. Whole rock analyses from the FDF have been omitted from the isochron calculation. The isochron regression for the whole rock and pyrochlore analyses is based on 49 samples. The more precise age estimate obtained by regressing the pyrochlore analyses on their own is based on 34 samples. LA-MC-ICPMS pyrochlore analyses are shown with ± 2σ error ellipses. Whole rock analyses are shown with basic symbols as the errors are too small to be observed on the scale of this diagram. The box surrounding the whole rock data is shown in detail in Fig. 7.7.

The altered pyrochlores have a relatively constant $^{208}Pb/^{204}Pb$ at variable $^{206}Pb/^{204}Pb$ ratios, ranging from 37.65 to 68.42 with one anomalously high sample at 103.06. The independent behaviours of thorogenic and uranogenic lead may represent fractionation of U over Th during crystallisation of the parental magma from which the pyrochlores crystallised. Alternatively, it might be interpreted as mobilisation of U and Th under sub-solidus conditions. The most obvious explanation for this trend is for U to exsolve from the pyrochlore structure, mobilised as uranyl complexes under a U6+ oxidation state. Airborne gamma spectrometry surveying during the SYDURAN project revealed significant Th anomalies in several localities in the roof zone of the MSF and notable thorium anomalies were identified during the surface sampling program of Angus and Ross plc, suggesting that Th may be localised in the roof zone of the centre through ponding of residual fluids. It is

therefore plausible that in addition to U, which may be mobilised when oxidized to the 6+ state, Th may also be mobilised during the sub-solidus and locally concentrated in unidientified Th rich phases within the high-level units of the formation.

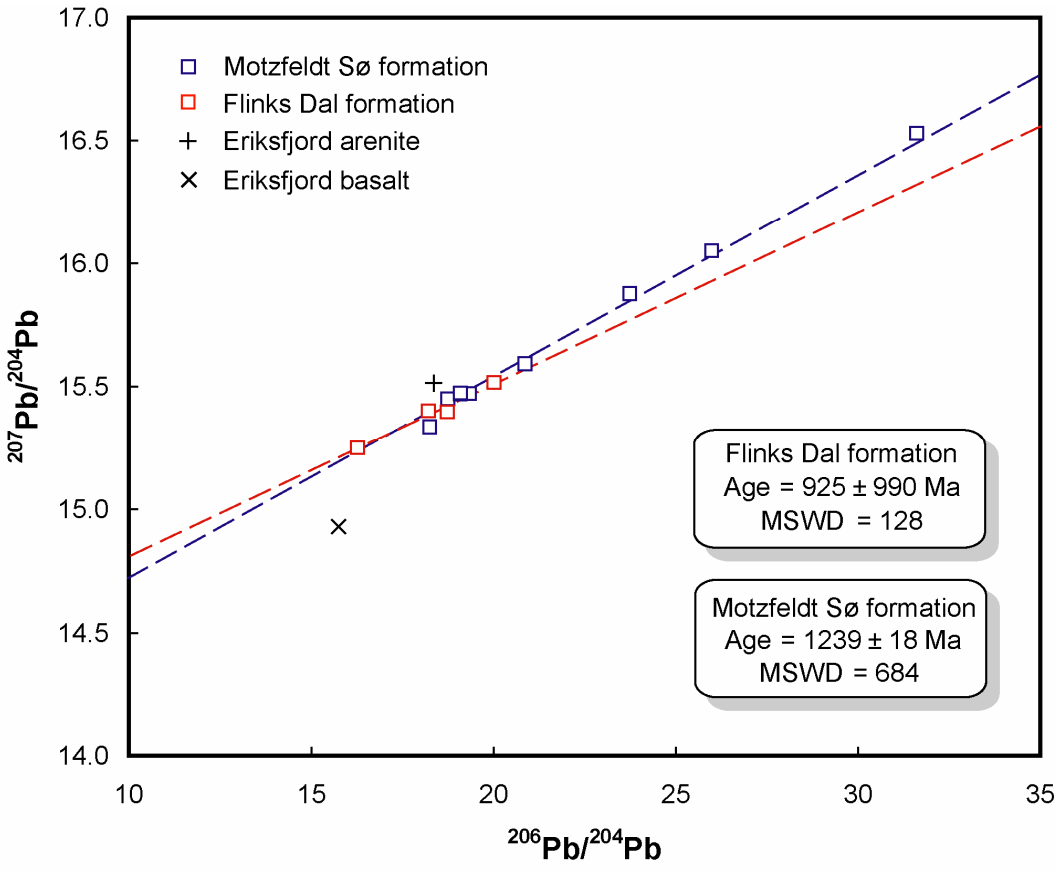

Figure 7.7. Pb-Pb isochron diagram for whole rock analyses for the MSF and FDF. Sample GJM06-24 plots at 84.06 $^{206}Pb/^{204}Pb$ and 20.77 $^{207}Pb/^{204}Pb$ and has been used during the isochron regression but is not shown on the diagram to allow other features to be observed. Analyses of Eriksfjord basalt and arenite are also shown for reference.

Although thorium is usually considered immobile in most geochemical environments, Keppler and Wyllie (1990) demonstrated that partitioning of Th (and U) into a fluid phase can occur in the presence of fluorine and/or chlorine. The Motzfeldt centre has been shown to have exceptionally high fluorine activity (chapter 5) and one of the highest inferred fluorine contents of all Gardar centres (Finch *et al.,* 1995). This inference is supported by the high modal abundance of fluorite in these rocks where it is found as intercumulus crystals and as late-stage veins. Additionally, localised fluorite mineralisation is found in the preserved roof zone of the centre suggesting ponding of F-rich fluids. Varied complexing of U and Th with fluorine-rich fluid ligands is therefore a plausible explanation for the geochemical separation

of U and Th. Although the exact process responsible for the independent behaviours of thorogenic and uranogenic lead remain unclear, it is likely that the intense subsolidus activity associated with the MSF, in particular the elevated activity of F-rich fluid ligands, played an important role in contributing to the isotopic character of pyrochlores from the MSF.

7.5 Discussion

7.5.1 Timing of Motzfeldt magmatism and its regional significance

The Gardar province has previously been interpreted in terms of three major episodes of rift related alkaline magmatism, occurring at 1350-1300, 1280-1260 and 1180-1140 Ma (Upton & Blundell, 1978). Advances in U-Pb age techniques have constrained these periods into two major episodes of igneous activity at ~1280 Ma and 1180 - 1140 Ma (Upton *et al.,* 2003 and references there in). Motzfeldt has been regarded as one of the oldest centres in the Gardar province; Blaxland *et al.* (1978) reported a whole-rock Rb-Sr age of 1282 ± 30 Ma for the centre (recalculated using decay constants of Steiger and Jäger (1977)), regarded as an estimate of the age of emplacement for the Motzfeldt centre. However this age is problematic. Feldspars and micas, usually the host of Rb in igneous rocks, have experienced intense alteration in the Motzfeldt centre which would permit significant opening of the isotopic system. Similar trends have been documented by Finch *et al.* (2001) in a Nunarsuit pegmatite. The U-Pb age of 1273 ± 8 Ma obtained during the present study from the MSF therefore provides a new age estimate for the magmatic emplacement of the Motzfeldt centre. This estimate is identical to the age of 1275 ± 1 Ma obtained form a Motzfeldt pegmatite cutting an Eriksfjord roof raft in the MSF (Salmon *et al.,* in prep, quoted in Upton *et al.* (2003)).

Finch *et al.* (2001) inferred from cross-cutting relations that the North Motzfeldt centre (1226 ± 27 Ma), a small satellite intrusion north-east of the MSF, predates the emplacement of the Motzfeldt centre and proposed that Motzfeldt is younger than the age estimate of Blaxland *et al.* (1978). They tentatively suggested that Motzfeldt be divided into two periods of magmatism termed 'Early' and 'Late' Motzfeldt, separated by a significant hiatus in magmatism. Early Motzfeldt (comprising the FDF) was suggested as Early Gardar and Late Motzfeldt (which includes the MSF and GF) postdates the emplacement of the North Motzfeldt syenites. However the contacts between the two centres are only observed in restricted outcrop in one locality. The rocks are mixed and clearly remelted and it is not trivial to determine which intrusion is younger (Finch, pers comm., 2007; Salmon, pers. comm.,

2005). The isotopic data of the present study dates the emplacement of the units north of the Motzfeldt Sø lake at 1273 ± 8 Ma, showing that the MSF is older than the North Motzfeldt centre (~1226 Ma, Finch *et al.,* 2001) and the oldest record of magmatism in the Igaliko complex. There is therefore no evidence to support the hypothesis of Finch *et al.* (2001) that the Motzfeldt complex is divided into two temporally distinct intrusive events.

One other key uncertainty surrounding Early Gardar magmatism is the age of the Eriksfjord Formation. Though not directly dated during this study, the presence of xenoliths and cross-cutting relations in the preserved roof demonstrate that the Eriksfjord local to the Motzfeldt centre is older than 1273 ± 8 Ma. This demonstrates further that Eriksfjord rocks in the Motzfeldt region are significantly older than the currently published dates of 1170 - 1200 Ma from Ulukasik Member on the Narsaq peninsula (Paslick *et al.,* 1993) and 1205 ± 12 Ma for the Mussartût member at Qassiarsuk (Andersen, 1997).

7.5.2 Timing and duration of alteration in the Motzfeldt Sø Formation

The geological history of the MSF is particularly complex, encompassing both a convoluted magmatic history and an extended alkaline hydrothermal phase. Determining the timing of alteration in the MSF is particularly important to the present study due to the role alteration has played in mobilising and locally concentrating certain elements within the formation. In most alkaline centres the separation of each phase is often poorly constrained owing to the continuum from the magmatic phase into the hydrothermal phase. In the MSF the evolution of a volatile enriched residual fluid in the presence of externally derived waters extended the crystallisation interval of the formation and gave rise to multiple phases of hydrothermal alteration, which is particularly well encoded in the pyrochlore group minerals of the formation (chapter 4).

Many studies assume that hydrothermal activity is immediately post-emplacement and therefore effectively synchronous (within the errors of radiometric age dating) with emplacement. In the MSF, multiple phases of hydrothermal alteration are encoded in pyrochlore group minerals associated with the evolution of the alkaline hydrothermal residua. In another part of the Igaliko complex, South Qôroq (Finch, 1995), fluids from one episode of magmatism overprint the chemistry of significantly and demonstrably older rocks. Hence it is credible that the age of the hydrothermal alteration that characterises the present-day MSF is significantly younger than MSF magmatism.

In the present study, one particular objective has been to develop methods to date the magmatic and hydrothermal episodes independently. This study uses a combination of luminescence petrography of zircons with selected area LA-MC-ICPMS to examine pristine and altered parts of zircon crystals. The magmatic zircons are generally concordant giving a robust age estimate for the emplacement of the MSF as 1273 ± 8 Ma. Analysing the altered zircons and interpreting the data at face value suggests that the hydrothermal alteration was, at least in part, Caledonian in age, a hypothesis inconsistent with the regional geology. This is therefore interpreted as an inaccurate age estimate. In contrast, the Pb-Pb isotope systematics from altered pyrochlores define a good (MSWD = 4.5) isochron age of 1267 ± 6 Ma for the hydrothermal event, which is within error of the magmatic age of 1273 ± 8 Ma obtained from magmatic zircons. Analysis of the pyrochlore textures using BSE imaging and EPMA demonstrates that the majority of the U in the pyrochlores is secdondary. Hence the age encoded in the altered pyrochlores represent the time of isotopic closure of the pyrochlore *after* alteration by the hydrothermal fluid(s) and therefore dates more accurately the hydrothermal activity. The overlap of the magmatic age and the hydrothermal age indicates that the magmatism and associated mineralisation of the MSF cannot be distinguished in time from the hydrothermal activity. Importantly, the hydrothermal activity was not a secondary event of significantly younger origin, as is for the case for the South Qôroq/Igdlerfigssalik centres, but is effectively synchronous with the emplacement and evolution of the centre. Detailed textural analysis of pyrochlore and zircon in the same intrusions followed by precise radiogenic isotopic analysis provides a route to deconvolute the magmatic and hydrothermal ages of igneous rocks.

7.6 Conclusions

Hf isotopic analyses from zircons from the MSF provide constraints for the Hf isotopic composition of the source material of magmatism in the Motzfeldt centre. Mixing of two or more components is needed to account for the present range of $^{176}Hf/^{177}Hf$ values. This is dominated by melts evolved directly from the global depleted mantle but also contains significant contributions from components with a notably lower $^{176}Hf/^{177}Hf$ signature, suggested to be a crustal component, corresponding to rocks from the 1.75-1.90 Ga Ketilidian crust and/or pre-Ketilidian Archaean age continental crust.

Dating igneous centres which have experienced metasomatic alteration under sub-solidus conditions often proves problematic due to the complexities introduced by sub-solidus

element mobility. Fluid-mineral interaction during the hydrothermal phase of the MSF resulted in pervasive alteration of zircons, which are often considered isotopically closed, even under extreme geological environments. Zircons from the MSF show strong isotopic discordance from altered areas of the crystal. Nevertheless concordant age estimates can be obtained from selective analysis of unaltered, magmatic parts of the same zircon crystals. Selected area analyses of preserved magmatic relicts provide a new age estimate of the magmatic emplacement of the Motzfeldt centre at 1273 ± 8 Ma. Pb-Pb isotope systematics from pyrochlore minerals, which show textural and microchemical evidence for polyphase fluid interaction, define an isochron age of 1267 ± 6 Ma for the age of isotopic closure of the pyrochlores following alteration under sub-solidus conditions. The overlap of the magmatic zircon age and alteration age from pyrochlore analyses suggests that the hydrothermal alteration encoded in the pyrochlore population of the MSF is a product of the alkaline hydrothermal phase, within ~5.6 Ma of the magmatic phase. However, in many centres multiphase hydrothermal activity may significantly post-date the magmatic history of the area, associated with repeated magmatism centred about, or close to, the same focus. Such settings provide excellent opportunity to study the timing of textural and chemical changes associated with fluid-rock interactions in poly-phase hydrothermal systems.

Chapter 8

Stable Isotope Geochemistry

8.1 Introduction

Throughout the Flinks Dal (FDF) and Motzfeldt Sø (MSF) Formations calcite and carbonate bearing mineral phases have been identified using optical and cathodoluminescence (CL) petrography. Calcite has been identified as the dominant carbonate phase, occurring throughout each formation in microveins, disseminated grains and as vug-filling crystalline calcite. Carbonate phases have also been identified under CL as sub-solidus alteration products associated with the rock's mafic mineralogy. In addition to calcite LREE-bearing carbonate phases rich in Ce, La and Nd (tentatively identified as bastnäsite, parisite or synchysite) have also been identified. Cancrinite has also been identified by previous authors in the rocks of the present study (Bradshaw, 1988; Schönenberger & Markl, 2008). The carbon and oxygen isotopic composition of carbonate phases were analysed by acidifying whole-rock powders with phosphoric acid (100%) to release CO_2 from the sample. Sample preparation and analytical procedure are detailed in appendix B.5. Results are given in the standard δ notation and expressed relative to PDB for carbon and SMOW for oxygen in per mille (‰). The analytical precision for the standards (NBS-18 and NBS-19) is ± 0.04‰ for oxygen and 0.02‰ for carbon.

8.2 Oxygen and carbon isotopes

14 whole-rock powders were analysed from carbonate-bearing syenite and nepheline syenite samples from the MSF and FDF and from late vein calcite from the FDF (Table 8.1). Whole-rock samples from the FDF have $\delta^{13}C_{PDB}$ values of -3.80 to -6.61 ‰ with $\delta^{18}O_{SMOW}$ ranging from +12.42 to +14.81 ‰. Similar values have been obtained by Schönenberger and Markl (2008) for acid rinsed whole-rock samples from the FDF and from late-stage vein calcite and calcite host in fluid inclusions from the FDF. The MSF samples span a larger range than the FDF with generally higher $\delta^{13}C_{PDB}$ from -1.37 to -3.43 ‰ and higher $\delta^{18}O_{SMOW}$ values of +12.71 to +19.18 ‰. One sample from the MSF (GJM05-06) has very high $\delta^{18}O_{SMOW}$ value of +20.89 ‰ and a $\delta^{13}C_{PDB}$ value of -5.30. This sample is from a dolerite dyke.

Table 8.1. *$\delta^{13}C$ and $\delta^{18}O$ composition of carbonates from the Motzfeldt centre*

Sample No.	Sample Description	$\delta^{13}C_{PDB}$	$\delta^{18}O_{SMOW}$
Motzfeldt Sø Formation			
GJM05/03	Altered syenite	-1.37	17.31
GJM05/06	Dolerite dyke	-5.30	20.89
GJM05/16	Pegmatitic syenite	-2.31	19.18
GJM05/21	Altered syenite	-2.65	12.71
GJM05/24	Pyrochlore syenite	-3.31	15.89
GJM05/41	Altered microsyenite	-2.73	14.58
GJM05/59	Altered syenite	-3.43	14.82
GJM05/66	Altered syenite	-3.15	12.71
Flinks Dal Formation			
GJM06/98	Nepheline syenite	-3.84	12.96
GJM06/99	Nepheline syenite	-5.19	12.42
GJM06/110	Lujavrite	-3.80	13.96
GJM06/119	Microsyenite	-4.03	14.81
GJM06/125	Syenite	-6.60	13.54
GJM06/126	Vein calcite	-3.47	9.50
Flinks Dal Formation (Schönenberger & Markl, 2008)			
JS67	Vein calcite	-4.4	7.8
JS109	Calcite crystal in fluid inclusion	-3.9	8.1
JS181	Whole-rock powder (Flinks Dal formation)	-3.2	24.2
JS159	Whole-rock powder (Flinks Dal formation)	-2.2	21.9
JS164	Whole-rock powder (Flinks Dal formation)	-2.1	21.9
North Motzfeldt Diatremes (Finch, Unpublished, 2005)			
AF/01/11	carbonatite xenolith	-5.33	10.04
AF/01/12	Ferrocarbonatite sheet	-7.27	9.46
AF/01/13	Carbonatite xenolith	-4.20	13.80

Typical precision is 0.02 per mil for C and 0.04 for O. Accuracy was maintained with reference to NBS-18 and NBS-19 standards

All of the data from the MSF and FDF are plotted as $\delta^{18}O_{SMOW}$ versus $\delta^{13}C_{PDB}$ (Fig. 8.1). Additional data of Schönenberger & Markl (2008) from the FDF and carbonate bearing mantle diatremes located in the country rocks immediately adjacent to the Motzfeldt centre (Finch, unpublished, 2005) are also shown. Also on the diagram are fields for Igaliko and Grønnedal-Ika carbonatite samples compiled from the literature (Coulson *et al.,* 2003; Goodenough, 1997; Pearce & Leng, 1996 and Pearce *et al.,* 1997). The box for expected O and C isotope compositions of primitive mantle-derived carbonatite magmas (Keller & Hoefs, 1995; Taylor *et al.,* 1967) is shown for reference. Samples from the FDF and MSF plot within two discrete groups, each showing considerable range in both isotope systems with several samples showing extremely high $\delta^{18}O_{SMOW}$ values. This is most apparent in the MSF which shows a notably larger range for both $\delta^{13}C_{PDB}$ and $\delta^{18}O_{SMOW}$ than in the FDF. Samples from the MSF have $\delta^{13}C_{PDB}$ values which are between 0.3-2 ‰ higher than is observed in samples from the FDF.

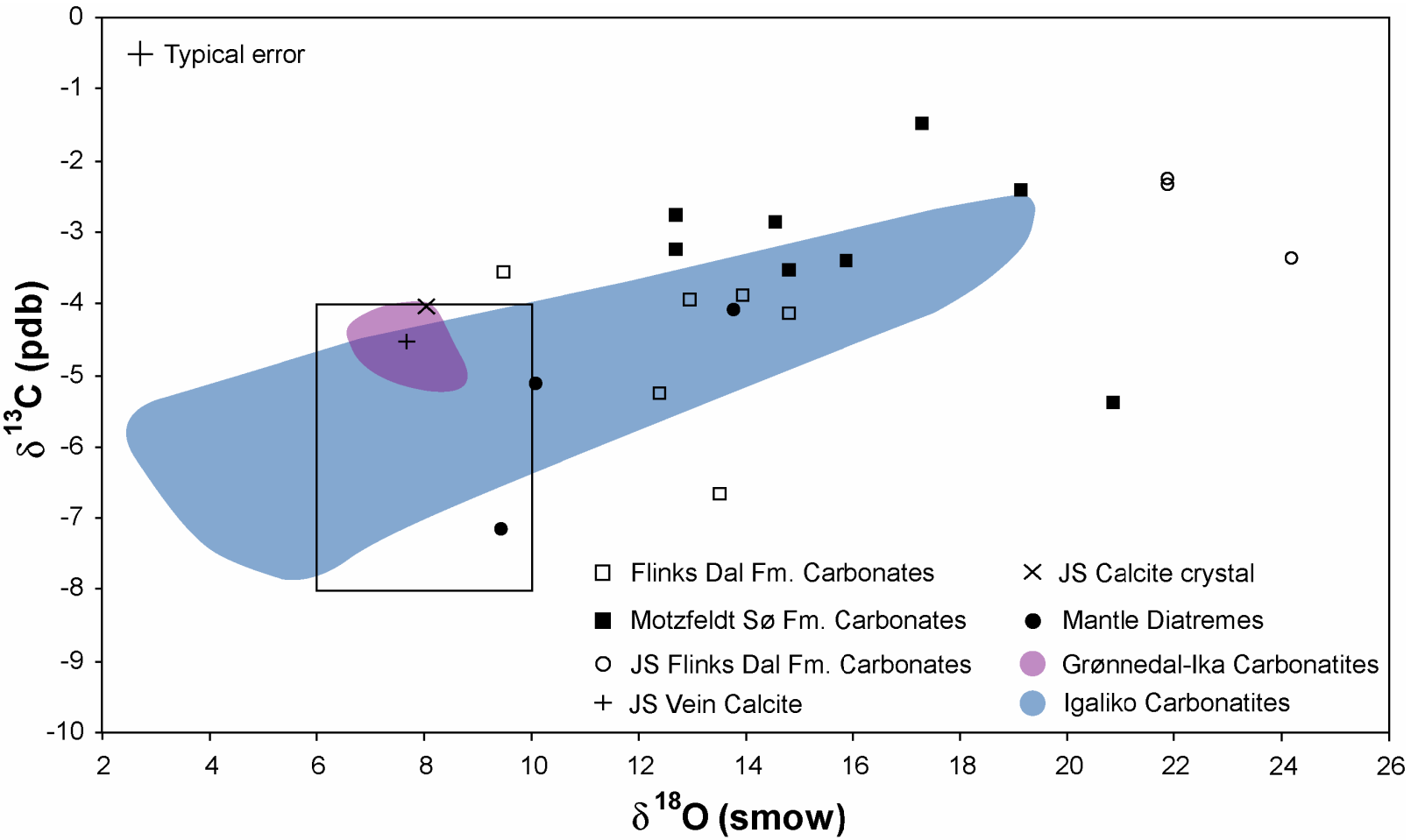

Figure 8.1. Plot of $\delta^{18}O_{SMOW}$ vs $\delta^{13}C_{PDB}$ for carbonates from the Motzfeldt Sø Formation and Flinks Dal Formation. Mantle carbonatite box from Taylor *et al.* (1967) and Keller and Hoefs (1995) shows the expected O and C isotope compositions of mantle derived carbonatites. Whole-rock, vein calcite and calcite crystals in fluid inclusions from the Flinks Dal formation from Schöenenberger & Markl (2008) are shown (JS). Fields for Igaliko and Gronnedal-Ika carbonatites compiled from the literature are also shown with data from mantle diatremes within the Igaliko (Finch, unpublished, 2005).

8.3 Discussion of stable isotope data

The results of the present study are broadly comparable with results from previous isotopic studies concerning Gardar carbonatites (Pearce & Leng, 1996; Coulson *et al.,* 2003). Many of the carbonatitic and lamprohyric units in the Igaliko province are generally considered to be of primitive mantle origin, though deviate from exclusively mantle derived isotopic signatures through a combination of fractionation processes, crustal assimilations and sub-solidus re-equilibration (Coulson *et al.,* 2003). Mantle derived carbonatites generally have $\delta^{18}O_{SMOW}$ and $\delta^{13}C_{PDB}$ values between +6 and +10 ‰ and -8 and -4 ‰, respectively (Keller & Hoefs, 1995; Taylor *et al.,* 1967). The oxygen isotope values from the whole-rock samples of the present study have $\delta^{18}O_{SMOW}$ values which are considerably higher than expected for exclusively mantle derived rocks. This is most extreme in samples from the MSF. The $\delta^{13}C_{PDB}$ values for the FDF generally fall within the suggested -8 to -4 ‰ range for mantle carbon, however the $\delta^{13}C_{PDB}$ values from the MSF are slightly richer in ^{13}C and lie at higher $\delta^{13}C_{PDB}$ than mantle values. This spread of data suggests carbonates from the MSF and FDF are either; 1) not of primary igneous origin, 2) have experienced isotopic contamination through assimilation of material with higher $\delta^{13}C$ and $\delta^{18}O$ ratios, or 3) have experienced isotopic re-equilibrium during secondary (subsolidus) processes.

Oxygen isotope variations in carbonatites are relatively common in shallow level intrusions (e.g. Andersen, 1987; Neilsen & Buchart, 1985; Reid & Cooper, 1992) however determining the processes which generate such changes can be problematic (Fig. 8.2). $\delta^{18}O_{SMOW}$ values greater than mantle levels may be attained through four possible processes: 1) Progressive partial melting (Rayleigh fractionation) and progressive depletion of light oxygen (^{16}O) and light carbon (^{12}O), 2) Interaction and assimilation of crustal rocks enriched in ^{18}O, 3) high-temperature hydrothermal exchange with high-$\delta^{18}O$ magmatic fluids, 4) low-temperature isotopic exchange with evolved magmatic fluids (H_2O-CO_2 fluids on Fig 8.2) (Deines, 1989; Demény *et al.,* 1998; Sharp, 2007). Exchange with pure meteoric waters ($\delta^{18}O_{SMOW}$ = 0.0) at high-temperatures often results in a negative oxygen isotope shift (Javoy *et al.,* 1986). This trend is not observed for any Motzfeldt samples, suggesting that any fluid-rock interaction involved largely primitive magmatic fluids or hybrid, H_2O-rich evolved magmatic fluid at lower temperatures. In the case of the MSF it seems likely that more than one process played an important role in the isotopic evolution of the formation.

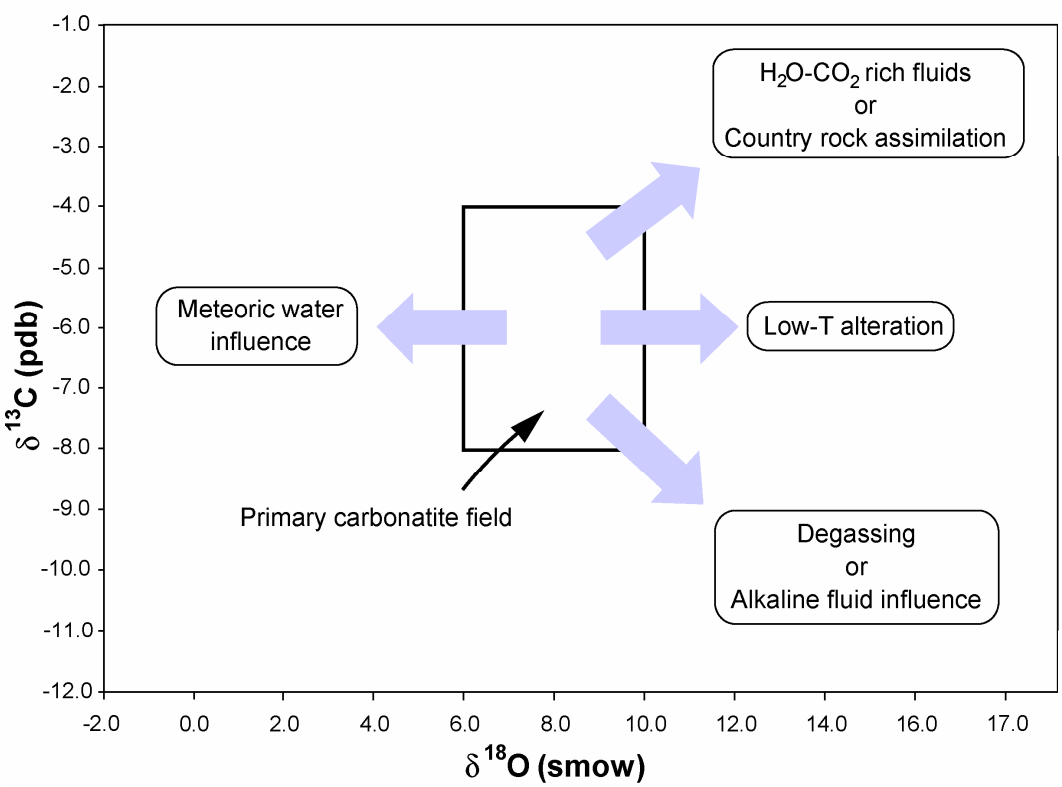

Figure 8.2. Schematic presentation of processes responsible for changes in O and C isotope compositions (after Demény *et al.,* 1998). Primary carbonatite field from Keller & Hoefs (1995) and Taylor *et al.* (1967)

Fractionation of carbon and oxygen during partial melting of a depleted lithospheric mantle source (as is suggested for Gardar magmas) would have generated primitive melts which were initially enriched in light carbon and oxygen with low $\delta^{18}O_{SMOW}$ and $\delta^{13}C_{PDB}$ values. With continued Rayleigh fractionation progressively more evolved melts fractions became depleted with respect to light carbon and oxygen as mantle CO_2 is partitioned between crystallising carbonate phases and coexisting vapour phases. This process would produce an increase in $\delta^{18}O_{SMOW}$ and, to a lesser degree, $\delta^{13}C_{PDB}$ as fractionation progressed (Deines, 1970; 1989; Neilsen & Buchart, 1985; Pearce & Leng, 1996). A similar model was suggested by Pearce and Leng (1996) for the evolution of the Igaliko dyke swarm and by Tichomirowa *et al.,* (2006) for the Tiksheozero and Siilinjarvi carbonatites of the Kola province. Following this model of isotopic evolution both formations would experience an increase in $\delta^{18}O_{SMOW}$ and $\delta^{13}C_{PDB}$ prior to any isotopic disturbance by the secondary processes.

Although magmatic isotope fractionation occurred during the generation and evolution of the parental melts of the Motzfedlt centre the exceptional range of oxygen and carbon values of the present study cannot be explained by fractionation processes alone.

Another process which likely contributed to the increased oxygen values in all samples is contamination from a component enriched in heavy oxygen. In the geological context of South Greenland this is likely through assimilation of carbonate-free basement and supracrustal rocks. Ketilidian and Archaean age crustal rocks have been demonstrated through Hf isotopic work (chapter 7) to be a notable component in the magmas of the centre. Therefore these rocks may also have contributed to the high $\delta^{18}O_{SMOW}$ signature of the centre. Despite a lack of field evidence for assimilation of Eriksfjord sediments during the present study, Bradshaw (1988) and Jones (1980) demonstrated that syenites of the MSF are mildly Si-oversaturated and attributed this to assimilation of significant amounts of silica-rich Eriksfjord supracrustal rocks during the formations stoped emplacement. Incorporation of arenitic country rocks would therefore introduce heavy oxygen and increase the $\delta^{18}O_{SMOW}$ signature of the melt. Samples from the FDF are largely undersaturated with respect to silica and have less extreme $\delta^{18}O_{SMOW}$ values than samples from the MSF. This observation reflects the enveloping geology into which the FDF was emplaced. Unlike the MSF which was emplaced into the arenite rich Massartût and Majût members of the Eriksfjord formation (Larsen & Tukiainen, 1985), the FDF was emplaced into a sequence of supracrustal rocks which were largely devoid of sedimentary components (Ilímaussaq member) (Jones, 1980). Additionally the FDF is inferred to be emplaced after the MSF through coring out of the MSF. Therefore FDF magmas did not experience crustal contamination during emplacement on the scale which is suggested for the MSF and is reflected in their oxygen isotope compositions.

In addition to contamination through assimilation of basement and supracrustal rocks, field relations and mineralogical and geochemical features from the MSF suggest an extended and convoluted sub-solidus history. Microtextural and microchemical analysis of pyrochlore group minerals from both formations suggest two principal phases of alteration associated with 1) high-temperature volatile-rich magmatic fluids, now only preserved in pyrochlores from the FDF, and 2) low-temperature alteration in the presence of an evolved magmatic fluid containing a significant meteoric component, as is found in the highly altered MSF pyrochlores. Similarly, fluid inclusion investigations in each of these formations suggest that late-stage fluids contained components of both juvenile and meteoric origin. From these observations it seems likely that the strongly positive $\delta^{18}O_{SMOW}$ values in the MSF, and to a lesser extent the FDF, may also be attributed to isotopic equilibration at low temperatures with evolved magmatic fluids, containing a notable contribution from hydrothermally convected surface waters. Bradshaw (1988) noted that the fugacity of oxygen (fO_2) appears increased in the MSF and attributes this to an influx and interaction of groundwaters with

volatile-rich residual magmatic fluids. This is supported by the intense hematite mineralisation throughout the MSF, suggesting that during the sub-solidus fO_2 increased above the hematite-magnetite (HM) buffer. This model is also favoured by Schönenberger & Markl (2008) who suggest a fluid mixing model for the evolution of the miaskitic units of the MSF and FDF. A similar model has also been suggested by Köhler *et al.* (2008) for the fluid evolution of the Ivigtût complex.

In addition to extremely enriched $\delta^{18}O_{SMOW}$ values the MSF also has $\delta^{13}C_{PDB}$ values which are consistently higher than the FDF and higher than the range expected for mantle derived melts. Similarly anomalous carbon values have been observed in carbonatites from other Gardar centres. Coulson *et al.* (2003) noted a high $\delta^{13}C_{PDB}$ value of -2.7 ‰ from a fluorite plug in the North Qôroq centre. Goodenough (1998) reported siderite samples from the Ivigtût stock with anomalously low $\delta^{13}C_{PDB}$ values (-7.2 to -8.4) and Pearce & Leng (1996) noted that samples from the Igaliko dyke swarm with low $\delta^{13}C_{PDB}$ values are rich in fluorine. Each of these studies suggests that anomalous carbon isotope ratios are strongly linked to centres or samples associated with elevated fluorine activity. It is known that light carbon (^{12}C) may be preferentially incorporated into F-rich melts through fluoro-carbonate complexing ($CO_3^{2-} + F^- = FCO_3^{3-}$) and it had been demonstrated by Rye & Ohmoto (1974) that $\delta^{13}C_{PDB}$ decreases with increasing pH (i.e. in alkaline melts). Based on the observations of Rye & Ohmoto (1974), Goodenough (1998) suggested that the anomalously low $\delta^{13}C_{PDB}$ values observed for the Ivigtût ore body were generated through interaction with late-stage alkaline fluids, which were not entirely derived from the granite. The present study has shown that the parental melts of the MSF are extremely enriched in fluorine (chapter 5). The unusually high F content of the melt may therefore have controlled the high $\delta^{13}C_{PDB}$ contents of these samples. This trend is particularly apparent in the MSF which has notably higher carbon values than the FDF and has also been demonstrated to have considerably higher F activity than the FDF (chapter 5). However, increased fO_2 (e.g. Bradshaw, 1988; Schönenberger & Markl, 2008) during the extended sub-solidus of the MSF should develop an increase in light carbon (^{12}C) thus reducing $\delta^{13}C_{PDB}$ values. This is not observed for the MSF. The systematic difference in carbon values between the MSF and FDF cannot be explained by the role of volatiles or by the assimilation of crustal components. The importance of infiltrating groundwaters in the evolution if the MSF has already been suggested in previous chapters. and is also suggested to exhibit some control over the oxygen isotopes of the formation. The influence of externally derived groundwaters on carbon and oxygen isotopes has been demonstrated in previous work on the Rødberg carbonatite complex (Andersen, 1984). This study demonstrated that

during sub-solidus re-equilibration with hydrothermally convected groundwaters $\delta^{13}C_{PDB}$ can be increased. Although the processes which controlled the systematically different carbon isotope content of samples from the MSF are unclear, it is likely that the unique sub-solidus evolution associated with this formation exhibited a strong control over the stable isotope composition of carbonates.

8.4 Conclusions

The isotopic composition of carbonates from the present study are broadly comparable with the isotope composition of carbonatites from pervious work in the Igaliko complex and Gardar province. However they do not reflect the isotopic composition of melts derived exclusively from a depleted lithospheric mantle source, as is suggested for Gardar magmatism as a whole. Heavy oxygen isotopes are enriched in both the MSF and FDF. Enrichment of oxygen, and to a lesser extent carbon, through Rayleigh fractionation is common in many carbonatitic mantle derived melts, however the extreme enrichment in the samples of the present study cannot be accounted for through this process alone. Enrichment to the levels observed in all the Motzfeldt samples is though to be generated through assimilation of crustal rocks in middle to shallow crustal levels and during the stoped emplacement of the centre. Variation in the oxygen isotopic signature of the two formations is though to reflect the mode of emplacement and composition of the host rocks into which they were emplaced. In the MSF isotopically significant amounts of Eriksfjord supracrustal sediments have been assimilated into the melt during emplacement. In the FDF the enveloping geology is dominated by sequences of trachyte and basalt, which is now reflected in the isotopic composition of the formation. The high $\delta^{18}O$ values in the MSF may also be attributed to fluid-rock interaction evolving hybrid water-rich magmatic fluids containing a component of meteoric origin. Similar explanations have been given by Goodenough (1998) and Köhler *et al.* (2008) for the isotopic evolution of the Ivigtût complex, where externally derived ground waters mixed with late-stage juvenile fluids.

The carbon composition of the FDF is consistent with derivation from a mantle source, however samples from the MSF are consistently higher. The processed which contributed to the anomalously high carbon content of the MSF remains somewhat enigmatic. The distinct difference in carbon isotopes between the MSF and FDF is inferred to reflect the striking difference in sub-solidus activity between the MSF and FDF. Subsolidus re-equilibration is therefore inferred to be the principal control over the high carbon isotope

composition of the MSF, through processes involving the elevated halogen content of the formation cannot be discounted. In summary the isotopic evolution of carbonates from the Motzfeldt centre suggests derivation from a lithospheric mantle source, however subsequent crustal contamination and spatially varied sub-solidus re-equilibration has significantly altered the primary isotopic signature of carbonates from the centre.

Chapter 9

Petrogenesis of Ta-mineralisation in the Motzfeldt centre

9.1 Introduction

Rocks from the Motzfeldt Sø Formation (MSF) have been the focus of detailed study during this thesis since they host economically interesting amounts of Nb, Ta, Zr, U, Th and LREEs. This exceptional economic backdrop results from a unique and complex magmatic history involving repeated sheeting of small batches of evolved melts, followed by several cycles of sub-solidus hydrothermal alteration. This history is unique to the MSF and is not observed elsewhere in Gardar Province. In this final chapter the conclusions of previous chapters are drawn on to develop a petrogenetic model for the evolution of the Motzfeldt centre, to understand fully the magmatic and hydrothermal phases of the centre's evolution and hence the genesis of the economically interesting mineralisation within the MSF.

9.2 Generation, segregation and evolution of Gardar magmas

Evaluating the tectonic setting and the nature of the source rocks from which the Gardar melts were derived is the first issue in understanding their composition. In addition, the evolutionary trend these melt took from source to the emplacement will also be discussed with particular reference to the generation of melts enriched in halogens and incompatible elements which are common throughout the Gardar province.

The parental magmas to the Gardar province are believed to be picritic magmas derived by decompression of fertile mantle in an extensional (rift) tectonic setting (Upton & Emeleus, 1987; Upton *et al.,* 2003). Early Gardar basic members are uncommon in the Motzfeldt centre but picritic dykes of compositions similar to those envisaged as the primary magma are found as part of the Igaliko dyke swarm (Pearce, 1988). The FDF contains large (several km^2 size) rafts of trachytic and phonolitic lavas attributed to the Eriksfjord formation which are found in the stratigraphically higher parts of the formation. Furthermore, a 150 m thick succession of Eriksfjord basaltic lavas is preserved as an in situ roof to the MDF in the Angus and Ross plc locality 5 (Fig. 1.2). Throughout the Gardar province, basic rocks predating the formation and emplacement of the more evolved central complexes occur as extensive lava successions on the Narsaq peninsula between Tunugdliarfik and Nordre Sermilik and as xenolithic rafts in the Igaliko (Emeleus & Harry, 1970), Kûngnât (Upton,

1962) and Nunarsuit (Harry & Pulvertaft, 1963) complexes. Additionally extensive dyke swarms cut the province in an ENE-WSW trending belt, parallel to the cratonic margin, which include a number of larger composite 'giant' dykes (e.g. Upton & Thomas 1980).

Typically the less evolved rocks of the province display mildly alkaline basaltic to hawaiitic compositions (Upton & Emeleus, 1987; Upton *et al.,* 2003) and are characterised by incompatible element patterns with high La/Nb and low La/Ba, La/K and La/Rb (Upton & Emeleus, 1987). The trace element patterns described are inconsistent with direct derivation from a largely unmodified source within the upper asthenospheric mantle (Upton & Emeleus, 1987; Upton *et al.,* 2003). Instead the relatively evolved nature of these basic melts suggests a high-degree of fractionation during the interval between segregation and emplacement. Additionally, the wide range of Ce/Y and Zr/Nb ratios observed in Gardar rocks suggests that the mantle source from which they were segregated was geochemically heterogeneous (Upton *et al.,* 2003).

Based on the observations of Fitton *et al.* (1995), Upton (1996) and Upton *et al.,* (2003) suggest that the basic component of Gardar magmatism, from which the central complexes were later fractionated, was generated through partial melting of a fertile lithospheric mantle, which had previously experienced a period of melt extraction. The high Al content of the basic Gardar melts suggests partial melting and fractionation from a peridotite source which had previously undergone extensive diopside fractionation during earlier melt extraction (Upton *et al.,* 2003). In the context of southern Greenland it is likely that the earlier period of melt extraction is linked to subduction of the Archaean cratonic margin during the Ketilidian orogen (Chadwick *et al.,* 1994; Upton, 1996). The Ketilidian is interpreted as an Andean-type orogen and it is inferred that dehydration of the subducted slab caused metasomatism of the lithospheric mantle and promoted partial melting giving rise to the parental melts of the Julianehåb batholith, which now constitute the majority of the basement to Gardar rocks. Associated with this interval of melt segregation was the formation of a mantle restite. This later gave rise to the Gardar magmas which were generated during decompression of the mantle during the transtensional tectonic regime during the Proterozoic.

The geochemistry of the basic melts was largely controlled by multiple stages of crystal fractionation, during which alkali-basalt and hawaiitic melts, saturated with respect to plagioclase were generated. Further fractionation of these melts in the lower crustal regions of the Proterozoic craton generated anorthosite cumulates which are inferred to underlie much

of south Greenland (Bridgewater & Harry, 1968). The melt remaining from this phase of crystal fractionation is interpreted as the parental magma to all the major complexes, undergoing fractionation in storage chambers at depth to generate the evolved compositions, locally extending to peralkaline and agpaitic rocks, which now characterise the province.

The geochemical information encoded in the basic rocks of the province strongly suggests derivation from a depleted mantle source. Similarly the isotopic character of the central complexes, for the most part, suggests evolution largely from a mantle source region. This was demonstrated by the Rb-Sr work of Blaxland *et al.* (1978) who, in addition to proving the first detailed chronology for the emplacement of individual centres, demonstrated that the majority of Gardar alkaline complexes have initial $^{87}Sr/^{86}Sr$ values consistent with origin from a mantle source. Since this early work, subsequent investigations using the Sr, Nd and Pb isotope systems have been carried out on a number of Gardar intrusions (e.g. Andersen, 1997; Coulson *et al.,* 2001; Goodenough, 1997; Pearce & Leng, 1996; Taylor & Upton, 1993). The work of these authors has shown the isotopic character of the least evolved rare lamprophyres and carbonatites of the province are consistent with derivation from a depleted mantle lithosphere. However, in contrast to the initial findings of Blaxland *et al.* (1978) the Sr, Nd and Pb isotope data indicate that many more evolved central complexes show components of isotopically significant amounts of crustal material. This was described from the Kûngnât complex (Goodenough, 1997; Taylor & Upton, 1993), Ivigtût stock (Goodenough, 1997) and Tugtutôq Younger Giant Dyke (Taylor & Upton, 1993) and also within the basic volcanoclastics of the Qassiarsuk complex (Andersen, 1997).

It is likely that isotopically and geochemically significant amounts of crustal material are involved in the genesis of the Igaliko and Motzfeldt magmas. The Hf isotopic ratios of zircon crystals from the altered (MSF) syenites demonstrate that the melts of the Motzfeldt centre do not contain exclusively mantle signatures (Chapter 7). $^{176}Hf/^{177}Hf$ values range between 0.28185 and 0.28226, which indicates that in addition to a dominant depleted mantle source one or more crustal components also contributed to the magma. The crustal components inferred using the depleted mantle whole-rock age method (i.e. Griffin *et al.,* 2000) suggest contribution from a less radiogenic Hf source with model ages that correlate with age estimates for Ketilidian rocks (Garde *et al.,* 2002) and Archaean age crustal components (Knudsen *et al.,* 2001). These were incorporated during ascent and emplacement of the Motzfeldt magmas through the crust. This reinforces the range of data that show that evolved melts of the Gardar province assimilated significant amounts of crustal material

during the interval between fractionation in the lower crust and final emplacement. Chapter 7 provides the first evidence of such contributions in the central complexes of the Igaliko Complex.

9.3 Evolution of the Motzfeldt centre

9.3.1 Magmatic evolution of the Motzfeldt Sø Formation

The Motzfeldt Sø Formation (MSF) is the oldest identifiable intrusive event in the Motzfeldt complex. It comprises a suite of related units which are texturally and mineralogically highly variable. In addition, they show striking spatial variations in the degree of subsolidus alteration. Units of the MSF contain high concentrations of Th, U, Nb, Ta, Zr and light rare earth elements (LREE) within a range of minerals, including pyrochlore, zircon and LREE-bearing carbonates. The most important economic phase during the present study is pyrochlore. Conservative estimates from work carried out by Angus and Ross plc suggest a potential for over 500 million tons of ore from the MSF, containing over 1400 ppm Nb, 120 ppm Ta and 60 ppm U. From facies of syenite hosting the highest modal abundance of pyrochlore smaller masses of 30 Mt with a potential for >250 ppm Ta have been suggested (Thomassen, 1988; Armour-Brown, 2001).

The heterogeneous mineralised units of the MSF differ from the homogeneous and largely unmineralized units of the FDF in the relative concentration of volatile elements. Variation in the volatile content of magmas throughout the Gardar has been demonstrated by Finch *et al.* (1995). Of the centres studied, Motzfeldt has one of the highest F contents. The F content of biotites from the present study shows that there are also significant differences in the inferred F activity between the individual formations of the Motzfeldt centre (Chapter 5). The high halogen content of all Gardar centres (Finch *et al.,* 1995) suggests that halogen ions were particularly enriched in the source. Upton and Emeleus (1987) and Upton *et al.* (2003) suggest that the relative enrichment of halogens throughout the Gardar may be attributed to infiltration of volatiles into the lithospheric mantle during crustal attenuation and depressurisation of the underlying asthenospheric mantle, associated with the transtensional tectonic regime during the Gardar. The cyclicity of Gardar magmatism may therefore reflect multiple phases of lithospheric mantle metasomatism and partial melting during periods of volatile infiltration. Central complex magmatism during the Early Gardar initiated in the Igaliko Complex with the emplacement of the Motzfeldt centre (1273 ± 8 Ma, U-Pb zircon,

present study). From cross-cutting relationships it is inferred that the MSF was the first major intrusive unit of the Motzfeldt centre. Following the suggestion that the magmatic cyclicity within the Gardar was generated through volatile-induced metasomatism and partial melting of a mantle source it may be suggested that the exceptionally high F content of the first intrusive unit of the Early Gardar magmatism (Motzfeldt) reflects the high volatile influx within the Gardar source region.

To generate incompatible element-rich, evolved melts requires fractionation between segregation and emplacement in the shallow crust. Therefore a model for the fractionation of the Motzfeldt magmas calls for the emplacement of incompatible element rich partial melts into a deep-seated crustal storage chamber, followed by a protracted interval of in situ fractionation to generate the evolved melts parental to the Motzfeldt centre and Igaliko Province. The exceptionally high volatile and incompatible element content of the MSF may therefore reflect the first batches of extremely evolved and F-rich melt extracted from the top a stratified storage chamber at depth. The relative lower F content of the FDF may therefore reflect a reduction in the volatile content of subsequent melt batches extracted from this storage chamber, following the extraction of the MSF. Additionally Finch *et al.* (1995) showed that the F content of other intrusions within the Igaliko complex (i.e. unaltered South Qôroq) show a relatively low F content, relative to the Motzfeldt centre, in progressively younger units. Progressive reduction in F content is true for all of the centres emplaced during the Early Gardar period of magmatism; however melts associated with the Igdlerfigssalik centre (1142 ± 15 Ma, Blaxland *et al.,* 1978) show a considerable increase in F content, with a Maximum Fluorine Line comparable to that of the FDF (Fig. 10, Finch *et al.,* 1995). Emplacement of this F-rich intrusion during the Late Gardar (~1180 – 1140 Ma) may reflect regeneration of halogen-rich partial melts from the lower lithosphere, during an influx of volatiles from the asthenospheric mantle.

Enrichment of volatile components in alkaline magmas significantly affects their physicochemical properties, reducing viscosity and increasing the crystallisation interval of the magma. This permits continued fractionation down to relatively low temperatures (~400°C has been suggested in the case of the agpaites of the Ilímaussaq intrusion, Sørensen, 1962). Evidence for the relatively high fluidity of magmas in the Motzfeldt centre comes from wide spread development of cumulate features and pseudo-sedimentary flow features in the rocks of the MSF and FDF. Importantly for the present study, enrichment of volatiles increases the melts potential to dissolve and retain incompatible elements (Kogarko, 1974; 1990), hence

highly fractionated and volatile rich magmas are often exceptionally rich in HFSE and REEs. This is exemplified in the rocks of the Motzfeldt centre, particularly so in the MSF.

Fractionation at depth and the timing of melt extraction exerted a strong control over the character of the magmas within the MSF and FDF. However there are a number of local processes which operated during emplacement which have strongly influenced the evolution of the rocks of the Motzfeldt centre. Throughout previous chapters (e.g. Chapter 2, 3, 5 & 6) the importance of the relative exposure levels, depth of emplacement and enveloping host geology of the MSF and FDF have been stressed, in particular the influence these have had on the magmatic and hydrothermal evolution of the MSF.

Within the MSF the textural and mineralogical diversity of rocks increases towards the top of the intrusion. Motzfeldt is an exceptional natural laboratory to study this aspect of the evolution of the complex since nearly 1.5 km of vertical relief is present of which over 1 km has been studied in the present study. Within the inferred roof-zone, the diversity of rock types is most extreme and hosts the highest concentrations of HFSE and REE. At lower levels in the intrusion, HFSE and REE contents are reduced and texturally the rocks are laterally homogeneous. The variation in textural diversity and localisation of HFSE and REE rich units towards the top of the intrusion indicates that the proximity to the roof of the MSF played a pivotal role in the genesis of highly evolved and economically interesting units. It has been suggested that the melts which form the MSF were tapped from the top of a stratified magma chamber at depth. The concentration of evolved units in the top of the MSF may therefore represent the product of a further stage of in situ fractionation at the final depth of emplacement. This is reflected in the concentration of texturally varying facies of syenite and localised intercumulus fluorite towards the top of the chamber. In addition to in situ fractionation, the role of the Eriksfjord in modifying the composition of the magmas has been stressed by previous authors. Jones (1980) and Bradshaw (1988) observed significant silica enrichment in the rocks of the MSF. The pegmatites at the roof-zone contain zircon, astrophyllite and alkali amphibole, a mineral assemblage similar to the pegmatites in silica-oversaturated centres such as Nunarsuit (Harry & Pulvertaft, 1963) and Kûngnât (Upton, 1962). Eudialyte, present in pegmatites of silica-undersaturated centres, is absent. In addition, quartz-rich veins cross-cut the roof zone and quartz is a relatively common phase in miarolitic cavities at high levels. As part of the present study, an assessment of the textures associated with dislodged quartzite rafts into the MSF was undertaken. In this case the evidence for assimilation into the magma was minimal – the edges of the xenoliths are sharp and those

dislodged progressively further showed precisely the same textures as those proximal to the raft. Although no field evidence for large scale assimilation of Eriksfjord sedimentary components into the MSF was observed during the present study, saturation with respect to Si in the MSF and not in the FDF seems only possible through local processes at the site of emplacement. The oxygen isotope character of calcite from the MSF suggests incorporation of a significant amount of material rich in ^{18}O, which may be attributed, in part, to assimilation of crustal rocks during the stoped emplacement of the formation. The role silica played in the magmatic evolution of the MSF relates to the melt's capacity to dissolve volatiles, principally F, which in turn dictates the melts capacity to carry incompatible elements through volatile complexing. It is recognised that the capacity for evolved alkaline melts (peralkaline) to carry incompatible elements increases with increasing volatile content (Kogarko, 1990). However with increasing Si content this capacity is significantly reduced (Sørensen & Larsen, 1978). Therefore the introduction of silica into the evolved melts in the roof-zone of the MSF may have been one of the major driving forces controlling the localised precipitation of HFSE-rich minerals in the high level units of the formation. Alternatively the progressive reduction in the confining pressure at shallow levels may have promoted exsolution of an F-rich fluid phase from the melts, thereby reducing HFSE solubility in the melt and promoting the precipitation of HFSE-rich minerals.

The highest concentration of pyrochlore-bearing rocks lies within the roof-zone and suggests that the occurrence of this particular facies of syenite is linked to the in situ fractionation of the formation and concentration of volatile, incompatible element rich melt batches in the roof of the intrusion. Although pyrochlore is a rare accessory mineral in all facies of syenite from the MSF, the presence of the particular pyrochlore-rich facies shows that this particular melt fraction was exceptionally rich in Nb, Ta, U, Th and LREEs. A number of microsyenite sheets cut the formation and are also notably rich in pyrochlore-group minerals. These are inferred to be late-magmatic in origin sheeted into the partially crystallised MSF during the final stages of magmatism in the formation.

9.3.2 Sub-solidus evolution of the Motzfeldt Sø Formation

In addition to the economically interesting HFSE content, the MSF is also characterized by the pervasive alteration associated with the subsolidus evolution of the formation. Although petrography indicates more than one phase of fluid induced alteration occurred (e.g. alteration of pyrochlore group minerals, Chapter 4) it is likely that fluids

associated with each phase are genetically linked through fluid evolution during stabilization of the hydrothermal system. Therefore rather than being considered as separate hydrothermal events, the subsolidus within the MSF should be considered as continuum from a high temperature phase of alteration dominated by juvenile magmatic fluids, to a low temperature phase, associated with evolved fluids containing a significant contribution from groundwaters, indicated by the progressive alteration of pyrochlore minerals and fluid inclusion salinities.

The most characteristic feature of alteration in the MSF is the pervasive and widespread oxidation of alkali-feldspars, giving the formation a characteristic brick-red colour visible even from satellite photographs. The feldspars are coarsely exsolved and highly altered (Chapter 3). The cathodoluminescence character of feldspars is a particularly useful indicator of the degree of subsolidus alteration (Chapter 3). Samples from low in the stratigraphy are characterized by blue luminescent magmatic cores and deep red metasomatised rims. Traversing to higher stratigraphic locations, alteration increases. This is reflected in the luminescence of feldspars which only display red luminescence. Variation in the luminescence character with depth shows that fluid-induced alteration and metasomatism was greatest at high levels in the intrusion. This is expected given the high concentration of F-rich fluids ponding within the roof-zone of the formation. Subsolidus alteration of arfvedsonite amphiboles to a secondary assemblage of aegirine pyroxene, biotite micas and magnetite is the principal subsolidus reaction associated with the mafic mineralogy of the MSF (Chapters 4 & 5). The fluid composition of the MSF is considered to be dominated by juvenile orthomagmatic fluids, however the influence of externally-sourced groundwaters in the system is also evident. It is therefore suggested that contemporaneous to the exsolution of F-rich juvenile fluids, heat transfer into the Ketilidian wall-rocks and Eriksfjord roofing sequence initiated convection of externally-derived groundwater through the MSF. Fluorite host secondary fluid inclusions from the altered facies of the MSF contain saline (<9 wt. % NaCl equiv.) aqueous liquids which record trapping temperatures of 150 – 360°C. Within the roof of the formation trapped fluids are of higher salinity (12-20 wt. % NaCl equiv.) demonstrating that an exceptional, highly saline hydrothermal environment existed immediately below the roof. The higher salinity inclusions trapped within the roof of the formation are inferred to encode fluid chemistries which have experienced minimal dilution though interaction with externally-derived fluids. The relatively low temperatures of these are thought to relate to the late-stage exsolution of these fluids during the final stages of the magmatic evolution, associated with the emplacement of peralkaline microsyenite sheets in the roof-zone. Throughout the rest of the formation fluid salinities are lower. It is inferred that there has

been km-scale mixing of juvenile fluids with externally derived groundwaters, effectively diluting the salinity of the fluids circulating throughout the MSF. This is consistent with the model of Schönenberger and Markl (2008) who demonstrated that the Cl/Br ratio of inclusions from the MSF characterise a fluid mixing model for the Motzfeldt centre. The Cl/Br ratios from this study are comparable with other Gardar alkaline intrusions (e.g Ivigtût, Köhler *et al.,* 2008), suggesting a common halogen source throughout the province. This enhances the argument for a mantle halogen source discussed above.

Mineralogical and textural evidence for fluid mixing is particularly well encoded in the pyrochlore population of the formation. These are highly altered through a network of fluid induced microfractures, associated with which is extensive mobilization and leaching of Na, F, variable enrichment or depletion of Ca and enrichment of Sr, K, Fe and REEs (Chapter 4). These features are characteristic of the secondary to transitional alteration trends of Lumpkin and Ewing (1995) in the presence of medium to low temperature fluids (200 - 300°C) with a low pH and low HF activity. Pyrochlore from the FDF retain primary zoning and only display diffusive alteration fronts relating to high temperature (ca. 500°C) fluids with high pH and high HF activity, hence predominantly juvenile fluids. Pyrochlore has also been used as a chronological tool for determining the timing of alteration in the MSF. In the neighbouring South Qôroq centre, fluid-induced metasomatism and alteration is related to the emplacement and permeation of fluids from the Late Igdlerfigssalik intrusion, separated by ~20 Ma (Blaxland *et al.,* 1978)

The independent dating of the hydrothermal and magmatic events in the MSF has been a particular target of the present study, given the suggestion by Finch *et al.* (2001) that the Motzfeldt Centre may combine rocks of Early and Late Gardar age. In addition, it is possible that the hydrothermal alteration is significantly later (e.g. 100 Ma) than the magmatism. To explore these hypotheses, a method was developed that compares and contrasts pristine and altered parts of individual pyrochlore and zircon crystals. The magmatic age is 1273 ± 8 Ma from magmatically zoned zircon. Dating of altered zircon gave spurious results and was unsuccessful in giving an age for the hydrothermal alteration. However analysis of altered pyrochlore gave a Pb-Pb isochron age of 1267 ± 6 Ma (Chapter 7), which is synchronous, within error, of the magmatic emplacement of the formation, providing no evidence for a significant hiatus between emplacement and alteration. Hence the hypothesis of Finch *et al.* (2001) that Motzfeldt is a site of repeated magmatism and hydrothermal activity throughout the Gardar is discounted.

Other mineralogical features in the MSF which indicate the influx of groundwater include pervasive oxidation of feldspars and extensive hematite formation throughout the high-levels of the formation, suggesting that within the top of the intrusion fluids became progressively oxidized during mixing, raising the oxygen fugacity of the fluid above the hematite-magnetite buffer during the waning stages of the hydrothermal phase. In addition to the possible assimilation of carbonate free Eriksfjord crustal rocks, the enriched oxygen isotopes in the MSF can also be explained by interaction and isotopic re-equilibration of carbonate phases with evolved H_2O-rich fluids as is the case in many shallow crustal syenite and carbonatite intrusions.

The principal focus of this study has been the genesis of Ta-bearing minerals. However throughout the altered facies of the MSF, late-stage incompatible element mobilization associated with the subsolidus phase is evident, most noticeably in the formation of LREE carbonates such as bastnäsite and parasite along grain-boundaries and localised high Th concentrations within the roof-zone of locality 5 (Fig. 1.2). The genesis of these sub-solidus mineralized facies is intimately related to the evolving composition of fluids through influx of groundwater. It is suggested that the effective dilution of magmatic fluids by groundwater decreased the fluids potential to complex incompatible elements. Finch (1990) discussed the complexing potentials of various different ligands, the most important of which include F^-, Cl^-, CO_2 and FCO_3^-. This study suggest that the fluids with high fluoride and CO_2 activity, $a(F^-)$ and $a(CO_2)$ respectively, have greater potential to complex incompatible elements. F was an important ligand in fluids of the Motzfeldt centre, given the exceptionally high F levels associated with this intrusion. Rare CO_2-H_2O fluid inclusions have been identified by Schönenberger and Markl (2008), suggesting that CO_2 complexing may also have been significant in the intrusion. Additionally, late-stage carbonates are also relatively common indicating the activity of C bearing complexes. The model proposed for the origin of REE and HSFE mineralisation in high-level units of the formation during the subsolidus is one involving fluid mixing and oxidation. Dilution of halogen rich juvenile fluids decreased HFSE and REE solubility in the roof zone promoting precipitation of incompatible element and REE-rich minerals such as fluorite and REE fluorcarbonates.

The complex fluid history encoded in the altered rocks of the MSF reflects contributions from juvenile orthomagmatic fluids and externally derived groundwater. Alteration at high-levels in the intrusion is dominated by a lower temperature, pervasive alteration associated with a mixed fluid. Subsolidus HFSE and REE mineralisation in the

formation is intimately associated with change in the physical and chemical properties of the fluid from dominantly juvenile to an oxidizing groundwater-rich fluid during the final stages of the hydrothermal phase.

9.4 Genetic relationship of the Flinks Dal and Motzfeldt Sø Formations

Although part of the same intrusive complex, the FDF and MSF are wholly different in texture, mineralogy and chemistry. It is suggest that the lower F and incompatible element concentrations in the FDF, relative to the MSF, relates to the timing of emplacement, or, more specifically, the timing of melt tapping from a stratified storage chamber at depth. The enrichment of F and incompatible elements in the MSF therefore represents the first highly evolved melts extracted from the tops of storage chambers. Subsequent melts (including FDF) were less enriched in these components. In addition, the influence of silica saturation and pervasive fluid-rock alteration is also absent in the FDF, reflected in the rock's mineralogy and largely homogeneous texture and chemistry. The same processes did not operate during the subsolidus of the FDF as are inferred for the MSF. This raises that question as to why these processes were restricted to the MSF and largely absent in the FDF.

Aside from the lower F content the major difference in the magmas of the FDF was the emplacement and the host geology into which they were emplaced. The Eriksfjord sequence seems to be the principal source of silica in the MSF, incorporated into the magmas during the stoped emplacement of the formation. The outliers of Eriksfjord north of Motzfeldt Sø comprise a sequence of supracrustal rocks comprising a basal trachyte overlain by thick sequences of quartz arenite and fluvial conglomerates. Subordinate sub-aerial basaltic components are also present, however the sequence is dominated by sedimentary rocks. Correlation of these units with the Eriksfjord sequence exposed on the Narsaq peninsula suggest that the components in the country rocks adjacent to the MSF belong to the sediment dominated Majût and Mussartût members of the Eriksfjord (Larsen, 1977; Larsen & Tukiainen, 1985; Poulsen, 1964). Throughout the high plateaus of the MSF, preserved or partially assimilated xenoliths of arenite from these members are notably absent. However occurrences of highly altered basalt have been observed. Hence assimilation of arenite rafts may have been so successful that xenoliths are now fully digested and unrecongised, unlike the basalts higher in the sequence. The volcanic components were more resistant to the assimilation process and are preserved as highly metasomatised rafts and xenoliths.

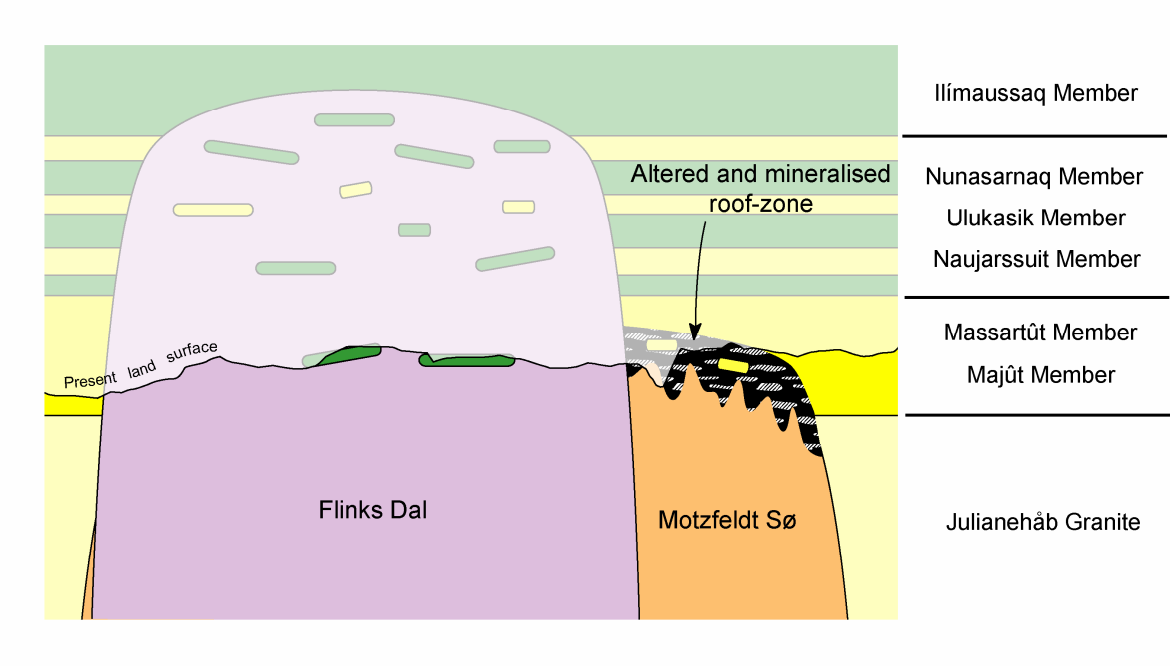

Figure 9.1: Schematic representation of relative emplacement depths and host geology of the Motzfeldt Sø and Flinks Dal formations. Green units are volcanic and yellow units are siliciclastic components of the Eriksfjord Formation.

Within the FDF an in situ roof is absent, although large rafts of trachyte and basalt are found up to ~200 m thick and covering several km^2 in area. Sedimentary rocks within the rafts of the FDF are exceptionally rare. Jones (1980) correlated these large volcanic rafts with the Ilímaussaq member of the Eriksfjord, suggested to be ~1.5 km above the base of the Mussartut member in the exposed sequence on the Narsaq peninsula (Poulsen, 1964). The different xenolithic cargo within the MSF and FDF would suggest that each formation was emplaced at different stratigraphic levels in the crust. The depth of emplacement in the MSF appears to be largely controlled by the unconformity between the Ketilidian and base of the Eriksfjord, intruding to a maximum of several hundred meters into the Eriksfjord sequence. The FDF, intruded following the emplacement of the MSF may have reached higher stratigraphic heights in the Eriksfjord, intruding up to 1.5 km higher into the sequence than the MSF. The large rafts of trachyte and basalt now hosted by the FDF therefore represent large sections of roofing material which have delaminated and sunk into the intrusion during its emplacement to higher crustal levels. The present surface exposure of the centre dissects the MSF along the roof zone of the formation however the present exposure of the FDF is inferred to be some 1-1.5 km below the roof of the formation.

From these observations it is suggested that, in addition to variation in volatile content, the depth of emplacement and the roof into which each formation was emplaced were other major controls over the differences between the two formations. The Majût and Mussartût members into which the MSF were emplaced are dominated by sedimentary components. It is likely that these were more permeable to water circulation during the formation of a hydrothermal cell within the MSF. Furthermore the MSF was the first intrusive unit, emplaced directly into the crust, and may have been one of the first large magma chambers to establish convection cells in the surrounding basement rocks. As a result hydrothermally circulated groundwater went directly from Ketilidian rocks into syenite and a greater degree of wall and roof-rock alteration occurred. In effect the MSF acted as a buffer, reducing the circulation of groundwater through the FDF. The relative height of exposure in each formation must also be taken into account. The current exposure of the FDF, based on reconstruction of the Eriksfjord, is ~1.5 km below the top of the intrusion. Therefore, although the rocks at current exposure are laterally homogeneous, those at the FDF roof may have more closely resembled the rocks currently in the roof-zone of the MSF. Indeed relatively weakly altered and laterally homogeneous rocks are now observed ~1 km below to roof of the MSF. It is therefore possible that the rocks from the MSF and FDF both experienced similar magmatic and hydrothermal histories, yet the depth of emplacement and current surface exposure dissects each formation at a different level within the intrusive column (Fig. 9.1).

9.5 Economic implications and final comments

The aim of this project was to understand more fully the genesis of Ta-mineralisation and evaluate the possibility of identifying a particularly Ta-rich facies of syenite within the formation. The Ta-bearing minerals in the rocks of the MSF are sourced largely form the basic parental magmas tapping a mantle source that became enriched in HFSE (including Ta) during a partial melting event in Ketilidian (1.8 Ga) times. Rifting allowed the influx of volatile elements, notably F, from the asthenospheric mantle that mobilised the HFSE from the mantle into the parental Gardar melts. During fractionation of these melts the HFSE were concentrated, and the consistently high halogen (particularly F) contents of the magma, allowed the magma to retain these elements. This magma eventually formed a HFSE-enriched nepheline syenitic magma that intruded the Greenland crust. Many batches of these fractionated melts were emplaced beneath the unconformity between the Ketilidian basement and Early Gardar supracrustals (the Eriksfjord) creating the MSF. In addition, a number of

late-magmatic peralkaline microsyenite sheets cross-cut the formation immediately after its emplacement. Associated with these magmas is a cargo of Ta-bearing pyrochlore group minerals. The present study shows that the highest concentrations of Ta are mostly within the high-level units, and relates to fractionation, migration and ponding of evolved melt batches in the roof-zone of the chamber. Although Ta is disseminated across the roof-zone, it is inferred that a large body of incompatable element-rich syenite at depth within the MDF is unlikely. The presence of pyrochlore-bearing microsyenite sheets throughout the formation suggests that there may be an evolved feeder chamber located below current exposure, however the depth of such a unit is unknown and there are no means of directing drilling to intersect it. The flat-lying, agpaitic SM6 unit (Schönenberger & Markl 2008) in the FDF shows that evolved, late-stage microsyenite bodies are possible within less-evolved sequences, but their location is impossible to predict. Analyses of pyrochlore crystals have revealed significant quantities of a number of other elements in addition to Ta. Separation of pyrochlores in the enriched zones suggests that efforts to extract Ta may also yield significant quantities of Nb, U, Th, Zr and LREEs. If estimates of mineralised ore tonnages of $30x10^6$ with a potential for over 250 ppm Ta are accurate for pyrochlore-enriched zones (Armour-Brown, 2001) then typical extractable values of ~30Mt of Ta can be expected. With these estimated values significant quantities of the other elements (Nb, U, Th, Zr and LREE) would inevitably also be retrieved from the pyrochlore. By comparing the estimate of the possible tonnage of Ta in pyrochlore (30 Mt) with the composition of typical pyrochlore, extraction may also yield: Nb – 200 Mt, Zr – 30 Mt, Th – 1.6 Mt U – 16 Mt $\sum$REE – 20 Mt.

Although Ta-mineralisation is now understood to be largely a consequence of the magmatic history of the centre, multiple sub-solidus hydrothermal phases have played an important role in complexing and remobilising elements. Although the F content was notably high, causing the mobilisation of many HFSE including Nb, this did not mobilise Ta. Yet, also associated with the late magmatic and sub-solidus history are REE bearing carbonates, enriched in La (10-12 wt. %), Ce (22-29 wt. %) and Nd (5-8 wt %). These are often intimately associated with pyrochlore and fluorite. These REE carbonates may easily be extracted by dilute acid rinsing and may provide recoverable amounts of REE.

The present study has demonstrated that the mineralisation and highly atypical character of the rocks within the MSF were generated through a combination of processes relating to the magma chemistry, emplacement process and the unusual hydrothermal regime in the formation. Despite the complex hydrothermal history encoded in the rocks of the MSF,

the genesis of Ta-mineralisation is suggested to be largely a magmatic feature, masked by the pervasive subsolidus features of the area.

References

References

Allart, J.H. (1976) Ketilidian mobile belt in South Greenland. In A. Escher, and W.S. Watt, Eds. *Geology of Greenland*, p. 121-51. Geological Survey of Greenland, Copenhagen.

Andersen, T. (1984) Secondary processes in carbonatites: Petrology of "Rødberg" (hematite-calcite-dolomite carbonatite) in the fen central complex, Telemark (South Norway). *Lithos*, **17**, 227-45.

Andersen, T. (1986) Magmatic fluids in the fen carbonatite complex, S.E. Norway. *Contributions to Mineralogy and Petrology*, **93**, 491-503.

Andersen, T. (1987) A model for the evolution of hematite carbonatite, based on whole-rock major and trace element data from the Fen complex, Southeast Norway. *Applied Geochemistry*, **2**, 163-80.

Andersen, T. (1997) The age and petrogenesis of the Qassiarsuk carbonatite-alkaline silicate volcanic complex in the Gardar rift, South Greenland. *Mineralogical Magazine*, **61**, 499-514.

Andersen, T., and Griffin, W. (2004) Lu-Hf and U-Pb isotope systematics of zircons from the Storgangen intrusion, Rogaland intrusive complex, SW Norway: Implications for the composition and evolution of Precambrian lower crust in the Baltic sheild. *Lithos*, **73**, 271-88.

Andersen, T., Griffin, W.L. and Pearson, N. (2002) Crustal evolution of the SW part of the Baltic sheild: The Hf isotope evidence. *Journal of Petrology*, **43**, 1725-47.

Andersen, T., Griffin, W.L. and Sylvester, A.G. (2007)Sveconorwegian crustal underplating in southwestern Fennoscandia: LAM-ICPMS U-Pb and Lu-Hf isotope evidence from granites and gneisses in Telemark, southern Norway. *Lithos*, **93**, 273-87

Armour-Brown A. (2001) Tantalum exploration: Review of previous exploration, results of benefication studies and recommendations for future work, Angus & Ross plc report 1

Armour-Brown, A., Tukiainen, T., Wallin, B., Bradshaw, C. and Emeleus, C.H. (1983) Uranium exploration in South Greenland. *Rapport Grønlands Geologiske Undersøgelse*, **115**, 68-75.

Bailey, S.W. (1984) Classification and structures of the micas. In S.W. Bailey, Ed. *Micas: Reviews in Mineralogy and Geochemistry*, *Mineralogical Society of America,* **13**, p. 1-12.

Blaxland, A.B., Vanbreemen, O., Emeleus, C.H., and Anderson, J.G. (1978) Age and origin of major syenite centers in Gardar province of South Greenland - Rb-Sr studies. *Geological Society of America Bulletin*, **89**, 231-44.

Blichet-Toft, J. and Albarède, F. (1997) The Lu-Hf geochemistry of chondrites and the evolution of the mantle-crust system. *Earth and Planetary Science Letters*, **148**, 243-58.

Bodnar, R.J. (1993) Revised equation and table for determining the freezing point depression of H_2O-NaCl solutions. *Geochimica et Cosmochimica Acta*, **57**, 683-4.

Bodnar, R.J. (1994) Synthetic fluid inclusions: XII. The system H_2O-NaCl. Experimental determination of the halite liquidus and isochores for a 40 wt. % NaCl solution. *Geochimica et Cosmochimica Acta*, **58**, 1053-63.

Bohse, H., Brooks, C. and Kunzendorf, K. (1971) Field observations on the kakortokites of the Ilímaussaq intrusion, South Greenland. *Rapport Grønlands Geologiske Undersøgelse*, **38**, 43.

Bonazzi, P., Bindi, L., Zoppa, M., Capitain, G. and Olmi, F. (2006) Single-crystal diffraction and transmission electron microscopy studies of "silicified" pyrochlore from Narssarssuk, Julianehåb district, Greenland. *American Mineralogist*, **91**, 794-801.

Bradshaw, C. (1985) The alkaline rocks of the Motzfeldt centre: Progress report on the 1984 field season. *Rapport Grønlands Geologiske Undersøgelse*, **125**, 62-4.

Bradshaw, C. (1988) *A petrographic, structural and geochemical study of the alkaline igneous rocks of the Motzfeldt centre, South Greenland*. Unpublished PhD thesis, University of Durham.

Bradshaw, C and Tukiainen, T. (1983) Geological and radiometric mapping of the Motzfeldt centre of the Igaliko Complex, Unpublished Internal GGU report. p. 35

Bridgewater, D. anf Harry, W.T. (1968) Anorthosite xenoliths and plagioclase megacrysts in Precambrian intrusions in South Greenland. *Grønlands Geologiske Undersøgelse Bulletin*, **77**

Brigatti, M.F., Caprilli, E., Malferrari, D. and Mottana, A. (2007) Crystal structure and crystal chemistry of fluorannite and its relationships to annite. *Mineralogical Magazine*, **71**, 683-90.

Chadwick, B., Erfurt, P., Frisch, T., Garde, A.A., Schonwandt, H.K., Stendal, H and Thomassen, B. (1994) Sinistral transpression and hydrothermal activity during emplacement of the Early Proterozoic Julianhab batholith, Ketilidian orogenic belt, South Greenland. *Rapport Grønlands Geologiske Undersøgelse,* **163**, 5-22

Chakhmouradian, A.R. and Mitchell, R.H. (1999) Primary, agpaitic and deuteric stages in the evolution of accessory Sr, REE, Ba and Nb-mineralisation in nepheline-syenite pegmatites at Pegmatite peak, Bearpaw mountains, Montana. *Mineralogy and Petrology*, **67**, 85-110.

Chakhmouradian, A.R. and Mitchell, R.H. (2002) New data on pyrochlore- and perovskite-group minerals from the Lovozero alkaline complex, Russia. *European Journal of Mineralogy*, **14**, 821-36.

Chakoumakos, B. (1984) Systematics of the pyrochlore structure type, ideal $A_2B_2X_6Y$. *Journal of solid state chemistry*, **53**, 120-9.

Chakoumakos, B. and Lumpkin, G.R. (1990) Pressure-temperature constraints on the crystallisation of the Harding pegmatite, Taos Country, New Mexico. *Canadian Mineralogist*, **28**, 287-98.

Coulson, I.M. (2003) Evolution of the north Qôroq centre nepheline syenites, South Greenland: Alkali-mafic silicates and the role of metasomatism. *Mineralogical Magazine*, **67**, 873-92.

Coulson, I.M., Goodenough, K.M., Pearce, N. and Leng, M. (2003) Carbonatites and lamprophyres of the Gardar Province - a 'window' to the sub-Gardar mantle? *Mineralogical Magazine*, **67**, 855-72.

Davis, W.D., Lowenstein, T.K. and Spencer, R.J. (1989) Melting behavior of fluid inclusions in laboratory grown halite crystals in the systems NaCl-H_2O, NaCl-KCl-H_2O, NaCl-$MgCl_2$-H_2O and NaCl-$CaCl_2$-H_2O. *Geochimica et Cosmochimica Acta*, **54**, 591-601.

De St. Jorre, L. and Smith, D.G.W. (1988) Cathodoluminescent gallium-enriched feldspars from the Thore Lake rare metal deposits, Northwest Territories. *Canadian Mineralogist*, **26**, 301-8.

Deer, W.A., Howie, R.A. and Zussman, J. (1992) *An introduction to the Rock Forming Minerals*. Longman, Essex.

Deines, P, (1970) Carbon and oxygen isotopic composition of carbonates from the Oka carbonatite, Quebec, Canada. *Geochimica Et Cosmochimica Acta*, **34**, 1199-1225.

Deines, P. (1989) Stable isotope variations in carbonatites. In K. Bell, Ed. *Carbonatites: Genesis and Evolution*, p. 301-59. Unwin and Hyman, London.

Demény, A., Ahijado, A., Casillas, R. and Vennemann, T. (1998) Crustal contamination and fluid/rock interaction in the carbonatites of Fuerteventura (Canary Islands, Spain): A C, O, H isotope study. *Lithos*, **44**, 101-15.

Edge, R.A., and Taylor, H.F.W. (1969) Crystal structure of thaumasite, a mineral containing $[Si(OH)_6]^{2-}$ groups. *Nature*, **224**, 364

Emeleus, C.H. and Harry, W.T. (1970) The Igaliko nepheline syentie complex. General description. *Grønlands Geologiske Undersøgelse Bulletin*, **85**, 116.

Emeleus, C.H. and Upton, B.G.J. (1976) The Gardar period in South Greenland. In A. Escher, and W.S. Watt, Eds. *Geology of Greenland*, p. 152-81. Geological Survey of Greenland Copenhagen.

Fall, A., Bodnar, R.J., Szabo, C. and E, Pal-Molnar. E. (2007) Fluid evolution in the nepheline syenites of the Ditrau Alkaline Massif, Transylvania, Romania. *Lithos*, **95**, 331-45.

Ferguson, J. and Pulvertaft, C. (1963) Contrasted styles of igneous layering in the Gardar Province of South Greenland. *Mineralogical Society of America*, **1**, 10-21.

Finch, A.A. (1990) *The chemical and isotopic nature of fluids associated with alkaline magmatism, South Greenland.* Unpublished PhD thesis, University of Edinburgh.

Finch, A.A. (1991) Conversion of nepheline to sodalite during subsolidus processes in alkaline rocks. *Mineralogical Magazine*, **55**, 459-63.

Finch, A.A. (1995) Metasomatic overprinting of juvenile fluids, Igdlerfigssalik, South Greenland. *Contributions to Mineralogy and Petrology*, **122**, 11-24.

Finch, A.A., Goodenough, K.M., Salmon, H.M. and Andersen, T. (2001) The petrology and petrogenesis of the North Motzfeldt centre, Gardar Province, South Greenland. *Mineralogical Magazine*, **65**, 759-74.

Finch, A.A. and Klein, J. (1999) The causes and petrologic significance of cathodoluminescence emissions from alkali-feldspars. *Contributions to Mineralogy and Petrology*, **135**, 234-43.

Finch, A.A., Mansfeld, J. and Andersen, T. (2001) U-Pb radiometric age of Nunarsuit pegmatite, Greenland: Constraints on the timing of Gardar magmatism. *Bulletin of the Geological Society of Denmark*, **48**, 1-7.

Finch, A.A., Parsons, I. and Mingard, S.C. (1995) Biotites as indicators of fluorine fugacities in late-stage magmatic fluids: The Gardar province of South Greenland. *Journal of Petrology*, **36**, 1701-28.

Finch, A.A. and Walker, F.D.L. (1991) Cathodoluminescence and microporosity in alkali-feldspars from the Blå Måne Sø perthosite, South Greenland. *Mineralogical Magazine*, **55**, 583-9.

Finger, L.W. and Hazen, R. (1991) Crystal chemistry of six-coordinated silicon: A key to understanding the earth's deep interior. *Acta Crystallographica*, **47**, 561-80.

Fitton, J.G., Saunders, A.D., Larsen, L.M., Fram, L.M., Demant, A., Sinton, C. and Leg 152 Shipboard Scientific Party. (1995) Magma sources and plumbing system during the break-up of the SE Greenland margin: Prelimenary results from ODP Leg 152. *Journal of the Geological Society London*, **152**, 985-90.

Fitton, J.G. and Upton, B.G.J. (1987) *Alkaline igneous rocks*. Geological Society of London. Blackwell.

Flohr, M.J.K. (1994) Titanium, vanadium and niobium mineralisation and alkali metasomatism from the Magnet Cove Complex, Arkansas. *Economic Geology*, **89**, 105-30.

Frantz, J.D., and Marshall, W.L. (1984) Electrical conductances and ionization constants of acids and bases in supercritical aqueous fluids: Hydrochloric acid from 100°C to 700°C and at pressures of 4,000 bars. *Carnegie Institute of Washington, Yearbook 1982*, 372-7.

Garde, A.A., Hamilton, M.A., Chadwick, B., Grocott, J. and McCaffrey, K.J.W. (2002) The Ketilidian origin of South Greenland: Geochronology and techtonics, magmatism and fore-arc accretion during Palaeoproterozoic oblique convergence. *Canadian Journal of Earth Science*, **39**, 765-93.

Geake, J.E., Walker, G., Telfer, D.J. and Mills, A.A. (1977) The cause and significance of luminescence in lunar plagioclase. *Philosophical Transactions of the Royal Society of London. Series A, Mathematical and Physical Sciences*, **285**, 403-8.

Geisler, T., Schaltegger, U. and Tomaschek, F. (2007) Re-equilibration of zircon in aqueous fluids and melts. *Elements*, **3**, 43-50.

Goodenough, K.M. (1997) *Geochemistry of Gardar intrusions in the Ivigtût area, South Greenland.* Unpublished PhD thesis. University of Edinburgh.

Goodenough, K.M., Upton, B.G.J. and Ellam, R. (2000) Geochemical evolution of the Ivigtût granite, South Greenland: A fluorine-rich "A-type" intrusion. *Lithos*, **51**, 205-12

Götze, J., Habermann, D., Neuser, R.D. and Richter, D.K. (1999) High-resolution spectrometric analysis of rare earth elements-activated cathodoluminescence in feldspar minerals. *Chemical Geology*, **153**, 81-91.

Götze, J., Krbetschek, M.R., Habermann, D., and Wolf, D. (2000) High-resolution cathodoluminescence studies of feldspar minerals. In M. Pagel, V. Barbin, P.H. Blanc, and D. Ohnenstetter, Eds. *Cathodoluminescence in Geosciences*, p. 245-70. Springer Verlag, Berlin.

Götze, J., Plötze, M., Götte, T., Neuser, R.D. and Richter, D.K. (2002) Cathodoluminescence (CL) and electron paramagnetic resonance (EPR) studies of clay minerals. *Mineralogy and Petrology*, **76**, 195-212.

Griffin, W., Pearson, N., Belousova, E., Jackson, S., Van Achterbergh, E., O'Reilly, S. and Shee, S. (2000) The Hf isotope composition of the craytonic mantle: LAM-MC-ICPMS analysis of zircon megacrysts in kimberlites. *Geochimica Et Cosmochimica Acta*, **64**, 133-47.

Guidotti, C.V. and Dyar, M.D. (1991) Ferric iron in metamorphic biotite and its petrologic and crystallochemical implications. *American Mineralogist*, **76**, 161-75.

Gulson, B. and Krogh, T. (1972) U/Pb zircon studies on the age and origin of post tectonic intrusions in South Greenland. *Rapport Grønlands Geologiske Undersøgelse*, **45**, 48-53.

Gunow, A.J., Ludington, S. and Munoz, J.L. (1980) Fluorine in micas from the Henderson molybdenite deposit, Colorado. *Economic Geology*, **75**, 1127-37.

Hansen, B.T. and Friderichsen, J.D. (1989) The influence of recent lead loss on the interpretation of disturbed U-Pb systems in zircons from igneous rocks in East Greenland. *Lithos*, **23**, 209-23.

Harley, S. and Kelly, N. (2007) Zircon: Tiny but timely. *Elements*, **3**, 13-8.

Harper, C.L. (1988) *On the nature of time in cosmological perspective*. Unpublished PhD thesis. University of Oxford.

Harry, W.T. and Pulvertaft, C. (1963) The Nunarssuit intrusive complex, South Greenland. *Grønlands Geologiske Undersøgelse Bulletin*, **36**, 136.

Hayward, C.L. and Jones, A.P. (1991) Cathodoliminescence petrography of the Middle Proterozoic extrusive carbonatite from Qasiarsuk, South Greenland, *Mineralogical Magazine*, **55**, 591-603

Henley, R.W. and McNabb, A. (1978) Magmatic plumes and ground-water interaction in a porphyry copper emplacement. *Economic Geology*, **73**, 1-20.

Hodgson, N.A. and Le Bas, M.J. (1992) The chemistry and cryptic zonation of pyrochlore from San Vicente, Cape Verde Islands. *Mineralogical Magazine*, **56**, 201-14.

Hogarth, D.D. (1977) Classification and nomenclature of the pyrochlore group. *American Mineralogist*, **35**, 403-10.

Hogarth, D.D., Williams, C.T. and Jones, P. (2000) Primary zoning in pyrochlore group minerals from carbonatites. *Mineralogical Magazine*, **64**, 683-97.

Hoskin, P. and Black, L. (2000) Metamorphic zircon formation by solid-state recrystallization of protolith igneous zircon. *Journal of Metamorphic Geology*, **18**, 423-39.

Imeokparia, E.G. (1982) Tin contents of biotites from the Afu Younger Granite Complex, central Nigeria. *Economic Geology*, **77**, 1710-24.

Javoy, M., Pineay, F. and Delorme, H. (1986) Carbon and nitrogen isotopes in the mantle. *Chemical Geology*, **57**, 41-62.

Johan, V. and Johan, Z. (1994) Accessory minerals of the Cinovec (Zinnwald) granite cupola, Czech Republic Part 1: Nb-, Ta-, and Ti-bearing oxides. *Mineralogy and Petrology*, **51**, 323-43.

Jones, A.P. (1980) *The petrology and structure of the Motzfeldt centre, Igaliko, South Greenalnd.* Unpublished PhD thesis. University of Durham.

Jones, A.P. (1984) Mafic silicates from the nepheline syenites of the Motzfeldt centre, South Greenland. *Mineralogical Magazine*, **48**, 1-12.

Jones, A.P. and Larsen, L.M. (1985) Geochemistry and REE minerals of nepheline syenites from the Motzfeldt centre, South Greenland. *American Mineralogist*, **70**, 1087-100.

Jones, A.P. and Peckett, A. (1980) Zirconium-bearing aegirines from Motzfeldt, South Greenland. *Contributions to Mineralogy and Petrology*, **75**, 251-5.

Keller, J. and Hoefs, J. (1995) Stable isotope characteristics of recent natrocarbonatites from Oldoinya Lengai. In K. Bell, and J. Keller, Eds. *Carbonatite volcanism: Oldoinya Lengai and the petrogenesis of natrocarbonatites*. IAVCEI proceedings in volcanology 4. Springer, Berlin.

Keppler, H. and Wyllie, P.J. (1990) Role of fluids in transport and fractionation of uranium and thorium in magmatic processes. *Nature*, **348**, 531-3.

Kinny, P. and Maas, R. (2003) Lu-Hf and Sm-Nd isotope systems in zircon. In J. Hanchar, and P. Hoskin, Eds. *Zircon*, **53**, p. 327-39. Mineralogical Society of America, Reviews in Mineralogy.

Knudsen, T., Griffin, W., Hartz, E., A, A. and Jackson, S. (2001) In-situ hafnium and lead isotope analyses of detrital zircons from the Devonian sedimentary basin of NE Greenland: A record of repeated crustal reworking. *Contributions to Mineralogy and Petrology*, **141**, 83-94.

Köhler, J., Konnerup-Madsen, J. and Markl, G. (2008) Fluid chemistry in the Ivigtût cryolite deposit, South Greenland. *Lithos*, **103**, 369-92.

Kogarko, L.N. (1974) Role of volatiles. In H. Søresnsen, Ed. *The Alkaline Rocks*. Wiley, London. p. 474-87

Kogarko, L.N. (1990) Ore-forming potential of alkaline magmas. *Lithos*, **26**, 167-175

Konnerup-Madsen, J. (2001) A review of the composition and evolution of hydrocarbon gases during solidification of the Ilímaussaq alkaline complex, South Greenland. *Geology of Greenland Survey Bulletin*, **301**, 159-66.

Konnerup-Madsen, J., Dubessy, J. and Rose-Hansen, J. (1985) Combined Raman microprobe spectrometry and microthermometry of fluid inclusions in minerals from igneous rocks of the Gardar province (South Greenland). *Lithos*, **18**, 271-80.

Konnerup-Madsen, J. and Rose-Hansen, J. (1982) Volatiles associated with alkaline igneous rift activity; fluid inclusions in the Ilímaussaq intrusion and the Gardar granitic complexes (South Greenland). *Chemical Geology*, **37**, 79-93.

Konnerup-Madsen, J. and Rose-Hansen, J. (1984) Composition and significance of fluid inclusions in the Ilímaussaq peralkaline granite, South Greenland. *Bulletin de Mineralogie*, **107**, 317-26.

Kovalenko, V.I., Tsaryeve, G.M., Goreglyad, A.V., Yarmoluk, V.V, and Troitsky, V.A. (1995) The peralkaline-granite related Khaldzan-Buregtey Rare metal (Zr, Nb, REE) deposit, West Mongolia. *Economic Geology*, **90**, 530-47.

Lanier, G., Raab, W.J., Folsom, R.B. and Cone, S. (1978) Alteration of equigranular monzonite, Bingham mining district, Utah. *Economic Geology*, **73**, 1270-86.

Larsen, L.M. (1977) Petrology of the late lavas of the Eriksfjord Formation, Gardar Province, South Greenland. *Grønlands Geologiske Undersøgelse Bulletin*, **125**, 31.

Larsen, L.M., and Tukiainen, T. (1985) New observations on the easternmost extension of the Gardar supracrustals (Eriksfjord Formation), South Greenland. *Rapport Grønlands Geologiske Undersøgelse Undersøgelse*, **125**, 64-6.

Lee, M.R., Parsons, I., Edwards, P.R. and Martin, R.W. (2007) Identification of cathodoluminescence activators in zoned alkali-feldspars by hyperspectral imaging and electron-probe microanalysis. *American Mineralogist*, **92**, 243-53.

Long, J.V.P. and Agrell, S.O. (1965) The cathodo-luminescence of minerals in thin section. *Mineralogical Magazine*, **34**, 318-26.

Ludwig, K.R. (2003) User's manual for Isoplot 3.00. A geochronological toolkit for Microsoft Excel. Berkley, California, Berkley Geochronology Centre Special Publication, 4a.

Lumpkin, G. (1989) *Alpha-decay damage, geochemical alteration and crystal chemistry of pyrochlore group minerals*. Unpublished PhD thesis. University of New Mexico.

Lumpkin, G.R., Chakoumakos, B. and Ewing, R.C. (1986) Mineralogy and radiation effects of microlite from the Harding pegmatite, Taos Country, New Mexico. *American Mineralogist*, **71**, 569-88.

Lumpkin, G.R. and Ewing, R.C. (1992) Geochemical alteration of pyrochlore group minerals: Microlite subgroup. *American Mineralogist*, **77**, 179-88.

Lumpkin, G.R. and Ewing, R.C. (1995) Geochemical alteration of pyrochlore group minerals: Pyrochlore subgroup. *American Mineralogist*, **80**, 732-43.

Lumpkin, G.R. and Ewing, R.C. (1996) Geochemical alteration of pyrochlore group minerals: Betafite subgroup. *American Mineralogist*, **81**, 1237-48.

Manceau, A., Bonnin, D., Stone, W.E.E. and Stanz, J. (1990) Distribution of Fe in the octahedral sheet of trioctahedral micas by polarized EXAFS. *Physics and Chemistry of Minerals*, **17**, 319-29.

Mariano, A.N. (1976) The application of cathodoluminescence for carbonatite exploration and characterization. *In: Simposio Internacional de Carbonatitos*, 1. Pocos de Daldas.

Mariano, A.N. and Ring, P.J. (1975) Europium-ctivated cathodoluminescence in minerals. *Geochimica Et Cosmochimica Acta*, **39,** 649-660.

Marshall, D.J. (1988) *Cathodoluminescence of Geologic Materials*. Unwin Hyman.

Mason, R. (1992) Models of order and iron-fluorine avoidance in biotite. *Canadian Mineralogist*, **30**, 343-54.

Munoz, J. (1984) F-OH and Cl-OH exchange in micas with applications to hydrothermal ore deposits. In S.W. Bailey, Ed., *Micas: Reviews in Mineralogy and Geochemistry*, *Mineralogical Society of America,* **13**, p. 469-94.

Munoz, J. and Ludington, S. (1974) Fluoride-hydroxyl exchange in biotite. *American Journal of Science*, **274**, 396-413.

Munoz, J. and Swenson, A. (1981) Chloride-hydroxyl exchange in biotite and estimation of relative HCl/HF activities in hydrothermal fluids. *Economic Geology*, **76**, 2212-21.

Nickel, E. (1992) Solid solutions in mineral nomenclature. *Canadian Mineralogist*, **30**, 231-4.

Nielsen, T.F.D. and Buchardt, B. (1985)Sr-C-O isotopes in nephelinitic rocks and carbonatites, Gardiner Complex, Tertiary of East Greenland. *Chemical Geology*, **53**, 207-17

Oberti, R., Ungaretti, L., Cannillo, E. and Hawthorne, F.C. (1993) The mechanism of Cl incorporation in amphibole. *American Mineralogist*, **78**, 746-52.

Parsons, I. (1972) A perlimenary description of the Klokken intrusion. *Rapport Grønlands Geologiske Undersøgelse*, **45**. 29-32.

Parsons, I. (1979) The Klokken gabbro-syenite complex, South Greenland: Cryptic variation and origin of inversely graded layering. *Journal of Petrology*, **20**, 653-94.

Parsons, I. (1981) The Klokken gabbro-syenite complex, South Greenland: Quantative interpretation of mineral chemistry. *Journal of Petrology*, **22**, 233-60.

Parsons, I., Mason, R., Becker, S. and Finch, A.A. (1991) Biotite equilibria and fluid circulation in the Klokken intrusion. *Journal of Petrology*, **32**, 1299-333.

Partington, G.A., McNaughton, N.J. and Williams, I.S. (1995) A review of the geology, mineralisation and geochronology of the Greenbushes pegmatite, Western Australia. *Economic Geology*, **90**, 616-35.

Paslick, C.R., Halliday, A.N., Davies, G.R., Mazger, K. and Upton, B.G.J. (1993) Timing of Proterozoic magmatism in the Gardar Province, southern Greenland. *Geological Society of America Bulletin*, **105**, 272-8.

Patchett, P.J. (1983) Importance of the Lu-Hf isotopic system in studies of planetary chronology and chemical evolution. *Geochimica et Cosmochimica Acta*, **47**, 81-91.

Patchett, P.J., Kouvo, O., Hedge, C. and Tatsumoto, M. (1981) Evolution of continental crust and mantle heterogeneity: Evidence from Hf isotopes. *Contributions to Mineralogy and Petrology*, **78**, 279-97.

Pearce, N. (1988) *The Petrology and Geochemistry. of the Igaliko Dyke Swarm, South Greenland.*. Unpublished PhD thesis, University of Durham.

Pearce, N. and Leng, M. (1996) The origin of carbonatites and related rocks from the Igaliko dyke swarm, Gardar Province, South Greenland: Field geochemical and C-O-Sr-Nd isotope evidence. *Lithos*, **39**, 21-40.

Pearce, N., Leng, M., Emeleus, C.H. and Bedford, C. (1997) The origins of carbonatites and related rocks from the Grønnedal-Ika nepheline syenite complex, South Greenland: C-O-Sr isotope evidence. *Mineralogical Magazine*, **61**, 515-29.

Pearce, T.H. (1994) Recent work on oscillatory zoning in plagioclase. In I. Parsons, Ed. *Feldspars and their Reactions*, p. 313-49. Kluwer Academic, Dordrecht.

Piper, J.D.A., Thomas, D.N., Share, S. and Zhang, Q.R. (1999) The paleomagnetism of (Mesoproterozoic) Eriksfjord group red beds, South Greenland: Multiphase remagnetization during the Gardar and Grenville episodes. *Geopyhsics Journal International*, **136**, 739-56.

Poulsen, V. (1964) The sandstones of the Precambrian Eriksfjord Formation in South Greenland. *Rapport Grønlands Geologiske Undersøgelse*, **2**, 16.

Putnis, A., Hinrichs, R., Putnis, C.V., Golla-Schindler, U. and Collins, L.G. (2007) Hematite in porous red-coloured feldspars: Evidence of large-scale crustal fluid-rock interaction. *Lithos*, **95**, 10-8.

Rancourt, D.G., Christie, I.A.D., Royer, M., Kodama, H., Robert, J.L., Lalonde, A.E. and Murad, E. (1994) Determination of accurate $^{[4]}Fe^{3+}$, $^{[6]}Fe^{3+}$ and $^{[6]}Fe^{2+}$ site populations in synthetic annite by Mössbauer spectroscopy. *American Mineralogist*, **79**, 51-62.

Reid, D. and Cooper, A. (1992) Oxygen and carbon isotope patterns in the Dicker Willem carbonatite complex, southern Namibia. *Chemical Geology*, **94**, 293-305.

Rimsaite, J. (1970) Structural formulae of oxidized and hydroxyl-deficient micas and decomposition of the hydroxyl group. *Contributions to Mineralogy and Petrology*, **25**. 225-40.

Robert, J.L., Beny, J.M., Della Ventura, G. and Hardy, M. (1993) Fluorine in micas: Crystal-chemical control of the OH-F distribution between trioctahedral and dioctahedral sites. *European Journal of Mineralogy*, **5**, 7-18.

Roedder. E. (1984) *Fluid inclusions: Reviews in Mineralogy*. Mineralogical Society of America.

Roedder, E. and Bodnar, R.J. (1980) Geologic pressure determinations from fluid inclusion studies. *Earth and Planetary Science Letters*, **8**, 263-301.

Rosenberg, P.E. and Foit, F.F. (1977) Fe^{2+}-F avoidance in silicates. *Geochimica Et Cosmochimica Acta*, **41**, 345-6.

Ross, N., Shu, J., Hazen, R., and Gasparik, T. (1990) High-pressure crystal chemistry of stishovite. *American Mineralogist*, **75**, 739-47.

Rye, R., and Ohmoto, H. (1974) Sulfur and carbon isotopes and ore genesis: A review. *Economic Geology*, **69**, 826-42.

Salters, V., and White, W. (1998) Hf isotope constraints on mantle evolution. *Chemical Geology*, **145**, 447-60.

Salvi, S. and Williams-Jones, A.E. (2006) Alteration, HFSE mineralisation and hydrocarbon formation in peralkaline igneous systems: Insights from the Strange Lake pluton, Canada. *Lithos*, **91**, 19-34.

Schönenberger, J. (2008) *Evolution of agpaitic rocks from mantle melts, with reference to the Motzfeldt complex, South Greenland.* Unpublished PhD thesis, Univerity of Tübingen.

Schönenberger, J. and Markl, G. (2008) The magmatic and fluid evolution of the Motzfeldt intrusion in South Greenland: Insights into the formation of agpaitic and miaskitic rocks. *Journal of Petrology*, **49**, 1549-77.

Shannon, R.D. and Prewitt, C.T. (1969) Effective ionic radii on oxides and fluorides. *Acta Crystallographica*, **B25**, 925.

Sharp, Z. (2007) *Principles of Stable Isotope Geology*. Prentice Hall, New Jersey.

Shepherd, T.J., Rankin, A.H. and Alderton, D.H.M. (1985) *A practical guide to fluid inclusion studies*. Blackie, Glasgow.

Sheppard, S.M.F. (1986) Igneous rocks: III. Isotopic case studies of magmatism in Africa, Eurasia and oceanic islands. *Mineralogical society of America Special Publications*, **16**, 319-71.

Shore, M. and Fowler, A.D. (1996) Oscillatory zoning in minerals: A common phenomenon. *Canadian Mineralogist*, **34**, 1111-26.

Sinha, A.K., Wayne, D.M. and Hewitt, D.A. (1992) The hydrothermal stability of zircon - preliminary experimental and isotopic studies. *Geochimica et Cosmochimica Acta*, **56**, 3551-60.

Smith, J.V. and Stenstrom, R.C. (1965) Electron excited luminescence as a petrologic tool. *Journal of Geology*, **73**, 627-35.

Smith, P., Tatsumoto, M. and Farquhar, R. (1987) Zircon Lu-Hf systematics and the evolution of the Archean crust in the southern Superior Province, Canada. *Contributions to Mineralogy and Petrology*, **97**, 93-104.

Sørensen, H. (1962) On the occurrence of steenstrupine in the Ilimaussaq massif, Southwest Greenland, *Meddelelser om Grønland,* **167**,251

Sørensen, H. (1969) Rhythmic igneous layering in peralkaline igneous intrusions. *Lithos*, **2**, 261-83.

Sørensen, H. (1970) Internal structures and geological setting of three agpaitic intrusions - Khibina and Lovozero of the Kola peninsula and Ilímaussaq intrusion, South Greenland. *Canadian Mineralogist*, **10**, 299-334.

Sørensen, H. (1974) *The Alkaline Rocks*. Wiley, London.

Sørensen, H. and Larsen, L.M. (1978) Aspects of crystallization of volatile-rich peralkaline undersaturated magmas – exemplified by the Ilimaussaq intrusion, South Greenland. *Jornal de Mineralogia Recife,* **7**, 135-42

Stanz, J. and Stone, W.E.E. (1979) NMR study of micas II. Distribution of Fe^{2+}, F- and OH- in the octahedral sheet of phlogopites. *American Mineralogist*, **64**, 119-26.

Stanz, J. and Stone, W.E.E. (1983) NMR applied to minerals: IV. Local order in the octahedral sheet of micas: Fe-F avoidance. *Clay Minerals*, **18**, 187-92.

Steiger, R.H. and Jäger, E. (1977) Convention on the use of decay constants in geo- and cosmochronology. *Earth and Planetary Science Letters*, **36**, 359-62.

Stewart, J.W. (1970) Precambrian Alkaline-Ultramafic-carbonatite volcanism ot Qagssiarsuk, South Greenland. *Grønlands Geologiske Undersøgelse Bulletin, 84*.

Subramanian, M., Aravamundan, G. and Subba Rao, G.V. (1983) *Oxide Pyrochlores - A Review*. Oxford, New York.

Taubald, H., Morteani, G. and Satir, M. (2004) Geochemical and isotopic (Sr, C, O) data from the alkaline complex of Grønnedal-Ika (South Greenland): Evidence for unmixing and crustal contamination. *International Journal of Earth Science*, **93**, 348-60.

Taylor, H., Frechen, J. and Degens, E. (1967) Oxygen and carbon isotope studies of carbonatites from the Laacher See district, West Germany and the Alno District Sweden. *Geochimica Et Cosmochimica Acta*, **31**. 407-30.

Taylor, H. and Upton, B.G.J. (1993) Contrasting Pb isotopic compositions in two intrusive complexes of the Gardar magmatic province of South Greenland. *Chemical Geology*, **104**, 261-8.

Tichomirowa, M., Grosch, G., Gotze, J. Baltyatsky, B.V., Savva, E.V., Keller, J. and Todt, W. (2006) The mineral isotopic composition of two Precambrian carbonatite complexes from the Kola alkaline Province – Alteration versus primary magamtic signatures. *Lithos*, **91**, 229-49.

Tilton, G. (1960) Volume diffusion as a mechanism for discordant lead ages. *Journal of Geophysical Research*, **65**, 2933-45.

Tirsgaard, H. and Øxenvad, I.E.I. (1998) Preservation of pre-vegetational mixed fluvio-aeolian deposits in a humid climatic setting: An example from the Middle Proterozoic Eriksfjord Formation, Southwest Greenland. *Sedimentary Geology*, **120**, 295-317.

Thomassen, B. (1988) The Motzfeldt 87 Project, Final Report. Open file Series 88/1, *Grønlands Geologiske Undersøgelse*

Tukiainen, T. (1985) Geological mapping and mineral explotation in the Motzfeldt centre of the Igaliko nepheline syenite complex. *Rapport Grønlands Geologiske Undersøgelse,* **125***,* 78-79.

Tukiainen, T. (1988) Niobium-tantalum mineralisation in the Motzfeldt centre of the Igaliko nepheline syenite complex, South Greenland. In J. Boissonnas, and P. Omenetto, Eds. *Mineral deposits within the European Community*, p. 230-46. Springer-Verlag, Berlin Heidelberg.

Tukiainen, T., Bradshaw, C. and Emeleus, C.H. (1984) Geological and radiometric mapping of the Motzfeldt centre of the Igaliko Complex, South Greenland. *Rapport Grønlands Geologiske Undersøgelse*, **102**, 78-83.

Upton, B.G.J. (1961) Textural features of some contrasted igneous cumulates from South Greenland. *Grønlands Geologiske Undersøgelse Bulletin*, **29**, 1-32.

Upton, B.G.J. (1962) Geology of Tugtutôq and Neighbouring Islands, South Greenland. I. *Bulletin Grønlands Geologiske Undersøgelse,* **34**, 60.

Upton, B.G.J. (1974) The alkaline province of south-west Greenland. In H. Sorensen, Ed. *The Alkaline Rocks*, p. 221-38. Wiley, New York.

Upton, B.G.J. (1996) Anorthosites and troctolites of the Gardar Province. In: D. Demaiffe, Ed. *Petrology and Geochemistry of Magmatic Suites of Rocks in Continental and Oceanic Crusts. A volume dedicated to Professor Jean Michot: Universite´ Libre de Bruxelles*, pp. 19– 34. Royal Museum for Central Africa.

Upton, B.G.J. and Blundell, D.J. (1978) The Gardar Igneous Province: Evidence for Proterozoic continental rifting. In E.R. Neumann, and I.B. Ramberg, Eds. *Petrology and Geochemistry of Continental Rifts*, p. 163-72. Reidel, Dordrecht.

Upton, B.G.J. and Emeleus, C.H. (1987) Mid-Proterozoic alkaline magmatism in Southern Greenland: The Gardar Province. In J.G. Fitton, and B.G.J. Upton, Eds. *Alkaline Igneous Rocks, Special Publication*, **30**, p. 449-71. Geological Society of London.

Upton, B.G.J., Emeleus, C.H., Heaman, L.M., Goodenough, K.M. and Finch, A.A. (2003) Magmatism of the Mid-Proterozoic Gardar Province, South Greenland: Chronology, petrogenesis and geological setting. *Lithos*, **68**, 43-65.

Upton, B.G.J. and Thomas, J.E. (1980) The Tugtutoq younger giant dyke complex, Fractional crystallisation of transitional olivine basalt magama*, Journal of Petrology*, **21**, 167-98

Van Breemen, O., Aftalion, M. and Allart, J.H. (1974) Isotopic and geochronologic studies on granites from the Ketilidian mobile belt of South Greenland. *Bulletin of the Geological Society of America*, **85**, 403-12.

Van den Kerkhof, A.M. and Hein, U.F. (2001) Fluid inclusion petrography. *Lithos*, **55**, 27-47.

Vittorio, L., Griffith, C., Blackford, M. and Hanna, J. (2005) Structural and ion exchange properties of nanocrystaline Si-doped antimony pyrochlore. *Journal of Materials Chemistry*, **15**, 564-72.

Volfinger, M. and Pascal, M.-L. (1989) Partitioning of chlorine between muscovite and HCl-buffered solutions from 400 to 600°C at 2 kbar. *European Journal of Mineralogy*, **1**, 791-800.

Volfinger, M., Robert, J.L., Vielzeuf, D. and Neiva, A.M.R. (1985) Structural control of the chlorine content of OH-bearing silicates (micas and amphiboles). *Geochimica et Cosmochimica Acta*, **49**. 1813-23

Voloshin, A., Pakhomovskiy, Y., Nadezhina, T., Bakhchisaraitsev, A., and Kobyashev, Y. (1989) Strontiopyrochlore: Composition and structure. *Trudy Mineralogicheskogo Muzeya and SSSR*, **36**, 12-24 (In Russian).

Webster, J.D. (2004) The exsolution of magmatic hydrosaline chloride liquids. *Chemical Geology*, **210**, 33-48.

Wetherill, G. (1956) Discordant uranium-lead ages - Part I. *Transactions of the American Geophysical Union*, **37**, 320-6.

Wetherill, G. (1963) Discordant uranuim-lead ages - Part 2: Discordant ages resulting from diffusion of lead and uranium. *Journal of Geophysical Research*, **68**, 2957-65.

Wilkinson, J.J. (2001) Fluid inclusions in hydrothermal ore deposits. *Lithos*, **55**, 229-72.

Wood, S.A. (1990) The aqueous geochemistry of the rare earth elements and yttrium: Part I. Review of available low temperature data for inorganic complexes and the inorganic REE speciation of natural waters. *Chemical Geology*, **82**, 159-86.

Wood, B.J. and Nicholls, J. (1978) The thermodynamic properties of reciprocal solid solutions. *Contributions to Mineralogy and Petrology*, **66**, 389-400.

Worden, R.H., Walker, F.D.L., Parsons, I. and Brown, W.L. (1990) Development of microporisity, diffusion channels and deuteric coarsening in perthitic alkali-feldspars. *Contributions to Mineralogy and Petrology*, **104**.

Zhang, D., Xu, G., Zhang, W. and Golding, S.D. (2007) High salinity fluid inclusions in the Yinshan polymetallic deposit from the Le-De metallogenic belt in Jiangxi Province, China: Their origin and implications for ore genesis. *Ore Geology Reviews*, **31**, 247-60.

Zhang, D., Yu, C., Bao, Z. and Tang, Z. (1997) Ore zoning and the dynamics of ore-forming processes in the Yinshan polymetallic deposit, Jiangxi. *Chinese Journal of Geochemistry*, **16**, 123-32.

Zhu, C. and Sverjensky. (1992) F-Cl-OH partitioning between biotite and apatite. *Geochimica Et Cosmochimica Acta*, **56**, 3435-67.

Zhu, C. and Sverjensky, D. (1991) Partitioning of F-Cl-OH between minerals and hydrothermal fluids. *Geochimica Et Cosmochimica Acta*, **55**, 1837-58.

Appendices

Appendices

Appendix A: Sample locations and descriptions

List of sample numbers, locations (Fig. A.1 & A.2) and a brief sample description. All samples are those of J. McCreath (JAM) at the University of St Andrews collected during the present study, except those labelled A&R, which are drill core samples collected by Angus and Ross plc during 2001 and those labelled JS which where donated by J. Schönenberger.

Type of analyses carried out on each sample is indicated: TS - polished thin section/EPMA analyses, X - XRF analyses, U - U-Pb zircon analyses, Lu - Lu-Hf zircon analyses, Pb - whole-rock Pb-Pb analyses, Py - Pyrochlore Pb-Pb analyses. FI - Fluid inclusion analyses and O - stable isotope analyses.

Sample	Lat	Long	Description	Fm.	Coll.	TS	X	U	Lu	Pb	Py	FI	O
05/01	N61.21004	W44.95847	Fine-grain microsyenite dyke	MSF	JAM								
05/03	N61.21004	W44.95847	Med-grain altered syenite	MSF	JAM		x			x			x
05/04	N61.20998	W44.95872	Fluorite vein	MSF	JAM								
05/05	N61.20976	W44.95978	Med-grain syenite with lower alteration	MSF	JAM								
05/06	N61.21068	W44.96344	Porphyritic dolerite dyke	MSF	JAM		x						x
05/07	N61.21068	W44.96344	Mafic poor altered syenite	MSF	JAM								
05/08	N61.21145	W44.96684	Med-coarse grain altered syenite	MSF	JAM		x			x			
05/09	N61.21149	W44.96705	Highly altered syenite	MSF	JAM								
05/11	N61.21165	W44.96613	Pegmatitic altered syenite	MSF	JAM		x			x			
05/12	N61.21312	W44.96123	Med-grain altered syenite	MSF	JAM								
05/13	N61.21451	W44.95895	Microsyenite dyke	MSF	JAM								
05/14	N61.21836	W44.97054	Microsyenite	MSF	JAM								
05/15	N61.21735	W44.97339	Less altered zone of med-grain syenite	MSF	JAM								
05/16	N61.21735	W44.97339	Highly altered pegmatitic syenite	MSF	JAM		x						x
05/17	N61.21486	W44.97509	Highly altered pegmatitic syenite	MSF	JAM								
05/18	N61.21498	W44.97599	Med-coarse grain altered syenite	MSF	JAM								
05/19	N61.21651	W44.97385	Med-grain slightly altered syenite	MSF	JAM								
05/20	N61.21651	W44.97385	Med-grain altered syenite	MSF	JAM								
05/21	N61.20706	W44.97640	Biotite rich med-grain syenite	MSF	JAM	x	x			x			x
05/22	N61.20382	W44.99175	Med-grain altered syenite	MSF	JAM					x			
05/23	N61.20367	W44.99192	Fine-grain pyrochlore syenite	MSF	JAM	x							
05/24	N61.20355	W44.99178	Fine-grain pyrochlore syenite	MSF	JAM	x	x			x			x
05/25	N61.20178	W44.95108	Med-grain porphyritic syenite	MSF	JAM								
05/26	N61.20027	W44.95486	Med-grain altered syenite	MSF	JAM								
05/27	N61.20590	W44.95440	Marginal syenite surrounding quartzite	MSF	JAM								
05/28	N61.20586	W44.95474	Med-grain altered syenite	MSF	JAM								
05/29	N61.20453	W44.96442	Med-grain moderately altered syenite	MSF	JAM								
05/30	N61.18775	W44.94308	Quartzite with fine grain mafic clots	MSF	JAM	x							
05/31	N61.18775	W44.94308	Porphyritic microsyenite	MSF	JAM	x							
05/32	N61.19214	W44.95047	Quartzite raft	MSF	JAM								
05/33	N61.19238	W44.95114	Med-grain syenite/quartzite contact	MSF	JAM	x							
05/34	N61.19205	W44.94912	Porphyritic microsyenite	MSF	JAM	x	x						
05/35	N61.19261	W44.95000	Pegmatite/med-grain syenite contact	MSF	JAM	x							

Sample	Lat	Long	Description	Fm.	Coll.	TS	X	U	Lu	Pb	Py	FI	O
05/36	N61.19261	W44.95000	Med-grain porphyritic syenite	MSF	JAM								
05/37	N61.19265	W44.94963	Volcanic agglomerate	MSF	JAM								
05/38	N61.19385	W44.94926	Porphyritic basaltic raft	MSF	JAM								
05/39	N61.19385	W44.94926	Tracyite	MSF	JAM		x						
05/40	N61.19392	W44.94868	Quartzite with fine-grain mafic clots	MSF	JAM								
05/41	N61.19394	W44.94836	Fine-grain syenite	MSF	JAM	x	x						x
05/42	N61.19394	W44.94836	Med-grain porphyritic syenite	MSF	JAM	x							
05/43	N61.19383	W44.94827	Pegmatitic syenite	MSF	JAM								
05/44	N61.19383	W44.94827	FIne-grain syenite hosting pyrochlore	MSF	JAM	x							
05/45	N61.19387	W44.94861	Highly altered pegmatitic syenite	MSF	JAM								
05/46	N61.19454	W44.94958	Coarse altered syenite	MSF	JAM								
05/47	N61.19454	W44.94958	Coarse altered syenite	MSF	JAM								
05/48	N61.19433	W44.94853	Porphyritic pink siliceous rock	MSF	JAM								
05/49	N61.18596	W44.95527	Altered syenite	MSF	JAM								
05/50	N61.18740	W44.95336	Microsyenite dyke	MSF	JAM								
05/51	N61.18851	W44.95582	Pegmatitic altered syenite	MSF	JAM								
05/52	N61.18947	W44.95499	Basalt raft	MSF	JAM								
05/53	N61.18947	W44.95499	Basalt /highly altered syenite contact	MSF	JAM								
05/54	N61.18947	W44.95499	Highly altered syenite	MSF	JAM								
05/55	N61.18540	W44.96721	Pegmatitic syenite	MSF	JAM								
05/56	N61.18805	W44.97120	Pegmatitic syenite	MSF	JAM								
05/57	N61.18805	W44.97120	Fine-grain porphyritic syenite	MSF	JAM	x							
05/58	N61.19310	W44.97994	Pegmatitic syenite	MSF	JAM								
05/59	N61.19310	W44.97994	Unaltered syenite	MSF	JAM	x	x						x
05/60	N61.19166	W44.97885	Med-grain unaltered altered syenite	MSF	JAM	x							
05/61	N61.18555	W44.94698	Syenite surrounding basalt raft	MSF	JAM								
05/62	N61.18555	W44.94698	Basalt raft	EF	JAM	x							
05/63	N61.18829	W44.93962	Porphyritic dyke of microsyenite	MSF	JAM	x	x						
05/64	N61.19515	W44.94226	Porphyritic altered syenite	MSF	JAM	x	x						
05/65	N61.19545	W44.94392	Pegmatitic syenite	MSF	JAM	x							
05/66	N61.19545	W44.94392	Med-grain porphyritic syenite	MSF	JAM	x	x						x
05/67	N61.19545	W44.94392	Quartzite	EF	JAM	x							
05/68	N61.19549	W44.94647	Med-grain porphyritic syenite	MSF	JAM	x							
05/69	N61.19678	W44.94931	Secondary mica growth	MSF	JAM								
05/70	N61.19678	W44.94931	Secondary mica growth	MSF	JAM								
06/01	N61.21703	W44.95592	Diorite dyke	NM	JAM								
06/02	N61.21703	W44.95592	Unaltered med-grain syenite (NM1)	NM	JAM		x						
06/03	N61.21721	W44.96048	Unaltered med-grain syenite (NM1)	NM	JAM								
06/04	N61.21858	W44.96277	Porphyritic microsyenite	MSF	JAM								
06/05	N61.21933	W44.96273	Quartz pebbles in fine-grain syenite	MSF	JAM	x							
06/06	N61.22143	W44.95623	Porphyritic microsyente	MSF	JAM								
06/07	N61.22143	W44.95623	Porphyritic microsyente	MSF	JAM	x							
06/08	N61.22498	W44.96996	Versicular basalt lava	MSF	JAM								
06/09	N61.22057	W44.98150	Microsyenite dyke	MSF	JAM	x							
06/10	N61.20785	W44.95700	Microsyenite dyke	MSF	JAM								
06/11	N61.20785	W44.95700	Med-grain latered syenite	MSF	JAM								
06/12	N61.20788	W44.95767	Porpyritic microsyenite	MSF	JAM	x	x			x			
06/13	N61.20732	W44.95970	Coarse-grain syenite	MSF	JAM	x							
06/14	N61.21053	W44.97752	Med-grain syenite	MSF	JAM								
06/15	N61.21053	W44.97752	Microsyenite	MSF	JAM								
06/17	N61.20884	W44.97794	Med-grain biotite syenite	MSF	JAM	x							
06/18	N61.20355	W45.00197	Med-grain pyrochlore bearing syenite	MSF	JAM	x		x	x		x		
06/19	N61.20298	W44.95252	Aplite	MSF	JAM								
06/20	N61.20298	W44.95252	Med-grain syenite	MSF	JAM								
06/21	N61.20298	W44.95252	Aplite	MSF	JAM								
06/22	N61.20298	W44.95252	Aplite	MSF	JAM	x							
06/23	N61.20325	W44.95311	Med-grain altered syenite	MSF	JAM								
06/24	N61.20335	W44.95565	Aplite	MSF	JAM	x							
06/25	N61.20335	W44.95565	Microsyenite dyke	MSF	JAM								
06/26	N61.20355	W44.95812	Microsyenite	MSF	JAM								

Sample	Lat	Long	Description	Fm.	Coll.	TS	X	U	Lu	Pb	Py	FI	O
06/27	N61.20355	W44.95812	Med-grain syenite with mafic clusters	MSF	JAM								
06/28	N61.20355	W44.95812	Med-grain syenite with mafic clusters	MSF	JAM								
06/29	N61.20288	W44.95976	Med-grain syenite with large zircons	MSF	JAM	x		x	x				
06/30	N61.20288	W44.95976	Fluorite sample	MSF	JAM								
06/31	N61.20268	W44.95995	Biotite rich med-grain syenite	MSF	JAM	x							
06/32	N61.20272	W44.96073	Porphyritic fine-grain syenite	MSF	JAM	x							
06/33	N61.20069	W44.93642	Eriksfjord quartz arenite	EF	JAM	x	x			x			
06/34	N61.19292	W44.94333	Eriksfjord basalt	EF	JAM	x	x			x			
06/35	N61.19001	W44.97375	Dolerite dyke	MSF	JAM	x							
06/36	N61.19001	W44.97375	Fine-grain porpyritic syenite	MSF	JAM	x							
06/37	N61.19164	W44.97741	Fine-grain porpyritic syenite	MSF	JAM								
06/39	N61.20097	W44.96465	Microsyenite dyke	MSF	JAM								
06/40	N61.20522	W44.97587	Biotite rich med-grain syenite	MSF	JAM								
06/41	N61.20522	W44.97587	Med-grain syenite	MSF	JAM								
06/42	N61.22239	W44.96415	Highly altered microsyenite dyke	MSF	JAM								
06/43	N61.22385	W44.96806	Highly altered microsyenite dyke	MSF	JAM	x							
06/44	N61.22699	W44.97046	Vesicular basalt lava	EF	JAM								
06/45	N61.22699	W44.97046	Columnar jointed basalt lava	EF	JAM								
06/46	N61.22699	W44.97046	Highly altered microsyenite dyke	MSF	JAM								
06/47	N61.22554	W44.99192	Highly altered microsyenite dyke	MSF	JAM								
06/48	N61.21283	W44.96525	Fluorite sample	MSF	JAM							x	
06/49	N61.21277	W44.96621	Aplite	MSF	JAM								
06/50	N61.21261	W44.96668	Fine-grain porpyritic syenite	MSF	JAM								
06/51	N61.22514	W44.99535	Porpyritic microsyenite	MSF	JAM	x	x			x			
06/52	N61.22138	W45.01246	Med-grain syenite	MSF	JAM								
06/53	N61.21821	W45.02478	Highly altered microsyenite dyke	MSF	JAM								
06/54	N61.21641	W45.02365	Unaltered nepheline syenite	GF	JAM	x					x		
06/55	N61.21641	W45.02365	Unaltered nepheline microsyenite	GF	JAM								
06/56	N61.21491	W45.02235	Contact of altered/unaltered syenite	GF	JAM								
06/57	N61.22060	W45.00692	Fine-grain unaltered syenite	GF	JAM								
06/58	N61.19573	W45.02008	Coarse-grain unaltered syenite	MSF	JAM								
06/59	N61.19661	W45.01819	Med-grain porpyritic syenite	MSF	JAM	x	x			x			
06/60	N61.19661	W45.01819	Med-grain syenite	MSF	JAM								
06/61	N61.19937	W45.01071	Fine-grain syenite	MSF	JAM								
06/62	N61.20002	W45.00838	Microsyenite	MSF	JAM	x	x			x			
06/63	N61.20002	W45.00838	Biotite rich med-grain syenite	MSF	JAM	x							
06/64	N61.20510	W44.99737	Fine-grain pyrochlore bearing syenite	MSF	JAM	x					x		
06/65	N61.20522	W44.99654	Fine-grain pyrochlore bearing syenite	MSF	JAM	x					x		
06/66	N61.22131	W44.98720	Fine-grain nepheline syenite	MSF	JAM								
06/67	N61.22131	W44.98720	Med-grain syenite	MSF	JAM								
06/68	N61.22364	W44.98566	Roof zone fluorite	MSF	JAM							x	
06/69	N61.22364	W44.98566	Roof zone arenite/fluorite	MSF	JAM							x	
06/70	N61.22364	W44.98566	Roof zone syenite	MSF	JAM							x	
06/71	N61.22396	W44.98417	Highly altered microsyenite dyke	MSF	JAM								
06/72	N61.22459	W44.98318	Highly altered microsyenite dyke	MSF	JAM		x			x			
06/73	N61.20059	W44.93749	Aplite	MSF	JAM								
06/75	N61.20134	W44.96983	Unaltered nepheline syenite	MSF	JAM						x		
06/76	N61.19877	W44.97385	Med-grain syenite	MSF	JAM								
06/77	N61.21024	W45.13189	Unaltered nepheline syenite	MSF	JAM						x		
06/78	N61.21024	W45.13189	Phonolite dyke	MSF	JAM								
06/79	N61.21084	W45.10109	Fluorite sample	MSF	JAM								
06/80	N61.21023	W45.10707	Secondary biotite replacing amphibole	MSF	JAM								
06/81	N61.21023	W45.10707	Poikolitic fluorite	MSF	JAM							x	
06/82	N61.20968	W45.10659	Unaltered nepheline syenite	FDF	JAM								
06/83	N61.18776	W45.12063	Microsyenite	FDF	JAM								
06/84	N61.18776	W45.12063	Garnet bearing granitoid rock	EF	JAM								
06/85	N61.18796	W45.11880	Med-grain porpyritic syenite	FDF	JAM								
06/86	N61.18776	W45.12063	Coarse-grain nepheline syenite	FDF	JAM								
06/87	N61.18776	W45.12063	Med-grain syenite	FDF	JAM		x						
06/88	N61.19456	W45.11571	Mafic enclaves in med-grain syenite	FDF	JAM								

Sample	Lat	Long	Description	Fm.	Coll.	TS	X	U	Lu	Pb	Py	Fl	O
06/89	N61.20185	W45.13192	Carbonate vein	FDF	JAM								
06/90	N61.20748	W45.13245	Aplite	FDF	JAM		x			x			
06/91	N61.21178	W45.13276	Coarse-grain syenite	MSF	JAM						x		
06/92	N61.21024	W45.13189	Med-grain nepheline syenite	FDF	JAM								
06/93	N61.21024	W45.13189	Coarse-grain syenite	MSF	JAM								
06/94	N61.20971	W45.13058	MSF/FDF contact	MSF	JAM								
06/95	N61.18453	W45.12413	Coarse-grain syenite	FDF	JAM								
06/96	N61.18569	W45.10740	Fluorite sample	FDF	JAM							x	
06/97	N61.18370	W45.10488	Carbonate vein	FDF	JAM								
06/98	N61.18156	W45.10042	Coarse-grain nepheline syenite	FDF	JAM		x			x			x
06/99	N61.19813	W45.10657	Fine-grain nepheline syenite	FDF	JAM		x			x			x
06/100	N61.21080	W45.10097	Fluorite sample	FDF	JAM							x	
06/101	N61.21026	W45.10630	Contact traverse sample 1	MSF	JAM	x	x			x			
06/102	N61.21026	W45.10630	Contact traverse sample 2	MSF	JAM	x	x			x			
06/103	N61.21008	W45.10676	Contact traverse sample 3	MSF	JAM	x							
06/104	N61.20968	W45.10659	Contact traverse sample 4	MSF	JAM	x							
06/105	N61.20968	W45.10659	Contact traverse sample 5	FDF	JAM	x							
06/106	N61.20974	W45.10668	Contact traverse sample 6	FDF	JAM	x							
06/107	N61.20956	W45.10676	Contact traverse sample 7	FDF	JAM	x							
06/108	N61.20928	W45.10694	Contact traverse sample 8	FDF	JAM	x							
06/109	N61.20896	W45.10731	Contact traverse sample 9	FDF	JAM	x							
06/110	N61.15232	W45.21136	Mafic rich lujavrite	FDF	JAM		x			x			x
06/111	N61.15232	W45.21136	Felsic rich lujavrite	FDF	JAM								
06/112	N61.15232	W45.21136	Fine-grain syenite	FDF	JAM								
06/113	N61.20775	W45.10510	Aplite	FDF	JAM								
06/114	N61.20775	W45.10510	Fluorite	FDF	JAM								
06/115	N61.20775	W45.10510	Med-grain syenite/aplite contact	FDF	JAM								
06/116	N61.21047	W45.10780	Med-grain syenite	MSF	JAM		x			x			
06/117	N61.21232	W45.10817	Fine-grain spotty syenite	MSF	JAM								
06/118	N61.21232	W45.10817	Poikolitic fluorite	MSF	JAM								
06/119	N61.21259	W45.11065	Microsyenite	MSF	JAM		x			x			x
06/120	N61.21128	W45.11291	Fluorite sample	MSF	JAM								
06/121	N61.21164	W45.11341	MSF/FDF contact	MSF	JAM								
06/122	N61.21204	W45.11364	Med-grain syenite	MSF	JAM								
06/123	N61.20822	W45.11017	Aplite	MSF	JAM								
06/124	N61.19253	W45.12293	Locally altered med-grain syenite	FDF	JAM								
06/125	N61.19253	W45.12293	Locally altered med-grain syenite	FDF	JAM		x			x			x
06/126	N61.19212	W45.12524	Carbonate vein	FDF	JAM								x
06/127	N61.19169	W45.12899	Med-grain syenite	FDF	JAM								
10018	-	-	Drillcore sample	MSF	A&R	x							
10519	-	-	Drillcore sample	MSF	A&R	**x**							
10520	-	-	Drillcore sample	MSF	A&R	x							
11013	-	-	Drillcore sample	MSF	A&R	x							
11503	-	-	Drillcore sample	MSF	A&R	x							
JS53	-	-	Flinks Dal Formation roof zone	FDF	JS	x							
JS55	-	-	Flinks Dal Formation roof zone	FDF	JS	x							
JS66	-		Flinks Dal Formation roof zone	FDF	JS	x							

All samples collected by J. McCreath (JAM) are prefixed GJM.

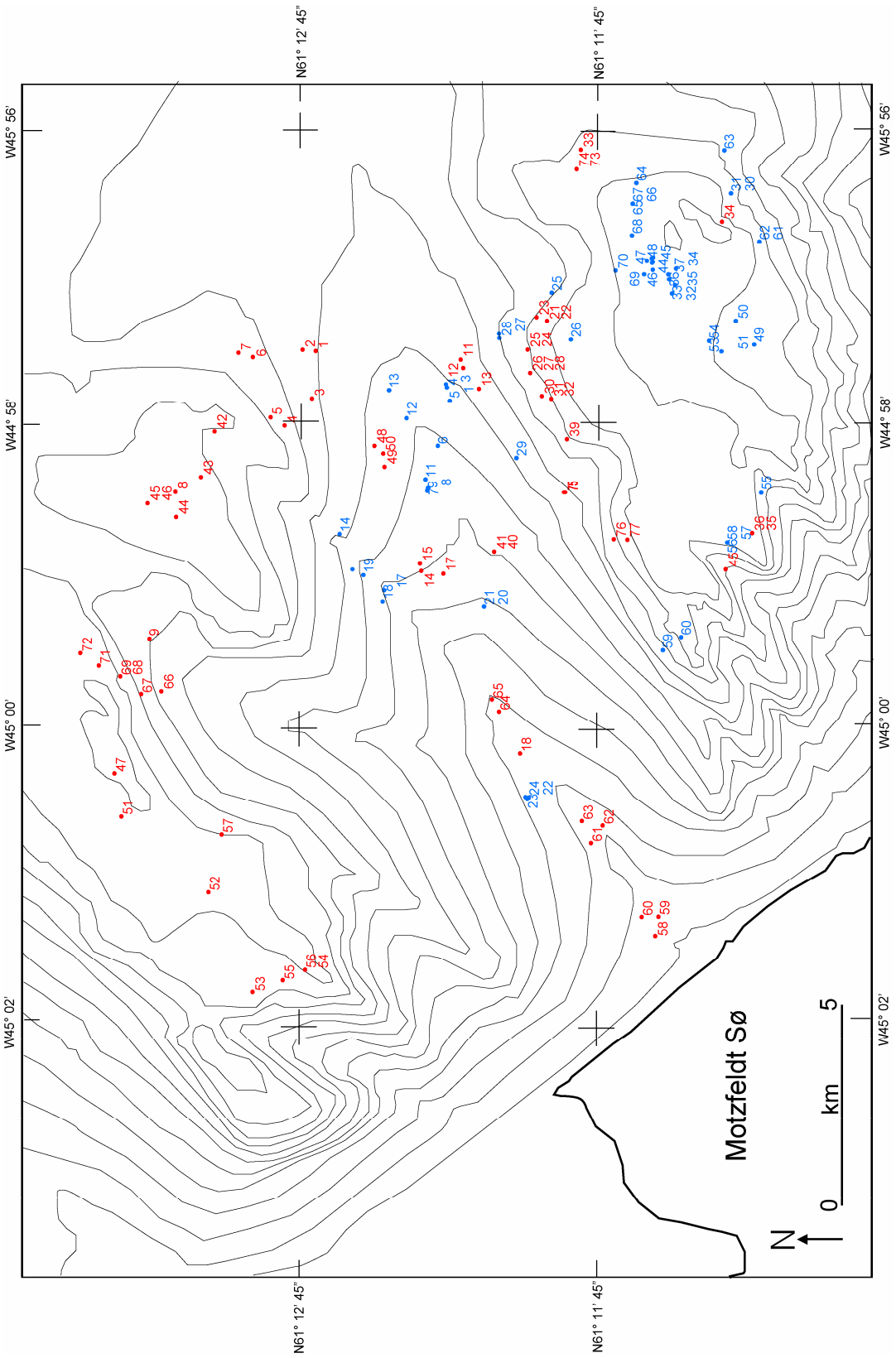

Figure A.1. Sample location map for samples from the Motzfeldt Sø Formation. Samples in blue are prefixed GJM05 and samples in red are prefixed GJM06

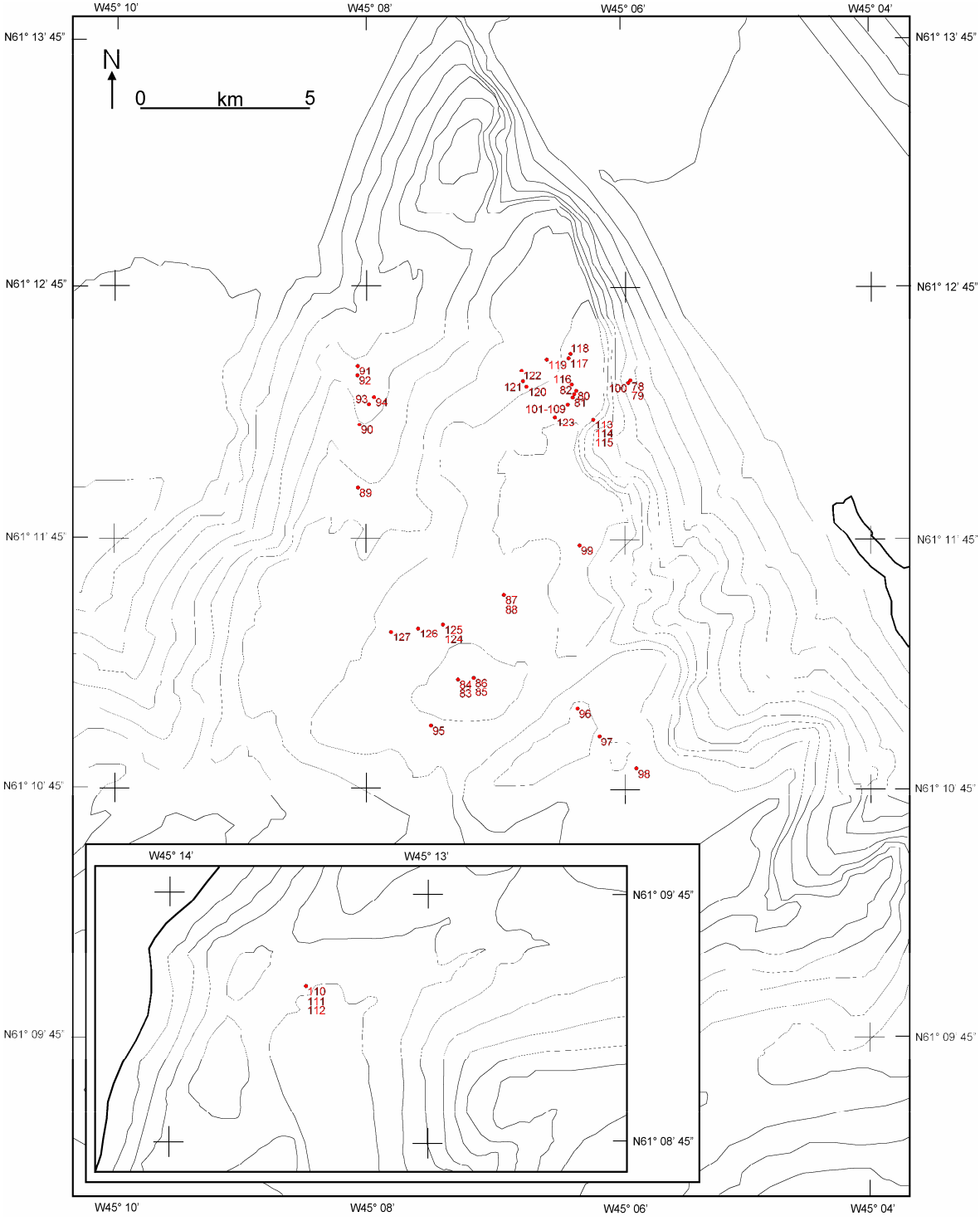

Figure A.2. Sample location map for samples from the Flinks Dal Formation. All samples are prefixed GJM06.

Appendix B: Analytical techniques

This appendix provides the details of the analytical methods used in the body of the thesis. Methodologies for EPMA (B.1), CL (B.2) mineral separate preparation (B.3), radiogenic isotope analyses (B.4) stable isotope analyses (B.5) and fluid inclusion microthermometry (B.6) are given.

B.1 Electron microprobe analyses

Electron microscopy and electron probe microanalyses (EPMA) were performed at the School of Geography and Geosciences at the University of St Andrews using a Jeol JCXA 8600 superprobe. A SAMIX Energy Dispersive System (EDS) was used to obtain qualitative estimates of mineral compositions prior to quantitative analysis, particularly to ensure that all significant elements were present in WDS analytical programs. Two mineral programs were used during Wavelength Dispersive (WDS) data acquisition. For pyrochlore group minerals a 28 element program was used with the electron beam operated at an accelerating voltage of 20 kV and a beam current of 30 nA. Peak searches were first performed for each element, followed by on peak count times of 10s and off-peak background counts of 5s either side of the peak. Analyses on biotites used a standard 10 element program using an accelerating voltage of 15 kV with a beam current of 20 nA. Peak and background count times were identical to the higher voltage/current program used for pyrochlore analyses. Data were processed using SAMIX software with fully quantitative ZAF corrections to obtain final element analyses. Well-characterised natural and synthetic standards (Table B.1) were measured at the beginning of each analytical session. Back-scattered electron imaging was carried out using an accelerating voltage of 15 kV with beam current of 20 nA to ensure a sharp image, unless images were taken during sampling procedure where the operating conditions where those mentioned for fully qualitative analyses. Sample images were processed using SAMIX software and later enhanced using Adobe Photoshop 6.0.

Table B.1 *Standards used during EPMA analysis*

Element	*Standard*	*Spec. Crystal*	*Element*	*Standard*	*Spec. Crystal*
Al	Corundum	TAP	Ta	Metal	LIF
Ba	Barite	LIF	Th	Metal	PET
Ca	Wollastonite	PET	U	Metal	PET
K	Orthoclase	LIF	W	Metal	PET
Na	Albite	TAP	F	MgF_2	LIF
P	Apatite	PET	La	Syn. Phosphate	LIF
Pb	Galena	PET	Ce	Syn. Phosphate	LIF
Si	Quartz	TAP	Pr	Syn. Phosphate	LIF
Sr	Celestine	PET	Nd	Syn. Phosphate	LIF
Zr	Zircon	PET	Sm	Syn. Phosphate	LIF
Ti	Rutile	PET	Gd	Syn. Phosphate	LIF
Fe	Metal	LIF	Dy	Syn. Phosphate	LIF
Mn	Metal	LIF	Y	Syn. Phosphate	TAP
Nb	Metal	PET	Yb	Syn. Phosphate	LIF

Mineral recalculations for pyrochlore were made using a Microsoft Excel spreadsheet. All pyrochlore analyses were calculated to structural formula based on a *B*-site cation total of 2 to allow for any *A*-site vacancies to be calculated One of the major problems of assigning structural formula is the determination of the oxidation state of Fe. In the reduced state (Fe^{2+}) iron preferentially enters the A-site. As Fe^{3+}, iron preferentially enters the *B*-site. During this study Fe is reported as FeO. Assignment of Fe to the *B*-site in highly altered samples, where Fe is often in high quantities, leads to overfilling of the B-site (>2.5 apfu). For this reason Fe is assumed to enter the *A*-site in the reduced state. This minimises *A*-site vacancies and prevents problems during recalculation of the *B*-site cations.

B.2 Cathodoluminescence petrography

Cathodoluminescence Petrography has been an important technique during this study for investigating fluid rock interaction and identifying carbonate bearing syenite facies. Cathodoluminescence was performed at the University of St Andrews using a Technocyn 8200 mk V cold-cathode luminoscope. Beam conditions were maintained at ~600 μA and ~15 kV with a corresponding power density of ~50 kW m^{-2}. Samples were placed in a vacuum chamber mounted on an optical microscope and viewed through either a x4 or x10 objective lens. The larger field of view was used to gain a more general view of the section (e.g. modal

abundance of intragranular fluorite or feldspar luminescence indices) and the higher power objective was used for detailed compositional variations (e.g. zircon zonation and alteration)

Images were collected with a DVC high sensitivity CCD camera mounted on a Nikon Optiphot microscope using EPIX software. Typical exposure times were ~8 s as longer exposures resulted in luminescence fading for some minerals (e.g. fluorite) under the beam. Images were enhanced after collection using Adobe Photoshop 6.0 or Microsoft Office Picture Manager software.

B.3 Mineral separate preparation

During this study both pyrochlore and zircon samples were selected for isotopic and electron probe analysis. Rock samples were crushed using a steel jaw crusher and sieved to <350 μm. Pyrochlore and zircon were then separated by a combination of Wilfley table washing, heavy liquid separation using tetrabromoethane (TBE) and magnetic separation, followed by hand picking under a binocular microscope. A total of 74 pyrochlore crystals were picked from the least magnetic, 1.3 A and 1 A magnetic fractions. These were then mounted in epoxy blocks and polished for microprobe and laser ablation microprobe-multi-collector inductively coupled plasma mass spectrometry (LAM-MC-ICPMS) analysis. The same procedure was followed for zircon, but crystals were picked only from the least magnetic fraction to avoid metamict grains. A total of 19 zircons were sampled.

B.4 Radiogenic isotope analysis

All isotopic analyses were carried out at the Department of Geosciences, University of Oslo using a Nu Plasma HR mass spectrometer equipped with a U-Pb collector block. U-Pb analyses were made in static mode, with masses 204, 206 and 207 in ion counters and 283 in a Faraday cup, positioned by adjusting the magnetic field and zoom lens voltages. Masses 235 and 232 were monitored in Faraday cups, but the counting statistics on the low intensity signal on mass 235 was insufficient for precise measurement, and ^{235}U was instead estimated from the signal on mass 238 using $^{238}U/^{235}U=137.88$ for natural uranium. The sensitivity at ^{238}U was ca. 10^{-4} V / ppm.

A New Wave / Merchantek LUV213 laser-ablation microprobe was used for the spot and raster analyses. The laser delivered 213 nm UV light from the 5th harmonic of a Nd:YAG

laser. Samples were ablated into He in a specially built ablation cell. The He aerosol was mixed with Ar in a Teflon mixing cell prior to entry into the plasma. The laser beam was focussed in aperture imaging mode with a circular spot geometry.

U-Pb analyses on zircon were carried out using a stationary beam and a spot size of ~40 μm with a pulse frequency of 10 Hz operating at 33% intensity delivering an energy of 0.1 J/cm^2/pulse. Ablation depth during a 60 s run with static beam is ca. 40 μm. The ablation pits had regular, circular shape and flat bottoms. A single laser ablation analysis of zircon included a 30 s on-peak background measurement with the laser turned off, followed by 60 s of ablation. Three natural zircons were used as calibration standards: GJ-01 (609 ± 1 Ma) 91500 (1065 ± 1 Ma) and A382 (1876 ±2 Ma). These were analysed in duplicate at the beginning and end of each analytical session, and at regular intervals during analyses. Tl correction for Pb isotope mass discrimination was not used for the analysis of zircons. A high background signal on mass 204 (typically ca. 10^3 cps) due to Hg contamination of the He and Ar gas was observed. However, there was no excess ionization of Hg during ablation at the laser and microscope light settings used, so that common lead in the zircons could be monitored at mass 204. Analyses showing common-lead above background were corrected using a common lead composition given by the Stacey-Kramers global lead isotope growth curve at the relevant time (Stacey & Kramers 1975).

Raw data from the Nu Plasma time-resolved analysis program were imported into a Microsoft Excel / VBA spreadsheet program (UPSB, written by T. Andersen) for interactive selection of isotopically homogeneous integration intervals, background correction, calibration to standards and calculation of ages.

The raw data from the calibration standards were fitted to a relationship:

$$y = x(a + bx + ct)$$

where y is the true isotope ratio, x is the observed ratio for the relevant depth interval, t is time since the first standard analysis in a series, and a, b and c are coefficients determined by the built-in linear regression algorithms of Microsoft Excel 2003. The second-order term was necessary to compensate for a deviation from linearity of the ion counters at high counting rates.

Laser ablation lead isotope analysis of pyrochlore was done in line-scan mode, using a 40-50 μm laser beam focused in aperture imaging mode, a frequency of 10 Hz and energy of ca. 0.12 J/cm^2/pulse. A dilute thallium solution was aspired through a desolvating nebulizer during ablation runs, and lead isotope ratios were corrected for mass bias relative to ^{203}Tl/^{205}Tl =2.3889. Masses 202, 203, 204, 205, 206, 207 and 208 were measured in Faraday collectors. Analyses were made in time-resolved mode, using 20 s on-peak background measurement for Pb and ^{202}Hg, followed by 20 s background measurement for Tl with the ion beam deflected by the electrostatic analyser. Data were reduced using the NU Plasma time-resolved analysis software. NIST glass standards were run at 10 Hz frequency using a 100 μm spot and energy of 12 to 20 J/cm^2/pulse.

Whole-rock powders were dissolved in a 9:1 concentration of HF-HNO_3 mixture in closed teflon beakers at 80°C for 48 hours. Pb was separated by standard anion exchange procedures. Purified lead salts were dissolved in 2% HNO_3, spiked by small amounts of Tl and introduced to the plasma through the desolvating nebulizer. The collector configuration was the same as for pyrochlore laser ablation analysis. Mass bias for lead isotopes were corrected relative to ^{203}Tl/^{205}Tl =2.3888, based on an observed, long-term relationship between Pb and Tl fractionation. The contribution from ^{204}Hg at mass 204 was corrected assuming ^{204}Hg/^{202}Hg=0.2299. Data were collected in two blocks of 20 measurements each consisting of 5 integrations.

Laser ablation Lu-Hf isotope analyses on zircons was carried out in situ using a 50 μm laser beam focused in aperture imaging mode with a pulse frequency of 5 Hz delivering an energy of 1 J/cm^2/pulse. Typical ablation times were 60 to 120 s. Ablated sample was transported from the ablation cell in a He aerosol via a mixing chamber where the sample was mixed with Ar gas prior to entry into the plasma torch. For this work we analysed for masses 172, 175, 176, 177, 178, 179 and 180 simultaneously in faraday cups and collected data were normalised to ^{179}Hf/^{177}Hf = 0.7325 to correct for mass bias. Initial setup of the instrument at the start of each analytical session was performed using a 1 ppm solution of JMC475 Hf, spiked with 40 ppb Yb. Processing of data was carried out using the NU Plasma time-resolved analysis software as was used for the U-Pb zircon and Pb-Pb pyrochlore data. During each analysis a 10 s background measurement was collected on peak with the laser turned off, followed by 30 s of ablation. At the beginning and end of each analytical session and at regular

intervals during analyses the Mud Tank zircon standard was ran at 5 Hz frequency using a 50 μm spot size delivering an energy of 1 J/cm^2/pulse

Isoplot 3.00 (Ludwig, 2003) was used for plotting radiogenic isotope data and for calculating U-Pb zircon model ages and pyrochlore Pb-Pb isochron ages. Lu-Hf data were processed using interactive Microsoft Excel spreadsheet designed by T. Andersen.

B.5 Stable isotope analysis

Stable isotope analyses were carried out at the University of St Andrews on whole-rock powders from samples known to contain carbonate up to ~5 % and from carbonate veins. Before isotopic analysis, an approximate measure of the CO_2 yield was measured for the whole-rock samples by acidifying 1 g of sample with phosphoric acid (H_3PO_4). The sample was weighed before and after addition of phosphoric acid and any weight loss was recorded as the CO_2 yield (%) from carbonate in the sample. This method only gives an approximate *maximum* CO_2 yeild for the sample as phosphoric acid will also react with fluorite to produce hydrofluoric acid (HF), therefore any weight lost will also be a product of this reaction. From these results it was calculated that to achieve a sufficient CO_2 yield from each of these samples 30 mg of sample should be measured. However following the first sample run it was discovered that several samples yield very low CO_2 contents. Therefore these samples were recalculated to determine how much sample was needed to generate sufficient CO_2 and were run again.

C and O isotope analysis of powder samples were performed using a Thermo Finnegan Delta plus XP continuous flow isotope ratio mass spectrometer. Attached to the spectrometer is a Thermo Finnegan Gasbench II fitted with a fully automated CTC GC-PAL robotic sampling arm controlled using the Thermoquest Finnegan data acquisition software – ISODAT 7.3.

Samples were weighed on a microbalance and transferred to clean and dry borosilicate sample vessels and capped with a rubber septum, which retains an airtight seal after being punctured by a needle. The sample vessels are loaded into the GasBench II sample holder and are automatically flush filled with helium carrier gas using a needle to inject, displace and replace air contained above the samples with helium. The samples and vessels of phosphoric acid used to acidify are left in the sample holder for 24 hr at a constant temperature of 30°C to

ensure the acid is at equal temperature to the sample before it is added. After the flush-fill process each sample is individually acidified with 100% anhydrous phosphoric acid. An air tight syringe was used to manually add enough acid to fully acidify each sample. Several large samples (> 1000 mg) were mixed with the acid using a vibrating mixer. The samples were left to react for a further 24 hr at 30˚C before automatic isotope analysis.

Data acquisition was carried out using the ThermoFinnegan ISODAT 7.3 software. Each sample run starts with a peak centering followed by three rectangular-shaped peaks of CO_2 reference gas. After peak centering 9 successive sample peaks are produced by introducing sequential aliquots of sample CO_2 into the ion source. Each successive aliquot of introduced sample sees a steady decrease in the molar mass. The internal precision measure over these 9 peaks is typically 0.01 – 0.03 per mille for $\delta^{13}C$ and 0.01-0.03 per mille for $\delta^{18}O$. A two point linear correction was performed on the raw data based on the intensity of the first sample peak. The difference this can make is dependant on the conditions of the mass spectrometer and may be negligible or significant. Recalculation of the raw data is achieved using the NIST NBS-18 and NBS-19 reference standards. The external precision calculated using 10 standards run during each sample run give typical values of 0.01-0.04 per mille for $\delta^{18}O$ and 0.01-0.02 per mille for $\delta^{13}C$

B.6 Fluid inclusion microthermometry

Fluid inclusions were analysed in 150-300 μm thick doubly-polished rock wafers prepared at the University of St Andrews following the procedure of Shephard (1985). Samples varying between 2-15 mm in diameter were cut and ground to ~500 μm before being polishing by hand using progressively finer grades of tungsten carbide powder. Final polishing was carried out by hand on an electric polishing machine using 6 μm diamond polishing paste followed by 1 μm diamond paste for the final polish. During preparation samples were mounted using dental wax with a low melting point to prevent decrepitation of inclusions prior to analysis. Microthermometric measurements were carried out at the Institut für Geowissenschaften, University of Tübingen, Germany on a Linkam THMS600 heating and freezing stage mounted on a Leica DMRX optical microscope. Temperature was controlled using a Linkam TMS94 stand alone temperature programmer, which can be set to ramp at a heating rate of 0.1 to 130˚C/min over the range -196 to 400˚C. Inclusions were imaged and processed using the DISCUS inclusion software program. At the beginning of each analytical session, two well-characterised synthetic standards were analysed in duplicate to calibrate the

inclusion stage. The standards measured were synthetic CO_2 inclusions in quartz and synthetic pure H_2O inclusions in quartz. The triple point temperature (-56.6 °C) was measured for the synthetic CO_2 standard and the final ice melting and critical homogenisation temperatures (0.0 and 374.2 °C respectively) were measured for the pure H_2O standard. The accuracy of the final melting temperatures is typically ± 0.3 °C and for homogenisation temperatures typically ± 0.8 °C. Samples measured during each analytical session were recalculated using the slope of the line defined by the H_2O and CO_2 final melting temperatures.

During the analysis procedure, inclusion samples were rapidly cooled to freezing (N.B. freezing temperature a lot lower than the final melting temperature) and heated back to room temperature at a rate of 130°C/min to establish a crude temperature of final melting. The inclusion was again cooled to freezing and heated to within a few degrees of the final melting temperature. Approaching the final melting temperature the heating rate was slowed to 10°C/min, followed by a further decrease to 1°C/min close to the critical phase change. The same approach was used for the homogenisation temperature however a rate of 10°C/min was used up until the point of homogenisation. Several samples show inclusion decrepitation before the homogenisation temperature is reached. For these samples the temperature of decrepitation was recorded and the sample was removed from the main data set. Salinity calculations for aqueous inclusions were made from final ice melting temperatures following the revised equation of Bodnar (1993).

$$Salinity = 0.00 + 1.78\theta - 0.0443\theta^2 + 0.000557\theta^3$$

where θ is the depression of the freezing point in degrees Celsius. All salinities are expressed in weight percent (Wt.%) NaCl equivalents.

Appendix C: Pyrochlore traverse lines

Travers lines from Flinks Dal Formation pyrochlores correlating with the element distribution profiles in figure 4.3